Ontwerp van microstructuur van functionele polymeermaterialen:
een modelgeleide aanpak

Microstructural Design of Functional Polymeric Materials:
A Model-Guided Approach

Stijn Fierens

Promotoren: prof. dr. M.-F. Reyniers, dr. ir. P. Van Steenberge
Proefschrift ingediend tot het behalen van de graad van
Doctor in de ingenieurswetenschappen: chemische technologie

UNIVERSITEIT
GENT

Vakgroep Materialen, Textiel en Chemische Proceskunde
Voorzitter: prof. dr. P. Kiekens
Faculteit Ingenieurswetenschappen en Architectuur
Academiejaar 2017 - 2018

ISBN 978-94-6355-077-2
NUR 952
Wettelijk depot: D/2017/10.500/112

Examination board (members ineligible to vote)

prof. dr. lic. Marie-Françoise Reyniers	Universiteit Gent
dr. ir. Paul H.M. Van Steenberge	Universiteit Gent

Examination board (voting members)

em. prof. dr. ir. Hendrik Van Landeghem	Universiteit Gent
prof. dr. ir. Guy B. Marin	Universiteit Gent
prof. dr. ir. Dagmar R. D'hooge	Universiteit Gent
prof. dr. lic. Richard Hoogenboom	Universiteit Gent
prof. dr. lic. Yohann Guillaneuf	Université d'Aix-Marseille

Universiteit Gent

Faculteit Ingenieurswetenschappen en Architectuur
Vakgroep Chemische Proceskunde en Technische Chemie
Laboratorium voor Chemische Techniek
Technologiepark 914
B-9052 Zwijnaarde, Gent
België
Tel.: +32 (0)9 331 17 57
Fax: +32 (0)9 331 17 59
http://www.lct.ugent.be

This work was supported by the Institute for the Promotion of Innovation through Science the Long Term Structural Methusalem Funding by the Flemish Government, the Interuniversity Attraction Poles Programme - Belgian State - Belgian Science Policy ((P7/05) – Functional Supramolecular Systems (FS2)) and the Fund for Scientific Research Flanders (FWO).

Contents

Preface

I would like to thank my supervisors prof. dr. Marie-Françoise Reyniers and dr. ir. Paul Van Steenberge for the support, discussions, and their profound knowledge.

Furthermore, I would like to thank:

Prof. dr. ir. Dagmar D'hooge for his guidance, suggestions, discussions and valued advice.

Prof. dr. ir. Guy Marin for giving for giving me the opportunity to commence a PhD at the Laboratory for Chemical Technology and careful reading of the manuscripts.

Dr. Jean-François Lutz for hosting me during three months at *Centre National de la Recherche Scientifique* in Strasbourg.

Prof. dr. lic. Richard Hoogenboom , prof. dr. lic. Yohann Guillaneuf, and em. prof. dr. ir. Hendrik Van Landeghem as jury members.

The present and past members of the 'polymer group' for their help and friendship. In particular, my nearest colleagues Nils, Gilles, Dries, Lies, Yoshi and Pieter for the many laughs, memorable dinners, and for being a pleasure to work with.

All LCT colleagues.

My friends, for taking my mind of work when needed.

You, for reading this.

Finally and essentially, my deepest thanks go out to my mother, father, and sisters for bringing joy in my life and for their continuous support and trust in me.

Stijn Fierens

September 2017

Nederlandstalige samenvatting

Het eerste synthetische polymeer, Bakeliet, is ontstaan rond 1907 en is vernoemd naar zijn uitvinder, de Belgisch-Amerikaanse scheikundige Leo Baekeland (°Gent, 1863 - †New York, 1944), en markeerde het begin van de moderne kunststofindustrie. Polymeren zijn op de dag van vandaag onmisbaar in het moderne leven. Vrije radicalaire polymerisatie (FRP), een type kettingpolymerisatie, is één van de meest gebruikte synthetische routes voor commerciële polymeren met een jaarlijkse productie van miljoenen tonnen. Veel verschillende monomeertypes kunnen eenvoudig gepolymeriseerd worden via FRP met als doel de synthese van een polymeerproduct met de gewenste mechanische en chemische eigenschappen, bv. hardheid, ketenflexibiliteit, chemische weerstand. Synthetische polymeren hebben talrijke toepassingen, vooral in eerder simpele verbruiksgoederen zoals verpakkingsmateriaal.

Een groot nadeel van FRP is de gelimiteerde controle over de (co)polymeer microstructuur. Midden jaren ’50 ontstonden nieuwe synthetische routes, bv. anionische en kationische polymerisatie, die controle toelaten over de microstructuur door het minimaliseren van terminatie- en ketentransferreacties. Deze zogenaamde levende polymerisatie reacties vereisen echter strenge reactie condities en zijn slechts compatibel met een beperkt aantal monomeer types. Midden jaren ’80 ontstonden er nieuwe technieken dewelke de voordelen van vrije- en levende radicalaire polymerisaties combineren gebaseerd op de reversibele deactivering van het radicalaire species en worden reversibele deactivering radicalaire polymerisatie (RDRP) genoemd. De drie belangrijkste RDRP technieken zijn nitroxide gemedieerde polymerisatie (NMP), atoom transfer radicalaire polymerisatie (ATRP), en reversibele additie/fragmentatie keten transfer (RAFT) polymerisatie. Deze RDRP technieken laten de synthese van geavanceerde complexe macromoleculaire structuren zoals gradiënt-, blok-, en ster copolymeren. Hoewel er momenteel slechts een beperkt aantal RDRP producten de weg naar commercialisering heeft

gevonden, wordt er verwacht dat RDRP gebaseerde producten zullen leiden tot de ontwikkeling van producten met een hoge toegevoegde waarde in bv. de (bio)medische, elektronica en andere niche industrieën.

In deze doctoraatsthesis worden verschillende RDRP technieken onderzocht. Een gecombineerd experimenteel en modelgebaseerde aanpak wordt toegepast om inzichten te verwerven in de kinetische karakteristieken van RDRP processen. Het generiek LCT-modeleringsplatform wordt hiertoe uitgebreid. Dit platform omvat een snelle deterministische oplossingsmethode dewelke gebruikt kan worden voor het schatten van snelheidscoëfficiënten en, voor de eerste maal, Pareto optimalisatie van RDRP processen. De tweede oplossingsmethode is een matrix-gebaseerde kinetische Monte Carlo techniek (stochastisch) dewelke toelaat gedetailleerde kinetische en microstructurele inzichten te verwerven, echter tegen een hogere computationele kost. Dit laat het opvolgen van de expliciete microstructuur en *a posteriori* berekening van nieuwe distributies toe, dewelke toegepast zullen worden op verschillende gecontroleerde homo- en copolymerisaties. Zodoende mikt de gebruikte aanpak in deze thesis erop om een beter begrip en optimalisatie van RDRP processen te verwezenlijken zoals gedemonstreerd zal worden voor een aantal standaard RDRP processen.

In **Hoofstuk 1** wordt een algemene inleiding tot de in dit doctoraat toegepaste RDRP technieken, *i.e.* NMP, initiators voor continue activator regeneratie (ICAR) ATRP, en activators geregenereerd door elektron transfer (ARGET) ATRP, gegeven tezamen met het doel van deze doctoraatsthesis.

Hoofdstuk 2 geeft een overzicht van de huidige *state-of-the-art* modellen beschikbaar voor de beschrijving van copolymerisatieprocessen. De focus ligt bij zowel kinetische aspecten, zoals de propagatiesnelheid, als bij microstructurele aspecten specifiek voor copolymeren, zoals de

ordening van de comonomereenheden in de copolymeerketens. Verschillende modeleringstechnieken worden beschouwd naargelang hun mate van detail met betrekking tot de microstructuur van de polymeren en experimentele verificatie ervan. Zowel analytische als numerieke modellen worden besproken in volgorde van de hoeveelheid inzichten die ze verwerven in de kinetiek of de microstructuur van de polymeren. Gemiddelde eigenschappen, zoals de instantane copolymeersamenstelling, worden eerst besproken. Vervolgens komen univariate en bivariate modelleringsmethoden aan bod. De keuze om één of meerdere variabelen te gebruiken om de microstructuur te beschrijven vereist aannames en bijgevolg een verlies van informatie. In het geval dat veel details vereist zijn dient men zich te beroepen op expliciete modelleringstechnieken dewelke toelaten om de complete microstructuur van het (co)polymeer te volgen als functie van de tijd. Eén zulk expliciete stochastische modelleringstechniek, de matrix-gebaseerde kinetische Monte Carlo (*k*MC), is ontwikkeld aan het Laboratorium voor Chemische Technologie (Universiteit Gent) en zal doorheen deze doctoraatsthesis toegepast worden. Van belang is dat deze zogenaamde expliciete modelleringstechnieken het *a posteriori* berekenen van nieuwe distributies toelaat, zoals bv. activering-groei-deactivering cycli als functie van hun aantal propagatiestappen en de locatie van functionaliteiten, hetgeen nieuwe inzichten in de kinetiek van RDRP processen toelaat.

In **Hoofdstuk 3** wordt de MAMA-SG1 geïnitieerde NMP van styreen onderzoekt. MAMA-SG1, een NMP initiator (alkoxyamine) gecommercialiseerd door Arkema onder de merknaam BlocBuilder® is het meest gebruikte alkoxyamine voor NMP. Verscheidene kinetische studies van dit systeem zijn gerapporteerd maar desondanks is er een breed bereik aan kinetische snelheidscoëfficiënten gerapporteerd en is er geen fundamenteel model beschikbaar dat erin slaagt een breed bereik aan experimentele condities adequaat te beschrijven. In dit hoofdstuk

wordt een uitgebreide experimentele dataset vergaard voor een breed bereik aan temperaturen en beoogde ketenlengtes (*TCL*). Een deterministisch model, inclusief diffusielimiteringen en zijreacties zoals thermische initiatie van styreen en keten transfer reacties, gebaseerd op de momentenmethode wordt ontwikkeld en gebruikt voor data regressieanalyse. Op deze manier worden NMP specifieke Arrhenius snelheidscoëfficiënten bepaald op een statistisch verantwoorde manier. Deze snelheidscoëfficiënten worden vervolgens gebruikt in een meer geavanceerde, maar computationeel intensievere, *k*MC code om de microstructuur van de polymeerketens te visualiseren, voor de eerste keer, naargelang hun initiatie- of terminatiemechanisme. Gebaseerd op deze resultaten wordt het belang van de ketentransfer naar dimeer, een molecule gevormd gedurende het thermisch initiatie proces van styreen, gedemonstreerd. Deze reactie is de belangrijkste nevenreactie met betrekking tot controleverlies voor polymeerproducten met een hoge *TCL*. Finaal wordt het voordeel van een stapsgewijs temperatuurprogramma *in silico* gedemonstreerd en experimenteel geverifieerd. Deze model-gebaseerde optimalisatiestrategie berust op een efficiëntere initiatie waardoor een lagere temperatuur toegepast kan worden en dus thermische initiatiereacties, en de daar bijhorende zijreacties, geminimaliseerd worden voor een gelijke batch tijd.

Hoofdstuk 4 verkent het volledige potentieel van RDRP technieken gebruikmakende van *multi-objective optimization* (MOO) algoritmes. Deze algoritmes zijn ontwikkeld voor probleemstellingen waarin conflicterende objectieven geoptimaliseerd dienen te worden, leidende tot de identificatie van een zogenaamd Pareto-optimaal front. Het vaak gebruikte NSGA-II algoritme werd geïmplementeerd en toegepast ter optimalisatie van ARGET ATRP van butyl methacrylaat met twee objectieven ter beschouwing, *i.e.* batch tijd om een monomeerconversie (X_M) van 0.75 te bereiken en finale dispersiteit ($Đ$). Een deterministisch literatuur-gebaseerd

model wordt gebruikt en optimalisatie van programma's voor (i) temperatuur, (ii) monomeer additie, en (iii) reducerend agens additie worden beschouwd alsook hun combinaties. De drie verschillende individuele optimalisatiestrategieën leiden tot de identificatie van een Pareto optimaal front en dus de *in silico* optimalisatie van ten minste één objectief. Uit de vergelijking van de verschillende strategieën blijkt monomeeradditie het meest veelbelovend en de gecombineerde strategieën tonen synergetische effecten leidende tot een verbeterd Pareto optimaal front. Een verklaring van de optimalisatiestrategieën wordt voorzien aan de hand van de kinetische significantie van verschillende reactiesnelheden, zoals terminatie en de verhouding van de propagatie tot deactivering probabiliteit (P_{prop}/P_{deac}). Als tweede RDRP techniek wordt NMP van styreen beschouwd, gebruikmakende van het kinetisch model verkregen in Hoofdstuk 3, met drie objectieven, *i.e.* batch tijd (X_M = 0.75), $Đ$, en EGF. Opnieuw worden temperatuur-, monomeer additie-, en initiale nitroxide hoeveelheid programma's beschouwd. Pareto-optimale fronten worden geïdentificeerd en een temperatuurprogramma lijkt het meest veelbelovend, zoals reeds aangekaart in Hoofdstuk 3. Een kinetische verklaring van de geoptimaliseerde strategieën wordt gegeven aan de hand van de terminatieprobabiliteit en P_{prop}/P_{deac}, alsook de reactieprobabiliteit van de transfer naar dimeer reactie, hetgeen het belang van het ontwikkelde model in Hoofdstuk 3 aantoont.

In **Hoofdstuk 5**, wordt een transitie naar copolymeersystemen gemaakt. De *k*MC code wordt toegepast voor verbeterde inzichten en optimalisatiestrategieën in de synthese van sequentie-gecontroleerde polymeren via NMP. Deze sequentie-gecontroleerde polymerisatietechnieken hebben de laatste jaren veel aandacht gekregen omwille van de mogelijkheid die ze bieden om functionaliteiten langsheen de polymeerketen in te bouwen op de gewenste positie, gebruikmakende van een elektron-donor (styreen) en een elektron-acceptor monomeer (N-benzyl

maleimide; het functioneel monomeer). Een experimentele data set, gebruikmakende van BlocBuilder als NMP initiator, wordt verworven en gebruikt voor modelverificatie. Vervolgens wordt het *k*MC model gebruikt voor de expliciete visualisering van de copolymeerketens. *A posteriori* analyse laat toe nieuwe inzichten te verkrijgen in de accuraatheid van de inbouw van functionaliteiten in de ketens. Er wordt aangetoond dat hieruit eerder brede distributies van de plaatsing van het functionele monomeer volgen, zowel op een absolute als relatieve basis. Een ander kwaliteitscriterium is de verdeling van de functionele monomeren over de polymeerketens heen. Hieruit volgt ook dat bij een batch proces gemedieerd door SG1 een verre van ideaal beeld volgt met een brede distributie. Voor de eerste maal worden de activering-groei-deactivering cycli als functie van het aantal propagatiestappen gekwantificeerd. *In silico* optimalisatiestrategieën worden verkend. Er wordt aangetoond dat de additie van styreen toelaat om zowel de relatieve als absolute positionering van de BzMI functionaliteit te verbeteren. De invloed van het mediërend agens wordt onderzocht met behulp van *grid* simulaties waarin de activering (k_a) en deactivering (k_{da}) snelheidscoëfficiënten van het macrospecies gewijzigd worden. Gebaseerd op deze resultaten wordt aangetoond dat SG1 niet de ideale mediërende kwaliteiten bezit met betrekking tot de synthese van sequentie-gecontroleerde polymeren. Een nitroxide met een hogere k_{da} waarde zou leiden tot een betere distributie van de verdeling van het functioneel monomeer over de ketens heen. Finaal wordt de model-geoptimaliseerde strategie toegepast voor een tri-gefunctionaliseerd sequentie-gecontroleerd poly(styreen) product.

Hoofdstuk 6 omvat een *in silico* kinetische studie gebruikmakende van de *k*MC code om het belang van *penultimate* monomeereenheid (PMU) aan te tonen voor de reactiviteit van macroradicalen en slapende macrospecies in de ICAR ATRP van *n*-butyl acrylaat (*n*BA) en methyl methacrylaat (MMA) met een literatuur-gebaseerd kinetisch model. PMU effecten worden

beschouwd op zowel propagatie als (de)activering reacties. Grid simulaties laten toe geschikte batch reactie condities te identificeren waaruit besloten wordt dat de aard van de ATRP initiator cruciaal is voor succesvolle ICAR ATRP. Een tertiaire ATRP initiator wordt verkozen boven een secondaire omdat deze laatste leidt tot trage initiatie en dus slechtere controle over de microstructuur. De aanwezigheid van een tweefasige initiatie stap voor de tertiaire initiator, omwille van sterke reactiviteitsverschillen tussen de verschillende macrospecies, wordt aangetoond. Voor de batch simulaties wordt onafhankelijk bewezen dat PMU effecten op propagatie en (de)activering van groot belang zijn. PMU effecten op propagatie zijn vooral van belang voor de initiatiefase en PMU effecten op (de)activering beïnvloeden vooral het (de)activeringsevenwicht bij hogere conversies. Er wordt aangetoond dat de temperatuurafhankelijkheid van de reactiviteitsverhoudingen, een vaak genegeerd aspect in kinetische studies, van belang is. De batch ICAR ATRP van *n*BA en MMA met een equimolaire voeding vertoont een "natuurlijke" gradiënt dewelke verbeterd kan worden door een monomeeradditieprogramma. Er wordt gedemonstreerd dat PMU effecten de gradiëntkwaliteit (<*GD*>) beïnvloeden. De *in silico* bepaling van ideale voedingsprofielen is sterk afhankelijk van de beschouwde PMU effecten. In het algemeen toont dit hoofdstuk aan dat mogelijke PMU effecten steeds in beschouwing genomen dienen te worden gezien ze een sterk effect op copolymerisaties kunnen hebben.

Hoofdstuk 7 omvat een gecombineerde experimentele en modeleringsstudie voor NMP van MMA met en zonder een kleine hoeveelheid styreen geïnitieerd door BlocBuilder. NMP van MMA gemedieerd door SG1 lijdt onder een zijreactie, *i.e.* disproportionering van SG1 met MMA macroradicalen, en een te grote (de)activeringsevenwichtscoëfficiënt. Weloverwogen homopolymerisatiecondities worden gekozen om een ge-updatete snelheidscoëfficiënt voor deze

zijreactie te bepalen. Er wordt aangetoond dat laboschaal polymerisatie-experimenten niet-isothermiciteit vertonen, hetgeen geïncorporeerd moet worden in het model voor betrouwbare parameterbepaling. Door een kleine hoeveelheid styreen toe te voegen wordt de globale (de)activeringsevenwichtscoëfficiënt verlaagd. Voor de copolymerisatie, laat het tunen van de radicaalreactiviteitsverhouding voor activering (voor macrospecies met terminale styreeneenheid) toe om een adequate beschrijving van een grote set experimentele data te verkrijgen. De *k*MC code wordt gebruikt om de invloed van de initiële hoeveelheid styreen in kaart te brengen en een drempelwaarde te kwantificeren voor aanvaardbare controle. Inzichten in de expliciete microstructuur van het copolymeer en de activering-groei-deactivering cycli als functie van hun aantal propagatiestappen worden verkregen, dewelke een atypische vorm tonen voor een RDRP proces gezien de cycli zonder groei oververtegenwoordigd zijn door de aanwezigheid van een kleine hoeveelheid styreen.

Tot slot vat **Hoofdstuk 8** de belangrijkste conclusies van deze doctoraatsthesis samen en worden perspectieven voor toekomstig onderzoek geformuleerd.

English summary

The first synthetic polymer, Bakelite, emerged around 1907 and is named after its inventor, the Belgian-American chemist Leo Baekeland (°Ghent, 1863 - †New York, 1944), and marked the beginning of the modern plastics industry. Polymers nowadays are indispensable in modern everyday life. Free radical polymerization (FRP), a type of chain polymerization, is one of the most applied synthetic pathways for the synthesis of commercial polymers with a multi-million ton annual production. Many monomer types can be easily polymerized via FRP in order to synthesize a polymer product with the desired mechanical and chemical properties, *e.g.* toughness, chain-flexibility, chemical resistance. Synthetic polymers have numerous applications mainly in rather simple utilities such as packaging material.

A major drawback of FRP is the limited control over the (co)polymer microstructure. In the mid-50s novel synthetic pathways, *i.e.* anionic and cationic polymerization, emerged allowing control over this microstructure by minimization of termination and transfer reactions. However, these so-called living radical polymerization (LRP) required stringent reaction conditions and only allowed the polymerization of limited number of monomer types. In the mid-80s novel techniques appeared combining the benefits of FRP and LRP based on a reversible deactivation of the radical species and are called reversible deactivation radical polymerization (RDRP). The three most important RDRP techniques are nitroxide mediated polymerization (NMP), atom transfer radical polymerization (ATRP), and reversible addition/fragmentation chain transfer (RAFT) polymerization. These RDRP techniques allow the synthesis of tailor-made complex macromolecular architectures such as gradient-, block-, and star copolymers. Although currently a limited number of RDRP products have found their way towards commercialization, it is envisioned that RDRP derived products will lead to many high-added value applications in the (bio)medical, electronic and other niche industries.

In this PhD thesis, several RDRP techniques are investigated. A combined experimental and model-based approach is used to gain insight in the kinetic characteristics of RDRP processes. The generic LCT modeling platform is therefore extended. This platform consists out of a fast deterministic solver which will be used for estimation of rate coefficients and, for the first time, Pareto optimization of RDRPs. The second solver is a matrix-based kinetic Monte Carlo technique (stochastic) which allows highly detailed kinetic and microstructural insights albeit at a higher computational cost. This allows tracking of the explicit microstructure and *a posteriori* calculation of novel distributions, which will be applied for several controlled radical homo- and copolymerizations. As such, the approach applied in this thesis aims at a better understanding and optimization of RDRP in general as will be illustrated for a number of standard RDRPs.

In **Chapter 1**, a brief general introduction to the RDRP techniques used in this work, i.e. NMP, initiators for continuous activator regeneration (ICAR) ATRP, and activators regenerated by electron transfer (ARGET) ATRP is given together with the scope of this PhD thesis.

Chapter 2, provides an overview of the state-of-the-art models available for the description of copolymerization processes. Focus is both on kinetic aspects, such as the propagation rate, and microstructural aspects specific to copolymers, *e.g.* the arrangement of the comonomers in the polymer chains. Modeling techniques considering various levels of complexity in microstructural detail are discussed as well as their experimental verification. Analytical and numerical models are discussed according to the level of kinetic or microstructural detail they are able to provide. Average properties, such as the instantaneous copolymer composition, are first discussed. Next, univariate and bivariate models are covered. The choice of one or more variables to describe the microstructure requires certain assumptions and thus loss of information. In case a high level of detail is needed, one should use explicit modeling techniques which allow tracking of the time

evolution of the complete microstructure of the (co)polymer. One such explicit stochastic modeling technique, matrix-based kinetic Monte Carlo (*k*MC), has been developed at the Laboratory of Chemical Technology (Ghent University) and will be used throughout this thesis. Importantly, such explicit modeling techniques allow the *a posteriori* calculation of novel distributions of *e.g.* activation-growth-deactivation cycles with respect to their number of propagation steps and location of functionalities which allows novel insights into RDRP kinetics.

Chapter 3 investigates the MAMA-SG1 initiated NMP of styrene. MAMA-SG1, a NMP initiator (alkoxyamine) commercialized by Arkema under the tradename BlocBuilder®, is the most used alkoxyamine for NMP. Several kinetic studies of this system have been reported but nevertheless a broad scatter in reported kinetic rate coefficients has been reported and a fundamental model able to adequately predict a broad range of experimental data is lacking. In this chapter, an extensive experimental data set covering a broad temperature and targeted chain length (TCL) range is gathered. A deterministic model, including diffusional limitations and side reactions such as thermal initiation and chain transfer reactions, based on the method of moments is constructed and used for data regression analysis. This results in the determination of the NMP specific Arrhenius rate coefficients in a statistically sound manner. These rate coefficients are subsequently imported in a more advanced, computationally expensive *k*MC code to visualize the microstructure of the polymer chains, for the first time, according to their initiation or termination mechanism. Based on these results, the importance of the chain transfer reaction to dimer, a molecule formed during the styrene thermal initiation mechanism, is demonstrated. This reaction is the main deteriorating factor for synthesizing a polystyrene product with a high chain length in a controlled fashion. Finally, the beneficial use of a stepwise temperature program is demonstrated *in silico* and confirmed experimentally. This model-guided optimization strategy

relies on a more efficient initiation phase thereby allowing a lower reaction temperature, and thus minimizing thermal initiation and related side reactions, for the same batch time.

In **Chapter 4**, the full potential of RDRP techniques is explored via the use of multi-objective optimization (MOO) algorithms. These algorithms have been developed for problems in which conflicting objectives need to be optimized, leading to the identification of the so-called Pareto-optimal front. The widely used NSGA-II algorithm was implemented and applied for the optimization of the ARGET ATRP of butyl methacrylate considering two conflicting objectives, *i.e.* batch time to reach a monomer conversion (X_M) of 0.75 and final dispersity ($Đ$). A literature based deterministic kinetic model is used and optimization programs for (i) temperature, (ii) monomer addition, and (iii) reducing agent addition are considered as well as their combinations. All three single objective optimization strategies resulted in the identification of a Pareto optimal front and thus the *in silico* optimization of at least one objective. The comparison of these single objective optimization strategies allows to conclude that the monomer addition program is the most promising and that combined optimization strategies show a synergistic effect leading to an even more improved Pareto-optimal front. Explanation of the optimization strategies for the ARGET ATRP of butyl methacrylate is provided based on the kinetic significance of several key reactions rates, such as termination and the ratio of propagation to deactivation probability (P_{prop}/P_{deac}). Secondly, the NMP of styrene, using the kinetic model developed in Chapter 3, is considered using three objectives: batch time (X_M = 0.75), $Đ$, and EGF. Again temperature -, monomer addition -, and initial nitroxide amount programs are considered. Pareto-optimal fronts are optimized showing that a temperature program is most promising, as hinted by the simpler stepwise temperature program as introduced in Chapter 3. A kinetic explanation of the obtained optimization stategies is provided by considering the termination probability and P_{prop}/P_{deac}, as

well as the reaction probability for the transfer to dimer reaction, highlighting the importance of the model developed in Chapter 3.

In **Chapter 5**, a transition towards copolymer systems is made. The *k*MC code is applied for improved insights and optimization pathways into the synthesis of sequence-controlled polymers via NMP. These sequence-controlled polymers have attracted a lot of attention as they allow the incorporation of functionalities at desired positions in the polymer chain via the use of an electron-donor (styrene) and an electron-acceptor comonomer (*N*-benzyl maleimide, BzMI; the functional monomer). First, an experimental data set, using BlocBuilder as NMP initiator, is gathered and used for model validation. Subsequently, the *k*MC model is used for explicit visualization of the copolymer chains. *A posteriori* analysis allows novel insights into the preciseness of the functional monomer placement in the chains. It is shown that a rather broad distribution of the functional monomer results, both around its absolute and relative position along the polymer chain. Another quality criterion for sequence-controlled polymers is the distribution of the number of functional monomer over the polymer chains. Here also, for the batch process mediated by SG1, a far from ideal picture arises with a rather broad distribution. For the first time, the distribution of activation-growth-deactivation cycles with respect to their number of propagation steps is quantified. Therefore, *in silico* optimization strategies are explored. Fed-batch addition of styrene shows to improve both the relative and absolute position of the BzMI functionality. The influence of the mediating agent is investigated by means of grid simulations varying the activation (k_a) and deactivation rate coefficients (k_{da}) of the macrospecies. Based on these results, it is shown that SG1 does not possess ideal mediating capabilities in light of sequence-controlled polymer synthesis. A nitroxide possessing a higher k_{da} would lead to a better distribution of the functional monomer units among the polymer chains. Finally, the

model-based optimized strategy is demonstrated for a trifunctionalized sequence-controlled poly(styrene) product.

Chapter 6 encompasses an *in silico* kinetic study using the *k*MC code to demonstrate the importance of penultimate monomer unit (PMU) for the reactivity of macroradicals and dormant macrospecies in the ICAR ATRP of *n*-butyl acrylate (*n*BA) and methyl methacrylate (MMA) using a literature based kinetic model. PMU effects are considered on both the propagation and (de)activation steps. Grid simulations are used to identify suitable batch reaction conditions from which it was concluded that the nature of the ATRP initiator is crucial for successful ICAR ATRP. A tertiary ATRP initiator is preferred over a secondary one as the latter leads to too slow initiation, thereby deteriorating the microstructural control. The occurrence of a two-step initiation stage is found for the tertiary initiator, due to strong differences in the reactivities of the different (meth)acrylic macrospecies. For the batch simulations, the importance of PMU effects on propagation and (de)activation is independently demonstrated and proves to be crucial. The former are more relevant for the initiation stage whereas the latter mostly influence the (de)activation equilibrium at higher conversions. The temperature dependence of the reactivity ratios, often neglected in kinetic studies, shows to be non-negligible. The batch ICAR ATRP of *n*BA and MMA with an equimolar initial feed composition yields a so-called "natural" gradient copolymer which can be improved via a fed-batch program. It is demonstrated how the PMU affects the gradient quality (<*GD*>). The *in silico* determination of an ideal fed-batch program depends strongly on the PMU effects considered. Overall, this chapter strongly suggests that possible PMU effects should be considered whenever possible as they can have a profound effect on the copolymerization.

Chapter 7 presents a combined experimental and modeling study for NMP of MMA with and without a small amount of styrene initiated by BlocBuilder. The NMP of MMA mediated by SG1 is deteriorated due to a side-reaction in which the nitroxide SG1 may disproportionate with MMA macroradicals along with a too large (de)activation equilibrium. Dedicated homopolymerization conditions are designed to determine an updated rate coefficient for this side reaction. It is demonstrated that lab-scale polymerization experiments are non-isothermal, which needs to be incorporated in the model in view of parameter assessment. By adding a small amount of styrene, the overall (de)activation equilibrium is decreased. In this copolymerization, adjusting the activation radical reactivity ratio (styrene terminal unit) allows an adequate prediction of a large set of experimental data. The *k*MC code is applied to map the influence of the initial styrene content and identify thresholds for acceptable control. Insights into the explicit copolymer microstructure are provided as well as into the individual activation-growth-deactivation cycles which display atypical distributions for RDRP processes as the zero-growth cycles are promoted by the presence of a small styrene amount.

Finally, in **Chapter 8** the main conclusions of this PhD are summarized and an outlook for possible future research is provided.

List of symbols

Abbreviations

AIBN	2,2-azobisisobutyronitrile
BDE	bond dissociation energy
BMA	butyl methacrylate
BPO	benzoyl peroxide
BzMI	N-benzylmaleimide
CTA	chain transfer agent
CaH_2	Calcium hydride
CDCl3	deuterated chloroform
CEF	crystallization elution fractionation
CLD	chain length distribution
CoC-CLD	copolymer composition-chain length distribution
CoCD	copolymer composition distribution
CRP	controlled radical polymerization (also known as RDRP)
CRP	controlled radical polymerization
CRYSTAF	crystallization analysis fractionation
Cu(II)Br2/PMDETA	N,N,N′,N″,N″-pentamethyldiethylenetriamine
D	dimer
DBNO	di-tert-butyl nitroxide
DCM	Dichloromethane
EGF	end-group functionality
EPR	electron paramagnetic resonance
FID	flame ionization detector
FRP	free radical polymerization

FT-IR	Fourier-transform infrared
GC	gas chromatography
GPC	gel permeation chromatography (also known as SEC)
HPLC	high-pressure liquid chromatography
ICAR	initiators for continuous activator regeneration
kMC	kinetic Monte Carlo
LLDPE	Linear low-density polyethylene
MALDI-TOF MS	matrix assisted laser desorption/ionization time-of-flight analyzer mass spectroscopy
MCD	monomer-monomer complex participation
MCP	monomer-monomer complex dissociation
MMA	methyl methacrylate
MSTD	monomer sequence type distributions
$Mt^{n+1}X_2/L$	ATRP deactivator
$Mt^{n}X/L$	ATRP activator
*n*BuA	*n*-butyl acrylate
NMP	nitroxide mediated polymerization
NMR	nuclear magnetic resonance
PID	proportional-integral-derivative
PLP	pulsed laser polymerization
PMU	penultimate monomer unit
ppm	parts per million
PSSA	pseudo-steady state assumption
R0X	ATRP initiator
RDRP	reversible deactivation radical polymerization

RI	refractive index
R^{II}	reducing agent
R_iX	dormant macrospecies
SG1	N-*tert*-butyl-N-[1-diethylphosphono-(2,2-dimethylpropyl)]
SLD	segment length distribution
Sn(EH)$_2$	tin(II) 2-ethylhexanoate
TCL	targeted chain length
TEMPO	2,2,6,6-tetramethylpiperidinyl-1-oxy
THF	tetrahydrofuran
TIPNO	2,2,5-trimethyl-4-phenyl-3-azahexane-3 oxyl
TPMA	tris[(2-pyridyl)methyl]amine
TREF	temperature rising elution fractionation
UV	ultraviolet
X	halogen moiety

Symbols

$(l_{i,inst})_k$	instantaneous segment length of monomer type *i* with length *k*	-
$\overline{l_{1,inst,}}$	instantaneous average segment lengths	-
<BD>	block deviation index	-
<GD>	gradient deviation index	-
<K>	overall (de)activation equilibrium	-
$<k_p>$	average propagation rate coefficient	L mol^{-1} s^{-1}
A	pre-exponential factor	(L mol^{-1}) s^{-1}
A^*	reparametrized pre-exponential factor for	((L mol^{-1}) s^{-1})

	regression analysis	
$\boldsymbol{b}$	vector with parameter estimates	(kJ mol^{-1}/s^{-1}/L mol^{-1} s^{-1})
E_a	activation energy	kJ mol^{-1}
F_1	cumulative copolymer composition	-
$F_{1,inst}$	instantaneous copolymer composition	-
f_i	monomer type i feed composition	-
$f_{m,inst}(n,y)$	instantaneous mass fraction of chains with length n and relative composition γ	-
f_{rec}	fraction of termination via recombination	-
k	rate coefficient	(L mol^{-1}) s^{-1}
K_{eq}	activation/deactivation equilibrium coefficient	-
M	monomer	-
M_1	monomer type 1 (MMA)	-
M_2	monomer type 2 (styrene)	-
MM	molar mass	g mol^{-1}
N_o	offspring population number	-
N_p	parent population number	-
P_i	parent generation number i	-
p_{ij}	probabilities propagation of terminal radical type i with monomer j	-
P_x	reaction probability of reaction x	-
Q_i	off-spring generation number i	-
R	radical macrospecies	-
R	universal gas constant	J $(K\ mol)^{-1}$

$R_{0,1}$	NMP initiator radical	-
$R_{0,1}X$	alkoxyamine or NMP initiator	-
$R_{0,2/3}$	initiators radicals formed upon thermal initiation with 3 referring to the dimer radical; corresponding dormant species $R_{0,2/3}$X	-
$R_{0,4}$	radical formed upon chain transfer to monomer; corresponding dormant species $R_{0,4}X$	-
R_0X	alkoxyamine initiator	-
$r_i^{(')}$	monomer radical reactivity ratio (i=1 or 2)	-
R_iX	dormant macrospecies	-
R_x	reaction rate of reaction *x*	mol (L s)$^{-1}$
S	objective function for regression analysis (-)	-
s_{ai}	activation radical reactivity ratio (i=1 or 2)	-
s_i	propagation radical reactivity ratio (i=1 or 2)	-
t_{ret}	retention time	s
T_{set}	temperature set-point	K
W	matrix containing the weights for regression (-)	-
XH	hydroxylamine	-
X_M	overall monomer conversion	-
X_{MMA}	MMA conversion	-
x_n	number average chain length	-
$\boldsymbol{y}$	vector containing the measured values for responses for the *i*th experimental data point (-)	-
μ	mean average	-
σ	standard deviation	-

Sub and superscripts

0	initiator related
a	activation
d	Diels-Alder dimerization
da	deactivation
dis	dissociation of conventional initiator
dr	retro Diels-Alder dimerization
i,j	chain length
p	propagation
tc	termination via recombination
td	termination via disproportionation
td,X	disproportionation with nitroxide
thi	molecule assisted homolysis
trd	chain transfer to dimer
trm	chain transfer to monomer

List of publications and conference contributions

Publications in international peer reviewed journals

Accepted

1. *Fierens, S.K.; D'hooge, D.R.; Van Steenberge, P.H.M.; Reyniers, M.-F.; Marin, G.B.* ***MAMA-SG1 initiated nitroxide mediated polymerization of styrene: from Arrhenius parameters to model-based design*** Chemical Engineering Journal **2015**, 278, p.407-420
2. *Fierens, S.K.; D'hooge, D.R.; Van Steenberge, P.H.M.; Reyniers, M.-F.; Marin, G.B.* ***Exploring the full potential of reversible deactivation radical polymerization using Pareto-optimal fronts*** Polymers **2015**, 7(4). p.655-679
3. *Fierens, S.K.; Van Steenberge, P.H.M.; Telitel, S.; Reyniers, M.-F.; Marin, G.B.; Lutz, J.-F.; D'hooge, D.R.* ***Model-based design to push the boundaries of sequence control*** Macromolecules **2016**, 49, p.9336-9344
4. *Fierens, S.K.; Van Steenberge, P.H.M.; Reyniers, M.-F.; Marin, G.B.; D'hooge, D.R.* ***How penultimate monomer unit effects and initiator choice influence ICAR ATRP of n-butyl acrylate and methyl methacrylate*** AIChE Journal **2017**, DOI: 10.1002/aic.15851

To be submitted

5. *Fierens, S.K.; Vermeire, F.; D'hooge, D.R.; Van Steenberge, P.H.M.; Reyniers, M.-F.; Marin, G.B.* ***A qualitative evaluation of the impact of SG1 disproportionation and the addition of styrene in nitroxide mediated polymerization of methyl methacrylate*** Macromolecules (envisioned)
6. *Fierens, S.K.; D'hooge, D.R.; Van Steenberge, P.H.M.; Reyniers, M.-F.; Marin, G.B.* ***Analytical and advanced models for characterization of chain-growth copolymerization: the state-of-the-art*** React. Chem. Eng. (envisioned)

Conference contributions

1. *Van Steenberge, P.H.M.; D'hooge, D.R.; Toloza Porras, C.; Fierens, S.K.; Reyniers, M.-F.; Marin, G.B.* ***Advanced kinetic Monte Carlo optimization of the synthesis of well-defined (co)polymers via atom transfer radical and nitroxide mediated polymerization*** American Institute of Chemical Engineers Annual Meeting (2013)
2. *Fierens, S.K.; D'hooge, D.R.; Reyniers, M.-F.; Marin, G.B.* ***Model-based design of nitroxide mediated polymerization*** 23rd International Symposium on Chemical Reaction Engineering (2014)
3. *Fierens, S.K.; D'hooge, D.R.; Van Steenberge, P.H.M.; Reyniers, M.-F.; Marin, G.B.* ***Model-based design of nitroxide mediated polymerization of styrene*** Annual meeting Belgian Polymer Group (2014)
4. *D'hooge, D.R.; Fierens, S.K.; Van Steenberge, P.H.M.; Reyniers, M.-F.; Marin, G.B.* ***The strength of model-based design for nitroxide mediated polymerization*** International Conference on Chemical Kinetics (2015)
5. *Fierens, S.K.; D'hooge, D.R.; Van Steenberge, P.H.M.; Reyniers, M.-F.; Marin, G.B.* ***A combined experimental and modeling study of the nitroxide mediated polymerization of styrene initiated by BlocBuilder*** IAP P7/08 Annual Meeting (2015)
6. *Fierens, S.K.; D'hooge, D.R.; Van Steenberge, P.H.M.; Reyniers, M.-F.; Marin, G.B.* ***Nitroxide mediated polymerization of styrene: from Arrhenius parameters to NMP kinetics and explicit visualization of microstructure*** BPG Annual Meeting, Belgian Polymer Group (2015)

7. *Van Steenberge, P.H.M.; Fierens, S.K.; D'hooge, D.R.; Reyniers, M.-F.; Marin, G.B.* ***Multi-objective optimization of feeding rates and temperature program for nitroxide mediated (co)polymerization of styrene and n-butyl acrylate*** 12th Workshop on Polymer Reaction Engineering (2016)
8. *Fierens, S.K.; Van Steenberge, P.H.M.; Telitel S.; Reyniers, M.-F.; Lutz J.-F.; D'hooge, D.R.; Marin, G.B.* ***In silico based design of nitroxide mediated polymerization: from homopolymers to sequence controlled polymers BPG*** Annual Meeting (2016)
9. *Fierens, S.K.; Van Steenberge, P.H.M.; Telitel S.; Reyniers, M.-F.; Lutz J.-F.; D'hooge, D.R.; Marin, G.B.* ***Design of nitroxide mediated polymerization via computer modeling: from homopolymers to sequence controlled polymers*** Chemical Research in Flanders (2016)

Chapter 1. Introduction and scope of thesis

1.1 Introduction

Reversible deactivation radical polymerization (RDRP), also known as controlled radical polymerization (CRP), has emerged as a powerful polymerization tool in recent decades allowing the synthesis of polymer products with a controlled composition and architecture.[1] RDRP finds its origins in classical free radical polymerization (FRP) techniques which can be considered a matured polymerization technique. FRP has been around since the 1950s and has since experienced an enormous growth partly thanks to its many beneficial attributes such as its compatibility with a large range of monomer families, the tolerance towards impurities and the absence of stringent reaction conditions. However, a poor control over the microstructure of the polymer product is achieved. This control over microstructure of polymers is an important prerequisite for many high-tech applications in markets such as, for example, the detergents, cosmetics, health, coating and electronics industries.[2] Control over the microstructure allows the synthesis of more complex polymer architectures. Figure 1.1 displays the variety of polymeric microstructures which can be achieved using RDRP techniques. These microstructures can differ in their composition, architecture, functionalization and conformation. Early attempts at achieving the required control over such polymer microstructures involved anionic and cationic polymerizations.[3, 4] However, these techniques show a strong intolerance towards impurities and require typically stringent reaction conditions, *e.g.* the complete absence of water, thereby limiting their industrial applicability. Nevertheless, living polymerization are employed industrially in for example the synthesis of poly(styrene-butadiene-styrene) rubber.

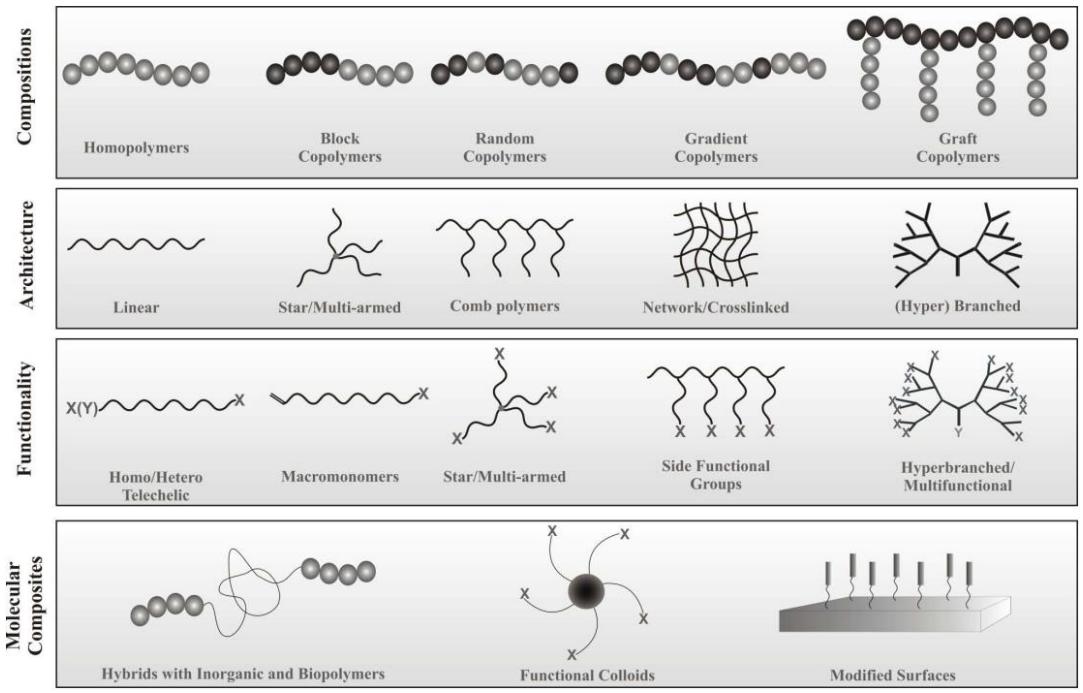

Figure 1.1. *Complex polymer microstructures achievable via RDRP techniques. Adopted from Toloza et al.*[5]

Therefore, in the past decades, novel polymerization techniques, so-called controlled radical polymerization techniques (CRP), have been investigated to establish control over polymer microstructure. Such CRPs combine the advantages of FRP (mild reaction conditions) with the positive characteristics of ionic polymerizations ("living" character). These CRPs are mostly based on reversible deactivation radical polymerization (RDRP) techniques and form the basis of this thesis. The three most important RDRP techniques are nitroxide mediated polymerization (NMP), atom transfer radical polymerization (ATRP), and reversible addition/fragmentation chain transfer (RAFT) polymerization. In this PhD, attention will be on NMP and several variations of the ATRP techniques. Below a short overview of these different RDRP techniques will be given.

1.1.1 Nitroxide mediated polymerization

Nitroxide mediated polymerization can be considered the easiest RDRP technique to apply and has been historically the earliest RDRP technique. Moad *et al.* published a pioneering paper in 1982 on the inhibition of the thermal initiation of styrene by scavenger nitroxide species, such as 2,2,6,6-tetramethylpiperidinyloxyl (TEMPO).[6] The principle of NMP relies on the temporary deactivation of the radicals by a nitroxide species, the mediating agent. The basic kinetic scheme of NMP is shown in Figure 1.2. Upon activation of the initiating alkoxyamine R_0X (k_{a0}), via a homolysis reaction, an initiator radical (R_0) and the mediating agent, the nitroxide (X), are released. The R_0 species may deactivate again (k_{da0}), or it can undergo a chain initiation (k_{p0}) by adding a monomer unit resulting in the formation of a macroradical (R_i). This macroradical will undergo several propagation steps (k_p) before it is deactivated (k_{da}) by the nitroxide. This temporary deactivation results in the formation of dormant macrospecies (R_iX) which remain in the dormant state before they are activated again. This deactivation maintains the radical concentration at much lower levels than comparable FRPs, thus leading to much less termination reactions (k_t) in comparison with FRP, as the rate of these termination reactions depend on the square of the radical concentration, ultimately avoiding formation of so-called dead polymer products (P_i).

Importantly, in NMP processes, deactivation reactions are favored due to the so-called persistent radical effect.[7-9] Initially, the alkoxyamines dissociate and produce the nitroxide mediating agents, *i.e.* the persistent radicals, and the radical initiating species, the so-called "transient radicals". In this early stage, the concentration of both radical types increases quasi-linearly as a function of time, leading to high transient radical concentrations and subsequent irreversible termination reactions, leading to the formation of dead polymer products. At the same time, the

transient radical concentration decreases whilst the persistent radical species are accumulating. This build-up of the nitroxide species favors the deactivation reaction, shifting the pseudo-equilibrium even further to the dormant side, lowering the transient radical concentration and minimizing the termination rate. For a more detailed explanation of this persistent radical effect, the reader is referred to the excellent article by Tang *et al.*[10]

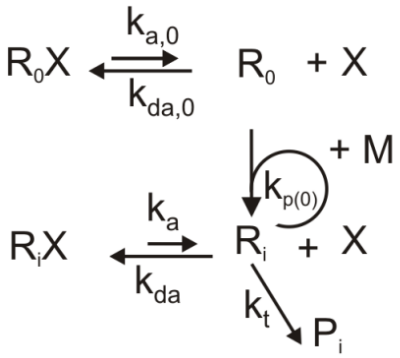

Figure 1.2. *Principle of nitroxide mediated polymerization (NMP); (d)a, p,t: (de)activation, propagation, termination; 0: NMP initiator related; M: monomer, R_0X: alkoxyamine, X: nitroxide.*

Next to using an alkoxyamine as initiating species, *i.e.* the so-called unimolecular pathway, also a bicomponent pathway to start a NMP is possible. This process uses a conventional thermal initiator (I_2), such as 2,2-azobisisobutyronitrile (AIBN) or benzoyl peroxide (BPO), in combination with so-called "free" nitroxide. Using the bicomponent pathway, an additional degree of freedom in the reaction conditions becomes available, namely the ratio of nitroxide to conventional initiator, which should be tuned for a successful NMP.[11, 12]

The success of a NMP depends strongly on the chemical structure of the mediating nitroxide agent. An overview of some of the most applied and historically important nitroxides is given in Figure 1.3. TEMPO was the earliest nitroxide proven to be an effective NMP initiator, but suffered from several drawbacks such as its incompatibility with many monomer families, due to

side reactions or a too high or low (de)activation equilibrium, mainly limiting its use to styrenic monomers and the necessity for high temperatures due to a low activation-deactivation equilibrium coefficient, leading to very slow polymerizations. The need for higher temperatures can be explained by both the high activation energy of the activation reaction and the near-zero activation energy of the deactivation reaction. Therefore, novel nitroxides have been investigated such as the acyclic ditertiary butyl nitroxide (DTBN/DBNO) which displays a higher (de)activation equilibrium coefficient than TEMPO and thus allowed lower reaction temperatures to be used.[13] This led to further investigation into these acyclic nitroxides, as done by Hawker *et al.*[14] who developed the more sterically hindered TIPNO nitroxide, the first nitroxide that was able to control a wider range of monomer families such as styrenics, acrylates and dienes. A further breakthrough came by introducing heteroatoms into these acyclic nitroxides which lead to the development of one of the most commonly used nitroxides called SG1 or DEPN.[15, 16] This β-phosphorylated nitroxide proved to be the most versatile nitroxide used in NMP so far which led to its commercialization by the French company Arkema in the form of the alkoxyamine BlocBuilder®, also known as MAMA-SG1. For an excellent review on the large variety of nitroxides and alkoxyamines developed the reader is referred to Nicolas *et al.*[17] In case of a unimolecular (initiation) pathway, the chemical structure of the R_0 radical needs to be carefully tuned, to ensure efficient chain initiation.[17]

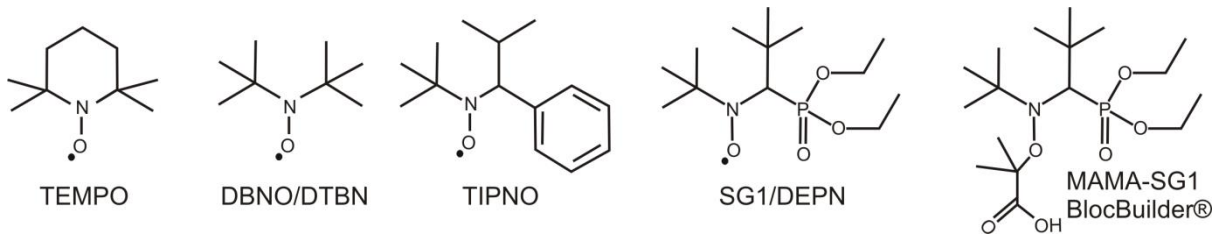

Figure 1.3. *Chemical structures of some historically important nitroxides/alkoxyamines*

1.1.2 Atom transfer radical polymerization

ATRP is a catalytic process which employs a transition metal complex, such as iron, nickel or copper. The latter has proven to be the most efficient transition metal and has been used for the RDRP of many types of monomers, such as styrenics, (meth)acrylates, (meth)acrylamides, *etc*. Many types of ATRP catalysts have been developed throughout the years. The most frequently applied ATRP catalysts are N,N,N',N",N"-pentamethyldiethylenetriamine (PMDETA), tris(2-pyridylmethyl)amine) (TPMA) and tris[2-(dimethylamino)ethyl]amine (Me_6TREN), which are complexes made out of copper bromide and/or copper chloride.

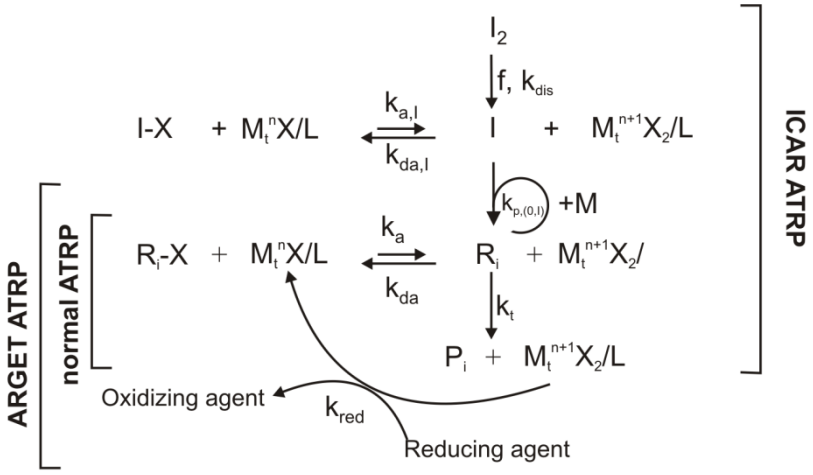

Figure 1.4. Principle of normal, ICAR, and ARGET ATRP.

The principle of atom transfer radical polymerization (ATRP) is shown in Figure 1.4. In this classical ATRP processes, typically, a Cu(I)-complex, *i.e*. the activator species, catalyses the

homolytic cleavage of the carbon-halide bond (*C-X*) of an ATRP initiator (R_0X). This reaction forms a transition metal complex in its higher oxidation state, *i.e.* $M_t^{(n+1)}$-complex or the deactivator species. The R_0 species will function as radical initiator and add monomer units, forming a macroradical. This macroradical continues growing until it reacts with the deactivator species, forming a carbon halide bond (C-X) and regaining the end-group functionality of the polymer molecule. This molecule remains dormant until the next activation reaction. Just as in NMP, termination is never fully suppressed, especially at low reaction times, and thus a build-up of the deactivator species occurs, also known as the persistent radical effect and leading to a decrease of the macroradical concentration. Normal ATRP has proven to be compatible with many monomers at relatively low reaction temperatures, which are two of the major drawbacks for NMP. However, normal ATRP suffers from various disadvantages. Firstly, all molecular oxygen must be removed from the reaction mixture, because the catalyst may react with oxygen. Secondly, to achieve a controlled normal ATRP, high catalyst concentrations are required, which is costly. Moreover, these metal complexes are toxic and must be removed from the product. This intensive purification step inhibits industrial realization. In order to overcome these drawbacks, improved initialization methods for ATRP have been developed, resulting in more commercially attractive ATRPs. The two best known examples of these alternative ATRP techniques, both of which are studied in this thesis, are activators regenerated by electron transfer (ARGET) ATRP and initiators for continuous activator regeneration (ICAR) ATRP and will be briefly discussed. They share common benefits, namely that the catalyst is initially present in its deactivated form, which does not react with molecular oxygen and that the required catalyst amounts are much lower than when initializing the ATRP normally, *i.e.* starting from the activator. These two ATRP techniques are introduced below.

The principle of ARGET ATRP is also shown Figure 1.4 and differs from the classical ATRP process in the presence of a reducing agent, for example tin(II) 2-ethylhexanoate ($Sn(EH)_2$). This reducing agent is added in excess with respect to the ATRP catalyst which is typically present in much lower amounts than in normal ATRP (typically 50-300 ppm vs. 500-1000 ppm with respect to monomer, respectively). The reducing agent will *in situ* reduce the deactivator species resulting in the regeneration of the activator species, thereby counteracting the build-up of deactivator species due to irreversible termination. Next to lowering the catalyst amount, this allows also to start the ARGET ATRP with the deactivator species instead of the activator species. As the former is much less sensitive to oxygen, this allows less stringent reaction conditions.

In ICAR ATRP (see Figure 1.4), the polymerization is again started with the oxygen insensitive deactivator in the presence of conventional radical initiator (I_2). As such, a FRP and "normal" ATRP process is mixed to allow for an acceptable polymerization rate and excellent microstructural control. Mechanistically, the I_2 will continuously generate radicals which can participate in the propagation reactions and react with deactivator molecules to (re)generate activator species to compensate for the build-up of deactivator species due to inevitable termination reactions.

1.1.3 Reversible addition/fragmentation chain transfer

RAFT polymerization is one of the most promising industrially attractive RDRP techniques which has been developed by the CSIRO group in Australia.[18] In contrast to NMP and ATRP, the RAFT process does not rely on the persistent radical effect but rather control is established through the degenerative transfer principle. Thiocarbonylthio compounds, the so-called RAFT chain transfer agent (CTA), are used as mediating agents. The process involves conventional free radical initiator (I_2) which generates radicals which propagate until they are either terminated or

react with the RAFT CTA to form the intermediate RAFT species. This intermediate radical has two pathways of fragmentation. An equilibrium between active chains and sleeping (macro) CTA-molecules is established resulting in controlled conditions. The RAFT polymerization technique is not considered in this thesis.

1.2 Objectives and outline

In this thesis, the generic modeling platform for radical polymerizations developed at the LCT is further extended. The advantage of the generic approach is that a single platform can be used to optimize many polymerizations, as opposed to developing a separate model for every individual polymerization. This generic platform consists of two numerical techniques for optimal flexibility. The first technique is the method of moments (deterministic) and is aimed toward fast computation of average microstructural characteristics (*e.g.* EGF, dispersity and average chain length), which can be used for estimation of rate coefficients and, for the first time, applied for Pareto optimization of RDRP. The second technique is a matrix-based kinetic Monte Carlo technique (stochastic) which is computationally expensive but ideally suited for highly detailed kinetic and microstructural insights on the arrangement of the monomer units (*i.e.* novel distributions of *e.g.* (de)activation-growth cycle and location of functionalities). The added value of both approaches is illustrated throughout this thesis for a number of standard RDRPs.

This generic modeling platform is used to model and optimizing several important RDRPs, considering, for the first time at the LCT, penultimate monomer units effects when feasible. The predictive abilities of the models are verified by validating against experimental data whenever possible, using dedicated reaction conditions to reliably capture competition between desired and undesired elementary reactions. In a next step, the model is used to guide experimental design of polymer microstructures, *i.e.* a model-guided approach is followed to obtain novel insights and

optimization strategies. These modeling insights into the kinetics of the RDRP processes, unattainable with exclusively experimental techniques, will be used to explain the observed experimental trends and to quantify and predict the reaction kinetics, a vital aspect for optimizing RDRP techniques. A more detailed, chapter-by-chapter, overview is given below.

The PhD-thesis is divided into 8 independent chapters, of which chapter 2-7 are related to journal papers which have been published or will be published in the near future. **Chapter 2** is a theoretical introductory chapter which provides an overview of the state-of-the-art computational, analytical and experimental techniques for predicting copolymerization properties. It serves as a basis for understanding the advanced modeling concepts used in later chapters. **Chapter 3** presents an investigation into the NMP of styrene initiated by BlocBuilder, a widely used alkoxyamine. A large experimental data set over a broad range of conditions was acquired to determine improved NMP specific rate coefficients using regression analysis and a deterministic kinetic model. The stochastic model was used to gain kinetic insights into the deteriorating effect of side reactions related to the thermal initiation of styrene and into the efficiency of the initiation stage of the NMP. A model-guided optimization strategy using a stepwise temperature program was identified and experimentally confirmed. In **Chapter 4**, the concept of Pareto optimality is applied for two RDRP processes, *i.e.* ARGET ATRP of butyl methacrylate and the NMP of styrene. Literature based deterministic models were employed in combination with a genetic multi-objective optimization algorithm to identify the optimization strategies via for example a temperature program or reagent addition profile and the trade-off between the conflicting objectives is quantified. Explanation of these optimization strategies is provided based on the kinetic significance of several key reaction rates. In **Chapter 5**, a shift is made towards copolymerization systems. More specifically, the synthesis of well-defined sequence-controlled

polymers synthesized via NMP of an electron-donor (styrene) and electron-acceptor (*N*-benzyl maleimide) initiated by BlocBuilder was investigated. Advanced kinetic Monte Carlo simulations allow to quantify the product quality, focusing on specific attributes related to these sequence-controlled polymers such as the precision of the functional monomer placement and the distribution of the functional monomer along the individual polymer chains. It is also shown that the nitroxide mediating capabilities and reaction conditions can be tuned to optimize the sequence-control. The observed trends are explained in terms of the individual activation-growth-deactivation cycles, which can only be accessed using a kinetic Monte Carlo modeling framework. In **Chapter 6**, the importance of penultimate monomer unit effects and the initiator choice for the ICAR ATRP of *n*-butyl acrylate and methyl methacrylate was assessed *in silico* using literature based stochastic models. Specific focus was on the synthesis of gradient copolymers. It is shown that PMU effects cannot be ignored, as is often done in kinetic studies, as they influence the identification of the most suited ICAR ATRP reactants and reaction conditions. Explanations of the formulated insights are provided again by means of interpreting the relative contribution of several key reaction steps. Finally, in **Chapter** 7, the NMP of methyl methacrylate with and without a small amount of styrene initiated by BlocBuilder is investigated. These polymerizations are notoriously difficult to control, due to a too high (de)activation equilibrium coefficient of terminal MMA macrospecies and side-reactions. Moreover, these uncontrolled conditions lead to a non-isothermal RDRP. Therefore, a small amount of styrene is added to decrease the (de)activation equilibrium coefficient. A dedicated experimental data set (methyl methacrylate without styrene) is used for the determination of Arrhenius parameters for the disproportionation to nitroxide reaction, the main side reactions leading to a failure of the NMP of MMA. Because such side reactions are activated, the relevance of incorporating the non-isothermicity of the copolymerization into the kinetic model is demonstrated. In a next step,

copolymerization data (methyl methacrylate with styrene) are described using the kinetic Monte Carlo model, improving the predictive power of the model. This model provides insights into the copolymer microstructure. Here also, explanations of the observed trends are provided by again looking at the relative contribution of several key reaction steps and by tracking the individual activation-growth-deactivation cycles.

As such, throughout this thesis, the strength of a model-based approach is demonstrated for several RDRP systems. Thorough interpretation of the results is each time provided by analysis of the kinetic characteristics of RDRP processes leading to an improved understanding of these RDRP processes in general.

References

1. Braunecker, W. A.; Matyjaszewski, K. Controlled/living radical polymerization: Features, developments, and perspectives. *Prog. Polym. Sci.* **2007,** 32, (1), 93-146.

2. Destarac, M. Controlled Radical Polymerization: Industrial Stakes, Obstacles and Achievements. *Macromol. React. Eng.* **2010,** 4, (3-4), 165-179.

3. Szwarc, M.; Levy, M.; Milkovich, R. Polymerization initiated by electron transfer to monomer. A new method of formation of block polymers. *J. Am. Chem. Soc.* **1956,** 78, (11), 2656-2657.

4. Szwarc, M. `Living' Polymers. *Nature* **1956,** 178, (4543), 1168-1169.

5. Toloza Porras, C. Model based design of functional polymer materials by initiators for continuous activator regeneration atom transfer radical polymerization (ICAR ATRP). PhD dissertation, Ghent University. Faculty of Engineering and Architecture, 2013.

6. Moad, G.; Rizzardo, E.; Solomon, D. H. A product study of the nitroxide inhibited thermal polymerization of styrene. *Polym. Bull.* **1982,** 6, (11-1), 589-593.

7. Fischer, H. The Persistent Radical Effect In “Living” Radical Polymerization. *Macromolecules* **1997,** 30, (19), 5666-5672.

8. Goto, A.; Fukuda, T. Kinetics of living radical polymerization. *Prog. Polym. Sci.* **2004,** 29, (4), 329-385.

9. Lutz, J. F.; Lacroix-Desmazes, P.; Boutevin, B. The persistent radical effect in nitroxide mediated polymerization: Experimental validity. *Macromol. Rapid Commun.* **2001,** 22, (3), 189-193.

10. Tang, W.; Fukuda, T.; Matyjaszewski, K. Reevaluation of persistent radical effect in NMP. *Macromolecules* **2006,** 39, (13), 4332-4337.

11. Veregin, R. P. N.; Odell, P. G.; Michalak, L. M.; Georges, M. K. The pivotal role of excess nitroxide radical in living free radical polymerizations with narrow polydispersity. *Macromolecules* **1996,** 29, (8), 2746-2754.

12. Gigmes, D.; Bertin, D.; Lefay, C.; Guillaneuf, Y. Kinetic Modeling of Nitroxide-Mediated Polymerization: Conditions for Living and Controlled Polymerization. *Macromol. Theory Simul.* **2009,** 18, (7-8), 402-419.

13. Moad, G.; Rizzardo, E. Alkoxyamine-Initiated Living Radical Polymerization: Factors Affecting Alkoxyamine Homolysis Rates. *Macromolecules* **1995,** 28, (26), 8722-8728.

14. Benoit, D.; Chaplinski, V.; Braslau, R.; Hawker, C. J. Development of a universal alkoxyamine for "living" free radical polymerizations. *J. Am. Chem. Soc.* **1999,** 121, (16), 3904-3920.

15. Grimaldi, S.; Finet, J.-P.; Le Moigne, F.; Zeghdaoui, A.; Tordo, P.; Benoit, D.; Fontanille, M.; Gnanou, Y. Acyclic β-Phosphonylated Nitroxides: A New Series of Counter-Radicals for "Living"/Controlled Free Radical Polymerization. *Macromolecules* **2000,** 33, (4), 1141-1147.

16. Benoit, D.; Grimaldi, S.; Robin, S.; Finet, J. P.; Tordo, P.; Gnanou, Y. Kinetics and mechanism of controlled free-radical polymerization of styrene and n-butyl acrylate in the presence of an acyclic beta-phosphonylated nitroxide. *J. Am. Chem. Soc.* **2000,** 122, (25), 5929-5939.

17. Nicolas, J.; Guillaneuf, Y.; Lefay, C.; Bertin, D.; Gigmes, D.; Charleux, B. Nitroxide-mediated polymerization. *Progress in Polymer Science* **2013,** 38, (1), 63-235.

18. Chiefari, J.; Chong, Y. K.; Ercole, F.; Krstina, J.; Jeffery, J.; Le, T. P. T.; Mayadunne, R. T. A.; Meijs, G. F.; Moad, C. L.; Moad, G.; Rizzardo, E.; Thang, S. H. Living free-radical polymerization by

reversible addition-fragmentation chain transfer: The RAFT process. *Macromolecules* **1998,** 31, (16), 5559-5562.

Chapter 2. Analytical and advanced models for characterization of chain-growth copolymerization: the state-of-the-art

Summary

A detailed overview is given on the currently developed models to calculate the key chain-growth copolymerization characteristics, differentiating between the polymerization rate and compositional properties (*e.g.* average copolymer composition, segment length distribution, and monomer sequences). Both terminal and penultimate reactivity models are included and the relevance of their parameters is highlighted through examples. Focus is first on analytical models which limit themselves to the description of the propagation kinetics and implicitly account for time dependencies. The focus is then shifted to advanced models, in particular multivariate ones that employ distributions with respect to a distinct number of microstructural variates of interest such as chain length and copolymer composition. Also the more recently developed explicit models in which the compositional and temporal changes are fully tracked along the copolymer chains are covered. This chapter is submitted in *React. Chem. Eng.*

2.1 Introduction

Many industrial polymerizations are chain polymerizations. The core reaction types of chain polymerizations are initiation, propagation, and termination/elimination, as illustrated for free radical polymerization (FRP) in Figure 2.1.[1, 2] The reactive species can be a free radical as in FRP,[2] an ion as in anionic and cationic polymerization,[3, 4] or can be bound to a metallo-organic center as in coordination polymerization.[5] If the reactive species is a radical the tolerance towards impurities and water is high, reaction conditions are mild, and a wide range of monomers can be polymerized.[6] FRP is one of the polymerization technique which allows facile copolymerization,

i.e. a polymerization in which two or more monomers are polymerized together. The interesting feature of copolymer products is that they allow modifying the material properties of the corresponding homopolymers, allowing a wide range of property tuning in case the appropriate comonomer concentrations and reaction temperature are selected. Some notable examples of commercialized copolymers are poly(ethylene-vinyl acetate), linear low density polyethylene (LLDPE), poly(methyl methacrylate – butyl acrylate), poly(styrene-butadiene), poly(styrene-acrylonitrile), and poly(acrylonitrile-butadiene-styrene).[1, 7, 8]

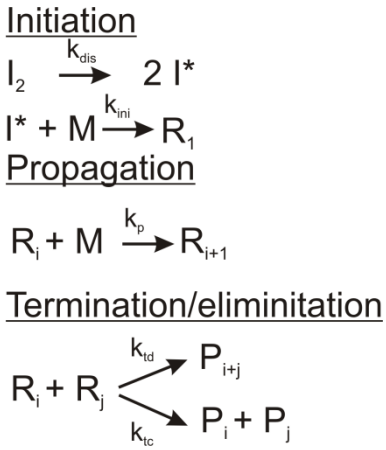

Figure 2.1. *Principle of basic chain polymerization illustrated for free radical polymerization; dis, ini, p, td, tc: dissociation, initiation, propagation, termination via disproportionation and termination via recombination; I_2: conventional radical initiator, R: radical species, P: dead polymer species; i,j = chain length.*

Due to the stochastic nature of chain growth polymerizations, the formed macrospecies are distributed with respect to their chain length (*e.g.* 1 to 10^5) and, in the case of copolymerization, with respect to their copolymer composition (*e.g.* 0 to 100% of comonomer 1). Moreover, these macrospecies can be branched with the type and locations of the branches as additional variables. In general, the composition and topology of every chain can thus be different. A control of the time evolution of the microstructure of these many polymer chains is crucial as their

intermolecular interaction determines the processability and properties of the final polymer product.[9] A detailed polymer characterization during synthesis is thus needed but the identification of multiple compositional and topological microstructural distributions is experimentally and computationally very demanding. Historically, main focus has therefore been on the role of propagation reactions as they are the main contributor to a variation in polymerization rate and control over polymer properties.[7, 10-14]

Several analytical models have been derived to calculate mostly instantaneous copolymer characteristics. Common in these models is the pseudo-steady state approximation (PSSA) for the calculation of the active macrospecies concentrations, which states that the temporal changes of these reactive species are assumed much smaller than the other species. To avoid the disturbance by other rate coefficients, the chain initiation and termination rates are assumed to be also balanced. In order to limit the number of propagation rate coefficients needed, it is further assumed that remote substituents, further away than a certain number of monomer units from the reactive center, have no effect on the propagation reactivity. Most often this number is assumed to be one or two. These (reactivity) models are referred to as terminal (first order Markov chains) and penultimate (second order Markov chains) models.[15-17] In rare cases and outside the scope of this work, the number is three and the associated model is denoted an ante-penultimate or pen-penultimate (third order Markov chains) model.[18, 19] Several research groups have also extended the analytical models if additional phenomena (*e.g.* depropagation and reversible radical deactivation polymerization) can take place.[20-24]

In a terminal description of the propagation rate coefficients, only the last monomer unit of the active macrospecies is considered and thus 4 distinct propagation rate coefficients result for a copolymerization involving two comonomers. Based on the 4 propagation rate coefficients, two

monomer (propagation) reactivity ratios are typically defined: $r_1 = k_{p,11}/k_{p,12}$ and $r_2 = k_{p,22}/k_{p,21}$ (first subscript: terminal unit of active macrospecies, second subscript: monomer type). Hence, upon knowing the homo-propagation rate coefficients the cross-propagation rate coefficients follow from these reactivity ratios. In case a penultimate description is considered eight propagation steps can be distinguished. This leads to 4 monomer reactivity ratios ($r_1 = k_{p,111}/k_{p,112}$, $r_2 = k_{p,222}/k_{p,221}$, $r_1' = k_{p,211}/k_{p,212}$, and $r_2' = k_{p,122}/k_{p,121}$ (first two subscripts penultimate and terminal unit of active macrospecies, third subscript monomer type) and 2 so-called radical reactivity ratios ($s_1 = k_{p,211}/k_{p,111}$ and $s_2 = k_{p,122}/k_{p,222}$), for which in contrast to a monomer reactivity ratio the radical type is varied and the monomer fixed.[22] A simplified so-called implicit penultimate model is obtained if the penultimate monomer unit (PMU) only influences the reactivity of the propagating radical and not the selectivity toward a monomer type.[25] This implies that $r_1 = r_1'$ and $r_2 = r_2'$. Monomer reactivity ratios can vary significantly. For example, monomer reactivity ratios near zero have been reported for alternating like copolymers (comonomers: styrene and maleic anhydride; $r_{1/2}$ = 0.00-0.02)[26] to rather high values (*e.g.* r_1 = 6.7 with r_2 = 0.02 for comonomers maleic anhydride and methyl methacrylate).[27] On the other hand, for radical reactivity ratios, a smaller range has been reported with values closer to unity (0.22-3.01).[28]

Reactivity ratios will appear in all analytical copolymerization models, as they determine to a large extent the microstructural arrangement of the monomer units within the copolymer. In general, it is accepted that terminal models can often not adequately describe the copolymerization kinetics and that penultimate models should be applied.[10, 29, 30] However, terminal models are still widely applied due to their simplicity and ease of use, in particular for process control.[10, 31] The most popular penultimate model is the implicit one.[10, 22] Although its

fundamental nature is questionable,[10, 29, 32, 33] it requires a limited number of parameters to be tuned while sharing features with the straightforward terminal model.

Determination of reactivity ratios is mostly done by regression analysis to analytical equations, using experimental data obtained from techniques for determination of the copolymer composition, such as nuclear magnetic resonance (NMR), infrared (IR) spectroscopy, or gas chromatography (GC).[7, 34, 35] Recently, matrix assisted laser desorption/ionization time-of-flight analyzer mass spectroscopy (MALDI-TOF MS) data have also been considered.[36] The advent of *ab initio* calculations lead in turn to the determination of reactivity ratios on a purely theoretical basis.[28, 37, 38] In addition, pulsed laser polymerization has been explored to study copolymerization parameters.[39-41]

Next to analytical models in the last decades also more advanced (kinetic) models have been developed that take into account more than the basic propagation reactions but also correct for possible side reactions and molecular diffusional limitations.[13, 14, 42-47] Both deterministic and stochastic modeling techniques have been developed which allow the simulation of copolymerization processes with different levels of microstructural detail and computational cost.[13, 14, 42, 44, 46, 48-51] The polymer microstructure can be described using average characteristics (*e.g.* number of average chain length or average copolymer composition) or using distributions with respect to a distinct number of microstructural variates of interest, such as chain length, branching degree, and (copolymer) composition.[46, 52-55] Most focus has been on univariate and bivariate deterministic models, although recently also more advanced stochastic models have been developed benefiting from the increased memory power of modern computers.[13, 43, 49, 55-58]

For models in which the number of microstructural variables is larger or equal than 2, leading to so-called multivariate models, and/or the number of reactions and the maximum chain length are

very high, a severe computational cost results. In such cases, so-called explicit modeling techniques are more recommended.[13, 42, 59-61] For example, Van Steenberge *et al.*[59] visualized monomer sequences of individual chains in controlled radical polymerization (CRP) or deactivation radical polymerization (RDRP), considering a detailed reaction scheme and diffusional limitations. The authors employed matrix-based kinetic Monte Carlo (*k*MC) simulations, starting from the basic Gillespie[62] algorithm and the theoretical developments of Szymanski,[63] and Wang and Broadbelt.[64] Any desired microstructural distribution, such as the chain length distribution (CLD) or the copolymer composition-CLD (CoC-CLD) describing the fraction of chains with a given length and fraction of a comonomer type, can be calculated *a posteriori*.[65, 66] Recently, Lemos and Pinto[60] applied this explicit modeling strategy for controlled polymerizations accounting for residence time distributions and D'hooge *et al.*[42] extended the matrix-based modeling strategy for CRPs with short chain branch formation (SCB). Not only the monomer sequences for the individual backbones but also the location and compositions of the SCBs could be visualized. Furthermore, Hernandez Ortiz *et al.*[67] applied the matrix-based *k*MC concept for polymer graft lengths.

In this contribution, an overview of the most important analytical and advanced models to obtain bulk/solution chain copolymerization characteristics is given, considering copolymerization with two comonomers unless stated otherwise. The text is organized according to the increase in desired modeled microstructural detail, starting with average polymer characteristics, over to uni- and multivariate descriptions, and ending with explicit kinetic modeling techniques. A further distinction is made between models for the calculation of the polymerization rate and the copolymer microstructure, focusing on linear polymers.

2.2 Basic models for average properties

The simplest copolymerization models describe a limited number of average properties as a function of the monomer feed composition (f_1; molar fraction of comonomer 1) and the propagation rate coefficients and/or reactivity ratios. Focus has been on (analytical) models for the calculation of the polymerization rate and average compositional properties.

2.2.1 Polymerization rate

The average propagation rate coefficient of a copolymerization $\langle k_p \rangle$, as defined with respect to the total radical and monomer concentration, is an important property of a copolymerization process as it allows to assess the time needed to polymerize a given monomer feed according to Equation (*2.1*) with M and R^* being the total monomer and radical concentration. The analytical formulas for $\langle k_p \rangle$ assuming a terminal and a penultimate polymerization model are given in Equation (2.2) and (2.3)-(2.5), respectively.[1, 43]

$$R_p = \langle k_p \rangle [M][R^*] \tag{2.1}$$

$$\langle k_p \rangle = \frac{r_1 {f_1}^2 + 2f_1(1-f_1) + r_2(1-f_1)^2}{r_1 f_1 / k_{p,11} + r_2(1-f_1)/k_{p,22}} \tag{2.2}$$

$$\langle k_p \rangle = \frac{\overline{r_1} {f_1}^2 + 2f_1(1-f_1) + \overline{r_2}(1-f_1)^2}{\overline{r_1} f_1 / \overline{k_{p,11}} + \overline{r_2}(1-f_1)/\overline{k_{p,22}}} \tag{2.3}$$

$$\overline{r_1} = \frac{r_1'(f_1 r_1 + (1-f_1))}{f_1 r_1' + (1-f_1)};\ \overline{r_2} = \frac{r_2'(f_1 + (1-f_1) r_2)}{f_1 + (1-f_1) r_2'} \tag{2.4}$$

$$\overline{k_{p,11}} = \frac{k_{p,111}(r_1 f_1 + (1-f_1))}{r_1 f_1 + {(1-f_1)}/{s_1}};\ \overline{k_{p,22}} = \frac{k_{p,222}(f_1 + r_2(1-f_1))}{r_2(1-f_1) + {f_1}/{s_2}} \tag{2.5}$$

Upon derivation of these formulas, the QSSA is applied to the macroradicals, *i.e.* it is assumed that the cross-propagation rates are balanced, and it is assumed that consumption of the monomer occurs only via propagation steps. For the terminal model, the monomer reactivity ratios appear in Equation (2.2) along with the two individual homo-propagation rate coefficients. Upon knowledge of the latter this equation thus allows to estimate the reactivity ratios or cross-propagation rate coefficients. For the penultimate model, a very similar equation is obtained as for the terminal model (Equation (2.3) vs. Equation (2.2)), although additional factors are needed that are a function of the additional monomer and radical reactivity ratios (r_i' and s_i; i=1,2) considered. For the special case in which the s values are unity the correction factors for the homopolymerization coefficients disappear (Equation (2.5)), and Equation (2.2) and (2.3) become even identical if also equal r and r' values are obtained (implicit PMU model). In general it can be expected that the $r^{(')}$ and s values do differ from unity and strong differences between penultimate and terminal model predictions can be established. The latter is theoretically illustrated in Figure 2.2 for a broad set of reactivity ratios, varying all reactivity ratios related to monomer type 1 one order of magnitude in both directions, with terminal reactivity results of unity as basic case (full red line in Figure 2.2). The other lines are perturbations on the reactivity ratios of this basic case, with a variation of r_1 (Figure 2.2 (a)), r_1' (Figure 2.2 (b)) and s_1 (Figure 2.2 (c)). In other words, in case PMU effects are sufficiently strong terminal descriptions inherently fail.

A weakness of the analytic models is that it is not straightforward to include an accurate time dependence. Either the f_1 temporal evolution needs to be known or kept constant through monomer addition. In that respect, any advanced kinetic model, either based on differential equations or the stochastic sampling of reaction events, always allows to calculate $\langle k_p \rangle$ a function

of f_1 and time and thus to obtain the copolymerization rate.[13, 14, 44] In particular, corrections for diffusional limitations can be made so that proper time dependencies can be simulated. For example, the apparent termination reactivity in radical polymerization is known to decrease significantly with increasing monomer conversions and viscosities.[68-71] A correction based on analytical expressions, typically with constant termination reactivities, is in this context too approximate and should be avoided.[70]

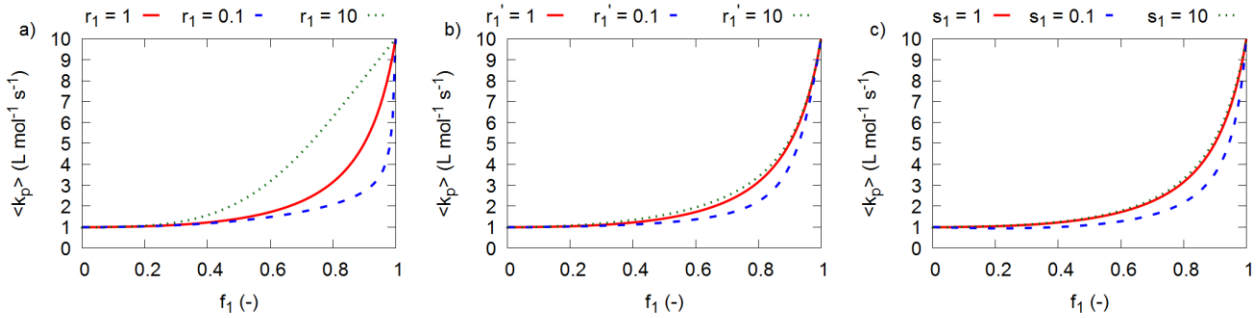

Figure 2.2. *Influence of PMU effect on the analytical average propagation rate coefficient <k_p> (Equation (2.2)- (2.5)) for $k_{p,111}$ = 10 L mol^{-1} s^{-1} and $k_{p,222}$ = 1 L mol^{-1} s^{-1} with $r_2 = r_2' = s_2 = 1$ and (a) $r_1 = 1$ (red full line; terminal reference case), $r_1 = 0.1$ (blue dashed line), $r_1 = 10$ (green dotted line), (b) $r_1' = 1$ (red full line), $r_1' = 0.1$ (blue dashed line), $r_1' = 10$ (green dotted line), and (c) $s_1 = 1$ (red full line), $s_1 = 0.1$ (blue dashed line), $s_1 = 10$ (green dotted line).*

2.2.2 Compositional and microstructural properties

The two most popular average compositional properties of copolymers are the instantaneous copolymer composition ($F_{1,inst}$) and the instantaneous average segment length of comonomer type 1 ($\overline{l_{1,inst,}}$). The former describes the average fraction of one comonomer type incorporated over all active chains. The latter is the average length of the segment of comonomer type 1, whereby a segment is defined as a sequence of comonomers of the same type. The cumulative properties are denoted without the subscript "inst".

Instantaneous copolymer composition

The so-called Mayo-Lewis model is the key calculation method for $F_{1,inst}$ and is given for a terminal copolymerization model by Equation (2.6).[16] Note that $F_{1,inst}$ does not depend on the individual absolute propagation rate coefficients but only on the monomer reactivity ratios. The equation for a penultimate copolymerization model is given in Equation (2.7) and as for $\langle k_p \rangle$ additional factors with respect to the terminal model are introduced.[17] Also here, only the monomer reactivity ratios are appearing, which implies that the radical reactivity ratios have no overall impact on the copolymer composition. Under the assumption that $r_{1/2} = r'_{1/2}$ or thus for an implicit PMU model, Equation (2.7) reduces to Equation (2.6). The impact of the penultimate parameters is in this case thus only present in $\langle k_p \rangle$ (Equation (2.2)-(2.3)) and not in $F_{1,inst}$.

$$F_{1,inst} = \frac{r_1 f_1^{\,2} + f_1 f_2}{r_1 f_1^{\,2} + 2 f_1 f_2 + r_2 f_2^{\,2}} \tag{2.6}$$

$$F_{1,inst} = \frac{r_1' \frac{1 + r_1 x}{1 + r_1' x} f_1^{\,2} + f_1 f_2}{r_1' \frac{1 + r_1 x}{1 + r_1' x} f_1^{\,2} + 2 f_1 f_2 + r_2' \frac{1 + r_2 \frac{1}{x}}{1 + r_2' \frac{1}{x}} f_2^{\,2}}; x = \frac{f_1}{f_2} \tag{2.7}$$

Note that under batch conditions compositional drift is obtained as $F_{1,inst}$ will continuously vary as f_1 alters. Hence, for the experimental determination of (f_1, $F_{1,inst}$) pairs in view of regression analysis to Equation (2.6)-(2.7) low monomer conversion data (*e.g.* up to 5 mol%) can only be used so that f_1 can be still seen as relatively constant. $F_{1,inst}$ is either determined directly using for example infrared, ultraviolet (UV[1]), or NMR spectroscopy[35] but can also be determined indirectly by analyzing the temporal evolution of the comonomer feed composition (f_1) using for example high-pressure liquid chromatography (HPLC) or GC.[34, 35] Several approximate methods, such as the Fineman-Ross[72] and Kelen-Tudos[73] method, which are graphical methods relying on the

linearization of Equation (2.6), have been developed to facilitate the fitting procedure for terminal models. For such linear models, analytical solutions for the linear regression problem are available. However, the most statistically sound method is conventional non-linear regression to the original non-linearized equations.[74]

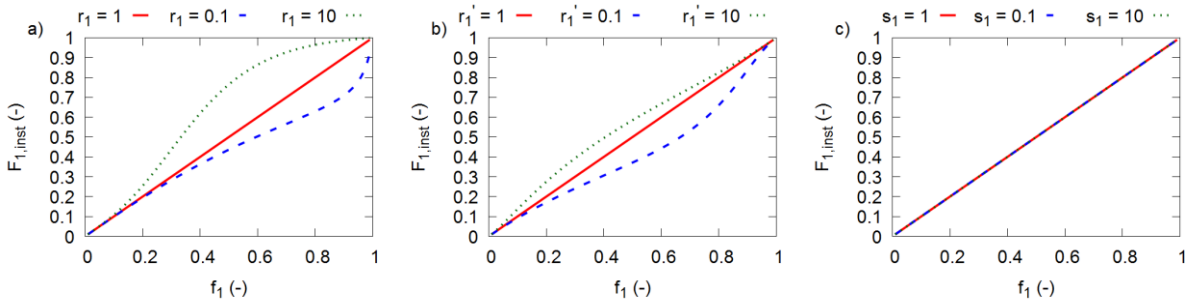

Figure 2.3. *Influence of PMU kinetics on the prediction of the instantaneous copolymer composition ($F_{1,inst}$; Equation (2.6)-(2.7)) for k_{p111} = 10 L mol^{-1} s^{-1} and k_{p222} = 1 L mol^{-1} s^{-1} with $r_2 = r_2' = s_2 = 1$ and (a) $r_1 = 1$ (red full line; terminal reference case), $r_1 = 0.1$ (blue dashed line), $r_1 = 10$ (green dotted line), (b) $r_1' = 1$ (red full line), $r_1' = 0.1$ (blue dashed line), $r_1' = 10$ (green dotted line), and (c) $s_1 = 1$ (red full line), $s_1 = 0.1$ (blue dashed line), $s_1 = 10$ (green dotted line).*

Figure 2.3 illustrates that in general a terminal and penultimate description of $F_{1,inst}$ are significantly different, considering the same range of reactivity ratios as for Figure 2.2 (basic case again red line in subplot (a)). Note that the *s* values (Figure 2.3(c)) have no effect they are not relevant. Importantly, the simulation results in these figures should in practice be interpreted along with the corresponding $\langle k_p \rangle$ descriptions (Equation (2.2)-(2.5)). For example, for the styrene and methyl methacrylate comonomer pair, a simultaneous fit of both the average propagation rate and (instantaneous) copolymer composition data under FRP conditions cannot be achieved using the terminal model, whereas a penultimate model allows an adequate fit.[25] Earlier studies most often considered the average copolymerization data only and the associated kinetic parameters must thus be treated with care. Currently, a large number of monomer pairs,

including next to styrene-methyl methacrylate,[25] the pairs styrene – butyl methacrylate,[75] styrene – butyl acrylate,[76] methyl methacrylate – vinyl acetate,[77] and many others,[10] have been critically tested against both average propagation rate and copolymer composition data. This testing indicates that the terminal model results in failure for most comonomer pairs. Notably this testing is typically done at one polymerization temperature and for simplicity temperature dependencies are therefore often ignored for reactivity ratios.[78]

An important consequence of the shape of Equation (2.6) and (2.7) is that f_1 is not necessarily the same as $F_{1,inst}$. Three limiting cases – assuming a terminal model - are typically used to discuss different types of copolymerization behavior in view of boundaries for the propagation reactivity ratios (r_1r_2 =1; << 1; and >> 1). The copolymerization in which the product r_1r_2 is unity (case 1) is referred to as an ideal copolymerization and by definition the terminal unit has no impact on the propagation preference ($k_{p,11}/k_{p,12}=k_{p,21}/k_{p,22}$). In the special situation that r_1 = 1 the comonomers show no preference towards one of the active macrospecies and thus $F_{1,inst}$ is always equal to f_1. This behavior is also referred to as random or Bernoullian.[79] If r_1 is larger/smaller than unity (still r_1r_2=1), monomer 1 is more/less involved in propagation. These different possibilities for case 1 are further illustrated in Figure 2.4 (a). The copolymerization behavior in which both r_1 and r_2 are smaller than one (case 2) is referred to as alternating copolymerization, as an active macrospecies will preferentially add a comonomer of a different type, *i.e.* cross-propagation is favored (ignoring concentration effects). A well-known alternating monomer pair is styrene and maleic anhydride.[26] As shown in Figure 2.4(b) the nature of the alternating behavior changes, depending on the value of both reactivity ratios, with a maximal *r* value of 1 for one of the two. For a copolymerization with both reactivity ratios much greater than unity (case 3), there is a tendency to form block copolymer segments as an active macrospecies will preferentially react

with the comonomer which relates to its terminal unit. Figure 2.4 (c) shows that also here the absolute values matter for the intensity of this block copolymer segment formation.

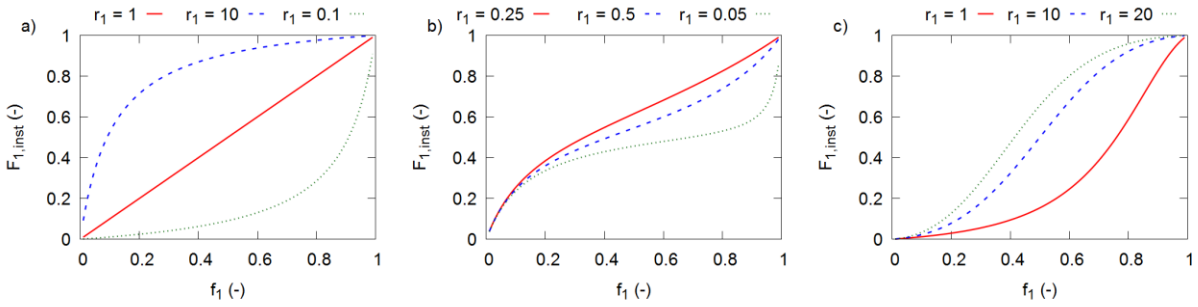

Figure 2.4. *Instantaneous copolymer composition of monomer 1 ($F_{1,inst}$; Equation (2.6)) as a function of the comonomer 1 feed fraction (f_1; molar) for (a) an ideal ($r_1r_2 = 1$; $r_1 = 1$ (red), $r_1 = 10$ (blue), $r_1 = 0.1$ (green)), and (b) an alternating ($r_2 = 0.25$; $r_1 = 1$ (red), $r_1 = 0.5$ (blue), $r_1 = 0.05$ (green)), and (c) an block like copolymerization ($r_2 = 10$; $r_1 = 1$ (red), $r_1 = 10$ (blue), $r_1 = 20$ (green)).*

The feed compositions that do lead to equal $F_{1,inst}$ and f_1 are called in analogy with distillation azeotropic points. They can be identified as intersections with the bisectors in Figure 2.4. For example, for a terminal model, the azeotropic point is given by Equation (2.8) (both reactivity ratios different from 1):

$$f_1 = \frac{1 - r_2}{2 - r_1 - r_2} \tag{2.8}$$

Analogously as for $\langle k_p \rangle$, advanced kinetic models allow to calculate the temporal evolution of $F_{1,inst}$ and f_1. A small compositional drift for the industrial copolymerization process can already lead to off-spec material, highlighting the relevance of these time based models.[6, 59] Only by adding comonomer(s), *i.e.* applying a semi-batch procedure, the monomer feed composition can be kept constant (not considering the azeotropic point) and thus also the average copolymer composition is constant.

Instantaneous segment length

The instantaneous copolymer composition characterizes the average fraction of comonomer units of a given type in the copolymer chains but does not yield information on the average connectivity of the comonomer units. This connectivity is for instance an important property for block- and gradient copolymers and can be characterized by the average instantaneous segment lengths ($\overline{l_{1,inst}}$ and $\overline{l_{2,inst}}$).[65]

Analytical expressions for terminal propagation reactivities have been derived and are given in Equation (2.9)-(2.10):[17]

$$\overline{l_{1,inst}} = 1 + \left(r_1 \frac{f_1}{f_2}\right) \tag{2.9}$$

$$\overline{l_{2,inst}} = 1 + \left(r_2 \frac{f_2}{f_1}\right) \tag{2.10}$$

The underlying assumption is that cross-propagation determines if an existing segment ends and a new segment begins. Hence, this model for the instantaneous average segment length depends only on the monomer reactivity and the monomer feed compositions. Experimental determination of the average segment length is difficult but has been attempted using UV-vis analysis up to relatively short segment lengths (< 5).[80]

For a penultimate model, Equation (2.9)-(2.10) are modified into:

$$\overline{l_{1,inst}} = 1 + \frac{r_1' x}{1 + r_1' x} \Big/ \left(1 - \frac{r_1 x}{1 + r_1 x}\right) \tag{2.11}$$

$$\overline{l_{2,inst}} = 1 + \frac{r_2' x^{-1}}{1 + r_2' x^{-1}} \Big/ \left(1 - \frac{r_2 x^{-1}}{1 + r_2 x^{-1}}\right) \tag{2.12}$$

Figure 2.5 highlights the effect of PMU effects for the calculation of the instantaneous average segment lengths by comparing terminal and penultimate model results again for the reactivity ratios considered in Figure 2.2 and Figure 2.3 (basic case of terminal model is the red line). As for Figure 2 no effect of an *s* variation is observed.

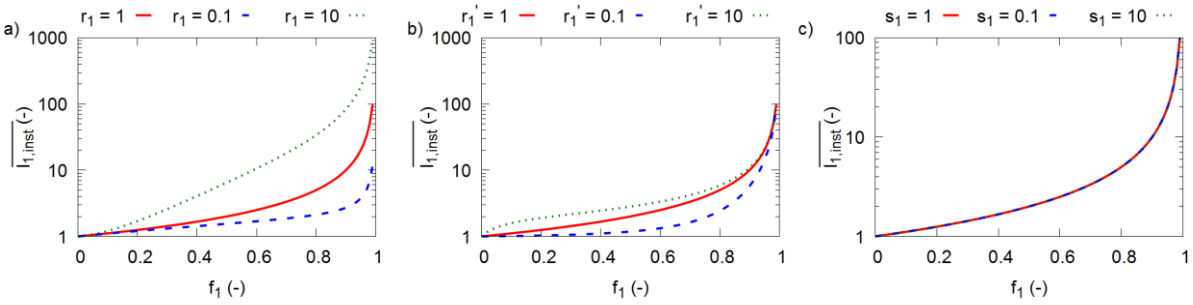

Figure 2.5. *Influence of PMU on the prediction of the average instantaneous segment length ($\overline{l_{1,inst}}$; Equation (2.9)-(2.12)) for k_{p111} = 10 L mol^{-1} s^{-1} and k_{p222} = 1 L mol^{-1} s^{-1} with $r_2 = r_2' = s_2 = 1$ and (a) $r_1 = 1$ (red full line; terminal reference case), $r_1 = 0.1$ (blue dashed line), $r_1 = 10$ (green dotted line), (b) $r_1' = 1$ (red full line), $r_1' = 0.1$ (blue dashed line), $r_1' = 10$ (green dotted line), and (c) $s_1 = 1$ (red full line), $s_1 = 0.1$ (blue dashed line), $s_1 = 10$ (green dotted line).*

Several advanced modeling studies have also focused on segment formation in copolymers.[43, 49, 52, 81] For example, Wang *et al.* developed a *k*MC model for nitroxide mediated polymerization (NMP) in which the segment formation is tracked throughout the simulation, resulting in data not only on average segment length but also on the (instantaneous) segment length distribution.[64, 81, 82] Van Steenberge *et al.* [59] developed a matrix-based *k*MC method allowing explicit tracking of the monomer incorporation of all macrospecies in atom transfer radical polymerization (ATRP). Post-processing allows the calculation of derived properties such as the instantaneous average segment length.

Cumulative copolymer composition

In order to describe the cumulative copolymer composition F_1, Skeist *et al.*[83] introduced an equation which is based on the differential material balance for comonomer 1 (Equation (2.13)) and in which $[M]_{(0)}$ is the total (initial) monomer concentration. This equation can be rearranged into its integral form (Equation (2.14)) with X_m the (overall) monomer conversion, so of both comonomers together. For the terminal model, this integral can be calculated analytically after substituting the Mayo-Lewis equation (Equation ((2.6))), which yields the so-called Meyer-Lowry equation (Equation (2.15)). Further rearrangement leads to the form with the cumulative copolymer composition F_1 explicitly appearing (Equation (2.16)).[84]

$$[M]\, f_1 - ([M] - \mathrm{d}[M])(f_1 - \mathrm{d}f_1) = F_1 \mathrm{d}[M] \tag{2.13}$$

$$\int_{[M]_0}^{[M]} \frac{d[M]}{[M]} = \ln \frac{[M]}{[M]_0} = \int_{f_{1,0}}^{f_1} \frac{df_1}{(F_1 - f_1)} \tag{2.14}$$

$$X_M = 1 - \frac{[M]}{[M]_0} = 1 - \left(\frac{f_1}{f_1^0}\right)^{\alpha} \left(\frac{f_2}{f_2^0}\right)^{\beta} \left(\frac{f_1^0 - \delta}{f_1 - \delta}\right)^{\gamma} \text{ with}$$
$$\alpha = \frac{r_2}{1 - r_2}; \beta = \frac{r_1}{1 - r_1}; \gamma = \frac{1 - r_1}{1 - r_2}; \delta = \frac{1 - r_2}{2 - r_1 - r_2} \tag{2.15}$$

$$1 - X_M = 1 - \left(\frac{f_1^0 - F_1 X_M}{f_1^0 (1 - X_M)}\right)^{\alpha} \left(\frac{1 - X_M - f_1^0 - F_1 X_M}{(1 - f_1^0)(1 - X_M)}\right)^{\beta} \left(\frac{(\delta - f_1^0)(1 - X_M)}{\delta - \delta X_M - f_1^0 + F_1 X_M}\right)^{\gamma} \tag{2.16}$$

The use of the integral form of the copolymer equation along with the equation for $\langle k_p \rangle$ is advised for the experimental determination of reactivity ratios, as it takes into account the change in the comonomer feed and does not limit the experiments to low monomer conversions. Care should although be taken by not increasing a threshold monomer conversion as at one point diffusional limitations can affect the validity of the derivations behind Equation (1.15).[13, 85] The

use of non-linear regression is again recommended, providing a quantification of the error in meaningful terms.[86, 87]

2.3 Extended models for average properties

An important question that arises is whether the above covered basic (analytical) models for the calculation of the average propagation rate and composition, which purely focus on propagation reactions, can also be easily extended for more detailed reaction schemes involving side reactions. In what follows, the most notable extensions are briefly discussed, with a main focus on the average polymerization rate and copolymer composition.

2.3.1 Reversible deactivation

With the advent of RDRP techniques during the past decades, it has been wondered whether the additional activation-deactivation reactions for macroradicals result in deviations from the copolymerization models derived for conventional chain growth/FRP kinetics (Equation (2.2)-(2.7)).

For example, for RDRPs based on the so-called persistent radical effect such as NMP and ATRP,[88-90] it has been indicated that $\langle k_p \rangle$ can be affected, as deactivation reactions lower the radical concentrations. The latter was theoretically explored by Charleux *et al.*[20] for NMP of methyl methacrylate and styrene, considering a terminal activation/deactivation model combined with a terminal propagation model (Equation (2.17)-(2.18)) and an implicit penultimate propagation model (Equation(2.19)-(2.20)):

$$\langle k_p \rangle \langle K \rangle = \frac{r_1 {f_1}^2 + 2 f_1 f_2 + r_2 {f_2}^2}{\frac{r_1 f_1}{k_{p,11} K_1} + \frac{r_2 f_2}{k_{p,22} K_2}} \qquad (2.17)$$

$$\langle K \rangle = \frac{\frac{r_1 f_1}{k_{p,11}} + \frac{r_2 f_2}{k_{p,22}}}{\frac{r_1 f_1}{k_{p,11} K_1} + \frac{r_2 f_2}{k_{p,22} K_2}} \tag{2.18}$$

$$\langle K \rangle = \frac{\frac{r_1 f_1}{\overline{k_{p,11}}} + \frac{r_2 f_2}{\overline{k_{p,22}}}}{\frac{r_1 f_1}{\overline{k_{p,11}} K_1} + \frac{r_2 f_2}{\overline{k_{p,22}} K_2}} \tag{2.19}$$

$$\langle k_p \rangle \langle K \rangle = \frac{r_1 {f_1}^2 + 2 f_1 f_2 + r_2 {f_2}^2}{\frac{r_1 f_1}{\overline{k_{p,11}} K_{eq,1}} + \frac{r_2 f_2}{\overline{k_{p,22}} K_{eq,2}}} \tag{2.20}$$

In these equations, $\langle K \rangle$ is an average equilibrium coefficient which is not only dependent on the individual equilibrium coefficients of both monomers types but also on the cross-propagation rate coefficients and the comonomer feed composition (f_1).

For the instantaneous average copolymer composition, early work by Matyjaszewski[91] and more recent work by Zapata-González *et al.* [92] indicated limited deviations from the FRP equations, mainly at lower monomer conversions and reaction times in agreement with results of Klumperman *et al.*[93] These deviations originate from a slower establishment of the balancing of the cross-propagation rates. When these are not balanced the PSSA is invalid and thus the classical FRP equations (Equation (2.6)-(2.7)) cannot be applied. However, once the PSSA can be applied the same ratios for the radical concentrations are obtained and the above formulated equations can be still used.

2.3.2 Depropagation at elevated temperatures

Depropagation is a well-known phenomenon which becomes important when a (co)monomer is (co)polymerized near or above the ceiling temperature.[1] For most comonomers this ceiling temperature is well above the reaction temperature but some comonomers such as α-methyl

styrene suffer from depropagation under typical copolymerization conditions. To account for depropagation the basic model needs to be extended as it influences the concentrations of the macrospecies.[21]

Several models for the instantaneous copolymer composition based on terminal propagation kinetics have been proposed in literature each one differing in their assumptions with respect to the ability of the different monomers to undergo depropagation. Most notable are the Kruger,[94] Wittmer,[95] and the three Lowry models.[96] Based on the latter model, an expression for $<k_p>$ has been derived by Kukulj *et al.*[97] in which terminal propagation kinetics are considered and it is assumed that only one monomer is near its ceiling temperature and depropagation occurs only if it is attached to a monomer of the same type.

2.3.3 Multicomponent copolymerization

In industry, also copolymerizations with more than two comonomers, *i.e.* so-called multicomponent copolymerizations, are conducted. For example, the ternary copolymerization of 2-acrylamido-2-methylpropane sulfonic acid, acrylamide and acrylic acid has been extensively studied.[85, 98, 99]

The developed models for these multicomponent copolymerizations rely on the knowledge of the underlying binary copolymerizations. For example, for a terminal model, the so-called Alfrey-Goldfinger equation (Equation (2.21)) has been developed for the relative instantaneous copolymer composition which can be solved knowing that $F_1+F_2+F_3 = 1$.[100] A more general analytical model (N monomers) has been formulated by Walling and Briggs.[101] For the equation for the penultimate model, the reader is referred to the work of Ham *et al.*[102]

$$F_1 : F_2 : F_3 = f_1 \left(\frac{f_1}{r_{31} r_{21}} + \frac{f_2}{r_{21} r_{32}} + \frac{f_3}{r_{31} r_{23}} \right) \times \left(f_1 + \frac{f_2}{r_{12}} + \frac{f_3}{r_{13}} \right) : \qquad (2.21)$$

$$f_2\left(\frac{f_1}{r_{12}r_{31}}+\frac{f_2}{r_{12}r_{13}}+\frac{f_3}{r_{32}r_{13}}\right)\times\left(\frac{f_1}{r_{21}}+f_2+\frac{f_3}{r_{23}}\right):$$

$$f_3\left(\frac{f_1}{r_{31}r_{21}}+\frac{f_2}{r_{23}r_{12}}+\frac{f_3}{r_{13}r_{23}}\right)\times\left(\frac{f_1}{r_{31}}+\frac{f_2}{r_{32}}+f_3\right)$$

2.4 Models based on univariate distributions

Basic copolymerization models, as covered above, allow a quick assessment of the average kinetic and microstructural properties for reaction schemes consisting mainly of propagation reactions. However, these averages are a simplified representation of a distributed polymer property, *e.g.* the chemical composition of the polymer chains and can be specifically biased in case multimodalities are present. A biased interpretation can also result due to the omittance of side reactions and/or diffusional limitations that significantly alter the microstructural distributions, such as the CLD and CoC-CLD.[54, 59, 103]

In view of the previous statements attention has been paid to both analytical and advanced models that do include complete microstructural distributions. In the most simple case the focus is restricted to one distribution and a so-called univariate model is constructed. The most important univariate models are discussed in this section, again differentiating between the polymerization rate and copolymer compositional properties.

2.4.1 Polymerization rate

The basic univariate distribution is the CLD. Important mathematical techniques to calculate this distribution are for instance the fixed pivot technique,[13, 55, 104] the extended method of moments,[105, 106] the probability generation function method,[107] advanced PSSA-based methods which allow to resolve CLDs,[56, 108] the Galerkin method,[109, 110] and the *k*MC technique.[49, 59]

Since polymerization reactions can be characterized by chain length dependency the shape and range of the CLD can affect the (co)polymerization kinetics and in particular the polymerization rate.[69, 111-113] In line with the discussion on the relevance of more advanced models for the calculation of average properties focus is again on the (apparent) termination reactivity in radical polymerization. Depending on the monomer type less mobile/longer chains can be created that affect the intensity of the gel-effect and thus the impact of diffusional limitations on termination in view of the calculation of the polymerization rate. Different time evolutions of the polymerization rate can thus be obtained for similar reactivity ratios in case the chain length dependencies for the diffusivity of the active macrospecies are different, *i.e.* average apparent termination rate coefficients that affect the radical concentrations need to explicitly account for the CLD shape.[112]

2.4.2 Compositional and microstructural properties

Using the basic models, the (instantaneous) average segment length can be calculated analytically (Equation (2.9)-(2.12)). However, segments are distributed with respect to their length, leading to a so-called (instantaneous) segment length distribution (SLD), *e.g.* $(l_{i,inst})_k$ for discrete lengths starting at unity and focusing on comonomer *i*. Quantifying this (number) distribution is important as it determines the properties of the final polymer product. For example, if a "hard" and "soft" monomer type are employed (*e.g.* styrene and butadiene), the final mechanical properties depend strongly on the micro-arrangement of the separate segments.[114-116]

The SLD can be obtained by noting that cross-propagations lead to the formation of segments. A segment of length *k* consisting of units of for instance comonomer 1, $(l_{1,inst})_k$, is formed by *k*-1 homopropagations of an active species, followed by a single cross-propagation. Introducing the terminal probabilities for homopropagation and cross-propagation (p_{11} and p_{12}):[1]

$$p_{11} = \frac{k_{p11}M_1}{k_{p11}M_1 + k_{p12}M_2} = \frac{r_1 f_1}{r_1 f_1 + f_2}; p_{12} = 1 - p_{11} \quad (2.22)$$

$(l_{1,inst})_k$ can be expressed as:

$$\left(l_{1,inst}\right)_k = {p_{11}}^{k-1} p_{12} \quad (2.23)$$

Note that, due to the power law shape of Equation (2.23) with probabilities lower than 1, the most likely segment always has a length of 1, irrespective of the monomer reactivity ratio and feed composition. It has been verified that the average of the distribution in Equation (2.23) is $1/p_{12}$, which is the result reported with the basic model (Equation (2.9)).[43] Hence, if the probability for cross-propagation is 0.2, then the average segment length is 5. The results for comonomer 2 are obtained by altering the subscripts 1 and 2.

Furthermore, following the concept behind Equation (1.22) penultimate probabilities can be combined, leading to following equations:[117]

$$p_{111} = \frac{r_1 f_1}{r_1 f_1 + f_2}; p_{112} = 1 - p_{111}; p_{211} = \frac{r_1' f_1}{r_1' f_1 + f_2}; p_{212} = 1 - p_{211} \quad (2.24)$$

$$\begin{gathered} \left(l_{1,inst}\right)_1 = 1 - p_{211} \\ \left(l_{1,inst}\right)_k = p_{211}(p_{111})^{k-2}(1 - p_{111}) \; for \; k > 1 \end{gathered} \quad (2.25)$$

The SLD results (comonomer 1) for three special cases - at an equimolar monomer feed composition - are given in Figure 2.6 (terminal reactivity model). Case 1 is an ideal copolymerization in which $r_1 = r_2 = 1$ (blue bars), meaning that all propagation steps have the same probability, accounting for the selected feed composition. A SLD is obtained in which sequences of length 1 have a number fraction of 0.5 but also longer segments are still present. For the case with $r_1 = 5$ and $r_2 = 0.2$ both radical types preferentially add comonomer 1 instead of 2 with a factor of 5. From Figure 2.6 (yellow bars) it can be seen that such conditions lead to a shift

towards higher segment lengths of comonomer 1 and a much broader distribution. Finally, a third case with r_1 = 0.1 and r_2 = 0.1, *i.e.* an alternating polymerization, is shown (purple bars). As expected a number fraction of 0.9 has a length of 1.

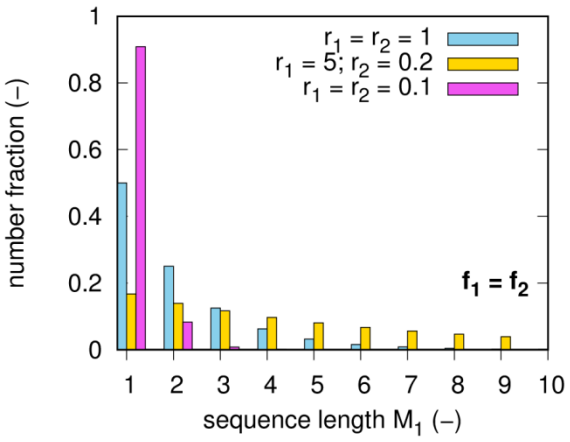

Figure 2.6. *Effect of monomer reactivity ratios on the instantaneous segment length distribution for comonomer 1, according to Equation (2.23) (terminal reactivity model). Focus restricted to equimolar feed composition.*

Experimental measurement of the SLD has been performed for a number of copolymer pairs (*e.g.* acrylonitrile and vinylidene chloride) mainly using high-resolution NMR (mostly ^{13}C NMR).[118] Based on these experiments, reactivity ratios have been determined due to the simplicity of *e.g.* Equation (2.22)-(2.25).[119] SLDs have also been accessed using Galerkin[52] and *k*MC modeling[65, 81] and this for more complex reaction schemes than covered with the analytical models capturing also effects related to for instance chain transfer, recombination, and (de)activation. In particular, Wang *et al.*[81] investigated the influence of RDRP conditions, in case of styrene/MMA gradient copolymers, on the segment formation compared with classical FRP. These authors conclude that segment formation is influenced by the temporary deactivation by RDRP mediating species (*e.g.* nitroxides) as they consider this to stop the instantaneous segment growth. However, it can be argued that deactivation only temporarily pauses the segment formation rather than stopping it.

Shi *et al.*[120] did not consider the temporary deactivation to halt the segment length formation. These authors concluded that under quasi-steady state conditions and, hence, at sufficiently long polymerization times, RDRP leads to identical instantaneous SLDs as FRP.

It should be further noted that the SLD focuses on segments considering the monomer type fixed, *i.e.* either comonomer 1 or 2 is focused on and the contributions of each segment length are specified. Often the reverse situation is of interest in which the sequence length is fixed at a low value (*e.g.* 2 or 3) and the univariate model allows to predict the distribution of the various monomer sequences of that number of monomer units. Mostly the length is fixed at 3, leading to so- called triads. Four triads can be defined for monomer type 1 as central monomer, *i.e.* 111, 212, 112, and 211, and their fractions ($F_{i,j,k,(inst)}$) define a (univariate) instantaneous distribution. These distributions are called monomer sequence type distributions (MSTDs).

For the instantaneous distribution, Equation (2.26) and (2.27) give the analytical expression for the terminal and penultimate model,[121] with Figure 2.7 highlighting some differences for again the reactivity ratios considered before (red line in left column each time basic terminal case). Again, also the *s* values do not matter (right column in Figure 2.7). Experimentally, the MSTD for a sequence length 3 is mostly derived from the spectral intensities of either ^{1}H or ^{13}C NMR spectroscopy measurements.[79]

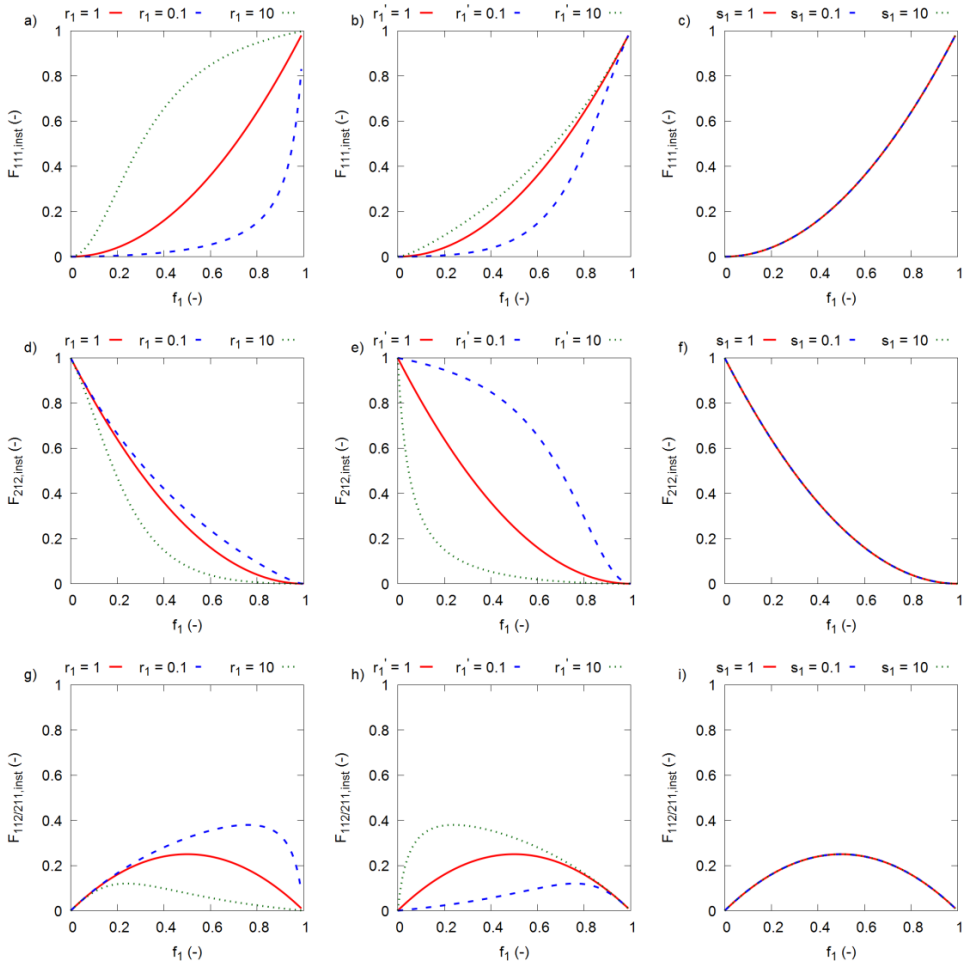

Figure 2.7. *Influence of PMU on the prediction of the instantaneous triad formation (Equations (2.26)-(2.27)) ((a-c) = 111, (d-f) = 212, (g-i) = 112/211) with* $r_2 = r_2' = s_2 = 1$ *and (a-d-g; terminal reference case)* $r_1 = 1$ *(red full line),* $r_1 = 0.1$ *(blue dashed line),* $r_1 = 10$ *(green dotted line), (b-e-h)* $r_1' = 1$ *(red full line),* $r_1' = 0.1$ *(blue dashed line),* $r_1' = 10$ *(green dotted line), and (c-f-i)* $s_1 = 1$ *(red full line),* $s_1 = 0.1$ *(blue dashed line),* $s_1 = 10$ *(green dotted line).*

$$F_{111,inst} = \frac{{r_1}^2 \left(\frac{f_1}{f_2}\right)^2}{1 + 2r_1 \frac{f_1}{f_2} + {r_1}^2 \left(\frac{f_1}{f_2}\right)^2}; F_{212,inst} = \frac{1}{1 + 2r_1 \frac{f_1}{f_2} + {r_1}^2 \left(\frac{f_1}{f_2}\right)^2}; \quad (2.26)$$

$$F_{112/211,inst} = \frac{r_1 \frac{f_1}{f_2}}{1 + 2r_1 \frac{f_1}{f_2} + {r_1}^2 \left(\frac{f_1}{f_2}\right)^2}$$

$$F_{111,inst} = \frac{r_1 {r_1}' \left(\frac{f_1}{f_2}\right)^2}{1 + 2{r_1}' \frac{f_1}{f_2} + r_1 {r_1}' \left(\frac{f_1}{f_2}\right)^2}; F_{212,inst} = \frac{1}{1 + 2{r_1}' \frac{f_1}{f_2} + r_1 {r_1}' \left(\frac{f_1}{f_2}\right)^2}; \quad (2.27)$$

$$F_{112/211,inst} = \frac{{r_1}' \frac{f_1}{f_2}}{1 + 2{r_1}' \frac{f_1}{f_2} + r_1 {r_1}' \left(\frac{f_1}{f_2}\right)^2}$$

2.5 Models based on multivariate distributions

As the degree of microstructural detail and complexity increases from univariate to multivariate, it is not surprising that less experimental and modeling copolymerization kinetics studies have been reported that focused on several variates. Most experimental reports relate to the measurement of (relative) bivariate distributions with respect to chain length and copolymer composition, *i.e.* Co-CLDs.[122-125] Certain analytical efforts are notable of which the most paramount one is the derivation of the so-called Stockmayer equation.[126]

Other analytical derivations for bivariate and for sure multivariate distributions are scarce and non-trivial and therefore advanced modeling needs to be performed by default in order to obtain information on these multivariate distributions. Both stochastic and deterministic methods have been used to calculate, for example, functional group - chain length,[127] segment length - chain length, and[128] long-chain branching - chain length distributions.[53]

2.5.1 Polymerization rate

For an accurate representation of the polymerization rate, a univariate calculation suffices provided that CLDs are calculated for every macrospecies type, correctly selecting either a terminal or penultimate reactivity model. The superposition of the individual CLDs becomes then the observed or measurable CLD. Hence, if the goal is only the calculation of the polymerization rate it is not worthwhile to increase the model complexity. Multivariate models are therefore only relevant in case compositional distributions are also of interest.

2.5.2 Compositional and microstructural properties

The best known bivariate distribution is the Stockmayer equation that describes the instantaneous mass CoC-CLD for a basic chain polymerization (see Figure 2.1) in which growth is stopped by disproportionation or elimination (in coordination polymerization of olefins), and terminal reactivities and identical molar masses of the comonomers are assumed:[126]

$$f_{m,inst}(n,\gamma) = \left(\frac{n}{{x_n}^2}\exp\left(-\frac{n}{x_n}\right)\right)\frac{1}{\sigma\sqrt{2\pi}}\exp\left(-\frac{\gamma^2}{2\sigma^2}\right) \tag{2.28}$$

in which $f_{m,inst}$ (n,y) is the instantaneous mass fraction of chains with length n and relative compositionγ with respect to the mean composition ($\bar{F}_{1,inst}$). This composition is defined as $F_{1,inst} - \bar{F}_{1,inst}$ with $\bar{F}_{1,inst}$ the average instantaneous copolymer composition, as provided by the Mayo-Lewis equation (Equation (2.6)). $F_{1,inst}$ is a stochastic variable equal to the ratio of the number of comonomer type 1 units in a polymer chain and the chain length of the same polymer chain. In addition, x_n is the number-average chain length. It is important to stress that the parameters in Stockmayer's distribution can be determined from observable quantities. The parameter σ^2 is defined as:

$$\sigma^2 = \frac{F_{1,inst}(1 - F_{1,inst})\kappa}{x_n} \tag{2.29}$$

in which κ is a parameter indicative of the compositional broadness depending on the product $r_1 r_2$ and $F_{1,inst}$:

$$\kappa = \sqrt{1 - 4F_{1,inst}(1 - F_{1,inst})(1 - r_1 r_2)} \tag{2.30}$$

If $r_1 r_2 = 1$, then κ is equal to 1 and the compositional broadness depends only on $F_{1,inst}$. Equation (1.35) also indicates that the compositional broadness will be largest for $F_{1,inst}$ = 0.5. Upon rewriting Equation (2.30) the instantaneous segment lengths (Equation (2.9)-(2.10)) can be introduced:

$$\kappa = \bar{F}_{1,inst}\left(\overline{l_{2,inst}} - 1\right) + (1 - \bar{F}_{1,inst})(\overline{l_{1,inst}} - 1) \tag{2.31}$$

Hence, κ is a type of average sequence length, which indicates that a high average instantaneous copolymer composition of one comonomer type combined with a low average segment length of the other comonomer type results in a large compositional broadness.. This is confirmed in shown in Figure 2.8 (a-c) in which $r_1 r_2$ is varied, assuming for simplicity $F_{1,inst}$ = 0.5. It can be seen that larger values lead to broader distributions. In Figure 2.8 (d-f) x_n is varied. Larger x_n lead to a smaller compositional broadness.

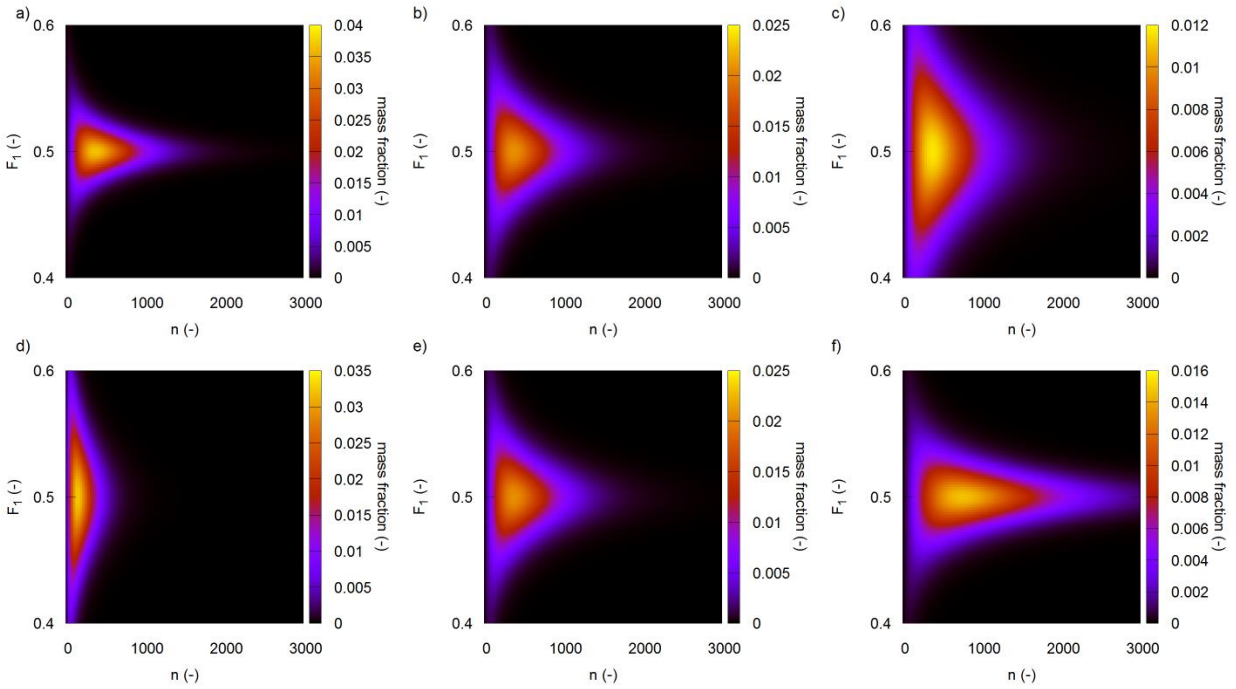

Figure 2.8. *Influence of r_1r_2 (top row) and x_n (bottom row) in copolymer composition – chain length distribution (CoC-CLD) as predicted by the Stockmayer equation (Equation (2.28)) with $F_{1,inst}$ = 0.5 for (a) r_1r_2 = 0.1, (b) r_1r_2 = 1, and (c) r_1r_2 = 10 for x_n = 250; and (d) x_n = 100, (e) x_n = 250, (f) x_n = 500 for r_1r_2 = 1.*

After integration of Equation (1.33) over the full γ domain, Flory's most probable distribution is obtained as the mass CLD:[129]

$$f_m(n) = \frac{n}{{x_n}^2} \exp\left(-\frac{n}{x_n}\right) \tag{2.32}$$

Analogously, integration over the *n* domain results in the corresponding mass copolymer composition distribution (CoCD):

$$f_m(\gamma) = \frac{3}{4\sqrt{2\frac{\sigma^2}{x_n}\left(1+\frac{\gamma^2}{2\frac{\sigma^2}{x_n}}\right)}^{2.5}} \tag{2.33}$$

Several extensions to the Stockmayer equation have been also derived, although focusing on terminal reactivities to not overload the mathematical treatment. For example, Tacx *et al.*[130] focused on the derivation with comonomers of unequal molar mass. Another extension is the adjustment for terpolymerizations, *i.e.* polymerizations including three comonomer types, and multicomponent copolymers as analytically derived by Anantawaraskul *et al* and confirmed using *k*MC simulations.[131] This Stockmayer equation has been further extended to a trivariate distribution by Soares *et al.* [132] for polymer products obtained via chain growth/coordination polymerization, in which long chain branches affect the product quality. An updated equation also exist with purely termination by recombination.[126] An additional extension is the more general case of competitive termination modes.. Therefore, the Stockmayer equation associated with Flory's most probable distribution has been formally extended by Stesjkal *et al.*[133] in order to incorporate the more general empirical Schulz-Zimm distribution. This distribution takes into account the broadness, *i.e.* dispersity (ratio of mass to number average chain length, x_m to x_n), of the polymerization:

$$f_{m,inst}(n,\gamma) = \left(\frac{b^{\,a+1}}{\Gamma(a+1)} n^a \exp(-b\,n)\right)\left(\frac{1}{\sigma\sqrt{2\pi}} \exp\left(-\frac{\gamma^2}{2\sigma^2}\right)\right)$$
$$a = \left(\frac{x_m}{x_n} - 1\right)^{-1}; b = \frac{a}{x_n} = \frac{a+1}{x_m} \quad (2.34)$$

Experimental verification of the CoC-CLD is not straightforward and only a limited number of experimental studies have been reported.[122-125] Using matrix-assisted laser desorption/ionization time-of-flight (MALDI-TOF) spectroscopy Haddleton *et al.*[134] managed to experimentally construct the CoC-CLD of MMA and *n*-butyl acrylate radical copolymerization via deconvolution of the m/z spectra. Similar experiments have been performed by van Herk *et al.*[36] Also temperature rising elution fractionation (TREF) combined with size exclusion

chromatography (SEC) and Fourier-transform infrared (FT-IR) spectroscopy combined with SEC have been used by Soares *et al.*[135] for experimental verification of the compositional characteristics of LLDPE obtained via coordination polymerization using a multiple of catalysts. By superimposing multiple Stockmayer distributions the contribution of each catalyst can be accounted for. Also, the univariate distributions obtained by integration over the full range of one of two variates have been experimentally investigated. Logically SEC chromatography is used for the CLD and techniques used for verification of the CoCD are for instance crystallization analysis fractionation (CRYSTAF) and crystallization elution fractionation (CEF).[136]

Using deterministic modeling techniques, such as the two-dimensional fixed-pivot technique[55] and stochastic modelling techniques (typically *k*MC techniques),[55, 59, 65, 137] bivariate distributions such as the CoC-CLD have been calculated, accurately accounting for more detailed reaction schemes and diffusional limitations.[55, 59, 65, 115] For example, Van Steenberge *et al.* highlighted that in FRP of MMA and styrene (terminal reactivity model) the shape and position of the CoCD is strongly dependent on the interplay of the gel-, cage and glass effect. Composite binary trees were also considered to allow for a fast simulation time.[59] For trivariate distributions, Kryven and Iedema[52] performed deterministic simulations in which the CoC-CLD and SLD have been tracked for FRP of styrene and acrylonitrile. A downside of these multivariate models remains although their computational cost explaining the development of the so-called explicit models.

2.6 Explicit models

In explicit models, the chain growth of individual copolymer macrospecies is tracked as a function of reaction time.[13, 14, 42, 44, 55, 61, 66, 103, 138] The macroscopic behavior of the copolymer can thus be related to the molecular structure of individual macrospecies at the micro-scale, with average properties always accessible *a posteriori*.[43, 139-141] Both basic and detailed reaction

schemes have been considered combined with mostly terminal but also recently penultimate reactivity models.[60, 139] Also intrinsic and apparent kinetics have been simulated. As for the bivariate and multivariate models, the explicit models are only of added value in case compositional characteristics are aimed at besides the calculation of the polymerization rate.

Typically vector or matrix-based stochastic simulations are performed in which the monomer incorporations are executed and stored. The monomer sequences are thus available from one chain end to the other. This leads to computationally more demanding computer codes but with an unprecedented amount of microstructural detail. The concept of a matrix representation has been originally introduced by Szymanski *et al.*[63] for the estimation of reactivity ratios for a very basic living polymerization aiming at a low final chain lengths, using bivariate distributions obtained out of the explicit matrix data. In parallel, Meimaroglou *et al.* [138] developed a vector based stochastic algorithm allowing reconstruction of the microstructure of individual highly branched homopolymer LDPE chains, based on the stored segment information. This information per segment was extended by Wang and Broadbelt[81] for NMP copolymerization aiming at gradient copolymer synthesis. Matrices were used to store the information on segments between active and dormant macrospecies. In the work of Van Steenberge *et al.* [59] a single matrix was employed for the growth of reactive chains in ATRP and the focus was shifted to the actual storage of the comonomer itself instead of a segment. Diffusional limitations were also fundamentally accounted for. The reaction event history and in particular the propagation reaction event history could be thus visualized for individual copolymerization chains at the level of the single comonomer unit. Typical results for RDRP copolymers are provided in Figure 2.9. A successful benchmark of the average properties with those obtained using the more conventional bivariate *k*MC technique has also obtained.

Similar algorithms were developed by Lemos *et al.*[60] later on whilst also incorporating continuous reactor configuration including residence time distributions. Currently, the single matrix-based *k*MC strategy has been applied to study to copolymer kinetics of a wide range of RDRP techniques.[60, 65, 139, 141-143] Its potential has also been illustrated for copolymer formation involving short chain branches[42] or grafting[67] through post-polymerization modification.

Next to the derivation of the (multi)variate distributions so-called structural deviations parameters have also been introduced, allowing the unbiased ranking of copolymers. Most notably are the gradient deviation index (<GD>)[65] and block deviation index (<BD>).[143] For values close to zero, a perfect gradient and block copolymer are respectively obtained. The worst-case scenario of a homopolymer is rescaled to a value of 1. Threshold values have been introduced to separate excellent from good and bad gradient and block copolymers. In addition, any information on compositional or kinetic information can be retrieved for each macrospecies. In particular for RDRP, the distribution reflecting the amount and type of comonomer units per activation-growth –deactivation cycle in a given monomer conversion interval can be obtained.[139, 141]

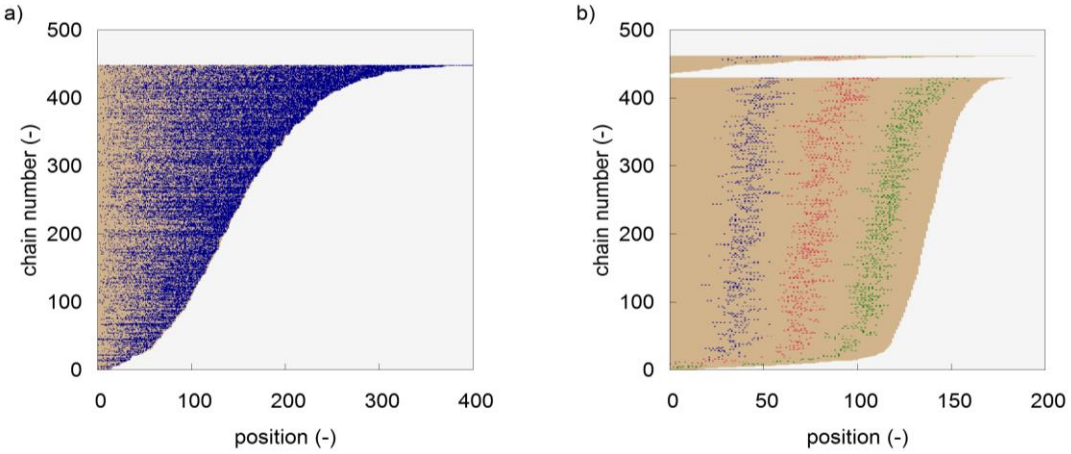

Figure 2.9. *Typical result from explicit matrix-based model to describe compositional properties;[59] color: different monomer unit; (a) gradient copolymer (b) sequence controlled polymer.*

2.7 Conclusions

A detailed overview has been provided on the current state-of-the-art on copolymerization models to calculate the average polymerization rate and compositional properties. Both terminal and penultimate reactivity models have been included. Despite their simplicity, analytical models allow a basic understanding of the copolymer microstructure evolution and can be used to obtain reactivity ratios. They are however less suited in case time dependencies need to be accurately accounted for and can lead to biased interpretations for more complex polymerization reaction schemes.

To resolve this disadvantage of analytical models advanced models are suited. Depending in the desired outcome, the model complexity can be increased. Interesting are multivariate descriptions in which the stochastic nature for chain length increase is fully acknowledged and the chemical composition variation is still treated on an average basis per chain length considered. To resolve the latter issue within a reasonable computational cost explicit-models have been developed, allowing to track each compositional change for individual macrospecies. The advent of the latter models allows to unambiguously rank copolymers and to understand both inter- and intramolecular compositional deviations in chain-growth polymerization.

References

1. Odian, G., *Principles of Polymerization*. 4th ed.; 2004.

2. Matyjaszewski, K.; Davis, T. P., *Handbook of Radical Polymerization*. Wiley: 2002.

3. Szwarc, M. Living polymers. Their discovery, characterization, and properties. *Journal of Polymer Science Part A: Polymer Chemistry* **1998,** 36, (1), IX-XV.

4. Szwarc, M. `Living' Polymers. *Nature* **1956,** 178, (4543), 1168-1169.

5. Chien, J. C. W., *Coordination polymerization: A Memorial to Karl Ziegler*. Elsevier Science: 2012.

6. Asua, J., *Polymer Reaction Engineering*. Wiley: 2007.

7. Dubé, M. A.; Saldívar-Guerra, E.; Zapata-González, I., Copolymerization. In *Handbook of Polymer Synthesis, Characterization, and Processing*, John Wiley & Sons, Inc.: 2013; pp 105-125.

8. McKee, G. E.; Kistenmacher, A.; Goerrissen, H.; Breulmann, M., Synthesis, Properties and Applications of Acrylonitrile–Styrene–Acrylate Polymers. In *Modern Styrenic Polymers: Polystyrenes and Styrenic Copolymers*, John Wiley & Sons, Ltd: 2003; pp 341-362.

9. Sperling, L. H., *Introduction to physical polymer science*. Wiley: 1986.

10. Coote, M. L.; Davis, T. P. The mechanism of the propagation step in free-radical copolymerisation. *Progress in Polymer Science* **1999,** 24, (9), 1217-1251.

11. Barner-Kowollik, C.; Vana, P.; Davis, T. P., The Kinetics of Free-Radical Polymerization. In *Handbook of Radical Polymerization*, John Wiley & Sons, Inc.: 2003; pp 187-261.

12. Coote, M. L.; Davis, T. P., Copolymerization Kinetics. In *Handbook of Radical Polymerization*, John Wiley & Sons, Inc.: 2003; pp 263-300.

13. D'hooge, D. R.; Van Steenberge, P. H. M.; Reyniers, M.-F.; Marin, G. B. The strength of multi-scale modeling to unveil the complexity of radical polymerization. *Progress in Polymer Science* **2016,** 58, 59-89.

14. Mastan, E.; Li, X.; Zhu, S. Modeling and theoretical development in controlled radical polymerization. *Progress in Polymer Science* **2015,** 45, 71-101.

15. Fukuda, T.; Ma, Y. D.; Inagaki, H.; Kubo, K. Penultimate-unit effects in free-radical copolymerization. *Macromolecules* **1991,** 24, (2), 370-375.

16. Mayo, F. R.; Lewis, F. M. Copolymerization. I. A Basis for Comparing the Behavior of Monomers in Copolymerization; The Copolymerization of Styrene and Methyl Methacrylate. *J. Am. Chem. Soc.* **1944,** 66, (9), 1594-1601.

17. Merz, E.; Alfrey, T.; Goldfinger, G. Intramolecular reactions in vinyl polymers as a means of investigation of the propagation step. *Journal of Polymer Science* **1946,** 1, (2), 75-82.

18. Ham, G. E. Antepenultimate Copolymer Composition Equation. *Journal of Macromolecular Science: Part A - Chemistry* **1971,** 5, (2), 453-458.

19. Ham, G. E. Antepenultimate Reactivity Ratios. *Journal of Macromolecular Science: Part A - Chemistry* **1971,** 5, (4), 815-818.

20. Charleux, B.; Nicolas, J.; Guerret, O. Theoretical Expression of the Average Activation−Deactivation Equilibrium Constant in Controlled/Living Free-Radical Copolymerization Operating via Reversible Termination. Application to a Strongly Improved Control in Nitroxide-Mediated Polymerization of Methyl Methacrylate. *Macromolecules* **2005,** 38, (13), 5485-5492.

21. Leamen, M. Kinetic Investigation and Modelling of Multi-Component Polymer Systems with Depropagation. UWSpace, 2005.

22. Fukuda, T.; Kubo, K.; Ma, Y.-D. Kinetics of free radical copolymerization. *Progress in Polymer Science* **1992,** 17, (5), 875-916.

23. Semchikov, Y. U. D. Preferential sorption of monomers and molecular weight effects in radical copolymerization. *Macromol. Symp.* **1996,** 111, (1), 317-328.

24. Harwood, H. J. Structures and compositions of copolymers. *Makromolekulare Chemie. Macromolecular Symposia* **1987,** 10-11, (1), 331-354.

25. Fukuda, T.; Ma, Y. D.; Inagaki, H. Free-radical copolymerization. 3. Determination of rate constants of propagation and termination for styrene/methyl methacrylate system. A critical test of terminal-model kinetics. *Macromolecules* **1985,** 18, (1), 17-26.

26. Klumperman, B. Mechanistic considerations on styrene-maleic anhydride copolymerization reactions. *Polymer Chemistry* **2010,** 1, (5), 558-562.

27. De Wilde, M. C.; Smets, G. Copolymérisation de l'Anhydride Maléique avec Différents Monomères Vinyliques. *Journal of Polymer Science* **1950,** 5, (2), 253-258.

28. Mavroudakis, E.; Cuccato, D.; Moscatelli, D. On the Use of Quantum Chemistry for the Determination of Propagation, Copolymerization, and Secondary Reaction Kinetics in Free Radical Polymerization. *Polymers* **2015,** 7, (9), 1483.

29. Coote, M. L.; Davis, T. P. Copolymerization Propagation Kinetics of Para-Substituted Styrenes: A Critical Test of the Implicit Penultimate Model. *Macromolecules* **1999,** 32, (11), 3626-3636.

30. Bertin, D.; Dufils, P. E.; Durand, I.; Gigmes, D.; Giovanetti, B.; Guillaneuf, Y.; Marque, S. R. A.; Phan, T.; Tordo, P. Effect of the penultimate unit on the C-ON bond homolysis in SGi-based alkoxyamines. *Macromol. Chem. Phys.* **2008,** 209, (2), 220-224.

31. Joseph Schork, F., Mathematical Modeling of Polymerization Reactors. In *Monitoring Polymerization Reactions*, John Wiley & Sons: 2013; pp 325-344.

32. Coote, M. L.; Davis, T. P.; Radom, L. Effect of the Penultimate Unit on Radical Stability and Reactivity in Free-Radical Polymerization. *Macromolecules* **1999,** 32, (9), 2935-2940.

33. Coote, M. L.; Davis, T. P.; Radom, L. Conformational Dependence of the Penultimate Unit Effect in Free-Radical Copolymerization. *Macromolecules* **1999,** 32, (16), 5270-5276.

34. Santos, A. F.; Silva, F. M.; Lenzi, M. K.; Pinto, J. C., Infrared (MIR, NIR), Raman, and Other Spectroscopic Methods. In *Monitoring Polymerization Reactions*, John Wiley & Sons: 2013; pp 107-134.

35. Duc, S.; Petit, A. Copolymerization of phenylacetylene and 1-hexyne using Ziegler-Natta and metathesis catalyst systems: copolymer compositions and reactivity ratios by 1H n.m.r. spectroscopy. *Polymer* **1999,** 40, (3), 589-597.

36. Huijser, S.; Mooiweer, G. D.; van der Hofstad, R.; Staal, B. B. P.; Feenstra, J.; van Herk, A. M.; Koning, C. E.; Duchateau, R. Reactivity Ratios of Comonomers from a Single MALDI–ToF–MS Measurement at One Feed Composition. *Macromolecules* **2012,** 45, (11), 4500-4510.

37. Noble, B. B.; Coote, M. L. First principles modelling of free-radical polymerisation kinetics. *International Reviews in Physical Chemistry* **2013,** 32, (3), 467-513.

38. Dossi, M.; Moscatelli, D. A QM Approach to the Calculation of Reactivity Ratios in Free-Radical Copolymerization. *Macromol. React. Eng.* **2012,** 6, (2-3), 74-84.

39. Hutchinson, R. A.; McMinn, J. H.; Paquet, D. A.; Beuermann, S.; Jackson, C. A Pulsed-Laser Study of Penultimate Copolymerization Propagation Kinetics for Methyl Methacrylate/n-Butyl Acrylate. *Industrial & Engineering Chemistry Research* **1997,** 36, (4), 1103-1113.

40. Coote, M. L.; Zammit, M. D.; Davis, T. P.; Willett, G. D. Copolymerization Propagation Kinetics of Styrene and Methyl MethacrylateRevisited. 1. Pulsed Laser Polymerization Study. *Macromolecules* **1997,** 30, (26), 8182-8190.

41. Willemse, R. X. E.; van Herk, A. M. Copolymerization Kinetics of Methyl Methacrylate−Styrene Obtained by PLP-MALDI-ToF-MS. *J. Am. Chem. Soc.* **2006,** 128, (13), 4471-4480.

42. D'hooge, D. R.; Van Steenberge, P. H. M.; Derboven, P.; Reyniers, M.-F.; Marin, G. B. Model-based design of the polymer microstructure: bridging the gap between polymer chemistry and engineering. *Polymer Chemistry* **2015,** 6, (40), 7081-7096.

43. D'hooge, D. R.; Van Steenberge, P. H. M.; Reyniers, M. F.; Marin, G. B., Modeling of Monomer Sequences in Chain-Growth Copolymerization. In *Reference Module in Chemistry, Molecular Sciences and Chemical Engineering*, Elsevier: 2016.

44. Zhou, Y.-N.; Luo, Z.-H. State-of-the-Art and Progress in Method of Moments for the Model-Based Reversible-Deactivation Radical Polymerization. *Macromol. React. Eng.* **2016,** 10, (6), 516-534.

45. Wang, A. R.; Zhu, S. P. Modeling the reversible addition-fragmentation transfer polymerization process. *J. Polym. Sci. Pol. Chem.* **2003,** 41, (11), 1553-1566.

46. Kiparissides, C. Polymerization reactor modeling: A review of recent developments and future directions. *Chem. Eng. Sci.* **1996,** 51, (10), 1637-1659.

47. Li, X.; Mastan, E.; Wang, W.-J.; Li, B.-G.; Zhu, S. Progress in reactor engineering of controlled radical polymerization: a comprehensive review. *Reaction Chemistry & Engineering* **2016,** 1, (1), 23-59.

48. Vale, H.; Daiss, A.; Naeem, O.; Seda, L.; Becker, K.; Hungenberg, K. D. Models in the Polymer Industry: What Present? What Future? *Macromol. Symp.* **2013,** 333, (1), 286-296.

49. Brandão, A. L. T.; Soares, J. B. P.; Pinto, J. C.; Alberton, A. L. When Polymer Reaction Engineers Play Dice: Applications of Monte Carlo Models in PRE. *Macromol. React. Eng.* **2015,** 9, (3), 141-185.

50. Becker, P.; Busch, M. Modeling of ethylene copolymerizations with acrylate monomers. *Macromol. Theory Simul.* **1998,** 7, (4), 435-446.

51. Van Steenberge, P. H. M.; D'hooge, D. R.; Vandenbergh, J.; Reyniers, M.-F.; Adriaensens, P. J.; Vanderzande, D. J. M.; Marin, G. B. Comparative Kinetic Monte Carlo study of the Sulfinyl and Dithiocarbamate Precursor Route toward Highly Regioregular MDMO-PPV. *Macromol. Theory Simul.* **2013,** 22, (4), 246-255.

52. Kryven, I.; Iedema, P. D. Deterministic Modeling of Copolymer Microstructure: Composition Drift and Sequence Patterns. *Macromol. React. Eng.* **2015,** 9, (3), 285-306.

53. Soares, J. B. P.; Hamielec, A. E. Bivariate chain length and long chain branching distribution for copolymerization of olefins and polyolefin chains containing terminal double-bonds. *Macromol. Theory Simul.* **1996,** 5, (3), 547-572.

54. Achilias, D. S.; Kiparissides, C. Development of a general mathematical framework for modeling diffusion-controlled free-radical polymerization reactions. *Macromolecules* **1992,** 25, (14), 3739-3750.

55. Krallis, A.; Meimaroglou, D.; Kiparissides, C. Dynamic prediction of the bivariate molecular weight–copolymer composition distribution using sectional-grid and stochastic numerical methods. *Chem. Eng. Sci.* **2008,** 63, (17), 4342-4360.

56. Zapata-González, I.; Hutchinson, R. A.; Payne, K. A.; Saldívar-Guerra, E. Mathematical modeling of the full molecular weight distribution in ATRP techniques. *AIChE Journal* **2016,** 62, (8), 2762-2777.

57. Zapata-González, I.; Saldívar-Guerra, E.; Flores-Tlacuahuac, A.; Vivaldo-Lima, E.; Ortiz-Cisneros, J. Efficient numerical integration of stiff differential equations in polymerisation reaction engineering: Computational aspects and applications. *The Canadian Journal of Chemical Engineering* **2012,** 90, (4), 804-823.

58. Pintos, E.; Sarmoria, C.; Brandolin, A.; Asteasuain, M. Modeling of RAFT Polymerization Processes Using an Efficient Monte Carlo Algorithm in Julia. *Industrial & Engineering Chemistry Research* **2016,** 55, (31), 8534-8547.

59. Van Steenberge, P. H. M.; D'hooge, D. R.; Reyniers, M. F.; Marin, G. B. Improved kinetic Monte Carlo simulation of chemical composition-chain length distributions in polymerization processes. *Chem. Eng. Sci.* **2014,** 110, 185-199.

60. Lemos, T.; Melo, P. A.; Pinto, J. C. Stochastic Modeling of Polymer Microstructure From Residence Time Distribution. *Macromol. React. Eng.* **2015,** 9, (3), 259-270.

61. Sosnowski, S. Software for Demonstration of Features of Chain Polymerization Processes. *Journal of Chemical Education* **2013,** 90, (6), 793-795.

62. Gillespie, D. T. Exact stochastic simulation of coupled chemical-reactions. *J. Phys. Chem.* **1977,** 81, (25), 2340-2361.

63. Szymanski, R., On the determination of the ratios of the propagation rate constants on the basis of the MWD of copolymer chains: A new Monte Carlo algorithm. In *e-Polymers*, 2009; Vol. 9.

64. Wang, L.; Broadbelt, L. J. Tracking Explicit Chain Sequence in Kinetic Monte Carlo Simulations. *Macromol. Theory Simul.* **2011,** 20, (1), 54-64.

65. Van Steenberge, P. H. M.; D'hooge, D. R.; Wang, Y.; Zhong, M. J.; Reyniers, M. F.; Konkolewicz, D.; Matyjaszewski, K.; Marin, G. B. Linear Gradient Quality of ATRP Copolymers. *Macromolecules* **2012,** 45, (21), 8519-8531.

66. Van Steenberge, P. H. M.; Verbraeken, B.; Reyniers, M.-F.; Hoogenboom, R.; D'hooge, D. R. Model-Based Visualization and Understanding of Monomer Sequence Formation in Gradient Copoly(2-oxazoline)s On the basis of 2-Methyl-2-oxazoline and 2-Phenyl-2-oxazoline. *Macromolecules* **2015,** 48, (21), 7765-7773.

67. Hernández-Ortiz, J. C.; Van Steenberge, P. H. M.; Reyniers, M.-F.; Marin, G. B.; D'hooge, D. R.; Duchateau, J. N. E.; Remerie, K.; Toloza, C.; Vaz, A. L.; Schreurs, F. Modeling the reaction event history and microstructure of individual macrospecies in postpolymerization modification. *AIChE Journal*, n/a-n/a.

68. Wang, A. R.; Zhu, S. ESR Study on Diffusion-Controlled Atom Transfer Radical Polymerization of Methyl Methacrylate and Ethylene Glycol Dimethacrylate. *Macromolecules* **2002,** 35, (27), 9926-9933.

69. D'hooge, D. R.; Reyniers, M.-F.; Marin, G. B. The Crucial Role of Diffusional Limitations in Controlled Radical Polymerization. *Macromol. React. Eng.* **2013,** 7, (8), 362-379.

70. Johnston-Hall, G.; Monteiro, M. J. Bimolecular radical termination: New perspectives and insights. *J. Polym. Sci. Pol. Chem.* **2008,** 46, (10), 3155-3173.

71. Barner-Kowollik, C.; Russell, G. T. Chain-length-dependent termination in radical polymerization: Subtle revolution in tackling a long-standing challenge. *Prog. Polym. Sci.* **2009,** 34, (11), 1211-1259.

72. Fineman, M.; Ross, S. D. Linear method for determining monomer reactivity ratios in copolymerization. *Journal of Polymer Science* **1950,** 5, (2), 259-262.

73. Kelen, T.; Tuds, F. Analysis of the Linear Methods for Determining Copolymerization Reactivity Ratios. I. A New Improved Linear Graphic Method. *Journal of Macromolecular Science: Part A - Chemistry* **1975,** 9, (1), 1-27.

74. Van Herk, A. M.; Dröge, T. Nonlinear least squares fitting applied to copolymerization modeling. *Macromol. Theory Simul.* **1997,** 6, (6), 1263-1276.

75. Davis, T. P.; O'Driscoll, K. F.; Piton, M. C.; Winnik, M. A. Copolymerization propagation kinetics of styrene with alkyl methacrylates. *Macromolecules* **1990,** 23, (8), 2113-2119.

76. Davis, T. P.; O'Driscoll, K. F.; Piton, M. C.; Winnik, M. A. Copolymerization propagation kinetics of styrene with alkyl acrylates. *Polym. Int.* **1991,** 24, (2), 65-70.

77. Ma, Y. D.; Won, Y. C.; Kubo, K.; Fukuda, T. Propagation and termination processes in the free-radical copolymerization of methyl methacrylate and vinyl acetate. *Macromolecules* **1993,** 26, (25), 6766-6770.

78. O'Driscoll, K. F. The Temperature Dependence of Copolymerization Reactivity Ratios. *Journal of Macromolecular Science: Part A - Chemistry* **1969,** 3, (2), 307-309.

79. Cheng, H. N., Polymerization and Statistical Models. In *eMagRes*, John Wiley & Sons, Ltd: 2007.

80. Winston, A.; Wichacheewa, P. Sequence Distribution in 1-Chloro-1,3-butadiene: Styrene Copolymers. *Macromolecules* **1973,** 6, (2), 200-205.

81. Wang, L.; Broadbelt, L. J. Kinetics of Segment Formation in Nitroxide-Mediated Controlled Radical Polymerization: Comparison with Classic Theory. *Macromolecules* **2010,** 43, (5), 2228-2235.

82. Wang, L.; Broadbelt, L. J. Factors Affecting the Formation of the Monomer Sequence along Styrene/Methyl Methacrylate Gradient Copolymer Chains. *Macromolecules* **2009,** 42, (21), 8118-8128.

83. Skeist, I. Copolymerization: the Composition Distribution Curve. *J. Am. Chem. Soc.* **1946,** 68, (9), 1781-1784.

84. Meyer, V. E.; Lowry, G. G. Integral and differential binary copolymerization equations. *Journal of Polymer Science Part A: General Papers* **1965,** 3, (8), 2843-2851.

85. Scott, A.; Kazemi, N.; Penlidis, A. AMPS/AAm/AAc Terpolymerization: Experimental Verification of the EVM Framework for Ternary Reactivity Ratio Estimation. *Processes* **2017,** 5, (1), 9.

86. Tidwell, P. W.; Mortimer, G. A. An improved method of calculating copolymerization reactivity ratios. *Journal of Polymer Science Part A: General Papers* **1965,** 3, (1), 369-387.

87. Dube, M.; Sanayei, R. A.; Penlidis, A.; O'Driscoll, K. F.; Reilly, P. M. A microcomputer program for estimation of copolymerization reactivity ratios. *Journal of Polymer Science Part A: Polymer Chemistry* **1991,** 29, (5), 703-708.

88. Fischer, H. The Persistent Radical Effect In "Living" Radical Polymerization. *Macromolecules* **1997,** 30, (19), 5666-5672.

89. Fischer, H. The persistent radical effect in controlled radical polymerizations. *J. Polym. Sci. Pol. Chem.* **1999,** 37, (13), 1885-1901.

90. Lutz, J. F.; Lacroix-Desmazes, P.; Boutevin, B. The persistent radical effect in nitroxide mediated polymerization: Experimental validity. *Macromol. Rapid Commun.* **2001,** 22, (3), 189-193.

91. Matyjaszewski, K. Factors Affecting Rates of Comonomer Consumption in Copolymerization Processes with Intermittent Activation. *Macromolecules* **2002,** 35, (18), 6773-6781.

92. Zapata-González, I.; Hutchinson, R. A.; Matyjaszewski, K.; Saldívar-Guerra, E.; Ortiz-Cisneros, J. Copolymer Composition Deviations from Mayo–Lewis Conventional Free Radical Behavior in Nitroxide Mediated Copolymerization. *Macromol. Theory Simul.* **2014,** 23, (4), 245-265.

93. Klumperman, B.; Chambard, G.; Brinkhuis, R. H. G., Peculiarities in Atom Transfer Radical Copolymerization. In *Advances in Controlled/Living Radical Polymerization*, American Chemical Society: 2003; Vol. 854, pp 180-192.

94. Krüger, H.; Bauer, J.; Rübner, J. Ein Modell zur Beschreibung reversibler Copolymerisationen. *Die Makromolekulare Chemie* **1987,** 188, (9), 2163-2175.

95. Wittmer, P., Copolymerization in the Presence of Depolymerization Reactions. In *Multicomponent Polymer Systems*, American chemical society: 1971; Vol. 99, pp 140-174.

96. Lowry, G. G. The effect of depropagation on copolymer composition. I. General theory for one depropagating monomer. *Journal of Polymer Science* **1960,** 42, (140), 463-477.

97. Kukulj, D.; Davis, T. P. Average Propagation Rate Coefficients in the Free-Radical Copolymerization of Styrene and α-Methylstyrene Measured by Pulsed-Laser Polymerization. *Macromolecules* **1998,** 31, (17), 5668-5680.

98. Valvassori, A.; Sartori, G., Present status of the multicomponent copolymerization theory. In *Fortschritte der Hochpolymeren-Forschung*, Springer Berlin Heidelberg: Berlin, Heidelberg, 1967; pp 28-58.

99. Dubé, M. A.; Soares, J. B. P.; Penlidis, A.; Hamielec, A. E. Mathematical Modeling of Multicomponent Chain-Growth Polymerizations in Batch, Semibatch, and Continuous Reactors: A Review. *Industrial & Engineering Chemistry Research* **1997,** 36, (4), 966-1015.

100. Alfrey, T.; Goldfinger, G. Copolymerization of Systems Containing Three Components. *The Journal of Chemical Physics* **1946,** 14, (2), 115-116.

101. Walling, C.; Briggs, E. R. Copolymerization. III. Systems Containing More than Two Monomers. *J. Am. Chem. Soc.* **1945,** 67, (10), 1774-1778.

102. Ham, G. E. Penultimate unit effects in terpolymerization. *Journal of Polymer Science Part A: General Papers* **1964,** 2, (9), 4191-4200.

103. Payne, K. A.; D'hooge, D. R.; van Steenberge, P. H. M.; Reyniers, M. F.; Cunningham, M. F.; Hutchinson, R. A.; Marin, G. B. ARGET ATRP of Butyl Methacrylate: Utilizing Kinetic Modeling To Understand Experimental Trends. *Macromolecules* **2013,** 46, (10), 3828-3840.

104. Kumar, S.; Ramkrishna, D. On the solution of population balance equations by discretization—I. A fixed pivot technique. *Chem. Eng. Sci.* **1996,** 51, (8), 1311-1332.

105. Hernández-Ortiz, J. C.; Vivaldo-Lima, E.; Dubé, M. A.; Penlidis, A. Modeling of Network Formation in Reversible Addition-Fragmentation Transfer (RAFT) Copolymerization of Vinyl/Divinyl Monomers Using a Multifunctional Polymer Molecule Approach. *Macromol. Theory Simul.* **2014,** 23, (3), 147-169.

106. D'hooge, D. R.; Reyniers, M. F.; Marin, G. B. Methodology for Kinetic Modeling of Atom Transfer Radical Polymerization. *Macromol. React. Eng.* **2009,** 3, (4), 185-209.

107. Fortunatti, C.; Sarmoria, C.; Brandolin, A.; Asteasuain, M. Modeling of the bivariate molecular weight distribution-copolymer composition distribution in RAFT copolymerization using probability generating functions. *Computational Materials Science* **2017,** 136, 280-296.

108. Saldívar-Guerra, E.; Infante-Martínez, R.; Vivaldo-Lima, E.; Flores-Tlacuahuac, A. Returning to Basics: Direct Integration of the Full Molecular-Weight Distribution Equations in Addition Polymerization. *Macromol. Theory Simul.* **2010,** 19, (4), 151-157.

109. Wulkow, M. Computer Aided Modeling of Polymer Reaction Engineering—The Status of Predici, I-Simulation. *Macromol. React. Eng.* **2008,** 2, (6), 461-494.

110. Wulkow, M. The simulation of molecular weight distributions in polyreaction kinetics by discrete Galerkin methods. *Macromol. Theory Simul.* **1996,** 5, (3), 393-416.

111. De Rybel, N.; D'hooge, D. R.; Van Steenberge, P. H. M.; Reyniers, M. F.; Marin, G. B. How chain length dependency interferes with the bulk RAFT polymerization rate and microstructural control. *Chem. Eng. Sci.* **2017**, submitted.

112. De Keer, L.; Van Steenberge, P. H. M.; Reyniers, M.-F.; Marin, G. B.; Hungenberg, K.-D.; Seda, L.; D'hooge, D. R. A complete understanding of the reaction kinetics for the industrial production process of expandable polystyrene. *AIChE Journal* **2017,** 63, (6), 2043-2059.

113. Peklak, A. D.; Butté, A.; Storti, G.; Morbidelli, M. Gel effect in the bulk reversible addition–fragmentation chain transfer polymerization of methyl methacrylate: Modeling and experiments. *Journal of Polymer Science Part A: Polymer Chemistry* **2006,** 44, (3), 1071-1085.

114. Kuhlman, R. L.; Klosin, J. Tuning Block Compositions of Polyethylene Multi-Block Copolymers by Catalyst Selection. *Macromolecules* **2010,** 43, (19), 7903-7904.

115. Mohammadi, Y.; Ahmadi, M.; Saeb, M. R.; Khorasani, M. M.; Yang, P.; Stadler, F. J. A Detailed Model on Kinetics and Microstructure Evolution during Copolymerization of Ethylene and 1-Octene: From Coordinative Chain Transfer to Chain Shuttling Polymerization. *Macromolecules* **2014,** 47, (14), 4778-4789.

116. Brandão, A. L. T.; Alberton, A. L.; Pinto, J. C.; Soares, J. B. P. Copolymerization of Ethylene with 1,9-Decadiene: Part II—Prediction of Molecular Weight Distributions. *Macromol. Theory Simul.*, 1700040-n/a.

117. Miller, R. L.; Nielsen, L. E. On the characterization of stereoregular polymers. I. Theory. *Journal of Polymer Science* **1960,** 46, (148), 303-316.

118. Bailey, D. B.; Henrichs, P. M. Diad, triad, and pentad sequence-distribution analysis of acrylonitrile–vinylidene chloride model copolymers by 13C-NMR. *Journal of Polymer Science: Polymer Chemistry Edition* **1978,** 16, (12), 3185-3199.

119. *RANDALL, JAMES C.* Academic Press: 1977.

120. Shi, Y.; Qin, X.; Guo, Y.; Xie, M.; Zhang, Y. The Effect of Activation/Deactivation Processes on the Microcomposition and Microsequence Structure of Controlled/Living Copolymers. *Macromol. Theory Simul.* **2008,** 17, (2-3), 130-136.

121. Koenig, J. L., Chapter 1 - Theory of polymer characterization. In *Spectroscopy of Polymers (Second Edition)*, Elsevier Science: New York, 1999; pp 1-33.

122. Cools, P. J. C. H.; Maesen, F.; Klumperman, B.; van Herk, A. M.; German, A. L. Determination of the chemical composition distribution of copolymers of styrene and butadiene by gradient polymer elution chromatography. *Journal of Chromatography A* **1996,** 736, (1), 125-130.

123. Ahmad, N. M.; Charleux, B.; Farcet, C.; Ferguson, C. J.; Gaynor, S. G.; Hawkett, B. S.; Heatley, F.; Klumperman, B.; Konkolewicz, D.; Lovell, P. A.; Matyjaszewski, K.; Venkatesh, R. Chain Transfer to Polymer and Branching in Controlled Radical Polymerizations of n-Butyl Acrylate. *Macromol. Rapid Commun.* **2009,** 30, (23), 2002-2021.

124. Ginzburg, A.; Macko, T.; Dolle, V.; Brüll, R. Multidimensional high-temperature liquid chromatography: A new technique to characterize the chemical heterogeneity of Ziegler-Natta-based bimodal HDPE. *J. Appl. Polym. Sci.* **2013,** 129, (4), 1897-1906.

125. Weidner, S. M.; Falkenhagen, J.; Bressler, I. Copolymer Composition Determined by LC-MALDI-TOF MS Coupling and "MassChrom2D" Data Analysis. *Macromol. Chem. Phys.* **2012,** 213, (22), 2404-2411.

126. Stockmayer, W. H. Distribution of Chain Lengths and Compositions in Copolymers. *The Journal of Chemical Physics* **1945,** 13, (6), 199-207.

127. Ali Parsa, M.; Kozhan, I.; Wulkow, M.; Hutchinson, R. A. Modeling of Functional Group Distribution in Copolymerization: A Comparison of Deterministic and Stochastic Approaches. *Macromol. Theory Simul.* **2014,** 23, (3), 207-217.

128. Saeb, M. R.; Mohammadi, Y.; Rastin, H.; Kermaniyan, T. S.; Penlidis, A. Visualization of Bivariate Sequence Length–Chain Length Distribution in Free Radical Copolymerization. *Macromol. Theory Simul.*, 1700041-n/a.

129. Flory, P., *Principles of Polymer Chemistry*. 1953.

130. Tacx, J.; Linssen, H. N.; German, A. L. Effect of molar mass ratio of monomers on the mass-distribution of chain lengths and compositions in copolymers - extension of the stockmayer theory. *J. Polym. Sci. Pol. Chem.* **1988,** 26, (1), 61-69.

131. Anantawaraskul, S.; Soares, J. B. P.; Wood-Adams, P. M. Chemical Composition Distribution of Multicomponent Copolymers. *Macromol. Theory Simul.* **2003,** 12, (4), 229-236.

132. Soares, J. B. P. The Use of Instantaneous Distributions in Polymerization Reaction Engineering. *Macromol. React. Eng.* **2014,** 8, (4), 235-259.

133. Stejskal, J.; Kratochvil, P. Statistical chemical heterogeneity of copolymers: modification of the Stockmayer distribution function of chemical composition. *Macromolecules* **1987,** 20, (10), 2624-2628.

134. Suddaby, K. G.; Hunt, K. H.; Haddleton, D. M. MALDI-TOF Mass Spectrometry in the Study of Statistical Copolymerizations and Its Application in Examining the Free Radical Copolymerization of Methyl Methacrylate and n-Butyl Methacrylate. *Macromolecules* **1996,** 29, (27), 8642-8649.

135. Faldi, A.; Soares, J. B. P. Characterization of the combined molecular weight and composition distribution of industrial ethylene/α-olefin copolymers. *Polymer* **2001,** 42, (7), 3057-3066.

136. Narkchamnan, K.; Anantawaraskul, S.; Soares, J. B. P. Bimodality Criterion for the Chemical Composition Distribution of Ethylene/1-Olefin Copolymers: Theoretical Development and Experimental Validation. *Macromol. React. Eng.* **2011,** 5, (5-6), 198-210.

137. Cho, A. S.; Broadbelt, L. J. Stochastic modelling of gradient copolymer chemical composition distribution and sequence length distribution. *Molecular Simulation* **2010,** 36, (15), 1219-1236.

138. Meimaroglou, D.; Kiparissides, C. A Novel Stochastic Approach for the Prediction of the Exact Topological Characteristics and Rheological Properties of Highly-Branched Polymer Chains. *Macromolecules* **2010,** 43, (13), 5820-5832.

139. Fierens, S. K.; D'hooge, D. R.; Van Steenberge, P. H. M.; Reyniers, M.-F.; Marin, G. B. How penultimate monomer unit effects and initiator choice influence ICAR ATRP of n-butyl acrylate and methyl methacrylate. *AIChE Journal* **2017**, DOI: 10.1002/aic.15851.

140. Fierens, S. K.; D'hooge, D. R.; Van Steenberge, P. H. M.; Reyniers, M.-F.; Marin, G. B. MAMA-SG1 initiated nitroxide mediated polymerization of styrene: From Arrhenius parameters to model-based design. *Chem. Eng. J.* **2015,** 278, 407-420.

141. Fierens, S. K.; Telitel, S.; Van Steenberge, P. H. M.; Reyniers, M.-F.; Marin, G. B.; Lutz, J.-F.; D'hooge, D. R. Model-Based Design To Push the Boundaries of Sequence Control. *Macromolecules* **2016,** 49, (24), 9336-9344.

142. Payne, K. A.; Van Steenberge, P. H. M.; D'Hooge, D. R.; Reyniers, M.-F.; Marin, G. B.; Hutchinson, R. A.; Cunningham, M. F. Controlled synthesis of poly[(butyl methacrylate)-co-(butyl acrylate)] via activator regenerated by electron transfer atom transfer radical polymerization: insights and improvement. *Polym. Int.* **2014,** 63, (5), 848-857.

143. Toloza Porras, C.; D'hooge, D. R.; Van Steenberge, P. H. M.; Reyniers, M.-F.; Marin, G. B. A Theoretical Exploration of the Potential of ICAR ATRP for One- and Two-Pot Synthesis of Well-Defined Diblock Copolymers. *Macromol. React. Eng.* **2013,** 7, (7), 311-326.

Chapter 3. MAMA-SG1 initiated nitroxide mediated polymerization of styrene: from Arrhenius parameters to model-based design

Summary

Activation and deactivation Arrhenius parameters are estimated for nitroxide mediated polymerization (NMP) of styrene initiated by BlocBuilder MA, based on an extensive set of experimental data covering a broad range of polymerization temperatures (90-120°C) and initial molar ratios of monomer to NMP initiator (100-1000). Data regression analysis is limited to conversions below 0.65 to avoid the possible influence of diffusional limitations on the activation/deactivation process. The applied kinetic model accounts for thermal initiation, chain transfer reactions and diffusional limitations on termination. A distinction is made between (de)activation of NMP initiator and macrospecies. The activation energy for the activation of the NMP initiator is 43 ± 3.5 kJ mol^{-1} lower than the one for the dormant macrospecies. At 120°C, the activation rate coefficients amount respectively to 1.18×10^{-1} s^{-1} and 7.08×10^{-3} s^{-1}, indicative of a fast NMP initiation. Using the obtained parameter estimates, a visualization of *ca.* 750 polymer chains is performed via advanced kinetic Monte Carlo simulations, explicitly specifying, for the first time, according to the living nature, and chain initiation and dead polymer mechanism. At 120°C, chain transfer to dimer lowers the level of control over chain length and end-group functionality. Model-based optimization reveals the beneficial effect of the use of a stepwise temperature program, as confirmed experimentally via a lowering of the dispersity from a conversion of 0.3 on due to a suppression of thermal initiation and chain transfer to dimer. This work was published in *Chemical Engineering Journal* 2015, 48, 492-501.

3.1 Introduction

In radical polymerizations, one of the most important industrially applied chemical processes, a crucial process condition is the temperature. For conventional free radical polymerization (FRP), the effect of temperature has been studied extensively.[1, 2] Reliable Arrhenius and thermodynamic parameters have been determined for the main FRP polymerizations, allowing a safe and efficient process control and the production of a wide variety of different product grades, including a variation in average chain length and overall comonomer incorporation.

Unfortunately, these FRP processes do not allow a facile incorporation of end-group functionality (EGF) or the production of polymers with a narrow chain length distribution (CLD; dispersity below 1.3), prohibiting the development of next-generation polymeric materials.[3-8] In particular, well-defined block, gradient and star copolymers (Figure 3.1 (a)) cannot be easily obtained according to the FRP mechanism. Hence, in the last decades significant attention has been focused on the development of so-called reversible deactivation radical polymerization (RDRP) (also called controlled radical polymerization (CRP)) techniques. These newly developed techniques allow, under well-selected conditions, the synthesis of well-tailored polymer molecules with almost uniform chain length and perfect EGF, opening the pathway to macromolecular engineering.[9] Alternatively, functional materials with complex architectures can be obtained via photopolymerization techniques.[10-14]

For styrene and (meth)acrylates as comonomers, one of the most important RDRP techniques is nitroxide mediated polymerization (NMP), the principle of which is given in Figure 3.1 (c).[15-20] For a sufficiently high polymerization temperature, a unimolecular alkoxyamine NMP initiator (R_0X) is cleaved into a NMP initiator radical (R_0) and a nitroxide (X), a persistent species. The R_0

species can either be deactivated reforming the original NMP initiator or it can undergo a couple of propagation steps, before it is deactivated into a dormant species (R_iX; i: chain length) or it can be involved in a termination reaction leading to the formation of a dead macrospecies (P). Alternatively, the NMP can be initiated via a bicomponent initiating system, *i.e.* with a conventional radical initiator, such as 2,2-azobisisobutyronitrile (AIBN) or benzoyl peroxide (BPO), and a stable free nitroxide. However, such reverse NMPs require an intensive tuning of the initial nitroxide to conventional radical initiator ratio.[18]

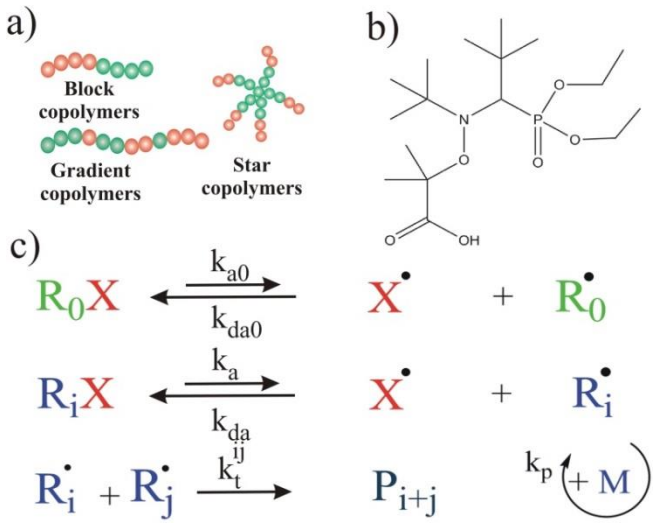

Figure 3.1. *(a) Macromolecular architectures that are difficult to access via free radical polymerization (FRP) but accessible via reversible deactivation radical polymerization (RDRP). (b) Chemical structure of MAMA-SG1/BlocBuilder MA. (c) Principle of nitroxide mediated polymerization (NMP), a main RDRP technique: $k_{a,da,p,t}$: rate coefficient for activation, deactivation, propagation and termination, subscript 0 related to NMP initiation; R_0X: NMP initiator; R_0: NMP initiator radical; X: nitroxide; i/j: chain length: R_iX: dormant macrospecies; P: dead species; termination by recombination is only shown.*

Importantly, in NMP, per termination reaction an excess of persistent nitroxide or deactivator species (X) is obtained, favoring deactivation over termination at sufficiently long polymerization times. Thanks to this so-called persistent radical effect,[21-24] the loss of end-group functionality X

can be limited, albeit at the expense of a lowering of the polymerization rate. Ideally, for a fast NMP initiation, at the end of the NMP all dormant polymer molecules possess a chain length equal to the initial molar ratio of monomer (*M*) to R_0X, which is also known as the targeted chain length (TCL).

To overcome the hurdle of a slow NMP, several optimization pathways, next to the development of novel nitroxides/alkoxyamines, have been explored by several research groups.[25-31] The use of long half-time conventional radical initiators,[26] small amounts of more sterically hindered alkoxyamines,[27] and the continuous addition of conventional radical initiator [28] have been put forward as possibilities to improve the NMP rate. A breakthrough for rate enhancement was achieved by the consumption of nitroxide radicals via deliberately added organic acids, such as camphorsulfonic acid [31]. Unfortunately, this addition method is accompanied by an increase of the dispersity. On the other hand, Malmström *et al.* [29] indicated that for certain nitroxides this penalty on the control over chain length can be avoided by using acetic anhydride (Ac_2O). However, as shown by Lansalot *et al.*,[30] Ac_2O does not result into a rate acceleration in SG1 based NMPs.

It should be stressed that in Figure 3.1 (c) only the main NMP reactions are represented and that side reactions can take place complicating the kinetic description and interpretation of the NMP process.[32] For example, in the NMP of acrylates both secondary and tertiary macrospecies can be formed due to intramolecular chain transfer reactions.[33, 34] Furthermore, for the NMP of styrene, it has been indicated that at polymerization temperatures above 100°C, thermal initiation cannot be neglected.[35-37] In particular, Bentein *et al.* [38] highlighted, via deterministic simulations, at 123°C the relevance of chain transfer to the dimer formed during this thermal initiation, when the NMP is mediated by N-(2-methyl-2-propyl)-N-(1-diethylphosphono-2,2-dimethylpropyl)-N-oxyl

(SG1/DEPN) or 2,2,6,6-tetramethylpiperidinyl-1-oxyl (TEMPO). These authors attributed the loss of control at higher TCLs mainly to this side reaction. In addition, several research groups have focused on the relevance of disproportionation reactions involving nitroxide moieties, which lead to the formation of hydroxylamines. For instance, based on experiments in the absence of monomer, Ananchenko *et al.* [39, 40] showed that the chemical nature and bulkiness of the nitroxide plays an important role for the intrinsic disproportionation reactivity. This was confirmed by Edeleva *et al.* [41, 42] via detailed ^{1}H-NMR analysis. In particular, these authors reported that in styrene NMP hydroxylamine formation can be neglected with SG1 as nitroxide.[43]

In general, optimization of the NMP process requires a detailed understanding of different reactions and their effect on the polymerization rate and control over chain length and EGF. In particular, as in FRP processes, the influence of the polymerization temperature on the NMP characteristics should be very clear. Many of the activation/deactivation parameters have however been determined under non-polymerization conditions, *i.e.* in solvent or at low temperature. In addition, most kinetic modeling studies have been focused on only one polymerization temperature and a limited range of TCLs,[38, 44, 45] imposing a barrier on the selection of the most optimal input parameters for subsequent model-based optimization. Interestingly, Chauvin *et al.* [46] indicated that, for NMP processes, a temperature program allows to improve the livingness and control over chain length. An efficient evaluation of this operation strategy implies, however, accurate NMP activation/deactivation Arrhenius parameters.

Currently, a relatively wide range of activation Arrhenius parameters have been reported, which are typically the result of a combination of different kinetic measurements. For example, Bertin *et al.* [47] reported an activation energy of 112 kJ mol^{-1} for NMP activation of MAMA-SG1, an important relatively new NMP initiator (Figure 3.1 (b); a.k.a. MAMA-SG1), based on a typical

but average pre-exponential factor of 2.4×10^{14} s^{-1}. Alternatively, Goto *et al.* [48] used the GPC peak resolution method to determine Arrhenius parameters. For activation of SG1 capped polystyrene species, these authors reported an activation energy of 130 kJ mol^{-1} and a value of 1.1×10^{-2} s^{-1} for k_a at 120 °C. Using the same method, Chevalier *et al.* [49] determined however a lower activation energy of 121 kJ mol^{-1} and a lower value of 3.4×10^{-3} s^{-1} at 120°C, illustrative of the scatter in literature on activation kinetic parameters. Similarly uncertainty exists concerning the deactivation kinetic parameters. For NMP deactivation of polystryryl radicals with SG1, Guillaneuf *et al.* [50] used the PLP-SEC method to determine k_{da} and reported a value of 5.3×10^5 L mol^{-1} s^{-1} at 120 °C. However, using laser flash photolysis, Fischer *et al.* [51] determined in the related phenylethyl-SG1 system a value of 4.6×10^6 L mol^{-1} s^{-1}. These authors also showed that the deactivation reaction shows a weak temperature dependency.

In this work, based on a broad set of experimental data and accounting for possible diffusional limitations on termination, regression analysis is first applied to estimate Arrhenius parameters for the NMP specific reaction steps under polymerization conditions. The regression analysis is performed for the NMP of styrene initiated by BlocBuilder MA, taking into account the effectiveness, versatility and commercial availability of this alkoxyamine.[52-54] Since regression analysis is performed, a reliable simultaneous identification of the involved pre-exponential factors and activation energies is possible, resolving the aforementioned pending issue in the polymer research community on accurate Arrhenius parameters for activation/deactivation.

Subsequently, the estimated parameter values are used to visualize, via detailed kinetic Monte Carlo (*k*MC) simulations,[55-57] the different macrospecies in the reaction mixture, while differentiating, for the first time, between their chain length, and dormant/dead chain formation. The *k*MC method is, in contrast to a deterministic solver, a stochastic method in which a

representative number of molecules is tracked throughout the polymerization process and reaction events are selected according to the reaction probabilities. In case all propagation reaction events are stored the chain length distribution and monomer sequences can be shown explicitly. In particular, a distinction is made between dormant chains which were started from initiator radicals formed upon chain transfer reactions or thermal initiation and between dead polymer chains formed via chain transfer or termination. Such differentiation not only allows a mapping of the different end-groups but also a detailed understanding of the relative importance of side reactions on the control over the NMP process.

Finally, the parameters are also used to illustrate the potential of stepwise temperature program to increase the control over the polymer properties for a fixed polymerization time and conversion. It is shown that such programs allow a suppression of chain transfer reactions and an increase of the livingness of the NMP product, as confirmed by the *k*MC simulations and experimental data.

3.2 Materials and methods

3.2.1 Materials

Styrene (Sty, monomer (M), ≥99%), Sigma-Aldrich) was passed through a column filled with basic aluminum oxide (Sigma-Aldrich) to remove the stabilizer (4-*tert*-butylcatechol). BlocBuilder MA ((MAMA-SG1 or NMP initiator ($R_{0,1}X$), ≥99%) was kindly provided by Arkema and used as received. Decane (≥99%), tetrahydrofuran (THF, ≥99%), and dichloromethane (DCM, ≥99%) were purchased from Sigma-Aldrich and used as received during analysis.

3.2.2 BlocBuilder MA initiated batch isothermal NMP of styrene

The batch isothermal polymerizations of styrene were performed in the presence of 6.25% (v/v, with respect to the monomer) decane, which is used as internal standard for gas chromatography

(GC) analysis. In-situ temperature control was performed via a proportional-integral-derivative (PID) controller, using refrigerated water as the cooling medium. The experiments were conducted for a sufficiently broad range of temperatures and TCLs (Table 3.1), allowing a reliable estimation of the activation/deactivation kinetic parameters. An overview of all experimental isothermal conditions used for the multi-response regression analysis can be found in Appendix (Entry 1-17: Table A.1).

Table 3.1. *Ranges of experimental conditions considered in regression analysis. An overview of all conditions is given in Table A.1 (Appendix)*

Temperature (°C)	TCL (-)	Time (h)	Conversion (-)
90-120	100-1000	0-55	0-0.65

A typical isothermal NMP experiment (entry 9 in Table A.1 in Appendix) was performed as follows. First 30 mL styrene, together with 2 mL decane were added to a 100-mL three-neck glass flask containing a magnetic stirrer bar. The desired amount of BlocBuilder MA (0.9979 g) was dosed and added to the mixture. A stopcock was attached to the one neck of the flask and a cold finger was attached to the second neck. The last neck was capped with a rubber septum. In a next step, the solution was degassed by performing three freeze-pump-thaw cycles. A thermocouple was inserted into the reaction flask through the rubber septum to allow for in situ temperature control. The reaction flask was immersed into the oil bath, which was already brought to the desired polymerization temperature. The reaction mixture was constantly stirred (350 rpm). Samples (0.75 mL) were withdrawn from the reaction flask through the septum at distinct reaction times, using 1 mL degassed syringes with stainless-steel needles. Samples were poured in a 1mL vial and immediately quenched in an ice-bath to prevent further polymerization.

For the additional experiment, in which a stepwise temperature program (TCL=1000) was applied, two oil baths each for one polymerization temperature were used with a fast manual switch of the flask to the second oil bath after 30 minutes by which the polymerization temperature was increased from 103 to 117°C. Again, in situ temperature control was applied.

3.2.3 Analytical techniques

Monomer conversion (X_m) was determined using both gas chromatography (GC) and gravimetric analysis allowing an additional reproducibility check (see Figure A.1 in Appendix). Size exclusion chromatography (SEC; a.k.a. gel permeation chromatography (GPC)) was used to determine the CLD and thus to measure the number average chain length (x_n) and the dispersity ($Đ$) as a function of (monomer) conversion.

A trace-GC ultra-Gas Chromatograph equipped with an AS3000 auto sampler, flame ionization detector (FID) detector and a CP Wax 52 CB 30m capillary column were employed for GC analysis. The injector and detector temperature were set at 275 °C. Helium (flow rate: 1.3 mL min^{-1}) was used as carrier gas and a stepwise temperature program was set as follows: 40 °C during 4 min, followed by a heating ramp of 20 °C min^{-1} until a temperature of 145 °C was reached, which was maintained for 2 minutes. Decane was used as internal standard and dichloromethane as solvent to prepare the samples. Data acquisition and processing were performed with Chrom-Card Trace-Focus GC software.

SEC analysis was performed with a PL-GPC*50* plus instrument equipped with a PL-AS RT auto sampler, refractive index (RI) detector, and the following columns connected in series: one Resipore 50×7.5mm guard column and two Resipore 300 × 7.5 mm columns. Measurements were performed in tetrahydrofuran flowing at a constant rate of 1 $mL.min^{-1}$ at a constant temperature of 30°C. Calibration was performed with narrow polystyrene standard samples (Medium EasiVials

kit, Agilent Technologies) ranging from 445 to 3.49×10^5 g mol^{-1}. Data acquisition and processing were performed with PL Cirrus GPC/SEC software.

As illustrated in Figure A.2 (Appendix), the reproducibility of the experimental data of the different responses is good. For completeness it is mentioned here that no reliable data on end-group functionality (EGF) could be obtained. As previously indicated, accurate measurements of the EGF, especially for high TCLs, are difficult to obtain in RDRP processes.[58] It should however be stressed that a sufficiently large range of response values can be obtained by considering the selected three responses, *i.e.* conversion, number-averaged chain length, and dispersity.

3.3 Kinetic model and regression analysis

An overview of the reactions included in the kinetic study for the NMP of styrene initiated by BlocBuilder MA is given in Table 3.2 with the reactants, *i.e.* the NMP initiator and the monomer, denoted as $R_{0,1}X$ and M. A distinction is made between styrene specific reactions steps, *i.e.* thermal initiation, propagation, termination, and chain transfer reactions, and NMP specific reaction steps, *i.e.* activation and deactivation reactions.

Since the polymerization temperature ranges from 90-120°C, thermal initiation reactions (reactions TI1-TI3 in Table 3.2) are included in the kinetic model.[35, 36, 59] For thermal initiation, the Mayo-mechanism [60, 61] is considered. In this mechanism, first a Diels-Alder cycloaddition takes place between two styrene molecules. The formed dimer can undergo a retro Diels-Alder reaction reforming two styrene molecules, but it can also undergo a molecule assisted homolysis with another styrene molecule, which results in the formation of two additional initiator radicals $R_{0,2}$ and $R_{0,3}$.

Table 3.2. *Overview of reactions in BlocBuilder initiated NMP of styrene; y,z = 1,2,3,4 and y^* = 2,3,4*

	Reaction step		k at 120°C ((L mol^{-1})s^{-1})	E_a (kJ mol^{-1})	A ((L mol^{-1})s^{-1})	Ref.
	Thermal initiation					
TI1	Diels-Alder dimerization	$2M \xrightarrow{k_d} D$	1.79×10^{-7}	93.5	4.74×10^{5}	38, 62 (a)
TI2	Retro Diels-Alder dimerization	$D \xrightarrow{k_{dr}} 2M$	1.36×10^{-4}	44.3	1.05×10^{2}	38, 62 (a)
TI3	Molecule assisted homolysis	$D + M \xrightarrow{k_{thi}} R_{0,2} + R_{0,3}$	9.07×10^{-8}	99.5	1.51×10^{6}	38, 62 (a)
	Chain initiation					
CI1		$R_{0,1} + M \xrightarrow{k_p^{0,1}} R_1$	1.00×10^{4}	16.5	1.55×10^{6}	46 (b)
CI2		$R_{0,2} + M \xrightarrow{k_p^{0,2}} R_1$	2.04×10^{3}	32.5	4.24×10^{7}	63(c)
CI3		$R_{0,3} + M \xrightarrow{k_p^{0,3}} R_1$	2.04×10^{3}	32.5	4.24×10^{7}	63(c)
CI4		$R_{0,4} + M \xrightarrow{k_p^{0,4}} R_1$	2.04×10^{3}	32.5	4.24×10^{7}	63(c)
P1	**Propagation**	$R_i \xrightarrow{k_p} R_{i+1}$	2.04×10^{3}	32.5	4.24×10^{7}	63
	Termination[(d)]					
T1		$R_{0,y} + R_{0,z} \xrightarrow{k_{tc,app}^{0,y;0,z}} R_0R_0$	composite k_t model[(d)]			61, 64 (d)
T2		$R_{0,y} + R_i \xrightarrow{k_{tc,app}^{0,y;i}} P_i$	composite k_t model[(d)]			61, 64 (d)
T3		$R_i + R_j \xrightarrow{k_{tc,app}^{i;j}} P_{i+j}$	composite k_t model[(d)]			61, 64(d)

Table 3.2. *Continued*

	Chain transfer					
CT1	to monomer	$R_{0,y} + M \xrightarrow{k_{trm}^{0,y}} P_0 + R_{0,4}$	2.09×10^{-1}	53.0	2.30×10^{6}	[61]
CT2		$R_i + M \xrightarrow{k_{trm}} P_i + R_{0,4}$	2.09×10^{-1}	53.0	2.30×10^{6}	[61]
CT3	to dimer	$R_{0,y} + D \xrightarrow{k_{trd}^{0,y}} P_0 + R_{0,3}$	1.50×10^{2}	27.5	6.76×10^{5}	[65, 66(e)]
CT4		$R_i + D \xrightarrow{k_{trd}} P_i + R_{0,3}$	1.50×10^{2}	27.5	6.76×10^{5}	[65, 66(e)]
	NMP (de)activation					
A1	Activation	$R_{0,1}X \xrightarrow{k_a^{0,1}} R_{0,1} + X$	1.18×10^{-1}	105.3	1.16×10^{13}	this work[(g)]
A2		$R_iX \xrightarrow{k_a} R_i + X$	7.08×10^{-3}	148.7	4.04×10^{17}	this work[(g)]
DA1	Deactivation	$R_{0,1} + X \xrightarrow{k_{da}^{0,1}} R_{0,1}X$	2.80×10^{6}	0.00.0[(f)]	2.80×10^{6}	this work[(g)]
DA2		$R_i + X \xrightarrow{k_a} R_iX$	1.09×10^{6}	0.0[(f)]	1.09×10^{6}	this work[(g)]

(a) Rate coefficients were taken from Bentein et al. [38] at 123°C with activation energies taken from Woloszyn et al.[62].(b) Propagation rate coefficient for R0,1 is assumed to be equal to be the one of the 2-(alkoxy)carbonylprop-2-yl radical [67].(c) Based on reference [62, 68], the propagation reactivity of the R0,2, R0,3 and R0,4 radicals is assumed to be equal.(d) Only recombination is considered as termination mode [2], no intrinsic rate coefficients needed as apparent rate coefficients are directly used (see Appendix).(e) Rate coefficient taken from Fu et al. [65] at 120°C with activation energy taken from Pryor et al. [66]. This activation energy is in agreement with quantum chemical calculations by Khuong et al. [69].(f) Activation energies for deactivation reactions were set equal to zero, since the deactivation rate coefficient exhibit a very weak temperature dependence [46, 51]. (g) Estimated in this work; confidence intervals are shown in Table 3.2 using reparametrized pre-exponential factors (Equation (3.1)).

Chain transfer to monomer as well as chain transfer to dimer are considered (reactions CT1-4 in Table 3.2), as it has been indicated that these side reactions play an important role at elevated temperatures, both under controlled and free radical polymerization conditions.[38, 70, 71]. Based on literature data,[72] chain transfer to polymer can be neglected, especially at the low/intermediate conversions (X_m < 0.65) considered in this kinetic study. Note that due to the presence of chain

transfer reactions, four initiator radical types (reactions CI1-4 in Table 3.2) are obtained: $R_{0,1}$, $R_{0,2}$, $R_{0,3}$ and $R_{0,4}$. For the former species, a different propagation reactivity compared to the macrospecies R_i is considered, as suggested in previous kinetic studies.[46, 52]

For NMP activation/deactivation (reactions A1 and A2 / DA1 and DA2 in Table 3.2), a distinction is made between initiator and macrospecies, in agreement with literature data.[19, 46] Note that the NMP activation relates to the cleavage of the N-OC bond in Figure 3.1(c). The competitive NO-C bond cleavage, which is a degradation reaction, can be safely neglected [19, 73] for the relatively mild reaction conditions studied, simplifying the kinetic description. Furthermore, as indicated above, for BlocBuilder MA initiated NMP, disproportionation reactions leading to hydroxylamine formation can be ignored.[40] Moreover, the absence of a rate acceleration in the conversion profiles (see 'Results and Discussion') indicates that also hydroxylamine formation via transfer reactions with SG1 can be ignored.

The Arrhenius parameters of the considered reactions and the corresponding intrinsic rate coefficients at 120°C are also given in Table 3.2. The NMP activation/deactivation parameters are estimated in this work using the Levenberg-Marquardt algorithm (ODRPACK v2.01),[74] while the other parameters are taken from literature. However, based on literature data, the activation energy for the deactivation reaction is assumed zero, leading to 6 Arrhenius parameters to be estimated (see Table 3.2). To minimize the binary correlation between the pre-exponential factors and the corresponding activation energies reparametrization is performed for the activation reactions, selecting a reference temperature $\bar{T}$ of 120°C:

$$k = A^* \exp\left(-\frac{E_a}{R}\left(\frac{1}{T}-\frac{1}{\bar{T}}\right)\right) \tag{3.1}$$

in which k is the intrinsic rate coefficient, A^* is the reparametrized pre-exponential factor and E_a the activation energy.

As objective function for the regression analysis Equation (*3.2*) is used:

$$S(\boldsymbol{b}) = \sum_{i=1}^{n} (\boldsymbol{y}_i - \hat{\boldsymbol{y}}_i)^T \boldsymbol{W} (\boldsymbol{y}_i - \hat{\boldsymbol{y}}_i) \tag{3.2}$$

In this equation, the parameter estimates are stored in the vector $\boldsymbol{b}$, and the vector $\mathbf{y_i}$ and $\hat{y}i$ respectively contain the measured and calculated conversions, number average chain lengths and dispersities for the i^{th} experimental data point. The weights of the regression are stored in the matrix $\boldsymbol{W}$. For a detailed description on the calculation of this weights and on the regression analysis procedure in general the reader is referred to the work of De Roo *et al.* [75] and Toloza Porras *et al.*[76] To avoid long simulation times during the parameter estimation, a deterministic solver is selected. The related continuity equations are integrated in a similar manner as described by Bentein *et al.*[38] It should be noted that dilution due to the addition of decane (internal standard) is taken into account in these simulations.

To account for the effect of the chain length dependency and viscosity increase on the diffusivity of the macroradicals,[77-80] chain length and conversion dependent apparent termination rate coefficients are considered. Apparent homo-termination rate coefficients, in which the chain length is assumed to be equal to the number average chain length, are calculated using the so-called composite k_t-model as developed by Johnston-Hall *et al.*[64] The corresponding parameters are provided in Table S.2 in Appendix. For simplicity, diffusional limitations on the activation/deactivation process, are neglected. As indicated in literature,[79, 81-83] only at conversions at which the viscosity has increased significantly (typically $X_m > 0.65$) and for sufficiently bulky nitroxides, such as SG1, the regular activation-growth-deactivation process can

be hindered by diffusional limitations. In this work, experimental data are therefore only analyzed up to intermediate conversions (X_m < 0.65) at which the effect of diffusional limitation on the activation/deactivation process can be expected to be limited, at least for sufficiently high polymerization temperatures. Similarly, diffusional limitations on propagation can be neglected as they are only important under very viscous conditions at low polymerization temperatures.[79]

For the detailed analysis of the simulation results after the regression analysis step, kinetic Monte Carlo (*k*MC) simulations are performed, allowing an explicit visualization of the polymer chains. The principle of this *k*MC method is explained in earlier work,[55-57] and includes a differentiation of chains based on their chain length and living/dead nature. In this contribution, the visualization procedure is extended with a classification according to the chain initiation mechanism (reactions CI1-4 in Table 3.2) and the dead polymer formation reaction path.

For the chain initiation involving dimer radicals (reactions CT3-4 in Table 3.2), an additional distinction is made according to the origin of the corresponding initiator radical $R_{0,3}$, which is either formed via chain transfer to dimer (reactions CT3-4 in Table 3.2) or thermal initiation (reaction TI3 in Table 3.2). In the remainder of the text, these species are denoted respectively as $R_{0,3*}$ and $R_{0,3**}$, as also specified in Figure 3.7. For the dead polymer formation, a subdivision is made according to dead polymer chains formed by recombination (reactions T1-3 in Table 3.2), chain transfer event to monomer (reactions CT1-2) and chain transfer to dimer (reactions CT3-4 in Table 3.2). Importantly, in Appendix, it is shown that both the deterministic and stochastic solver give identical results for the evolution of the conversion and average polymer properties with time, highlighting the high numerical accuracy of the developed kinetic model.

3.4 Results and discussion

In this section, a detailed kinetic study of the NMP of styrene initiated by BlocBuilder MA is presented. Based on an extensive experimental data set, covering both a broad range of temperatures (90-120°C) and TCLs (50-1000), experimental data on conversion, number averaged chain length, and dispersity are first used to estimate NMP specific (de)activation Arrhenius parameters. In a next step these parameters are employed to quantify the contribution of the various chain initiation steps, including the contribution of chain transfer to monomer and dimer. Finally, these parameters are used to perform a model-based optimization of the NMP process at elevated temperatures, focusing on the application of stepwise temperature programs.

3.4.1 Estimation of activation and deactivation kinetic parameters

Table 3.3 gives an overview of the estimated reparameterized activation pre-exponential factors, *i.e*. the estimated activation rate coefficients at 120°C (Equation (*3.1*)), the corresponding estimated activation energies and the estimated deactivation pre-exponential factors. All estimates are accompanied by their 95% confidence interval. It can be clearly derived that all six parameters have been estimated significantly. The F-value, which is a measure for the global significance of the regression, also largely exceeds the tabulated F-value (F_{calc} = 1.22 10^4 versus F_{tab} = 3.09), confirming the highly statistical relevance of the developed deterministic kinetic model.

Moreover, based on the correlation matrix (Table A.3 in Appendix) it follows that the estimates are only weakly correlated, *i.e.* the recorded experimental data allow a reliable assessment of each individual kinetic parameter in a relatively independent way. Hence, in the present study the strong correlation of the pre-exponential factor and the activation energy, as often encountered in literature, could be circumvented, further highlighting the high accuracy of the reported estimates.

Table 3.3. *Estimated Arrhenius parameters for (de)activation reactions in the NMP of styrene initiated by MAMA-SG1 (BlocBuilder MA) and their 95% confidence intervals; dormant macrospecies denoted as PS-SG1; for activation: reparameterized pre-exponential factor A* (Equation* (3.1)*) is given while the corresponding A is given in Table 3.2; subscript "0,1" refers to the NMP initiator MAMA-SG1 (Table 3.2).*

Reaction	Parameter		Estimated value
Activation MAMA-SG1	$A*_{a0,1}$	(s^{-1})	$(1.2 \pm 0.1) \times 10^{-1}$
	$E_{a,a0,1}$	(kJ mol^{-1})	105.3 ± 1.5
Activation PS-SG1	$A*_{a}$	(s^{-1})	$(7.1 \pm 0.5) \times 10^{-3}$
	$E_{a,a}$	(kJ mol^{-1})	148.8 ± 2.0
Deactivation MAMA + SG1[(a)]	$A_{da0,1}$	(L $mol^{-1}s^{-1}$)	$(2.1 \pm 0.5) \times 10^{6}$
Deactivation PS + SG1[(a)]	$A_{da0,1}$	(L $mol^{-1}s^{-1}$)	$(1.1 \pm 0.1) \times 10^{6}$

[(a)]Activation energy for deactivation reactions was fixed at zero based on literature data [53].

For the activation of the NMP initiator (MAMA-SG1) (reaction A1 in Table 3.2), both the resulting activation rate coefficient of 1.18×10^{-1} s^{-1} at 120°C and the activation energy of 105.3 kJ mol^{-1}, are well in line with typical values reported in literature. In particular, Bertin *et al.* [47] reported values of 2.80×10^{-1} s^{-1} and 112.3 kJ mol^{-1}. Similarly, for the activation of the dormant macrospecies (PS-SG1) (reaction A2 in Table 3.2), the intrinsic value obtained in this work at 120°C (k_a = 7.08×10^{-3} s^{-1}) agrees well with literature data. For instance, via electron paramagnetic resonance measurements (EPR) Bertin *et al.* [84] obtained a slightly lower average value of 5.6×10^{-3} s^{-1}, and using a GPC resolution method Goto *et al.* [48] obtained a slightly higher value of 1.1 x 10^{-2} s^{-1}. On the other hand, the corresponding estimated activation energy , *i.e.* 148.7 kJ mol^{-1}, is *ca.* 18 kJ higher compared to the one reported by Goto *et al.*[48] The latter and

present kinetic study confirm, however, the higher temperature dependency for activation of dormant macrospecies compared to the NMP initiator. In this contribution, an estimated difference of 43 kJ mol^{-1} is reported.

For the deactivation of polystyryl radicals with SG1 (reaction DA2 in Table 3.2), a rate coefficient of 1.09×10^6 mol L^{-1} s^{-1} is obtained in this work which is to a first approximation similar to the value of 5.30×10^5 mol L^{-1} s^{-1} determined by Guillaneuf *et al.* [50] and with the value of 5.70×10^5 mol L^{-1} s^{-1} obtained by Benoit *et al.* [52] Note that for the deactivation of the NMP initiator species (reaction DA1 in Table 3.2), to the best of the author's knowledge, no direct comparison can be made with literature data, highlighting the strength of the proposed regression approach to obtain all relevant activation/deactivation parameters simultaneously.

The corresponding parity diagrams are shown in Figure 3.2, while including a normalization with respect to the TCL for the second response, *i.e.* the number average chain length x_n. On an overall basis the three responses are modeled in a satisfactory manner, since all points are in the close vicinity of the bisector. The highest model performance is obtained for the conversion profiles and the number averaged chain length. For the dispersity, a somewhat larger discrepancy between experimental and calculated values is however observed, which can be partially attributed to the larger experimental error on the dispersity values, in particular at low average chain lengths.[85]

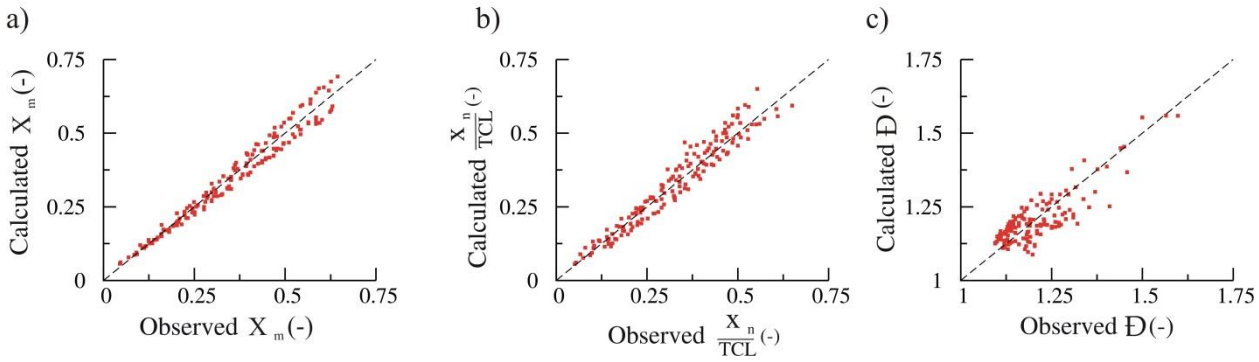

Figure 3.2. *Parity diagrams for (a) the conversion (X_m) (b) the ratio of the number averaged chain length (x_n) to the TCL (c) the dispersity (Đ).*

In Figure 3.3 the simulated and experimental responses are compared at distinct polymerization temperatures and TCLs (entry 1-11 in Table A.1), using the Arrhenius parameters given in Table 3.2. The plots for the other conditions (entry 12-16 in Table A.1) can be found in Appendix (Figure A.4). In agreement with the parity plots, the experimental trends are well captured by the kinetic model, in particular for the higher temperatures studied (110°C and 120°C).

The deviations for x_n and dispersity at lower temperatures (90°C and 100 °C) and higher conversions could be ascribed to the possible interference of diffusional limitations on the activation/deactivation process [79] and even on propagation, as also indicated by Roa Loa *et al.*[86] Diffusional limitations on (de)activation and propagation steps are however neglected in the current kinetic model, as indicated above. At low temperatures, chain transfer reactions can be neglected but a more viscous polymer-monomer mixture is obtained at a given conversion, in particular in case higher chain lengths are formed. As can be seen in Figure 3.3 (top two rows) a more pronounced deviation is obtained for a higher TCL at higher conversions, supporting the hypothesis that such diffusional limitations are indeed the reason for the observed discrepancy at the lower temperatures studied. It should however be stressed that these data points are of low added value in case the NMP process would be industrially applied.

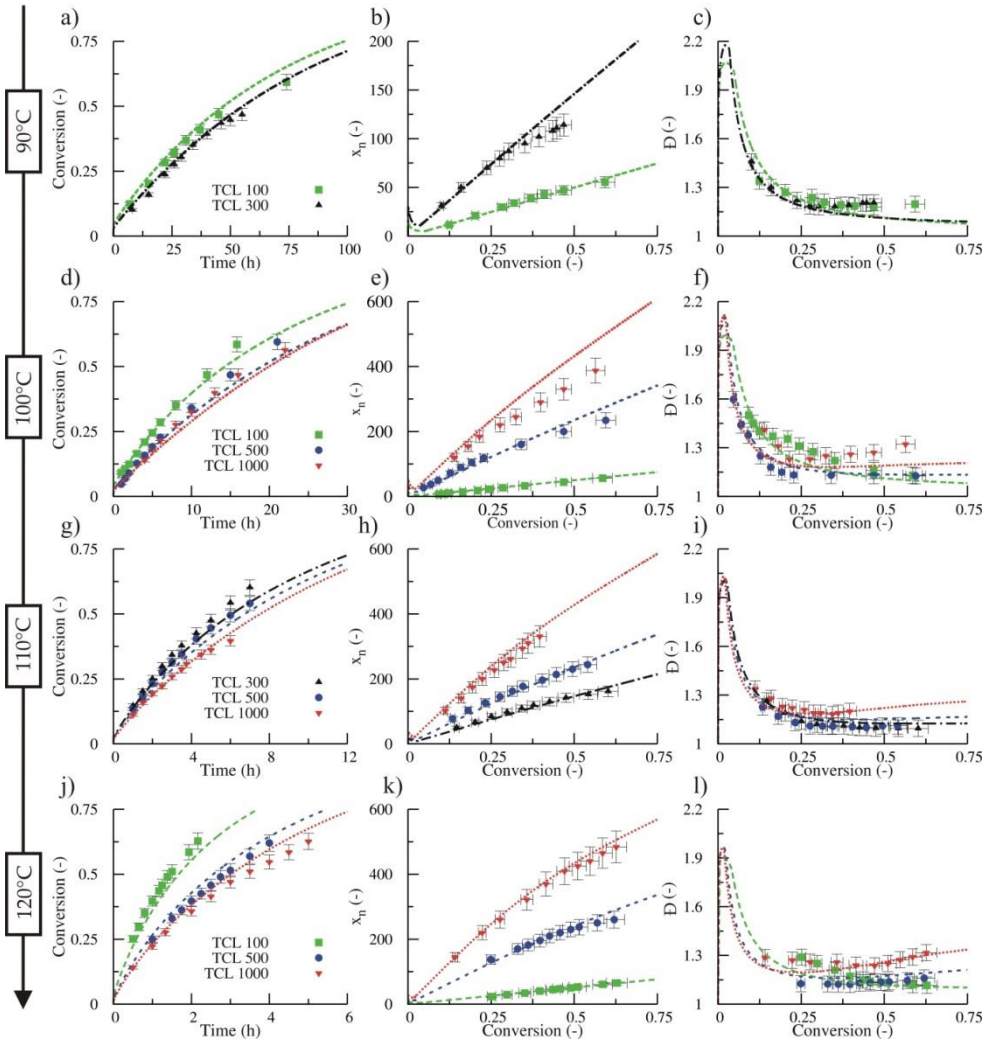

Figure 3.3. *Comparison between simulations and experiments: effect of temperature for different TCLs (a),(d),(g),(j) Conversion as a function of time; (b),(e),(h),(k) number-average chain length (x_n); (c),(f),(i),(l) dispersity (Đ) as a function of conversion for the NMP of styrene initiated by BlocBuilder MA at 90°C, 100°C, 110°C, and 120°C. (■, green) corresponds to a TCL of 100; (▲, black) corresponds to a TCL of 1000; (●, blue) corresponds to a TCL of 500; (▼, red) corresponds to a TCL of 1000; lines correspond to calculated values with set of parameters given in Table 3.2; deterministic solver used; entries 1-11 in Table A.1 in Appendix.*

Note that at the higher temperatures in Figure 3.3 (110°C and 120°C) the influence of the TCL on the conversion profile is rather limited. In contrast to classical RDRP systems, in styrene NMP at elevated temperatures thermal initiation occurs. Simulations indicated that upon an increase of

TCL thermal initiation compensates more for the lower number of radicals generated from the NMP initiator species.

Furthermore, the importance of the differentiation between the activation/deactivation kinetics of NMP initiator related species and macrospecies is given in Figure 3.4. In this figure, for a representative condition (entry 8 in Table A.1 in Appendix), the simulation results are compared in case the NMP initiator (de)activation rate coefficients are assumed equal to the corresponding rate coefficients for the macrospecies. Clearly, a strong deviation is obtained, highlighting the necessity to perform a multi-response regression analysis for a reliable estimation of (de)activation kinetic parameters.

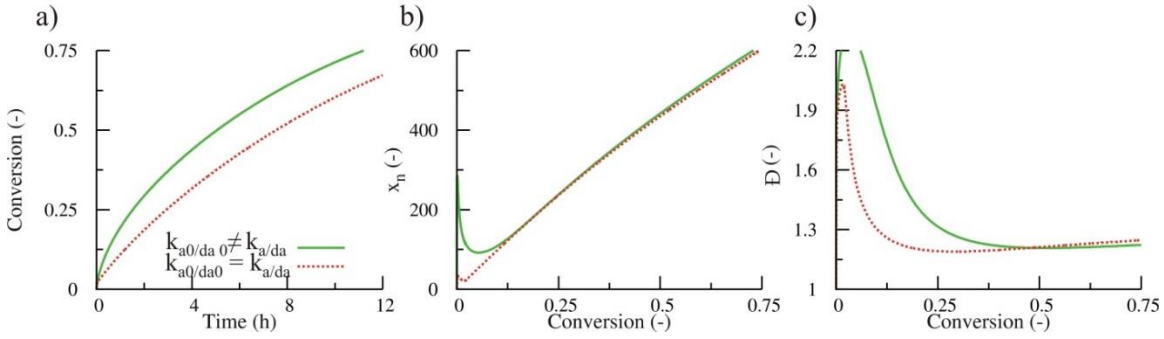

Figure 3.4. *Influence of NMP initiator (BlocBuilder) activation intrinsic rate coefficient on the simulation of the NMP of styrene at T = 110°C and TCL = 1000 (entry 8 in Table A.1 in Appendix).(a) conversion as a function of time, (b) number-average chain length (x_n) and (c) dispersity (Đ) as a function of conversion; red dashed lines correspond to the simulation with the kinetic parameter set given in Table 3.2, green full lines correspond to the simulation with the kinetic parameter set given in Table 3.2 but under the assumption that $k_{a,0} = k_a$ and $k_{da,0} = k_{da}$; deterministic solver.*

3.4.2 Importance of side reactions

As indicated in the previous section, the estimation of the activation/deactivation parameters has been performed using a deterministic solver considering three responses, namely the conversion,

the number averaged chain length, and the dispersity. The last two of these responses are, however, average properties of the measured CLD. Using the more advanced kinetic Monte Carlo (*k*MC) method [56, 57] the actual CLD can be simulated, as illustrated in Figure 3.5 (top row) for a TCL of 100, 500 and 1000 at a conversion of 0.50 and a polymerization temperature of 120°C (black dashed lines). This figure also includes a comparison with the experimentally obtained SEC traces (red dots). Importantly, as indicated above, the corresponding kMC conversion profile and evolution of the average properties benchmark with the deterministic simulation output used for the regression analysis.

As can be seen in Figure 3.5 (a)-(c), for all three TCLs, a good agreement between the simulation and experimental results is obtained. The slight deviations at lower chain lengths can be partly attributed to the difficulty of measuring the chain length of oligomeric chains. For the higher TCLs, a clear fronting, *i.e.* the significant presence of oligomeric chains, can be observed. For a TCL of 300, the good agreement between the SEC and simulated CLD data at distinct conversions is illustrated in Figure A.5 (Appendix). This good agreement between the experimental and the simulated CLD data for different reaction conditions thus strengthens the validity of the obtained parameter set during the regression analysis.

In Figure 3.5 (d)-(f) the CLDs presented in Figure 3.5 (a)-(c) are subdivided according to their "living nature", *i.e.* a differentiation is made between the contribution of the dormant polymer chains (blue) and the dead polymer chains (green), ignoring the negligible contribution of the macroradicals. Note that these additional profiles are scaled with respect to all polymer chains, and thus are not normalized *per se*, *i.e.* the area under the curves can be different from one. For the lower TCLs, it is observed that rarely any dead polymer chain is formed, indicative of the limited importance of termination and chain transfer reactions. For the higher TCLs, however, an

increase of the dead polymer population can be clearly observed and both the dead and dormant population are characterized by a fronting behavior, implying a significant contribution of chain transfer reactions, in agreement with literature data.[38]

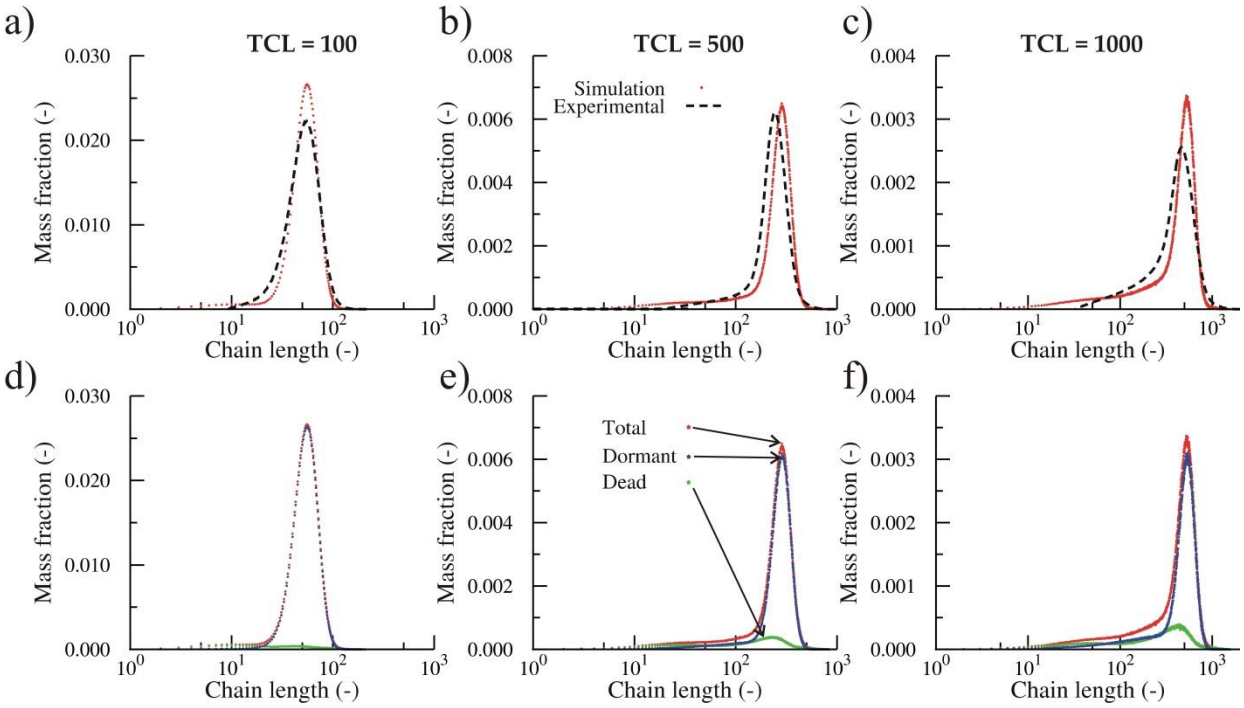

Figure 3.5. *Chain length distributions (CLDs) obtained via SEC measurements (black dashed line) and via kMC simulation results (red points) for a TCL of (a) 100 (X_m = 0.51), (b) 500 (X_m = 0.52), (c) 1000 (X_m = 0.48); Subdivision of CLD (red dots) into individual contribution of dormant polymer chains (blue dots) and dead polymer chains (green dots) at same conditions as for (a),(b),(c), respectively; entry in 9-11 in Table S.1 (Appendix).*

Moreover, the *k*MC technique allows to track the reaction event history, allowing a subsequent differentiation according to the chain initiation step, *i.e.* the step leading to the incorporation of the first monomer unit, and the nature of the dead polymer product. In these kMC simulations, a representative number of macrospecies (starting from *ca.* 2.5×10^7 monomer molecules) is tracked throughout the polymerization. For visualization purposes, however, a random selection

of maximum 750 chains is performed. A different number of chains can be actually obtained per selection, as the number of total chains tracked can be different taking into account that thermal initiation and chain transfer lead to extra chains, compared to the classical NMP reactions.

For a polymerization temperature of 120°C and a TCL of 1000 (entry 11 in A.1 (Appendix)), this explicit visualization is presented in Figure 3.6 at a conversion of 0.1, 0.4 and 0.7. A first distinction is made between the dead and dormant species (top vs. bottom part) and a second distinction is made via their chain initiation (reaction CI1-4 in Table 3.2) or dead polymer formation (reaction CT1-4 and T1-3 in Table 3.2) mechanism, following the colors of the reactions depicted in Figure 3.6 (c). As indicated above, for the dimer radicals ($R_{0,3}$ in Table 3.2) an additional superscript * or ** is introduced to denote their formation by chain transfer and thermal initiation, respectively.

The dormant polymers chains obtained via chain initiation involving a $R_{0,1}$ radical released by activation of BlocBuilder (reaction A1 in Table 3.2), are represented in blue. On the other hand, dormant species obtained via chain initiation of the radicals, $R_{0,3}^{*}$ or $R_{0,4}$, which are respectively formed upon chain transfer to dimer and monomer (reactions CT3-4 and CT1-2, respectively, in Table 3.2), are depicted in orange and green. Dormant species could alternatively have been initiated via the thermal initiation Mayo mechanism (yellow lines), in which 3 monomer units react forming two initiating radicals $R_{0,2}$ and $R_{0,3}^{* *}$(reaction T3 in Table 3.2) Note that, from a chemical point of view, and as shown in Figure 3.7, the initiator radical $R_{0,3}^{**}$ being formed via thermal initiation is identical to the radical formed by the transfer to dimer reaction ($R_{0,3}^{*}$).

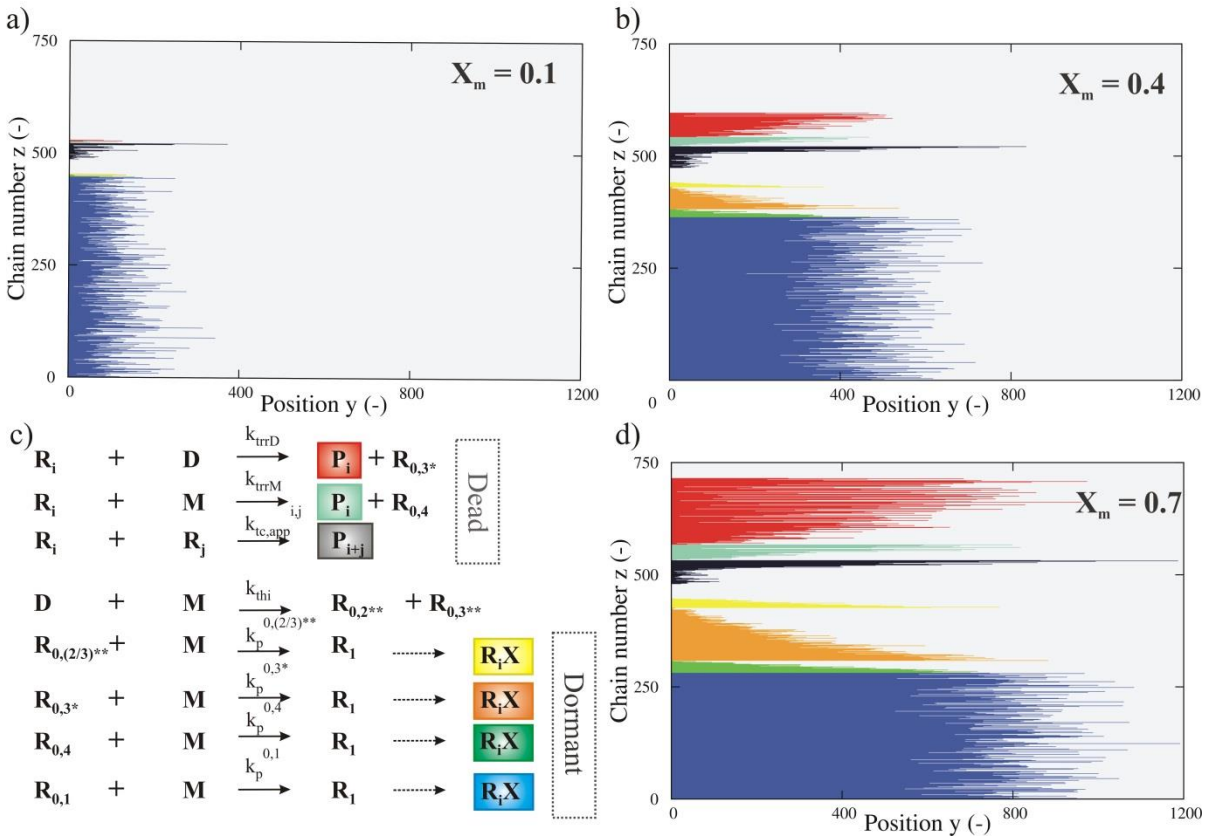

Figure 3.6. *Kinetic Monte Carlo based visualization of a representative number of polymer chains according to their dead or dormant nature and chain initiation for the NMP of styrene initiated by BlocBuilder MA (TCL = 1000; 120°C; entry 11 in Table A.1 (Appendix) at three different conversion: (a) X_m = 0.1, (b) X_m = 0.4, and (d) X_m = 0.7. (c) explanation of color code used with the boxed species corresponding to the macrospecies being visualized. From top to bottom: for dead polymer chains: termination product via transfer to dimer reactions (CT3-4 in Table 3.2; red), termination product via chain transfer to monomer (CT1-2 in Table 3.2; teal), termination via recombination (T1-3 in Table 3.2; black); for dormant chains a distinction is made according to the chain initiation event: chain initiation via radicals ($R_{0,2}$ and $R_{0,3*}$) formed upon thermal initiation(TI3 in Table 3.2; yellow), initiation by radical ($R_{0,3**}$) originating from chain transfer to monomer/dimer (CT1-2/3-4 in Table 3.2; green/orange), initiation via NMP initiator radical (A1 in Table 3.2; blue), initiator radical $R_{0,3}^{**}$ being formed via thermal initiation is identical to the radical formed by the transfer to dimer reaction ($R_{0,3}^{*}$): see Figure 3.7; note in Table 3.2:only $R_{0,3}$ is used and not $R_{0,3}^{*}$ and $R_{0,3}^{**}$.*

However, both products have to be distinguished to allow for a differentiation upon chain initiation, as envisaged in Figure 3.6. When a dead polymer chain is formed, *i.e*. via termination by recombination (reactions T1-3 in Table 3.2) or chain transfer to dimer or monomer (reactions CT3-4 and CT1-2, respectively, in Table 3.2), this chain is also labeled according to the underlying reaction event. The respective colors are black, red and teal. Note that for termination no further differentiation is made with respect to the end-groups involved to avoid overloading the figure.

At low conversion (X_m = 0.1) it can be seen that the dormant polymer chain fraction (bottom part in Figure 3.6 (a),(b),(d)) predominantly exists of chains initiated by the NMP initiator (EGF ≈ 0.90). The small dead fraction is primarily composed of dead polymer chains formed by termination reactions via recombination, taking into account that the persistent radical effect is not established instantaneously.[21] At the higher conversions, the fraction of dead chains is however gradually increasing, which can be mainly attributed to chain transfer to dimer reactions (red), especially at the highest conversion studied (X_m = 0.7). It can also be observed that chain transfer to monomer (teal) has a non-negligible contribution to the formation of the dead polymer product, and thus also to the formation of oligomeric dormant species (green).

A rather remarkable conclusion from Figure 3.6 is that only a limited fraction of dormant chains is formed directly via the thermal initiation mechanism (yellow) at the elevated temperature of 120°C. This can however be explained by the high importance of the chain transfer to dimer compared to the competitive molecule assisted homolysis. Both reactions consume a dimer molecule, but in the former a dead species is formed so that on a net basis no extra radicals are formed. In addition, the continuous formation of extra radicals via the molecule assisted

homolysis, leads to an imbalance for the mediating agent vs. the active species, enhancing the relevance of termination reactions.

Finally, it follows that despite the presence of diffusional limitations on termination, the formation of dead polymer chains cannot be avoided, which is visualized by the appearance of the longer (black) polymer chains at higher conversion. The latter is agreement with earlier work of Goto and Fukuda [87] and recent work of Zhong *et al.* [88] on related RDRP systems.

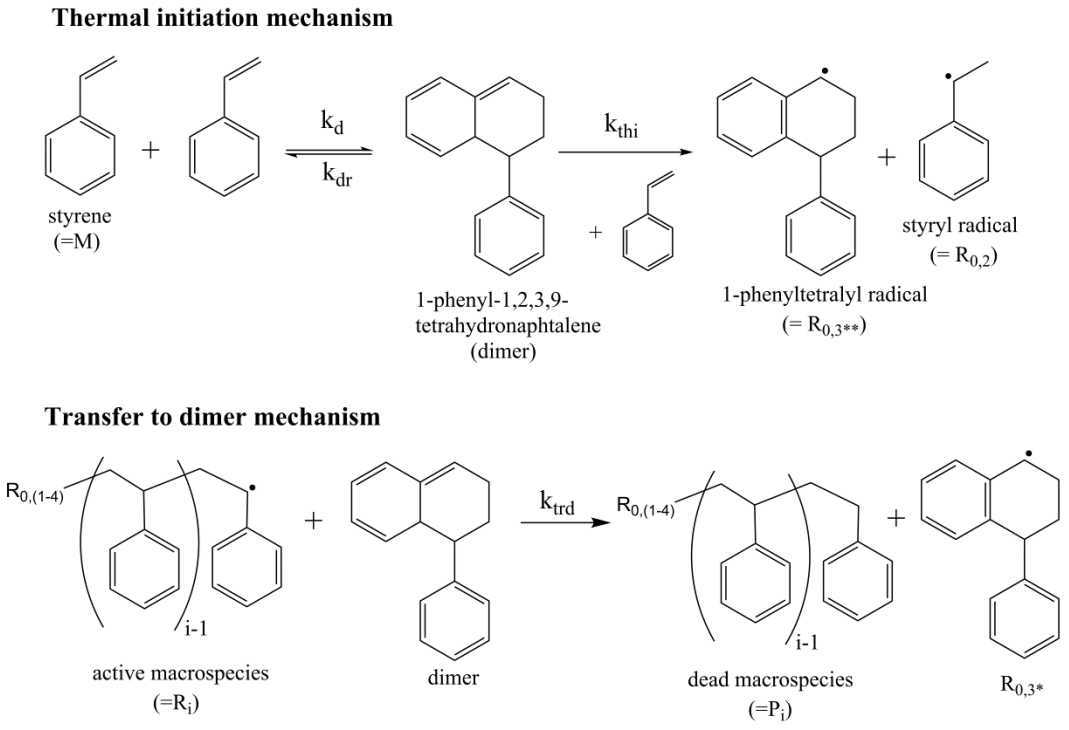

Figure 3.7. *Reactions leading to the chain initiating steps corresponding with Figure 3.6.*

3.4.3 Model-based optimization via a stepwise temperature program

In this section, a model-based optimization strategy is applied, benefiting from the aforementioned successful regression analysis procedure to retrieve reliable activation/deactivation Arrhenius parameters. A similar strategy was already followed for FRP [89] and very recently for atom transfer radical polymerization (ATRP), a related CRP technique.[90]

The aim of this optimization is the synthesis of a better defined polystyrene product at a TCL of 1000 within the same reaction time as for an isothermal NMP at 120°C to reach a conversion of 0.70. The latter polymerization temperature is selected as a reference temperature, since it allows a sufficiently high conversion within a reasonable reaction time.

Simulations indicated that following stepwise temperature program is most suited. First the polymerization temperature is set at 103°C for 30 minutes, after which the polymerization temperature is raised to a value of 117°C for the remainder of the polymerization. Note that the use of a temperature increase in the NMP process was previously highlighted by Chauvin *et al.*,[46] focusing mainly on the importance of a sufficiently high NMP initiator activation rate at low conversions and less on the optimization of the NMP process as such.

A comparison of the isothermal and non-isothermal case, is presented in Figure 3.8(a), in which the conversion, average chain length and dispersity profiles are given, as obtained by deterministic simulations and as experimentally recorded. As can be seen, the trends observed in the simulations are also confirmed by the experimental results, highlighting again the high accuracy of the Arrhenius activation/deactivation parameters obtained in this work. Despite the much lower polymerization temperature in the first 30 minutes and the slightly lower polymerization temperature throughout the remaining time of the polymerization, the conversion profile using the stepwise program converges towards the one of the isothermal polymerization. Importantly, under the selected non-isothermal conditions, slighty higher x_n, and lower dispersity values are obtained, reflecting a higher polymer product quality.

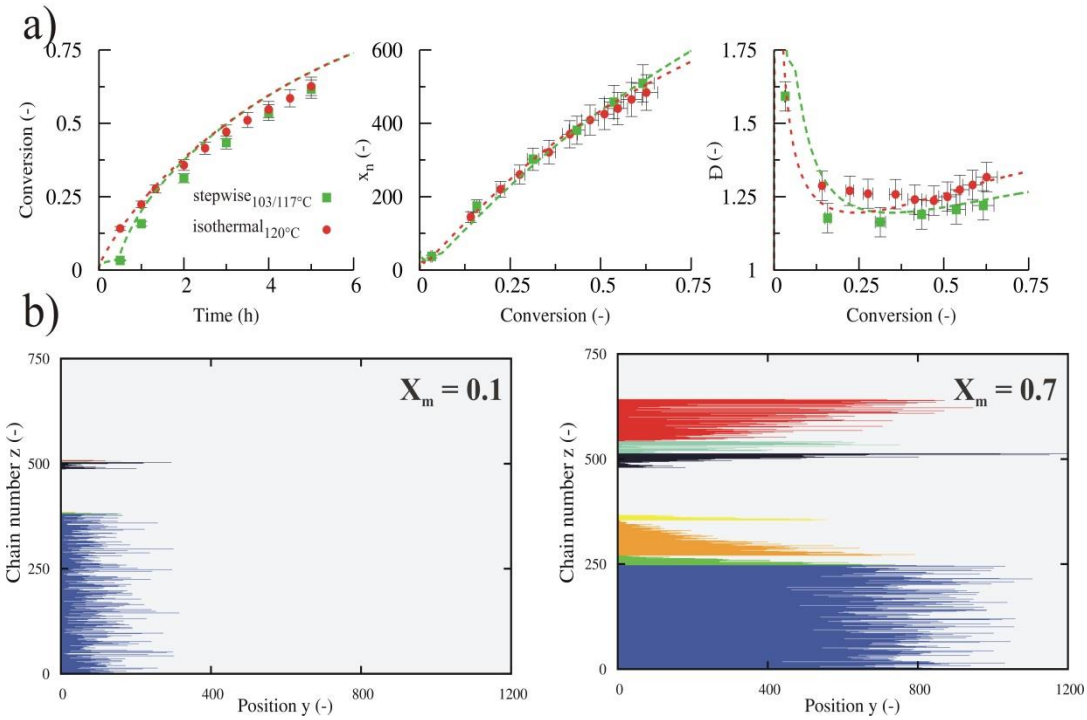

Figure 3.8. *(a) Comparison between experimental and deterministic simulation results for NMP of styrene initiated by BlocBuilder MA (TCL = 1000): (●,red) isothermal case (T = 120°C), and (■,green) the non-isothermal case with a stepwise temperature program (T = 103°C (0-0.5h) – T = 117°C (0.5-6h)); from left to right: conversion as a function of time, number average chain length and dispersity as a function of conversion; lines correspond to calculated values with the set of parameters given in Table 3.2 (b) detailed kMC representation of a representative number of polymer chain for the non-isothermal case; same colors as in Figure 3.6.*

Detailed kMC simulations for the non-isothermal case at X_m = 0.1 and X_m = 0.7 are displayed in Figure 3.8 (b) and reveal the underlying causes of the observed behavior. Comparison of the results at X_m = 0.1 with those from the isothermal polymerization (Figure 3.6 (a)) allows to deduce that a *ca.* 50% smaller fraction of dead chains is formed with the improved model-based method, implying a different intensity of the persistent radical effect at low polymerization times. Due to the lower initial polymerization temperature with the stepwise program, the release of $R_{0,1}$

species (reaction A1 in Table 3.2) is delayed (Figure 3.9 (a)), leading to less termination reactions and thus a higher livingness. The latter phenomenon implies a less pronounced build-up of nitroxide species (Figure 3.9 (b)), explaining the faster polymerization rate at higher polymerization times, eventually leading to the same polymerization time to reach the targeted conversion of 0.70 (Figure 3.8 (a)).

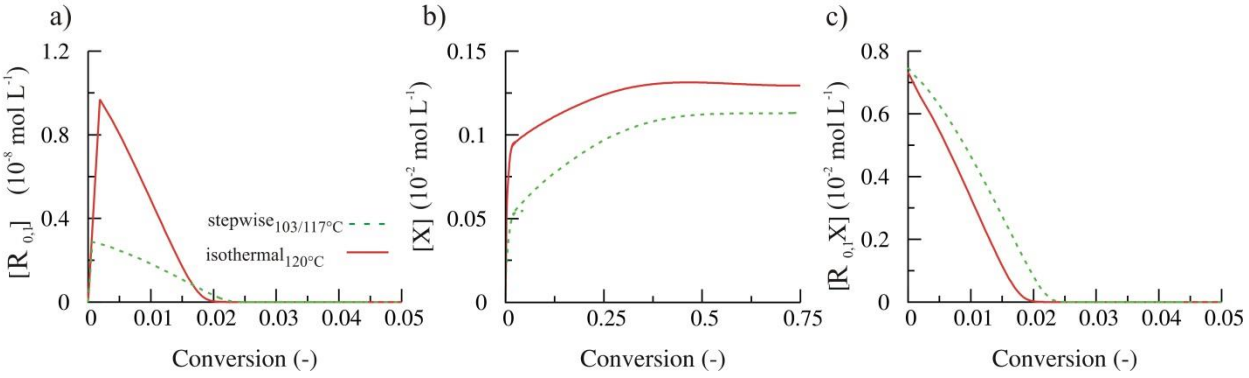

Figure 3.9. *(a) Concentration of the radical ($R_{0,1}$) released upon activation of the NMP initiator ($R_{0,1}X$); (b) Concentration of the persistent nitroxide radical (SG1) (X); (c) Concentration of the NMP initiator ($R_{0,1}X$) as a function of conversion; conditions see Figure 3.8 with green dashed lines (isothermal case) and red full lines (stepwise temperature program).*

On the other hand, a slower release of $R_{0,1}$ species is accompanied by a slower NMP initiation on a conversion basis (Figure 3.9 (c)), explaining the somewhat higher dispersity values at low conversions for the non-isothermal case (≤ 0.2). However, at higher conversions the latter effect is counteracted by the higher livingness, explaining the better control over chain length with the stepwise temperature program. The latter can also be inferred from a comparison of the explicit kMC visualizations at $X_m = 0.7$ (Figure 3.6 (d) vs. Figure 3.8 (b)). Clearly, the amount of dead polymer formed by chain transfer to dimer is smaller for the non-isothermal case (Figure 3.8 (b)), which can be linked to the lower temperature along the whole NMP, consistent with the lower measured dispersities (Figure 3.8 (a)).

3.5 Conclusions

For the NMP of styrene initiated by MAMA-SG1, regression to an extensive set of isothermal experimental data allowed to identify that the activation step for the NMP initiator is *ca.* 43 kJ mol^{-1} less activated than the corresponding macro-activation. At 120°C, values of 1.18×10^{-1} s^{-1} and 7.08×10^{-3} s^{-1} are obtained for the respective activation rate coefficients, in agreement with literature data. Deactivation is however slightly favored for the NMP initiator radicals (2.08×10^{6} vs. 1.09×10^{6} L mol s^{-1}).

A sufficiently high polymerization temperature (> 110°C) should be selected to ensure a high monomer conversion within a reasonable polymerization time. However, at such temperatures a clear fronting in the CLD is obtained at high TCLs (>300), which is reflected both in the dead and dormant population. Moreover, kMC simulations in which polymer chains are not only organized according to their dormant or dead nature but also with respect to their chain initiation, revealed that chain transfer to dimer is the main contributor to this loss of control over chain length. Based on these kMC simulations, it also follows that diffusion controlled termination reactions and chain transfer to monomer reactions cannot be neglected throughout the NMP.

A stepwise temperature program, as obtained via model-based optimization, can partially resolve the lack of control at 120°C and high TCLs by a suppression of chain transfer to dimer reactions, as experimentally confirmed by a drop of the dispersity at high conversions. The applied strategy of the consideration of a non-isothermal program for improved control can be extended to other RDRP processes, provided that the activation/deactivation Arrhenius parameters are obtained based on a multi-response regression analysis covering a broad temperature and TCL range.

References

1. Asua, J., *Polymer Reaction Engineering*. Wiley: 2007.

2. Matyjaszewski, K., *Handbook of Radical Polymerization*. 2002.

3. Gody, G.; Maschmeyer, T.; Zetterlund, P. B.; Perrier, S. Rapid and quantitative one-pot synthesis of sequence-controlled polymers by radical polymerization. *Nat. Commun.* **2013,** 4, 9.

4. Junkers, T.; Zang, L.; Wong, E. H. H.; Dingenouts, N.; Barner-Kowollik, C. Formation of Triblock Copolymers via a Tandem Enhanced Spin Capturing-Nitroxide-Mediated Polymerization Reaction Sequence. *J. Polym. Sci. Pol. Chem.* **2011,** 49, (22), 4841-4850.

5. Qiao, X. G.; Lansalot, M.; Bourgeat-Lami, E.; Charleux, B. Nitroxide-Mediated Polymerization-Induced Self-Assembly of Poly(poly(ethylene oxide) methyl ether methacrylate-co-styrene)-b-poly(n-butyl methacrylate-co-styrene) Amphiphilic Block Copolymers. *Macromolecules* **2013,** 46, (11), 4285-4295.

6. Matyjaszewski, K. Atom Transfer Radical Polymerization: From Mechanisms to Applications. *Israel Journal of Chemistry* **2012,** 52, (3-4), 206-220.

7. Vachaudez, M.; D'hooge, D. R.; Socka, M.; Libiszowski, J.; Coulembier, O.; Reyniers, M. F.; Duda, A.; Marin, G. B.; Dubois, P. Inverse dependencies on the polymerization rate in atom transfer radical polymerization of N-isopropylacrylamide in aqueous medium. *Reactive and Functional Polymers* **2013,** 73, (3), 484-491.

8. Jiang, J.; Zhang, Y.; Cao, D.; Jiang, P. Controlled immobilization of methyltrioxorhenium(VII) based on SI-ATRP of 4-vinyl pyridine from halloysite nanotubes for epoxidation of soybean oil. *Chem. Eng. J.* **2013,** 215–216, (0), 222-226.

9. Matyjaszewski, K. Macromolecular engineering: From rational design through precise macromolecular synthesis and processing to targeted macroscopic material properties. *Progress in Polymer Science* **2005,** 30, (8-9), 858-875.

10. Pedrón, S.; Anseth, K.; Benton, J. A.; Bosch, P.; Peinado, C. Bioapplications of Networks Based on Photo-Cross-Linked Hyperbranched Polymers. *Macromol. Symp.* **2010,** 291-292, (1), 307-313.

11. Sangermano, M.; Chiolerio, A.; Veronese, G. P.; Ortolani, L.; Rizzoli, R.; Mancarella, F.; Morandi, V. Graphene–Epoxy Flexible Transparent Capacitor Obtained By Graphene–Polymer Transfer and UV-Induced Bonding. *Macromol. Rapid Commun.* **2014,** 35, (3), 355-359.

12. Bella, F.; Lamberti, A.; Sacco, A.; Bianco, S.; Chiodoni, A.; Bongiovanni, R. Novel electrode and electrolyte membranes: Towards flexible dye-sensitized solar cell combining vertically aligned TiO2 nanotube array and light-cured polymer network. *Journal of Membrane Science* **2014,** 470, (0), 125-131.

13. Flores, M.; Fernández-Francos, X.; Ramis, X.; Sangermano, M.; Ferrando, F.; Serra, À. Photocuring of cycloaliphatic epoxy formulations using polyesters with multiarm star topology as additives. *J. Appl. Polym. Sci.* **2014,** 131, (6), n/a-n/a.

14. Ciftci, M.; Tasdelen, M. A.; Li, W.; Matyjaszewski, K.; Yagci, Y. Photoinitiated ATRP in Inverse Microemulsion. *Macromolecules* **2013,** 46, (24), 9537-9543.

15. Georges, M. K.; Veregin, R. P. N.; Kazmaier, P. M.; Hamer, G. K. Narrow molecular-weight resins by a free-radical polymerization process. *Macromolecules* **1993,** 26, (11), 2987-2988.

16. Hawker, C. J. Molecular Weight Control by a "Living" Free-Radical Polymerization Process. *J. Am. Chem. Soc.* **1994,** 116, (24), 11185-11186.

17. Hawker, C. J.; Barclay, G. G.; Orellana, A.; Dao, J.; Devonport, W. Initiating Systems for Nitroxide-Mediated "Living" Free Radical Polymerizations: Synthesis and Evaluation. *Macromolecules* **1996,** 29, (16), 5245-5254.

18. Veregin, R. P. N.; Odell, P. G.; Michalak, L. M.; Georges, M. K. The pivotal role of excess nitroxide radical in living free radical polymerizations with narrow polydispersity. *Macromolecules* **1996,** 29, (8), 2746-2754.

19. Nicolas, J.; Guillaneuf, Y.; Lefay, C.; Bertin, D.; Gigmes, D.; Charleux, B. Nitroxide-mediated polymerization. *Progress in Polymer Science* **2013,** 38, (1), 63-235.

20. Rosenfeld, C.; Serra, C.; Brochon, C.; Hessel, V.; Hadziioannou, G. Use of micromixers to control the molecular weight distribution in continuous two-stage nitroxide-mediated copolymerizations. *Chem. Eng. J.* **2008,** 135, Supplement 1, (0), S242-S246.

21. Fischer, H. The Persistent Radical Effect In "Living" Radical Polymerization. *Macromolecules* **1997,** 30, (19), 5666-5672.

22. Kothe, T.; Marque, S.; Martschke, R.; Popov, M.; Fischer, H. Radical reaction kinetics during homolysis of N-alkoxyamines: verification of the persistent radical effect. *Journal of the Chemical Society, Perkin Transactions 2* **1998**, (7), 1553-1560.

23. Ohno, K.; Tsujii, Y.; Miyamoto, T.; Fukuda, T.; Goto, M.; Kobayashi, K.; Akaike, T. Synthesis of a Well-Defined Glycopolymer by Nitroxide-Controlled Free Radical Polymerization. *Macromolecules* **1998,** 31, (4), 1064-1069.

24. Tang, W.; Fukuda, T.; Matyjaszewski, K. Reevaluation of persistent radical effect in NMP. *Macromolecules* **2006,** 39, (13), 4332-4337.

25. Veregin, R. P. N.; Odell, P. G.; Michalak, L. M.; Georges, M. K. Mechanism of rate enhancement using organic acids in nitroxide-mediated living free-radical polymerizations. *Macromolecules* **1996,** 29, (11), 4161-4163.

26. Greszta, D.; Matyjaszewski, K. TEMPO-mediated polymerization of styrene: Rate enhancement with dicumyl peroxide. *Journal of Polymer Science Part A: Polymer Chemistry* **1997,** 35, (9), 1857-1861.

27. Chang, C.-C.; Studer, A. Acceleration of the Styryl-TEMPO-Mediated Controlled Radical Styrene Polymerization by Addition of an Efficient Alkoxyamine. *Macromolecules* **2006,** 39, (12), 4062-4068.

28. He, J. P.; Chen, J. M.; Li, L.; Pan, J. Y.; Li, C. M.; Cao, J. Z.; Tao, Y. F.; Hua, F. J.; Yang, Y. L.; McKee, G. E.; Brinkmann, S. Rate enhancement of nitroxide-mediated living free-radical polymerization by continuous addition of initiator. *Polymer* **2000,** 41, (12), 4573-4577.

29. Malmström, E.; Miller, R. D.; Hawker, C. J. Development of a new class of rate-accelerating additives for nitroxide-mediated 'living' free radical polymerization. *Tetrahedron* **1997,** 53, (45), 15225-15236.

30. Lansalot, M.; Guillaneuf, Y.; Luneau, B.; Acerbis, S.; Dufils, P.-E.; Gaudel-Siri, A.; Gigmes, D.; Marque, S. R. A.; Tordo, P.; Bertin, D. A Step Towards High-Molecular-Weight Living/Controlled Polystyrene Using SG1-Mediated Polymerization. *Macromol. React. Eng.* **2010,** 4, (6-7), 403-414.

31. Georges, M. K.; Veregin, R. P. N.; Kazmaier, P. M.; Hamer, G. K.; Saban, M. Narrow Polydispersity Polystyrene by a Free-Radical Polymerization Process-Rate Enhancement. *Macromolecules* **1994,** 27, (24), 7228-7229.

32. Gryn'ova, G.; Lin, C. Y.; Coote, M. L. Which side-reactions compromise nitroxide mediated polymerization? *Polym. Chem.* **2013,** 4, (13), 3744-3754.

33. Hlalele, L.; Klumperman, B. In Situ NMR and Modeling Studies of Nitroxide Mediated Copolymerization of Styrene and n-Butyl Acrylate. *Macromolecules* **2011,** 44, (17), 6683-6690.

34. Ahmad, N. M.; Charleux, B.; Farcet, C.; Ferguson, C. J.; Gaynor, S. G.; Hawkett, B. S.; Heatley, F.; Klumperman, B.; Konkolewicz, D.; Lovell, P. A.; Matyjaszewski, K.; Venkatesh, R. Chain Transfer to Polymer and Branching in Controlled Radical Polymerizations of n-Butyl Acrylate. *Macromol. Rapid Commun.* **2009,** 30, (23), 2002-2021.

35. Kotoulas, C.; Krallis, A.; Pladis, P.; Kiparissides, C. A Comprehensive Kinetic Model for the Combined Chemical and Thermal Polymerization of Styrene up to High Conversions. *Macromol. Chem. Phys.* **2003,** 204, (10), 1305-1314.

36. Moad, G.; Rizzardo, E.; Solomon, D. H. A product study of the nitroxide inhibited thermal polymerization of styrene. *Polym. Bull.* **1982,** 6, (11-1), 589-593.

37. Fu, Y.; Cunningham, M. F.; Hutchinson, R. A. Modeling of Nitroxide-Mediated Semibatch Radical Polymerization. *Macromol. React. Eng.* **2007,** 1, (2), 243-252.

38. Bentein, L.; D'hooge, D. R.; Reyniers, M. F.; Marin, G. B. Kinetic Modeling as a Tool to Understand and Improve the Nitroxide Mediated Polymerization of Styrene. *Macromol. Theory Simul.* **2011,** 20, (4), 238-265.

39. Ananchenko, G. S.; Fischer, H. Decomposition of model alkoxyamines in simple and polymerizing systems. I. 2,2,6,6-tetramethylpiperidinyl- N-oxyl-based compounds. *Journal of Polymer Science Part A: Polymer Chemistry* **2001,** 39, (20), 3604-3621.

40. Ananchenko, G. S.; Souaille, M.; Fischer, H.; Le Mercier, C.; Tordo, P. Decomposition of model alkoxyamines in simple and polymerizing systems. II. Diastereomeric N-(2-methylpropyl)-N-(1-diethyl-phosphono-2,2-dimethylpropyl)-aminoxyl-b ased compounds. *J. Polym. Sci. Pol. Chem.* **2002,** 40, (19), 3264-3283.

41. Edeleva, M. V.; Kirilyuk, I. A.; Zubenko, D. P.; Zhurko, I. F.; Marque, S. R. A.; Gigmes, D.; Guillaneuf, Y.; Bagryanskaya, E. G. Kinetic Study of H-Atom Transfer in Imidazoline-, Imidazolidine-, and Pyrrolidine-Based Alkoxyamines: Consequences for Nitroxide-Mediated Polymerization. *J. Polym. Sci. Pol. Chem.* **2009,** 47, (23), 6579-6595.

42. Edeleva, M.; Marque, S. R. A.; Bertin, D.; Gigmes, D.; Guillaneuf, Y.; Morozov, S. V.; Bagryanskaya, E. G. Hydrogen-Transfer Reaction in Nitroxide Mediated Polymerization of Methyl Methacrylate: 2.2-Diphenyl-3-phenylimino-2,3-dihydroindol-1-yloxyl Nitroxide (DPAIO) vs. TEMPO. *J. Polym. Sci. Pol. Chem.* **2008,** 46, (20), 6828-6842.

43. Skene, W. G.; Scaiano, J. C.; Yap, G. P. A. An Improved Mimetic Compound for Styrene "Living" Free Radical Polymerization. An Initiator Containing the "Penultimate" Unit. *Macromolecules* **2000,** 33, (10), 3536-3542.

44. Gigmes, D.; Bertin, D.; Lefay, C.; Guillaneuf, Y. Kinetic Modeling of Nitroxide-Mediated Polymerization: Conditions for Living and Controlled Polymerization. *Macromol. Theory Simul.* **2009,** 18, (7-8), 402-419.

45. Bonilla, J.; Saldivar, E.; Flores-Tlacuabuac, A.; Vivaldo-Lima, E.; Pfaendner, R.; Tiscareno-Lechuga, F. Detailed modeling, simulation, and parameter estimation of nitroxide mediated living free radical polymerization of styrene. *Polym. React. Eng.* **2002,** 10, (4), 227-263.

46. Chauvin, F.; Dufils, P. E.; Gigmes, D.; Guillaneuf, Y.; Marque, S. R. A.; Tordo, P.; Bertin, D. Nitroxide-mediated polymerization: The pivotal role of the k(d) value of the initiating alkoxyamine and the importance of the experimental conditions. *Macromolecules* **2006,** 39, (16), 5238-5250.

47. Bertin, D.; Gigmes, D.; Marque, S. R. A.; Tordo, P. Polar, steric, and stabilization effects in alkoxyamines C-ON bond homolysis: A multiparameter analysis. *Macromolecules* **2005,** 38, (7), 2638-2650.

48. Goto, A.; Fukuda, T. Comparative study on activation rate constants for some styrene/nitroxide systems. *Macromol. Chem. Phys.* **2000,** 201, (16), 2138-2142.

49. Chevalier, C.; Robin, S.; Benoit, D.; Guerret, O.; Gnanou, Y. Controlled radical polymerization in the presence of beta-phosphonylated nitroxide - kinetics, mechanism and macromolecular architecture. *Polimery* **2003,** 48, (7-8), 499-504.

50. Guillaneuf, Y.; Bertin, D.; Castignolles, P.; Charleux, B. New experimental procedure to determine the recombination rate constants between nitroxides and macroradicals. *Macromolecules* **2005,** 38, (11), 4638-4646.

51. Sobek, J.; Martschke, R.; Fischer, H. Entropy Control of the Cross-Reaction between Carbon-Centered and Nitroxide Radicals. *J. Am. Chem. Soc.* **2001,** 123, (12), 2849-2857.

52. Benoit, D.; Grimaldi, S.; Robin, S.; Finet, J. P.; Tordo, P.; Gnanou, Y. Kinetics and mechanism of controlled free-radical polymerization of styrene and n-butyl acrylate in the presence of an acyclic beta-phosphonylated nitroxide. *J. Am. Chem. Soc.* **2000,** 122, (25), 5929-5939.

53. Mercier, C. L.; Lutz, J. F.; Marque, S.; Moigne, F. L.; Tordo, P.; Lacroix-Desmazes, P.; Boutevin, B.; Couturier, J. L.; Guerret, O.; Martschke, R.; Sobek, J.; Fischer, H., Use of Phosphonylated Nitroxides and Alkoxyamines in Controlled/"Living" Radical Polymerization. In *Controlled/Living Radical Polymerization*, American Chemical Society: 2000; Vol. 768, pp 108-122.

54. Lutz, J. F.; Lacroix-Desmazes, P.; Boutevin, B. The persistent radical effect in nitroxide mediated polymerization: Experimental validity. *Macromol. Rapid Commun.* **2001,** 22, (3), 189-193.

55. Van Steenberge, P. H. M.; Vandenbergh, J.; D'hooge, D. R.; Reyniers, M. F.; Adriaensens, P. J.; Lutsen, L.; Vanderzande, D. J. M.; Marin, G. B. Kinetic Monte Carlo Modeling of the Sulfinyl Precursor Route for Poly(p-phenylene vinylene) Synthesis. *Macromolecules* **2011,** 44, (22), 8716-8726.

56. Van Steenberge, P. H. M.; D'hooge, D. R.; Wang, Y.; Zhong, M. J.; Reyniers, M. F.; Konkolewicz, D.; Matyjaszewski, K.; Marin, G. B. Linear Gradient Quality of ATRP Copolymers. *Macromolecules* **2012,** 45, (21), 8519-8531.

57. Van Steenberge, P. H. M.; D'hooge, D. R.; Reyniers, M. F.; Marin, G. B. Improved kinetic Monte Carlo simulation of chemical composition-chain length distributions in polymerization processes. *Chem. Eng. Sci.* **2014,** 110, 185-199.

58. Päch, M.; Zehm, D.; Lange, M.; Dambowsky, I.; Weiss, J.; Laschewsky, A. Universal Polymer Analysis by 1H NMR Using Complementary Trimethylsilyl End Groups. *J. Am. Chem. Soc.* **2010,** 132, (25), 8757-8765.

59. Greszta, D.; Matyjaszewski, K. Mechanism of controlled/"living" radical polymerization of styrene in the presence of nitroxyl radicals. Kinetics and simulations. *Macromolecules* **1996,** 29, (24), 7661-7670.

60. Mayo, F. R. Chain Transfer in the Polymerization of Styrene. VIII. Chain Transfer with Bromobenzene and Mechanism of Thermal Initiation1. *J. Am. Chem. Soc.* **1953,** 75, (24), 6133-6141.

61. Hui, A. W.; Hamielec, A. E. Thermal polymerization of styrene at high conversions and temperatures. An experimental study. *J. Appl. Polym. Sci.* **1972,** 16, (3), 749-769.

62. Woloszyn, J. D.; McAuley, K. B. Application of Parameter Selection and Estimation Techniques in a Thermal Styrene Polymerization Model. *Macromol. React. Eng.* **2011,** 5, 453-466.

63. Buback, M.; Gilbert, R. G.; Hutchinson, R. A.; Klumperman, B.; Kuchta, F.-D.; Manders, B. G.; O'Driscoll, K. F.; Russell, G. T.; Schweer, J. Critically evaluated rate coefficients for free-radical polymerization, 1. Propagation rate coefficient for styrene. *Macromol. Chem. Phys.* **1995,** 196, (10), 3267-3280.

64. Johnston-Hall, G.; Monteiro, M. J. Bimolecular radical termination: New perspectives and insights. *J. Polym. Sci. Pol. Chem.* **2008,** 46, (10), 3155-3173.

65. Fu, Y.; Mirzaei, A.; Cunningham, M. F.; Hutchinson, R. A. Atom-Transfer Radical Batch and Semibatch Polymerization of Styrene. *Macromol. React. Eng.* **2007,** 1, (4), 425-439.

66. Pryor, W. A. L. L. D. Diels-Alder and 1,4-diradical Intermediates in the. Spontaneous Polymerization of Vinyl Monomers. *Adv. Free Radic. Chem.* **1975,** 5, (27), 27-99.

67. Zytowski, T.; Knuhl, B.; Fischer, H. Absolute rate constants for the addition of the 2-(methoxycarbonyl)propan-2-yl and the 3,3,3-trifluoracetonyl radicals to alkenes in solution. *Helv. Chim. Acta* **2000,** 83, (3), 658-675.

68. Saldivar-Guerra, E.; Bonilla, J.; Zacahua, G.; Albores-Velasco, M. Incubation period in the 2,2,4,4-tetramethyl-1-piperidinyloxy-mediated thermal autopolymerization of styrene: Kinetics and simulations. *J. Polym. Sci. Pol. Chem.* **2006,** 44, (24), 6962-6979.

69. Khuong, K. S.; Jones, W. H.; Pryor, W. A.; Houk, K. N. The mechanism of the self-initiated thermal polymerization of styrene. Theoretical solution of a classic problem. *J. Am. Chem. Soc.* **2005,** 127, (4), 1265-1277.

70. Zetterlund, P. B.; Saka, Y.; McHale, R.; Nakamura, T.; Aldabbagh, F.; Okubo, M. Nitroxide-mediated radical polymerization of styrene: Experimental evidence of chain transfer to monomer. *Polymer* **2006,** 47, (23), 7900-7908.

71. Olaj, O. F.; Kauffmann, H. F.; Breitenbach, J. W. The Diels-Alder intermediate as a chain transfer agent in spontaneous styrene polymerization 1. New evidence from the kinetic analysis of photoinitiated polymerization. *Die Makromolekulare Chemie* **1976,** 177, (10), 3065-3071.

72. A. Ueda, S. N., Transfer constants to monomers, polymers, catalysts and initiators, solvents and additives, and sulfur compounds in free radical polymerization. In *Polymer Handbook*, 4th ed.; J. Wiley & Sons: New York, 1989; pp 97-168.

73. Gaudel-Siri, A.; Siri, D.; Tordo, P. Homolysis of N-alkoxyamines: A computational study. *ChemPhysChem* **2006,** 7, (2), 430-438.

74. Boggs P.T., B. R. H., Rogers J.E., Schnabel R.B. *ODRPACK Software for Orthogonal Distance Regression*; National Institute of Standards and Technology: USA, 1992.

75. De Roo, T.; Wieme, J.; Heynderickx, G. J.; Marin, G. B. Estimation of intrinsic rate coefficients in vinyl chloride suspension polymerization. *Polymer* **2005,** 46, (19), 8340-8354.

76. Toloza Porras, C.; D'hooge, D. R.; Van Steenberge, P. H. M.; Reyniers, M.-F.; Marin, G. B. ICAR ATRP for Estimation of Intrinsic Macro-Activation/Deactivation Arrhenius Parameters under Polymerization Conditions. *Industrial & Engineering Chemistry Research* **2014**.

77. Vana, P.; Davis, T. P.; Barner-Kowollik, C. Easy Access to Chain-Length-Dependent Termination Rate Coefficients Using RAFT Polymerization. *Macromol. Rapid Commun.* **2002,** 23, (16), 952-956.

78. Buback, M.; Egorov, M.; Gilbert, R. G.; Kaminsky, V.; Olaj, O. F.; Russell, G. T.; Vana, P.; Zifferer, G. Critically Evaluated Termination Rate Coefficients for Free-Radical Polymerization, 1. The Current Situation. *Macromol. Chem. Phys.* **2002,** 203, (18), 2570-2582.

79. D'hooge, D. R.; Reyniers, M.-F.; Marin, G. B. The Crucial Role of Diffusional Limitations in Controlled Radical Polymerization. *Macromol. React. Eng.* **2013,** 7, (8), 362-379.

80. Shipp, D. A.; Matyjaszewski, K. Kinetic Analysis of Controlled/"Living" Radical Polymerizations by Simulations. 1. The Importance of Diffusion-Controlled Reactions. *Macromolecules* **1999,** 32, (9), 2948-2955.

81. Zetterlund, P. B. Compartmentalization in Atom Transfer Radical Polymerization to High Conversion in Dispersed Systems: Effects of Diffusion-Controlled Reactions. *Macromolecules* **2010,** 43, (3), 1387-1395.

82. Wang, A. R.; Zhu, S. Effects of Diffusion-Controlled Radical Reactions on RAFT Polymerization. *Macromol. Theory Simul.* **2003,** 12, (2-3), 196-208.

83. Bentein, L.; D'hooge, D. R.; Reyniers, M. F.; Marin, G. B. Kinetic modeling of miniemulsion nitroxide mediated polymerization of styrene: Effect of particle diameter and nitroxide partitioning up to high conversion. *Polymer* **2012,** 53, (3), 681-693.

84. Bertin, D.; Chauvin, F.; Marque, S.; Tordo, P. Lack of chain length effect on the rate of homolysis of polystyryl-SG1 alkoxyamines. *Macromolecules* **2002,** 35, (10), 3790-3791.

85. Payne, K. A.; D'hooge, D. R.; van Steenberge, P. H. M.; Reyniers, M. F.; Cunningham, M. F.; Hutchinson, R. A.; Marin, G. B. ARGET ATRP of Butyl Methacrylate: Utilizing Kinetic Modeling To Understand Experimental Trends. *Macromolecules* **2013,** 46, (10), 3828-3840.

86. Roa-Luna, M.; Diaz-Barber, M. P.; Vivaldo-Lima, E.; Lona, L. M. F.; McManus, N. T.; Penlidis, A. Assessing the importance of diffusion-controlled effects on polymerization rate and molecular weight development in nitroxide-mediated radical polymerization of styrene. *J. Macromol. Sci. Part A-Pure Appl. Chem.* **2007,** 44, (2), 193-203.

87. Goto, A.; Fukuda, T. Kinetics of living radical polymerization. *Prog. Polym. Sci.* **2004,** 29, (4), 329-385.

88. Zhong, M. J.; Matyjaszewski, K. How Fast Can a CRP Be Conducted with Preserved Chain End Functionality? *Macromolecules* **2011,** 44, (8), 2668-2677.

89. Biondi, M.; Borzacchiello, A.; Netti, P. A. Isothermal and non-isothermal polymerization of methyl methacrylate in presence of multiple initiators. *Chem. Eng. J.* **2010,** 162, (2), 776-786.

90. Mohammad Rabea, A.; Zhu, S. Achieving High-Conversion Bulk ATRP with Good Livingness and Well Controlled by Design and Optimization of Polymerization Temperature Profile. *Macromol. React. Eng.* **2014**, in press.

Chapter 4. Exploring the full potential of reversible deactivation radical polymerization using Pareto-optimal fronts

Summary

The use of Pareto-optimal fronts to evaluate the full potential of reversible deactivation radical polymerization (RDRP) using multi-objective optimization (MOO) is illustrated for the first time. Pareto-optimal fronts are identified for activator regenerated electron transfer atom transfer radical polymerization (ARGET ATRP) of butyl methacrylate and nitroxide mediated polymerization (NMP) of styrene. All kinetic and diffusion parameters are literature based and a variety of optimization paths such as temperature and fed-batch addition programs are considered. It is shown that improvements in the control over the RDRP characteristics are possible beyond the capabilities of batch or isothermal RDRP conditions. Via these MOO-predicted non-classical polymerization procedures, a significant increase of the degree of microstructural control can be obtained with a limited penalty on the polymerization time, specifically if a simultaneous variation of various polymerization conditions is considered. The improvements are explained based on the relative importance of the key reaction rates as a function of conversion. This work was published in *Polymers* 2015, 7(4). 655-679.

4.1 Introduction

During the last two decades, reversible deactivation radical polymerization (RDRP), which is also known as controlled radical polymerization (CRP), has shown to overcome disadvantages of conventional free radical polymerization (FRP), which allows mostly the synthesis of commodity polymer products,[1-7] unless expensive functional monomers are used.[8, 9] Under well-defined conditions, RDRP techniques are characterized by the establishment of a dynamic pseudo-equilibrium between propagating and dormant species, allowing the controlled incorporation of monomer units per activation-growth-deactivation cycle. This enables the production of polymers with a predetermined number average chain length and narrow chain length distribution (dispersity ($Đ$) < 1.3) that possess end-group functionality EGF. This brings the synthesis of well-defined macromolecular architectures such as block and star copolymers within reach. Two important RDRP techniques, which are studied in this work, are activators regenerated by electron transfer atom transfer radical polymerization (ARGET ATRP) [10-16] and nitroxide mediated polymerization (NMP).[17-21]

In traditional ATRP (Figure 4.1; left top), typically a Cu(I)-complex ($Cu^{I}X/L$; activator; X: halogen atom) catalyzes the homolytic cleavage of an ATRP initiator (R_0X') to yield an initiator radical (R_0') and a transition metal complex characterized by a higher oxidation state ($Cu^{II}X_2/L$; deactivator). This R_0 species propagates until it is temporarily deactivated by $Cu^{II}X_2/L$ to yield a halide capped dormant macrospecies (R_iX'; i: chain length). Typical monomers are styrene, (meth)acrylates and acrylamides. However, during the initial stage of the ATRP, termination reactions are also occurring at significant rates, thereby leading to a build-up of deactivator species. Hence, the deactivation reaction is favored over the termination reaction at higher

polymerization times, allowing microstructural control. This effect has been first described by Fischer *et al.* [22, 23] and is known as the persistent radical effect.[24] The commercial utilization of ATRP is however hampered by various challenges such as perfect oxygen removal, excessively high catalyst concentrations leading to extensive post-polymerization purifications, and the toxic characteristics of the transition metal complexes [1]. Therefore, alternative initiating procedures which result in a much more attractive ATRP have been investigated, *i.e.* systems in which the catalyst concentration is dramatically lowered and less stringent reaction conditions are employed.[25]

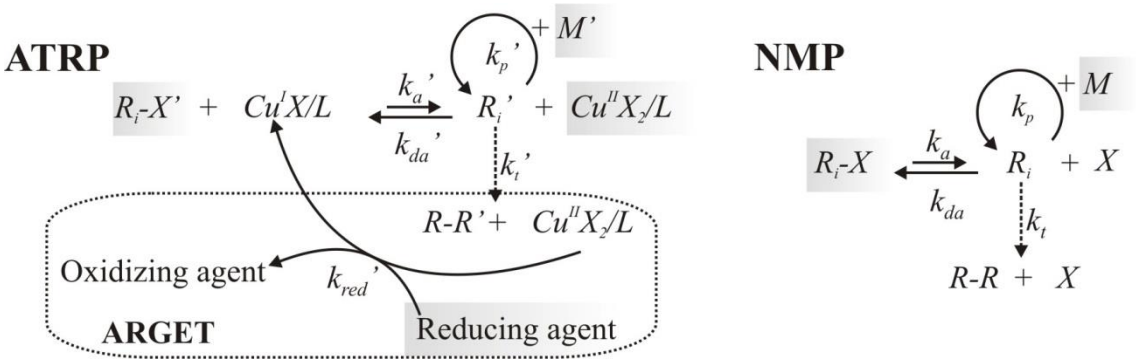

Figure 4.1. *Left: basic reaction scheme for Activators ReGenerated by Electron Transfer (ARGET) Atom Transfer Radical Polymerization (ATRP) using a Cu-based catalyst ($Cu^{II}X_2/L$; deactivator) and as ATRP initiator R_0X' (X: halogen atom), and monomer M'; Right: basic reaction scheme for Nitroxide Mediated Polymerization (NMP) using an alkoxyamine initiator R_0X and monomer M; k: rate coefficient; a,da,p,red,t: activation, deactivation, propagation, reduction, and termination; i: chain length with i=0 initiator related; grey box: initial presence of this species (i = 0); for simplicity only termination by recombination is shown; in traditional ATRP no reducing agent and also activator present at the start.*

One of these modified ATRPs is ARGET ATRP (Figure 4.1; left panel).[26-28] In this RDRP, a reducing agent, for example tin(II) 2-ethylhexanoate ($Sn(EH)_2$), is added in excess relative to the ATRP catalyst, which is present at very low amounts (< 300 ppm with respect to monomer;

molar). This allows the *in situ* reduction of the deactivator species and thus the regeneration of activator species. Moreover, ARGET ATRP allows the polymerization to be initiated by only the halide initiator and the deactivator, leading to less stringent reaction conditions compared to the classical ATRP process. It has been indicated that the outcome of the ARGET ATRP is very sensitive to the initial concentrations. In particular, the amount of reducing agent has to be selected carefully, taking into account a trade-off between polymerization rate and livingness.[29-32] Moreover, by switching to continuous operation, a more industrial relevant process can be obtained.[33, 34]

The basic kinetic scheme of the second studied RDRP, *i.e.* NMP,[17, 35] is shown in Figure 4.1 (right panel). NMP is one of the first discovered RDRP systems, due to the pioneering work of Rizzardo *et al.*[36] Since then, numerous studies have been devoted to clarify the mechanism and the kinetics of NMP,[37-42] focusing mostly on styrene and acrylates as monomers. In NMP, an alkoxyamine initiator (R_0X), undergoes a homolytic cleavage at elevated temperature which releases a R_0 species and a nitroxide radical (X), also called the persistent radical. As in ATRP, the initiator radical undergoes chain initiation and the persistent radical effect takes place allowing control at higher polymerization times.[43] Further optimization can be obtained via, for example, novel and highly active nitroxides/alkoxyamines [44, 45] such as N-(2-methyl-2-propyl)-N-(1-diethylphosphono-2,2-dimethylpropyl)-N-oxyl (MAMA-SG1; BlocBuilder®), the use of conventional radical initiators with a long half-life time,[46] the continuous addition of conventional radical initiator,[47] and rate-enhancing organic acids.[48]

However, both ARGET ATRP and NMP still display several shortcomings, which partly explains the limited industrial realization of RDRP.[49] Taking into account technical-economic considerations, several aspects should be still optimized. From a technical point of view an

improved polymer product, *i.e.* a better control over the narrowness of the CLD and a high EGF, are desired. On the other hand, the economic feasibility of the polymerization process necessitates that a predetermined conversion is reached within a minimal reaction time. These objectives are unfortunately often contradictory in nature, implying the need of multi-objective optimization (MOO) for the unbiased optimization of RDRP. Such optimization studies do not deliver a unique set of operating conditions, but result in a set of several equivalently optimal solutions. This so-called Pareto-optimal front offers the decision-maker useful insights in the compromise to be made and provides the flexibility to decide which is the preferred operating point taking into account specific constraints on polymerization time and microstructural control.[50, 51]

Several approaches have been developed which are suited for solving MOO-problems, such as fuzzy logic, neural networks, simulated annealing, and genetic algorithms.[52] The latter have shown to be very suited to solve MOO-problems involving many design variables, as in RDRP. A pioneering genetic algorithm is the so-called Nondominated Sorting Genetic Algorithm (NSGA) proposed by Srinivas and Deb.[53] This algorithm suffered from several drawbacks, which have been addressed by the development of an improved version NSGA-II.[54]

MOO has already been successfully applied for several conventional radical and non-radical polymerization processes, such as the production of nylon-6 in a semi-batch operated reactor,[55] the synthesis of polyester films,[56] semi-batch epoxy polymerization,[57] free radical (co)polymerization,[50, 58] and emulsion polymerization.[59, 60] Typically off-line optimization is performed, taking into account limitations for the calculation time of the MOO algorithm for complex kinetic schemes. For RDRP, however, this methodology has not yet been explored. In this work, for the first time, the potential of MOO for RDRP will be illustrated, considering ARGET ATRP of butyl methacrylate (BMA) and NMP of styrene as model cases and using

NSGA-II.[61-63] All kinetic and diffusion parameters are taken from literature [61, 64, 65] and a variety of optimization paths, such as temperature and fed-batch addition programs, are included, considering time, *Đ* and EGF as objectives. For simplicity, the objectives are evaluated only at a final conversion of 0.75. It is shown that significant progress can be made in the control over the RDRP characteristics via such non-classical polymerization procedures.

The reported improvements are explained by a comparison of the relative importance of the key reaction rates as a function of conversion. This involves a comparison of the propagation, deactivation and termination reaction probabilities and in addition probabilities related to important side reactions, such as chain transfer to dimer in the case of NMP of styrene.

4.2 Modeling procedure

4.2.1 Reaction schemes and rate coefficients

The reaction scheme for ARGET ATRP of BMA using $Sn(EH)_2$ as reducing agent (R^{II} in Table 4.1), ethyl 2-bromoisobutyrate as ATRP initiator (R_0X' in Table 4.2), and $CuBr_2$/*TPMA* (TPMA: tris[(2-pyridyl)methyl]amine; *D'* in Table 4.3) as deactivator is given in Table 4.3 (left column), considering bulk conditions for simplicity. The listed kinetic parameters are adopted from Payne *et al.* [64] and a distinction is made between ARGET ATRP specific and non-specific reaction steps. The main reactions are propagation, termination, and ATRP (de)activation. Both termination by disproportionation and recombination are considered. Chain transfer to monomer is neglected, based on previous studies.[66] Furthermore, a first and second reduction step for activator regeneration is included. Chain length and conversion dependent apparent termination rate coefficients are calculated via the composite k_t-model using the RAFT-CLD-T method, with improved parameters taken from the recent work from Derboven *et al.* [65] For the other reaction

steps, no diffusional limitations have to be accounted for, at least to a first approximation, as typically a maximal conversion of 0.75 is obtained. Note that the MOO-strategy can be extended to higher conversions, provided that reliable activation/deactivation parameters become available. A deterministic model based on the method of moments is used to describe the polymerization kinetics. More details on the method of moments can be found in Appendix.

An overview of the reactions included in the kinetic model of the NMP of styrene initiated by MAMA-SG1 ($R_{0,1}X$ in Table 4.3) is given in Table 4.3 (middle column). A distinction is made between styrene and NMP specific reaction steps. The corresponding Arrhenius parameters are taken from Fierens *et al.*,[61] who performed regression analysis on an extensive set of experimental polymerization data to obtain NMP (de)activation kinetic parameters while accounting for the reactivity difference between initiator and macrospecies. Importantly, for the styrene specific steps, thermal auto-initiation [67] is included, since for styrene, at elevated temperatures (> 100°C), auto-initiation occurs in which two styrene molecules undergo a Diels-Alder cycloaddition to form a dimer molecule (*D* in Table 4.3). This dimer can undergo a retro Diels-Alder reaction forming two styrene molecules or it can undergo a molecule assisted homolysis to yield two additional initiator radicals $R_{0,2}$ and $R_{0,3}$. Chain transfer reactions to monomer and dimer are considered, based on literature data.[62, 68] Again chain length and conversion dependent apparent rate coefficients are taken into account.[69, 70] Here, also, a deterministic model based on the method of moments has been used.

Table 4.3. *Reactions and Arrhenius parameters for the simulation of ARGET ATRP of butyl methacrylate (BMA; left column) and NMP of styrene initiated by MAMA-SG1 (middle column); Arrhenius parameters (A ((L mol^{-1}) s^{-1}) and E_a (kJ mol^{-1})) given in right column. Termination reactions are included in the kinetic model but not explicitly shown (for ARGET ATRP case: recombination and disproportionation; for NMP case: recombination); A' = $Cu^{I}X/L$, D'= $Cu^{II}X_2/L$, R^z=$Sn^z(EH)_2$, M' = butyl methacrylate, R_0X' = ethyl 2-bromoisobutyrate, M = styrene, R_0X = MAMA-SG1, D = dimer; j =1,2,3,4; j' = 2,3,4.*

Reactions		Arrhenius Parameters
ARGET ATRP [64]	**NMP [61]**	
ATRP (De)Activation	**NMP (De)Activation**	**ARGET ATRP**
$R_0X' + A' \underset{k_{da0'}}{\overset{k_{a0'}}{\rightleftharpoons}} R_0' + D'$	$R_{0,1}X \underset{k_{da0}}{\overset{k_{a0}}{\rightleftharpoons}} R_{0,1} + X$	$A_{a0'} = 5.38 \times 10^4$; $E_{a,a0'} = 27.7$
		$A_{da0'} = 3.94 \times 10^8$; $E_{a,da0'} = 7.98$
$R_iX' + A' \underset{k_{da'}}{\overset{k_{a'}}{\rightleftharpoons}} R_i' + D'$	$R_iX \underset{k_{da}}{\overset{k_a}{\rightleftharpoons}} R_i + X$	$A_{a'} = 3.99 \times 10^6$; $E_{a,a'} = 27.7$
		$A_{da'} = 1.97 \times 10^8$; $E_{a,da'} = 27.7$
Reduction	**Thermal Initiation**	$A_{r1'} = 5.55 \times 10^1$; $E_{a,r1'} = 14.9$
$D' + R^{II} \xrightarrow{k_{r1'}} A' + R^{III}$	$2M \underset{k_{rd}}{\overset{k_d}{\rightleftharpoons}} D$	$A_{r2'} = 1.87 \times 10^2$; $E_{a,r2'} = 14.9$
		$A_{p0'} = 3.80 \times 10^6$; $E_{a,p0'} = 22.9$
$D' + R^{III} \xrightarrow{k_{r2'}} A' + R^{IV}$	$D + M \xrightarrow{k_{thi}} R_{0,2} + R_{0,3}$	$A_{p'} = 3.80 \times 10^6$; $E_{a,p'} = 22.9$
		NMP
Chain Initiation	**Chain Initiation**	$A_{a0} = 1.16 \times 10^{13}$; $E_{a,a0} = 105$
$R_0' + M' \xrightarrow{k_{p,0'}} R_1'$	$R_{0,j} + M \xrightarrow{k_{p,0j}} R_1$	$A_{da0} = 2.80 \times 10^6$; $E_{a,da0} = 0.00$
		$A_a = 4.04 \times 10^{17}$; $E_{a,a} = 149$
Propagation	**Propagation**	$A_{da} = 1.09 \times 10^6$; $E_{a,da} = 0.00$
		$A_d = 4.74 \times 10^5$; $E_{a,d} = 93.5$
	$R_i + M \xrightarrow{k_p} R_{i+1}$	$A_{rd} = 1.05 \times 10^2$; $E_{a,rd} = 44.3$
	Chain Transfer	$A_{thi} = 1.51 \times 10^6$; $E_{a,thi} = 99.6$
$R_i' + M' \xrightarrow{k_{p'}} R_{i+1}'$	$R_i + M \xrightarrow{k_{trM}} P_i + R_{0,4}$	$A_{p01} = 1.55 \times 10^6$; $E_{a,p01} = 16.5$
		$A_{p0j'} = 4.24 \times 10^7$; $E_{a,p0j'} = 32.5$
		$A_p = 4.24 \times 10^7$; $E_{a,p} = 32.5$
	$R_i + D \xrightarrow{k_{trD}} P_i + R_{0,3}$	$A_{trM} = 2.30 \times 10^6$; $E_{a,trM} = 53.0$
		$A_{trD} = 6.76 \times 10^5$; $E_{a,trD} = 27.5$

4.2.2 Genetic optimization algorithm: NSGA-II

A solution, *i.e.* a set of variables (*e.g.* temperature and molar amounts for a given conversion interval), is said to be Pareto-optimal if there exists no other set of feasible variables that will

yield an improvement in one objective (*e.g. Đ)* without worsening at least one other objective (*e.g.* time to reach a given conversion). This set of conditions is said to be non-dominated and belongs to the Pareto-optimal front.[52]

In this contribution, the Nondominated Sorting Genetic Algorithm-II (NSGA-II) has been implemented in FORTRAN code and combined with literature deterministic kinetic models for ARGET ATRP of BMA and the NMP of styrene to perform MOO. In the first step of the NSGA-II algorithm (Scheme B.1; Appendix), a population of N_p parents (P_1; generation 1) is generated. This population refers to a set of initial variables which are randomly distributed in between minimum and maximum boundaries (*e.g.* a temperature range for a specific conversion). The polymerization characteristics of the population are evaluated at a predetermined conversion, after which the population is sorted based on non-domination, leading to a ranking of the individuals. This results in a so-called fitness value per population member, also known as the rank. Subsequently, each population member is assigned a crowding-distance, which allows to identify their level of remoteness in the objective space. This ensures the diversity of the population upon regeneration, which in this first generation refers to the creation of an initial offspring population (Q_i; $i = 1$) of size N_o. The latter population is obtained via selection, with rank as first decision criterion and crowding-distance as second, and subsequent crossover, and mutation.

In a next step, the ranks and crowding-distances of the combined population (R_i), *i.e.* parents and offspring population, are determined. Hereafter, a new generation for the parent population (P_{i+1}) of N_p members is created by selecting the best performing individuals out of the combined population with again the same decision criteria, *i.e.* rank and crowding-distance.

Additional generations are obtained by repeating the aforementioned process of offspring generation and reduction of population members to N_p size until a predefined maximum generation number is reached. If this number is sufficiently large the Pareto-optimal front is approached, provided that the other NSGA-II parameters (Table B.1; Appendix) are properly chosen. For more details on the NSGA-II algorithm, the reader is referred to Deb *et al.*[54]

An overview of the upper and lower bounds of the variables selected in this work is given in Appendix (Table B.2).

4.3 Results and Discussion

4.3.1 Multi-objective optimization of ARGET ATRP

The MOO of ARGET ATRP of BMA is explored considering time and *Đ* as objectives. Two objectives are selected in this case study to illustrate the strength of Pareto-optimal fronts, taking into that the simulated EGF variation is rather limited (<5%). Moreover, it has been verified that similar number averaged chain lengths are obtained for all cases considered. Several optimization pathways are considered, namely optimization via the application of a non-isothermal temperature program, fed-batch addition of monomer and fed-batch addition of reducing agent. The fed-batch addition of deactivator is ignored, since preliminary simulations revealed no improvement compared to the batch condition. Also the combination of several optimization pathways is examined and shown to be synergetic in particular cases. A constraint on the polymerization time of maximum 50 hours is imposed and the total molar amount of reactants is fixed with as reference case the following batch conditions **(**$[M]_0/[R_0X]_0/[Cu^{II}X_2/L]_0/[Sn^{II}(EH)_2]_0$ = 200/1/0.005/0.05; 90°C).

4.3.1.1 Variation of temperature

As a first individual optimization pathway the use of a temperature program is investigated. For simplicity, a piecewise linear temperature profile is selected, consisting of 6 distinct conversion intervals, each of equal size (ΔX_m = 0.125) with a maximal conversion of 0.75. Hence, 7 variables, *i.e.* the temperatures at the interval boundaries, have to be optimized by the MOO algorithm per simulation. Note that in practice these conversion points should be translated into times for a practical realization of the off-line optimization strategy. For completeness it is mentioned here that also in the remainder of the text temperature/fed-batch addition programs are always described per conversion interval of ΔX_m = 0.125. In other words, the boundary values of these intervals have to be determined per simulation. In the current situation of a temperature program, a variation between 60 and 90 °C is allowed for the 7 variables, based on literature data on isothermal batch ATRP of BMA [64]. The results of the MOO are shown in Figure 4.2 (a) (green dots). For the sake of comparison, the Pareto-optimal front for isothermal polymerizations is also shown (red dots).

It can be seen that the use of a temperature program is beneficial compared to the isothermal case. For example, for the synthesis of a polymer product with a $Đ$ of 1.35, a reduction of the polymerization time with *ca.* 3 hours results when using a temperature program. The values of the 7 variables describing the temperature program along the Pareto-optimal front are shown in Figure 4.2 (b). By linking this figure to Figure 4.2 (a) it follows that the final $Đ$ decreases if the ARGET ATRP is started at a lower temperature and the temperature is gradually increased throughout the polymerization. This increased control over chain length is although accompanied by a longer polymerization time. This becomes more clear when selecting three illustrative cases along the Pareto-optimal front (case 1, 2 and 3 in Figure 4.2 (a) and (b)). For completeness, the

complete temperature programs for these three cases are shown in Figure 4.2 (c). The most dynamic program is obtained for case 1, whereas case 2 corresponds to a less dynamic T-program providing a transition to the limiting case 3, in which an isothermal ARGET ATRP is conducted.

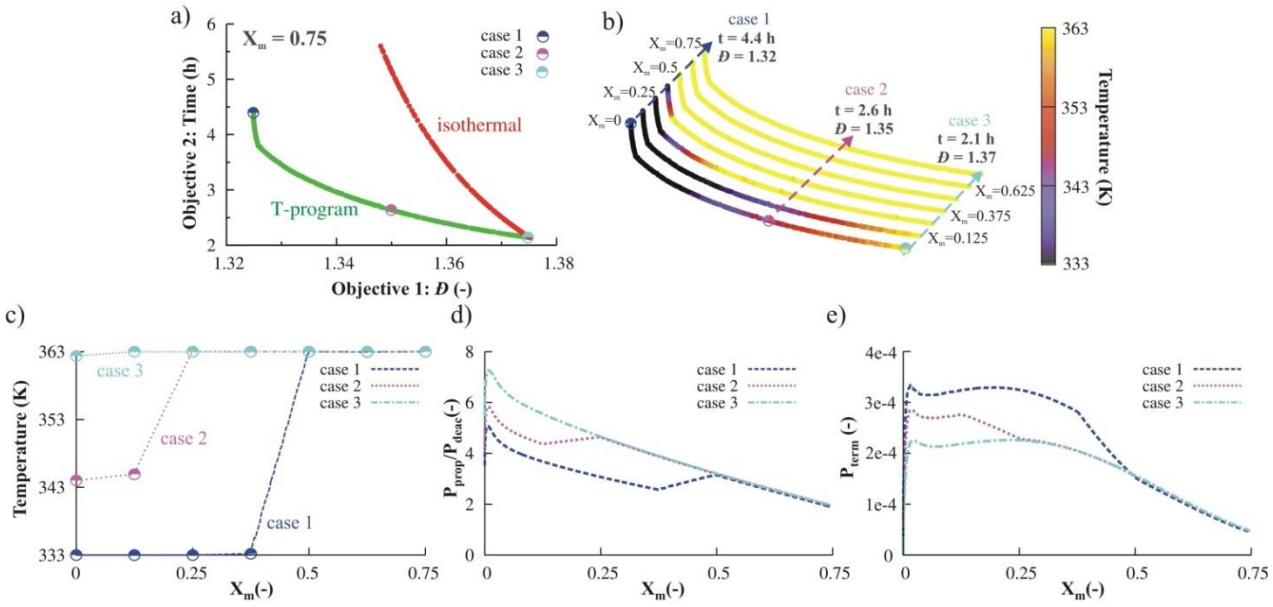

Figure 4.2. *Results for the multi-objective optimization (MOO) of ARGET ATRP of BMA using a piecewise linear temperature program (ΔX_m = 0.125 until X_m = 0.75; $[M]_0/[R_0X]_0/[Cu^{II}X_2/L]_0/[Sn^{II}(EH)_2]_0$ = 200/1/0.005/0.05) (a) Pareto-optimal front (green circles) and corresponding isothermal front (red circles); (b) Variation of the temperature at the interval boundaries along the Pareto-optimal front; (c) Temperature as a function of X_m for three selected cases in (a); (d) Ratio of probability for propagation to deactivation as a function of X_m for the selected cases; (e) Probability for termination as a function of X_m for the selected cases*

The observed differences in polymerization time and *Đ* can be explained by looking at the ratio of the reaction probability for a macroradical to propagate and to deactivate (P_{prop}/P_{deac}) (Figure 4.2 (d)) on one hand and the reaction probability for a macroradical to terminate (P_{term}) (Figure 4.2 (e)) on the other hand. The former characteristic is selected since simplified models assuming perfect livingness have shown that the ratio of the propagation and deactivation reactivity need to

be sufficiently low to guarantee the incorporation of a controlled amount of monomer units during each activation-propagation-deactivation cycle so that a low $Đ$ can be obtained.[1, 71] In reality, a perfect livingness cannot be achieved since termination is inevitable and thus P_{term} has to be considered as a second characteristic.[72, 73] Note that no additional characteristics are needed since other side reactions can be neglected.[64]

Figure 4.2 (d) shows that at low conversions a lower polymerization temperature clearly leads to a lower P_{prop}/P_{deac} and thus a slower ARGET ATRP and a better control over chain length. This can be understood by noting that propagation is much more activated (23 kJ mol^{-1} in Table 4.3) than deactivation (8 kJ mol^{-1} in Table 4.3). The beneficial effect of these lower P_{prop}/P_{deac} values on $Đ$ is however partly counteracted by the increase of P_{term} (Figure 4.2 (e)). The latter increase can be attributed to the as good as non-activated nature of termination and the limited importance on diffusional limitations on termination (Figure B.2 (a); Appendix) at these low conversions. This similar control over $Đ$ at low conversions for the three cases is confirmed in Appendix (Figure B.1 (a)). At higher conversions both P_{prop}/P_{deac} and P_{term} (Figure 4.2 (c) and (d)) become very similar for the 3 cases, but still the best control results for case 1, since the suppression of the absolute termination rate is more pronounced (Figure B.2 (b); Appendix). Hence, with a very dynamic temperature program, the lowest $Đ$ values are obtained at high conversions (Figure B.1 (a); Appendix and Figure 4.2 (a)-(b)).

4.3.1.2 Variation of monomer

A second individual optimization pathway for ARGET ATRP of BMA is a fed-batch monomer addition program. The latter implies an increase of the reaction volume as a function of polymerization time. This optimization is performed at the maximal temperature of 90°C, for illustration purposes only. Importantly, the term overall conversion ($X_{m,overall}$) needs to be

introduced [32]. This conversion is defined with respect to the initial molar amount of monomer used in the batch reference case ($n_{M,0,batch}$):

$$X_{m,overall} = \frac{n_{M,reacted}}{n_{M,0,batch}} \quad (4.1)$$

in which $n_{M,reacted}$ is the molar amount of monomer that has already reacted. This overall conversion thus differs from the actual or *in situ* conversion (X_m), which is defined with respect to amount of monomer added until the considered time. The overall conversion domain is divided into discrete subdomains of conversion increments of 0.125 until a final conversion of 0.75 is obtained as before. The addition profile is thus described by 7 variables, each representing the added fraction with respect to the corresponding initial batch amount for a given conversion interval. This normalization with respect to the initial batch amount implies thus an implicit constraint for the selected amount per conversion interval and guarantees an unbiased comparison of the different sets of conditions considered. For the first variable, this is the initial amount present, which has a lower limit of 15 mol% of the initial batch amount, whereas the other six variables represent the amount of monomer added in the interval. In each interval, a semi-continuous supply of monomer at a constant molar flow rate is provided per incremental conversion increase of 0.0025.

In Figure 4.3 (a), the Pareto-optimal front (green circles) is shown together with the batch reference case (red square), which clearly does not belong to this front, implying that an improvement of *Đ* can be obtained with a simultaneous decrease in the polymerization time. Close inspection reveals that with a minimal increase of the polymerization time a large improvement of *Đ* can be also accomplished, as long as *Đ* values above a critical value of *ca.* 1.23 are targeted. Note that a decrease with *ca.* 0.1 for *Đ* corresponds to an improvement of 20%

of the standard deviation of the chain length distribution. A lowering of the $Đ$ value below the critical value can be only obtained with a large penalty on the polymerization time, which can be clearly seen in the Pareto-optimal front displaying an L-shape.

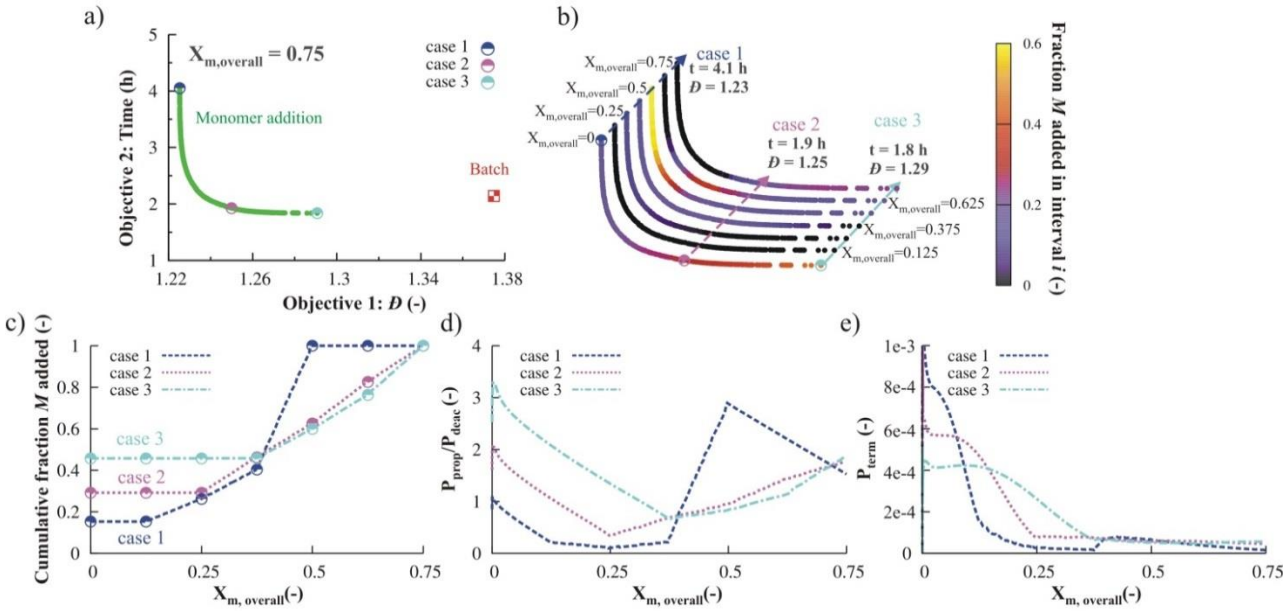

Figure 4.3. *Results for the multi-objective optimization (MOO) of ARGET ATRP of BMA using a fed-batch monomer program (constant molar flow rate per* $\Delta X_{m,overall}$ *of 0.125 until* $X_{m,overall}$ *= 0.75; 90°C;* $[R_0X]_0/[Cu^{II}X_2/L]_0/[Sn^{II}(EH)_2]_0$ *= 1/0.005/0.05; batch case:* $[M]_0/[R_0X]_0$ *= 200) (a) Pareto-optimal front (green circles) and reference batch polymerization (red square); (b) Variation of the 7 variables (fraction monomer added initially (variable 1) and during a conversion interval (variable 2-7) along the Pareto-optimal front; (c) Cumulative fraction of monomer added as a function of* $X_{m,overall}$ *for three selected cases in (a) (d) Ratio of probability for propagation over deactivation as a function of* $X_{m,overall}$ *for the selected cases; (e) Probability for termination as a function of* $X_{m,overall}$ *for the selected cases.*

Looking at the 7 variables describing the monomer addition program (Figure 4.3 (b)) it follows that more starved feed conditions at low overall conversions, *i.e.* lower monomer concentrations compared with the batch reference case, and the opposite conditions at high conversion are beneficial for control over chain length. This is shown in particular in Figure 4.4 (a) which shows

the change of the monomer concentration as a function of the overall monomer conversion for three illustrative cases of which the corresponding evolution of the cumulative molar fraction are depicted in Figure 4.3 (c). As for the temperature profile, case 1 clearly corresponds to the most dynamic case leading to the highest level of control over chain length.

The differences between the three cases in both objectives (Figure 4.3 (a)) can again be explained by looking at the evolution of P_{prop}/P_{deac} (Figure 4.3 (d)) and P_{term} (Figure 4.3 (e)). Note that the changes in reaction probabilities are now caused by differences in concentrations instead of differences in intrinsic/apparent rate coefficients. For low to intermediate overall conversions ($0.1 < X_{m,overall} < 0.4$), very low P_{prop}/P_{deac} values result, with the lowest ones for case 1, leading to a low $Đ$ for each case (Figure B.1 (b); Appendix). This beneficial effect is however slightly counteracted at very low overall conversion ($X_{m,overall} < 0.1$) by higher P_{term} values (Figure 4.3 (e)) since the radical concentration is also higher for a smaller reaction volume (Figure B.3 (a); Appendix). On the other hand, the counteracting effect is of limited importance at higher overall conversions ($X_{m,overall} > 0.1$) taking into account that the *in situ* conversions are high (Figure B.3 (b); Appendix) and thus already at low overall conversions the termination probability is strongly reduced. Hence, on an overall basis the positive effect on P_{prop}/P_{deac} is dominant up to intermediate conversions, explaining the enhanced control with the fed-batch monomer addition program. Moreover, due to the excellent suppression of termination reactions, it is possible to increase the polymerization rate at higher overall conversions, with an acceptable disturbance of the control over chain length.

In particular for case 1, which is characterized by the lowest P_{prop}/P_{deac} and P_{term} values it is afforded to add a large amount of monomer from intermediate overall conversions onwards ($X_{m,overall} > 0.4$). This only leads to a limited increase of P_{prop}/P_{deac} and a very limited increase of

P_{term}. The latter probability is only slightly increased since the large decrease of the radical concentration due to dilution compensates the corresponding increase of the apparent termination reactivity (Figure B.3 (a)-(b); Appendix). On the other hand, it should be reminded that a lower radical concentration leads to a lower propagation rate and thus higher polymerization times, consistent with the L-shape of the Pareto-optimal front.

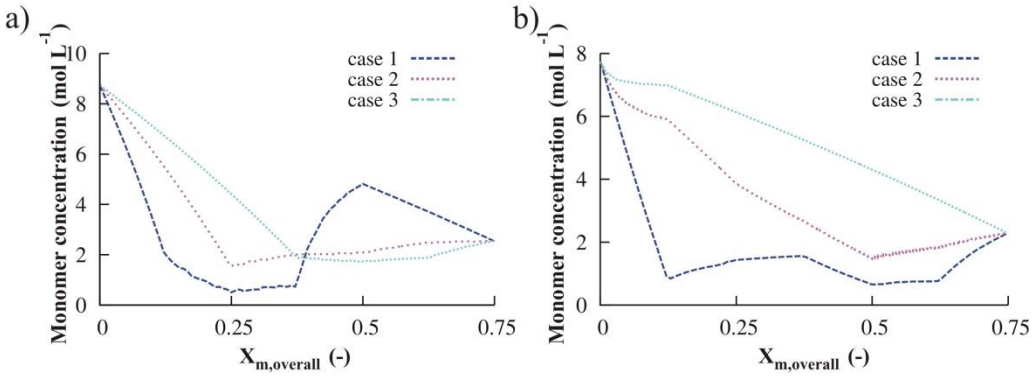

Figure 4.4. *Monomer concentration as a function of overall conversion for the three cases in (a) the multi-objective optimization (MOO) of ARGET ATRP of BMA using a fed-batch monomer program (Figure 4.3) and (b) MOO of NMP of styrene using a fed-batch monomer program (Figure 4.8).*

4.3.1.3 Variation of reducing agent

A final individual optimization pathway that is explored for the ARGET ATRP case study is the fed-batch addition of reducing agent. The total amount of reducing agent added is taken equal to the batch amount and is the same as used in the aforementioned simulations. Again a constant temperature of 90°C is chosen. The addition profile is described by 7 variables, again per conversion increment of 0.125. The first variable represents the fraction of the initial batch amount present at the start of the ARGET ATRP. The 6 remaining variables are the fractions of the initial batch amount added during an interval in a continuous manner at a constant molar flow rate.

The results (Figure 4.5 (a)) show that also in this case a trade-off between both objectives results in an L-shaped Pareto-optimal front. The values of the 7 variables, along the Pareto-optimal front, are shown in Figure 4.5 (b). From this figure it can be concluded that the fastest polymerization time is equal to the batch case. A lower initial fraction of reducing agent leads to a higher polymerization time, but lower *Đ*. Throughout the remainder of the polymerization smaller feed rates at low to intermediate conversion also lead to longer polymerization times and lower dispersities, whereas feeding the reducing agent at low conversions results in a faster polymerization but higher *Đ*.

The feeding profiles as a function of conversion for three illustrative cases are shown in Figure 4.5 (c). To explain the variation in the objectives the reaction probabilities are shown in Figure 4.5 (e)-(d). Looking at P_{prop}/P_{deac} (Figure 4.5 (d)), it can be seen that very limited differences can be observed, this in contrast to the application of a temperature and fed-batch monomer program. On the other hand, Figure 4.5 (e) shows that for case 1 (long polymerization time, low Đ; Figure B.1 (c); Appendix) P_{term} is practically zero for conversions lower than 0.5 and thus a good control over chain length can be obtained with a fed-batch addition of reducing agent. This is due to a very low radical concentration (Figure B.4; Appendix) since the reducing agent, needed for the reduction of a deactivator species, is only brought into the reaction mixture very slowly. This logically also leads to a decrease of the polymerization rate.

It can be concluded that the underlying reason of the examined individual optimization pathways can be different, as they can affect the reaction rates differently. Hence, additional improvement can be expected for specific combinations of individual optimization paths. This conjecture is explored in the next subsection.

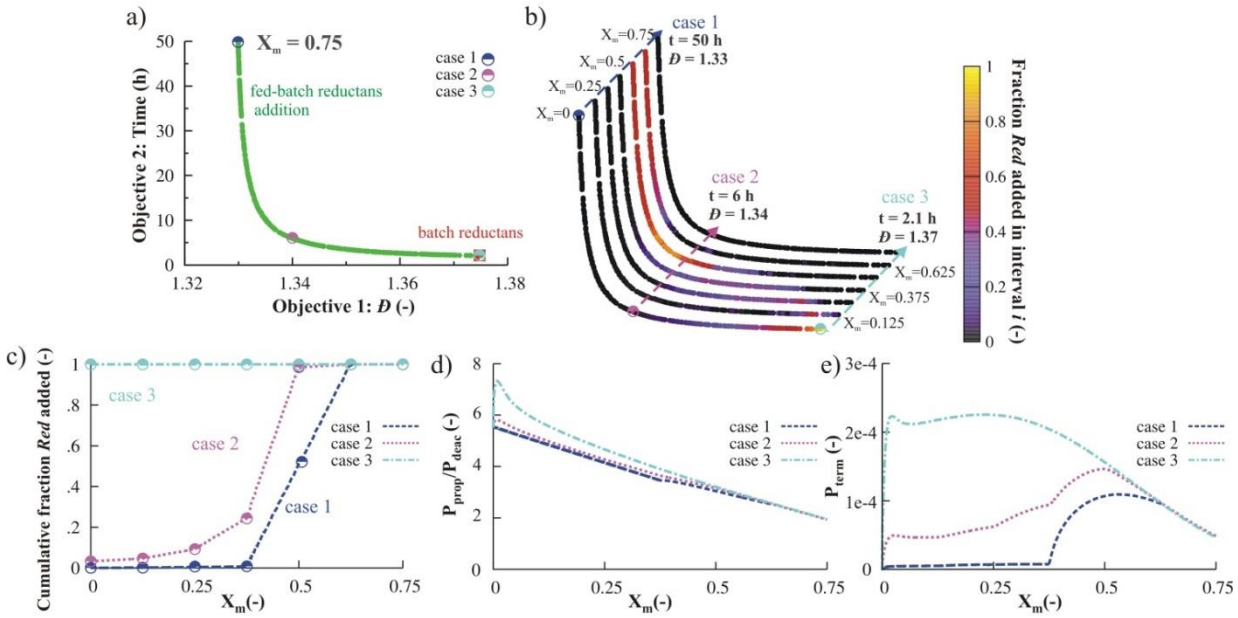

Figure 4.5. *Results for the multi-objective optimization (MOO) of ARGET ATRP of MBA using a fed-batch reducing agent program (constant molar flow rate per* ΔX_m *= 0.125 until* X_m *= 0.75;* $[M]_0/[R_0X]_0/[Cu^{II}X_2/L]_0$*= 200/1/0.005; 90°C: batch case:* $[R_0X]_0/[Sn^{II}(EH)_2]_0$*=0.05) (a) Pareto-optimal front (greencircles) and reference batch case (red square); (b) Variation of the 7 variables (fraction reducing agent added initially (variable 1) and during a certain conversion interval (variable 2-6)) along the Pareto-optimal front; (c) Cumulative fraction of reducing agent added as a function of* X_m *for three selected cases in (a); (d) Ratio of probability of propagation to deactivation as a function of* X_m *for the selected cases; (e) Probability for termination as a function of* X_m *for the selected cases.*

4.3.1.4 Simultaneous variation of different process conditions

In this subsection, a comparison between the different individual optimization pathways and combinations of these individual pathways are explored. The results of the individual optimizations and only the combinations leading to an improvement of the Pareto-optimal front (with respect to the individual optimizations) are shown in Figure 4.6. This figure shows that applying a fed-batch monomer program results in a Pareto-optimal front that dominates the Pareto-optimal fronts of the other two individual pathways, *i.e.* applying a temperature program

and fed-batch reducing agent program. Only two combinations lead to a synergetic effect. A first one is the combination of a fed-batch reducing agent program with a temperature program. An even more synergetic pathway is the combination of a fed-batch monomer and reducing agent addition program. In other words, combination of a temperature program with a fed-batch monomer program and combinations of all three do not result in a significant improvement of the Pareto-optimal front.

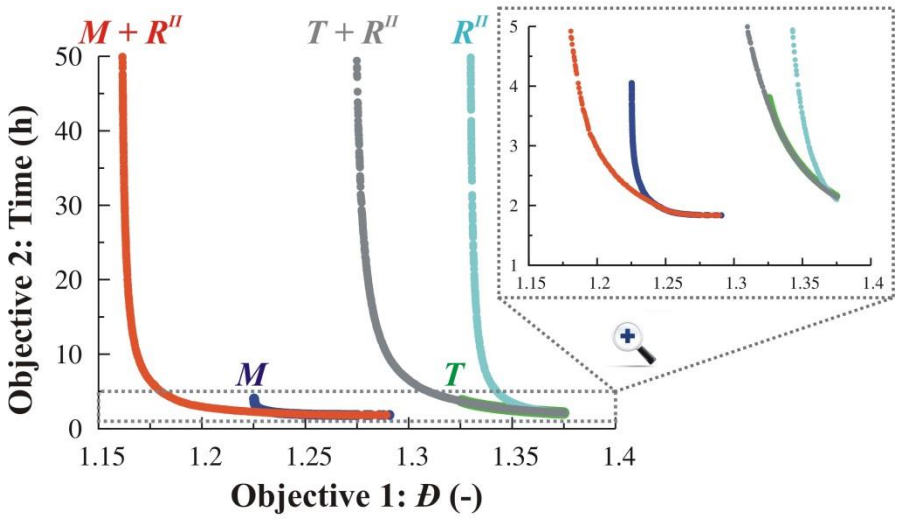

Figure 4.6. *Comparison between multi-objective optimization (MOO) results of the different individual optimization pathways: fed-batch addition of reducing agent (R^{II}) (teal; Figure 4.5 (a)), temperature program (T) (green; Figure 4.2 (a)), fed-batch addition of monomer (M) (blue; Figure 4.3 (a)), the synergetic combination of temperature program and fed-batch addition of reducing agent (grey), and the synergetic combination of fed-batch addition of monomer and reducing agent (red).*

To understand the improvement of the two synergetic cases, it is necessary to fully understand the differences of the individual optimization pathways, as previously discussed. For the temperature and the fed-batch monomer program, it was explained that both pathways lead at lower (overall) conversions to a lowered P_{prop}/P_{deac}, *i.e.* to a decrease in the average number of monomer units added per activation-growth-deactivation cycle. However, the beneficial effect on the *Đ* profiles

was partly diminished due to a higher P_{term}. Applying a fed-batch reducing agent program leads on the other hand to a reduction of P_{term} at lower conversion, but hardly influences P_{prop}/P_{deac}. Hence, it can be understood that combining the latter with a temperature or fed-batch monomer program leads to an improved Pareto-optimal front. In contrast, combining a temperature and fed-batch monomer program only results in a very limited improvement since both rely on suppressing/favoring the same reactions, which is also confirmed by the MOO.

4.3.2 Multi-objective optimization of NMP

The second case study involves the MOO of NMP of styrene initiated by MAMA-SG1 to optimize the process with respect to polymerization time, livingness and dispersity, *i.e.* 3 objectives are now considered. Several individual optimization pathways are again explored, namely optimization via a temperature program, fed-batch monomer addition, and fed-batch addition of free nitroxide, the persistent radical. Also the combination of optimization pathways is again examined. As before, for all optimizations considered, a constraint on the polymerization time of maximum 50 hours is imposed. The conditions, $[M]_0/[R_0X]_0$ = 1000/1 (120°C), are taken as batch reference conditions.

4.3.2.1 Variation of temperature

As a first optimization pathway the use of a temperature program is again investigated. The temperature program is described in the same way as with the MOO of ARGET ATRP. The 7 variables are now allowed to vary between 80 and 120 °C, based on literature data for the isothermal batch NMP of styrene.[61] The corresponding results are shown in Figure 4.7, considering three objectives, namely time, $Đ$, and EGF. For completeness it is mentioned here that a quasi-identical Pareto-optimal front is obtained in case only two objectives are selected (*e.g.* time and $Đ$; Figure B.5; Appendix). However, for decision making toward a preferred

operation point it is more suited to focus on the MOO case with three objectives (see Figure 4.7 (a)), taking into account that the EGF now varies significantly along the Pareto-optimal front. For isothermal NMP, the Pareto-optimal front is also shown in Figure 4.7 (a). Clearly, this front is not a subset of the Pareto-optimal front of the temperature program optimization. This means that a non-isothermal temperature program is always beneficial compared to the classical isothermal case.

From Figure 4.7 (b), which shows the variation of the temperature at the seven distinct conversions, it can be concluded that to find optimal trade-offs between the three objectives, a more complex temperature profile should be applied. This is also confirmed in Figure 4.7 (c), which displays the actual change of the temperature with conversion for three illustrative cases. The cases differ in the extent of their non-isothermicity but all start with a lower polymerization temperature. For the third case, which results in the lowest batch time but leads to the highest $Đ$ and lowest EGF, the temperature is maintained at the upper limit temperature throughout the major part of the polymerization and thus the isothermal case of 120°C is mimicked to a certain extent. In contrast, for the other two cases, which lead to a higher control over the NMP, the temperature is initially at its lower limit value, after which it is increased until a conversion of 0.125 is reached. Hereafter the temperature is lowered until a conversion of 0.25 results. Only at high conversion (X_m > 0.60) the temperature is significantly increased toward the maximum value and thus a strongly non-isothermal temperature profiles is established, in particular for the first case.

These at first sight counterintuitive trends in the temperature programs can be rationalized by considering the relative changes of the key reaction probabilities. As with the ARGET ATRP case, P_{prop}/P_{deac} (Figure 4.7 (d)) as well as P_{term} (Figure 4.7 (e)) play an important role in the

obtained microstructural control. As explained above, the lower P_{prop}/P_{deac}, the smaller the average number of monomer units incorporated per activation-growth-deactivation cycle and, hence, the lower the $Đ$ value. A higher P_{term} leads to an increase in $Đ$ but also to a lowering of EGF. In the case of the NMP of styrene, the reaction probability for chain transfer to dimer (P_{trD}; (Figure 4.7 (f)) needs also to be considered, specifically at elevated temperature.[62, 74]

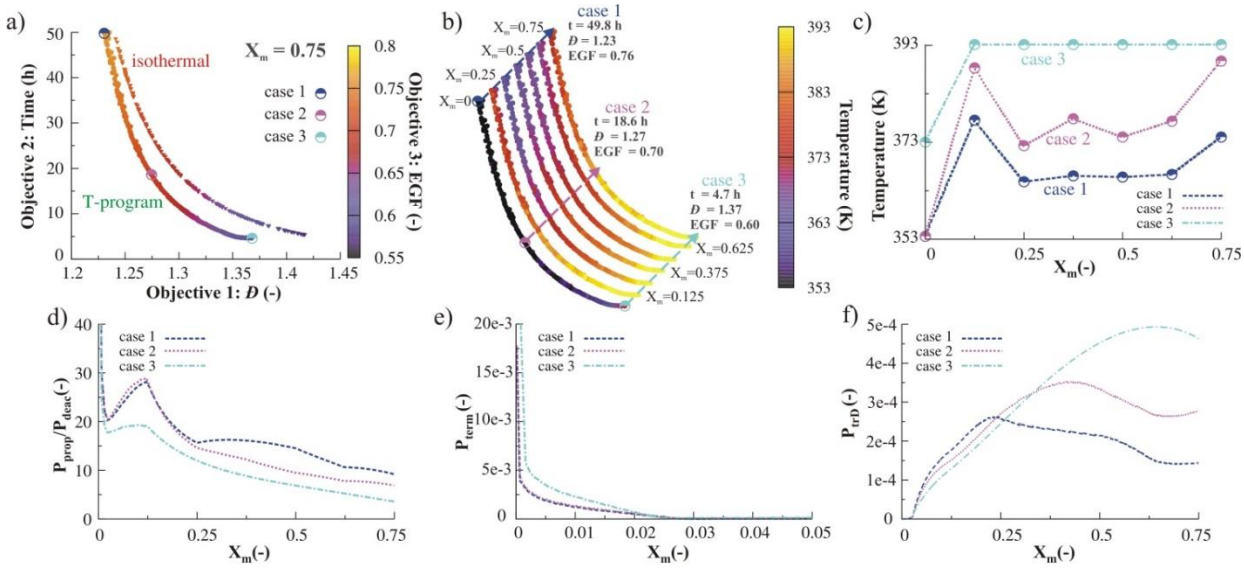

Figure 4.7. *Results for the multi-objective optimization (MOO) of NMP of styrene using a piecewise linear temperature program (ΔX_m = 0.125 until X_m = 0.75; $[M]_0/[R_0X]_0$ = 1000/1) (a) Pareto-optimal front and corresponding isothermal front; (b) Variation of the temperature at the interval boundaries along the Pareto-optimal front; (c) Temperature as a function of X_m for three selected cases; (d) Ratio of probability for propagation over deactivation as a function of X_m for the selected cases; (e) Probability for termination; (f) Probability for transfer to dimer as a function of X_m.*

At low conversion, the beneficial effect of starting with a lower temperature has already been explained in Fierens *et al.* [61] in which an isothermal NMP (120°C) was compared with a NMP conducted using a stepwise temperature profile with a lower initial temperature aiming to obtain a conversion of X_m of 0.75 within the same polymerization time as the isothermal case. With the stepwise profile less termination is occurring in the early stage of the NMP, leading to a less

dramatic manifestation of the persistent radical effect. This is confirmed in Figure 4.7 (e) in which P_{term} is clearly lowered and thus EGF is increased when starting at a lower initial temperature (decreasing temperature for case 3, 2 and 1). On the other hand, at these low conversions, P_{prop}/P_{deac} and P_{trD} are higher compared to the quasi-isothermal case 3, leading to higher initial $Đ$ values (Figure B.6 (a); Appendix) for case 1 and 2. From intermediate conversions onwards, in contrast, lowering the polymerization temperature is beneficial for the evolution of $Đ$ and EGF. This can be explained by looking at the pronounced change of P_{trD} (Figure 4.7 (f)). The lower temperature in case 2 and 3 for intermediate conversions suppresses the influence of the chain transfer to dimer, leading to the observed better control over $Đ$ and EGF. On the one hand, less dimer is formed via thermal auto-initiation and on the other hand chain transfer to dimer is suppressed, taking into account its relatively high activation energy (28 kJ mol^{-1} in Table 4.3). This, obviously, also leads to a decreased polymerization rate. Note that the increase of the temperature at the higher conversions (Figure 4.7 (c)) does not result in a severe penalty on the relevance of chain transfer to dimer (Figure 4.7 (f)) since the dimer concentration (Figure B.7 (a); Appendix) is already significantly decreased. This temperature increase will increase the polymerization rate. However, still a relatively slow NMP is obtained on an overall basis if a dynamic temperature profile is considered.

4.3.2.2 Monomer addition

A second optimization pathway for the NMP of styrene is the fed-batch addition of monomer. A constant temperature of 120°C is considered for illustration purposes. Again the overall conversion domain is divided into discrete subdomains of conversion increments of 0.125. The addition profile is again described by 7 variables, each representing the added fraction with respect to the corresponding initial batch amount. The initial fraction present has now a lower

limit of 10 mol%. Note that this monomer addition approach can be seen as an extension of the work of Bentein *et al.* [62] in which fixed small amounts of monomer were added for the NMP of styrene, using phenylethyl-SG1 as NMP initiator.

As can be seen in Figure 4.8 (a), fed-batch monomer addition results in an improvement compared to the batch case. Looking at the value of each variable along the Pareto-optimal front (Figure 4.8 (b)) some trends can be observed. It is beneficial to start the NMP with a low amount of monomer after which the remainder of the initial batch amount monomer is added continuously. As for the temperature variation, a more complex profile allows a higher level of control. Selecting again three illustrative cases, this becomes more clear when considering the explicit variation of the cumulative amount of monomer added with overall conversion (Figure 4.8 (c)). The corresponding monomer concentration profiles are provided in Figure 4.4 (b). For case 3, the total amount of monomer is already added in the first interval, leading to a high monomer concentration and a high polymerization rate but also to a higher $Đ$ and a lower EGF. For the other two cases, the addition of the remainder monomer amount occurs throughout the whole NMP. With the most starved-feed monomer conditions (case 1) the highest degree of control is obtained despite an increase in polymerization time.

At low conversions, the beneficial effect of starting with a low initial amount of monomer can be partially linked to P_{prop}/P_{deac} (Figure 4.8 (d)). This ratio is the lowest for case 1 where on average a lower amount of monomer is incorporated in each activation-growth-deactivation cycle, already from low conversion onwards. In other words, the initial spike in the $Đ$ profile (Figure B.6 (b); Appendix) is lower and $Đ$ declines to a lower value since controlled conditions are already obtained at a lower conversion. Additionally, the improved control can be related to the positive evolution of P_{term} (Figure 4.8 (e)) and P_{trD} (Figure 4.8 (f)). It is important to mention that case 1

has the highest living macroradical concentration of the three cases considered. Nevertheless, the rate of termination is the lowest since termination reactions are more diffusion controlled throughout the NMP. In case 1, the *in situ* conversion is namely very high (≈ 0.9) for the largest part of the polymerization (Figure B.8 (a); Appendix) and diffusional limitations are more pronounced, explaining the lower P_{term} values.

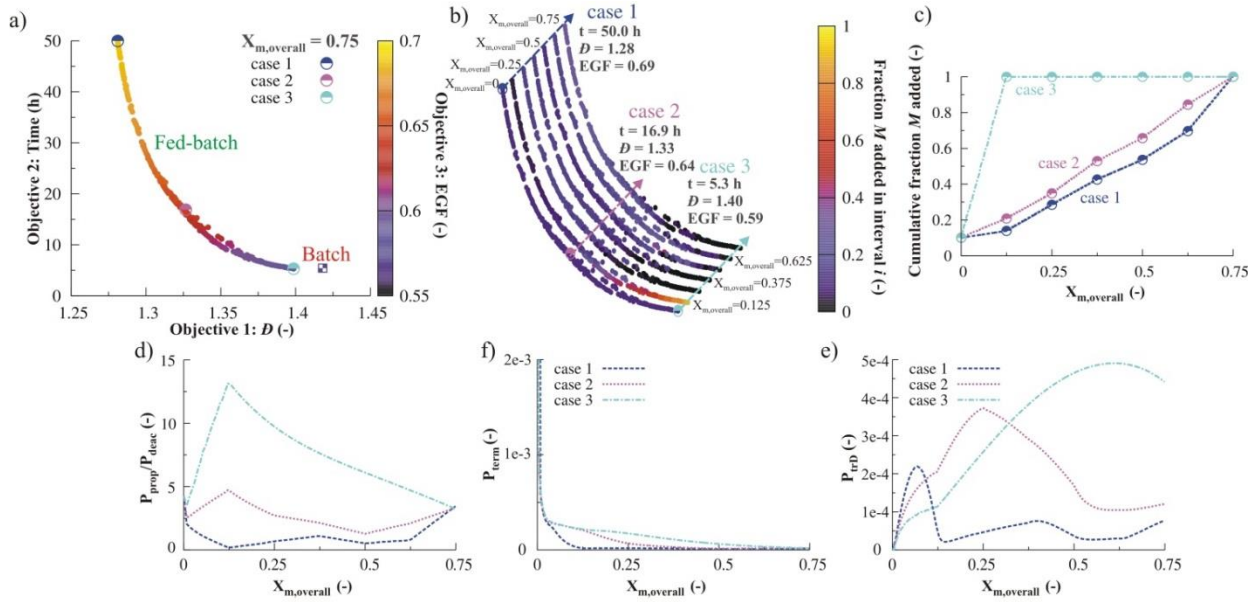

Figure 4.8. *Results for the multi-objective optimization (MOO) of NMP of styrene (120°C) using a fed-batch monomer program (constant molar flow rate per* $\Delta X_{m,overall}$ *of 0.125 until* $X_{m,overall}$ *= 0.75;* $[M]_0/[R_0X]_0$ *= 1000/1) (a) Pareto-optimal front and corresponding isothermal front; (b) Variation of the 7 variables (fraction monomer added initially (variable 1) and during a conversion interval (variable 2-7) along the Pareto-optimal front; (c) Cumulative fraction of monomer added as a function of* $X_{m,overall}$ *for three selected cases; (d) Ratio of probability for propagation to deactivation as a function of* $X_{m,overall}$ *for the selected cases; (e) Probability for termination as a function of* $X_{m,overall}$ *for the selected cases; (f) Probability for chain transfer to dimer as a function of* $X_{m,overall}$ *for the selected cases.*

The reduced importance of chain transfer to dimer can be understood by looking closely at the dimer formation in which two monomer molecules need to undergo a Diels-Alder reaction. If a

fed-batch monomer addition program is applied, especially under starved feed conditions, i.e. case 1 and case 2, the monomer concentration is kept low (Figure 4.4 (b)), thereby strongly reducing the dimer concentration (Figure B.8 (b); Appendix) and thus also lowering P_{trD}.

3.2.1. Variation of initial nitroxide loading

The beneficial influence of an excess of nitroxide with respect to NMP initiator, has already been discussed in literature.[39, 44, 75] Therefore, as a third possibility to optimize the NMP characteristics, the addition of nitroxide at the start of the polymerization is investigated. To stay within representative NMP conditions, the maximum initial ratio of nitroxide (X) to NMP initiator (R_0X) has been limited to 0.5. Again a constant polymerization temperature of 120°C is selected. For completeness it is mentioned here that also a MOO was performed with a nitroxide fed-batch addition program. However, this optimization revealed that the Pareto-optimal front only consists of points in which the total amount of nitroxide is added at the start of the polymerization, explaining why the initial loading was finally taken up as the only variable.

The Pareto-optimal front considering three objectives (time, $Đ$, and EGF) is given in Figure 4.9 (a). The corresponding variation of the initial molar ratio of nitroxide to NMP initiator is provided in Figure 4.9 (b). When an excess of nitroxide is initially present, termination is already strongly suppressed from the start of the NMP and almost no build-up of nitroxide is needed to create a sufficient high concentration of nitroxide species (Figure 4.9 (d)). This can also be inferred from Figure 4.9 (c) in which P_{prop}/P_{deac} is plotted as a function of conversion. At the initial stage, excess nitroxide leads to a sharp decrease in this ratio, since deactivation reactions are favored from the beginning of the polymerization, and thus the $Đ$ profile falls back to a much lower value from an early stage in the polymerization (Figure B.6 (c); Appendix). The beneficial effect is however counteracted at higher conversions by the higher importance of the chain

transfer to dimer reaction (Figure 4.9 (e)) leading to a rise in the *Đ* profile as a function of conversion. This higher importance can be related to the higher impact of radical generation via thermal initiation (Figure B.9 (a); Appendix), since a lower polymerization rates allows an increase of the dimer concentration (Figure B.9 (b); Appendix) during a significant period. Hence, the concentration of both reactants for chain transfer to dimer increases in such way that P_{trD} increases, explaining the observed *Đ* profiles.

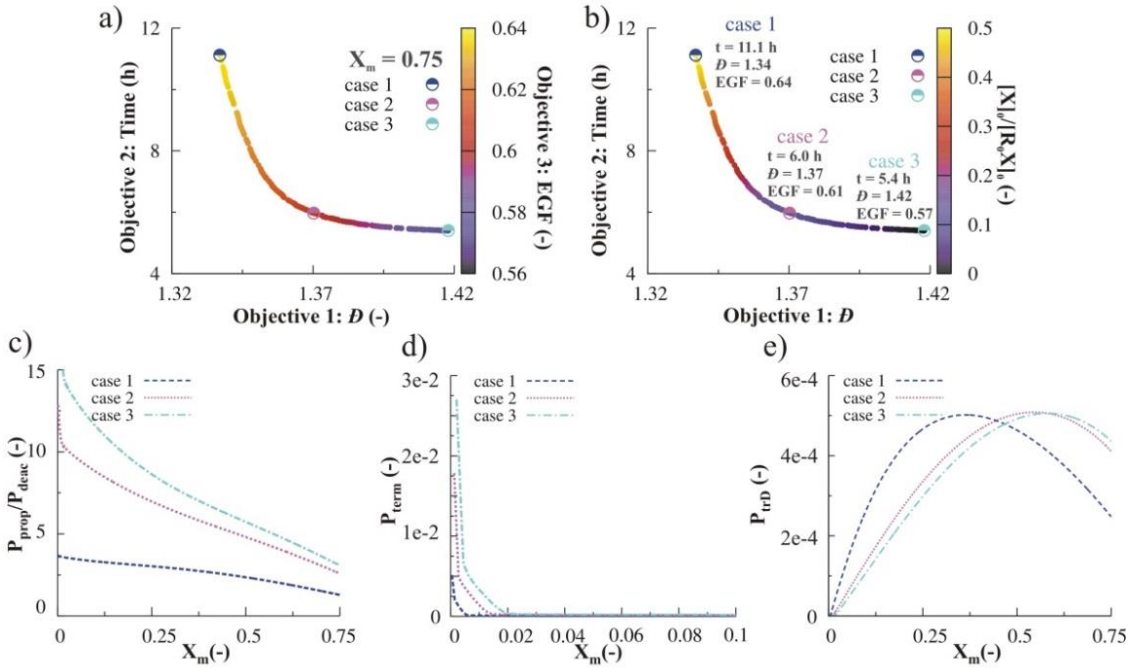

Figure 4.9. *Results for the multi-objective optimization (MOO) of NMP of styrene (120°C) using excess initial nitroxide (ΔX_m = 0.125 until X_m = 0.75; $([M]_0/[R_0X]_0$= 1000/1) (a) Pareto-optimal front and corresponding isothermal front; (b) Variation of $[X]_0/[R_0X]_0$ along the Pareto-optimal front; (c) Ratio of probability for propagation to deactivation as a function of conversion for the selected cases; (d) Probability for termination as a function of X_m for the selected cases; (e) Probability for chain transfer to dimer as a function of X_m for the selected cases.*

It should be stressed that overall still a large improvement of the *Đ* can be obtained with a relative small penalty in polymerization time, as witnessed from the L-shape of the Pareto-optimal front

(Figure 4.9 (a)). This result is corroborated by the reported observation that a small addition of nitroxide (< 10mol%) is beneficial for NMP processes in general, and that higher amounts decrease the polymerization rate excessively.[39]

4.3.2.3 Simultaneous variation of different process conditions

In a final step, combinations of the aforementioned individual pathways are explored, considering the most complex case of the three objectives time, *Đ* and EGF. The most interesting combinations of these advanced MOO simulations are shown in Figure 4.10, accompanied by the MOO fronts obtained via a single variation. To avoid misinterpretation, the Pareto optimal front is depicted twice using the time as the common objective. Looking only at the result of the individual optimization pathways it can be seen that applying a temperature program can be considered the best option with respect to all three objectives.

Further inspection shows that combination of a fed-batch monomer addition and an initial excess amount of nitroxide (yellow dots) is strongly synergetic, leading to a much improved Pareto-optimal front compared to the individual cases (green and red circles), especially for *Đ* (Figure 4.10**(**a)). This synergetic effect is due to positive effect of the initial presence of the free nitroxide which leads to a strongly decreased P_{prop}/P_{deac} and thus a lower *Đ* from low conversions onwards. Moreover, fed-batch addition of monomer additionally allows to suppress chain transfer to dimer reactions, which cannot be achieved if the nitroxide loading is the only variable, as explained in the previous subsection.

Finally, it follows that the combination of a temperature profile with a fed-batch monomer addition (purple dots) leads to Pareto-optimal fronts that cannot be represented by a single line, taking into account the 2D representation. This is a direct consequence of the definition of Pareto-optimality in which only improvement in one objective is needed, *i.e.* the simultaneous

improvement of both EGF and *Đ* is not strictly demanded. Hence, depending on the actual RDRP product requirements, it follows that a certain combination will be seen as suitable are not.

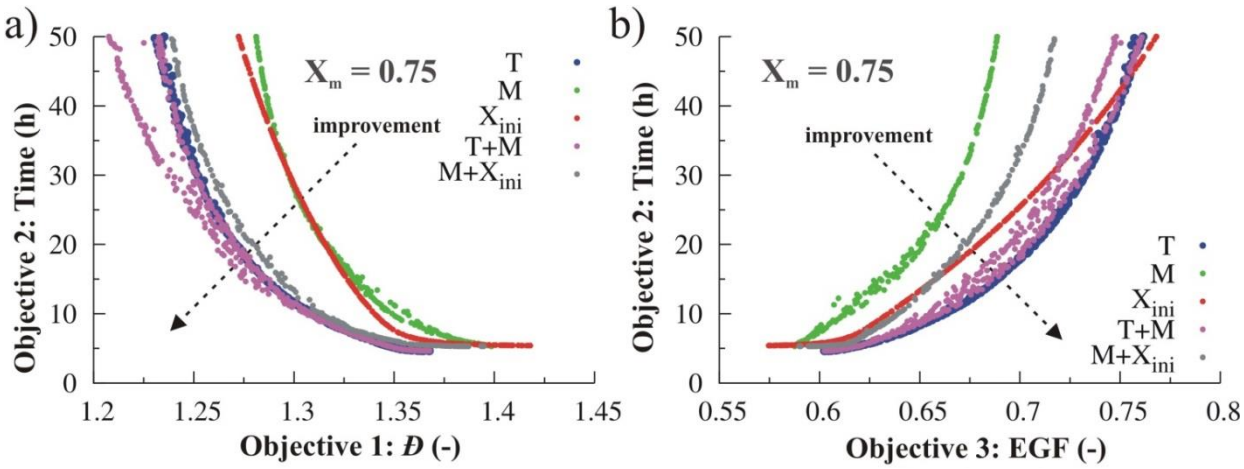

Figure 4.10. *Comparison between multi-objective optimization (MOO) results of NMP of styrene for the different individual optimization pathways: temperature program (T) (blue; Figure 4.7 (a)), fed-batch addition of monomer (M) (green; Figure 4.8 (a)), excess initial nitroxide (X_{ini}) (red; Figure 4.9 (a)), the synergetic combination of temperature program and fed-batch monomer addition (purple), the synergetic combination of fed-batch addition of monomer and excess initial nitroxide (grey) (a) projection for objective 1 (Đ) and objective 2 (time), and (b) projection for objective 3 (EGF) and objective 2 (time).*

4.4 Conclusions

For the first time, Pareto-optimal fronts have been determined for two important reversible deactivation radical polymerization (RDRP) techniques, *i.e.* activators regenerated electron transfer atom transfer radical polymerization (ARGET ATRP) and nitroxide mediated polymerization (NMP). For the simulations, the NSGA-II algorithm has been successfully implemented and combined with literature kinetic models. Diffusional limitations are accounted for on termination using a composite k_t-model. As design variables the temperature, and molar amounts of the involved species have been considered per conversion interval of 0.125, until a

conversion of 0.75 is reached. A distinction is made between 2-dimensional multi-objective optimization (MOO) for ARGET ATRP of BMA with as objectives time and *Đ*, and 3-dimensional MOO for NMP of styrene with as objectives time, *Đ*, and EGF.

In both RDRPs, the conditions belonging to the Pareto-optimal front perform better than the corresponding isothermal or batch conditions. In particular, significant gain in time is obtained for a given control over the RDRP. A typical Pareto-optimal front is L-shaped, implying that control can be improved without a significant penalty on time up to a critical *Đ*.

For ARGET ATRP of BMA, the strongest improvement for individual optimization pathways is obtained if a fed-batch addition of monomer is performed. Further improvement is obtained in case a combination of two optimization pathways is allowed. The most promising results are obtained when either a temperate program is combined with a fed-batch addition of reducing agent or a fed-batch addition of monomer is combined with a fed-batch addition of reducing agent. This can be explained by analyzing the reaction probabilities for the radical species. Fed-batch addition of a reducing agent allows to lower the termination reaction probability, whereas fed-batch addition of monomer and a temperature program allow to decrease the propagation to deactivation reaction probability which ensures a more controlled incorporation of monomer units per activation-growth-deactivation cycle on an average basis.

For NMP of styrene, considering individual optimization paths, a temperature program is the most suited, as it allows to suppress termination at low conversion, to decrease the propagation to deactivation reaction probability and to avoid a dominant occurrence of chain transfer to dimer at high conversion. A combination with fed-batch addition of monomer or a non-zero initial deactivator concentration allows further improvement. The former combination does however not automatically implies a simultaneous improvement in EGF and *Đ*.

Finally, it should be stressed that although NMP and ARGET ATRP are vastly different, it has been demonstrated that the road to maximize their potential consists of the common themes of optimizing the RDRP initiation process, mediating the activation/growth/deactivation cycles and suppressing termination and chain transfer reactions.

References

1. Braunecker, W. A.; Matyjaszewski, K. Controlled/living radical polymerization: Features, developments, and perspectives. *Prog. Polym. Sci.* **2007,** 32, (1), 93-146.

2. Matyjaszewski, K., *Handbook of Radical Polymerization*. 2002.

3. Chiefari, J.; Chong, Y. K.; Ercole, F.; Krstina, J.; Jeffery, J.; Le, T. P. T.; Mayadunne, R. T. A.; Meijs, G. F.; Moad, C. L.; Moad, G.; Rizzardo, E.; Thang, S. H. Living free-radical polymerization by reversible addition-fragmentation chain transfer: The RAFT process. *Macromolecules* **1998,** 31, (16), 5559-5562.

4. Chong, Y. K.; Le, T. P. T.; Moad, G.; Rizzardo, E.; Thang, S. H. A more versatile route to block copolymers and other polymers of complex architecture by living radical polymerization: The RAFT process. *Macromolecules* **1999,** 32, (6), 2071-2074.

5. Moad, G.; Chiefari, J.; Chong, Y. K.; Krstina, J.; Mayadunne, R. T. A.; Postma, A.; Rizzardo, E.; Thang, S. H. Living free radical polymerization with reversible addition-fragmentation chain transfer (the life of RAFT). *Polym. Int.* **2000,** 49, (9), 993-1001.

6. D'hooge, D. R.; Vachaudez, M.; Stadler, F. J.; Reyniers, M.-F.; Coulembier, O.; Bailly, C.; Dubois, P.; Marin, G. B. Assessment of end-group functionality in atom transfer radical polymerization of N-isopropylacrylamide. *Eur. Polym. J.* **2013,** 49, (8), 2344-2355.

7. Metz, N.; Theato, P. Controlled synthesis of poly(acetone oxime acrylate) as a new reactive polymer: Stimuli-responsive reactive copolymers. *Eur. Polym. J.* **2007,** 43, (4), 1202-1209.

8. Ferrari, R.; Yu, Y.; Morbidelli, M.; Hutchinson, R. A.; Moscatelli, D. ε-Caprolactone-Based Macromonomers Suitable for Biodegradable Nanoparticles Synthesis through Free Radical Polymerization. *Macromolecules* **2011,** 44, (23), 9205-9212.

9. Wang, W.; Hutchinson, R. A. PLP/SEC/NMR Study of Free Radical Copolymerization of Styrene and Glycidyl Methacrylate. *Macromolecules* **2008,** 41, (23), 9011-9018.

10. Wang, J.-S.; Matyjaszewski, K. Controlled/"living" radical polymerization. atom transfer radical polymerization in the presence of transition-metal complexes. *J. Am. Chem. Soc.* **1995,** 117, (20), 5614-5615.

11. Patten, T. E.; Matyjaszewski, K. Atom Transfer Radical Polymerization and the Synthesis of Polymeric Materials. *Advanced Materials* **1998,** 10, (12), 901-915.

12. Matyjaszewski, K.; Xia, J. Atom Transfer Radical Polymerization. *Chem. Rev.* **2001,** 101, (9), 2921-2990.

13. Vachaudez, M.; D'hooge, D. R.; Socka, M.; Libiszowski, J.; Coulembier, O.; Reyniers, M. F.; Duda, A.; Marin, G. B.; Dubois, P. Inverse dependencies on the polymerization rate in atom transfer radical polymerization of N-isopropylacrylamide in aqueous medium. *Reactive and Functional Polymers* **2013,** 73, (3), 484-491.

14. Teodorescu, M.; Matyjaszewski, K. Controlled polymerization of (meth)acrylamides by atom transfer radical polymerization. *Macromol. Rapid Commun.* **2000,** 21, (4), 190-194.

15. Lutz, J. F.; Matyjaszewski, K. Kinetic modeling of the chain-end functionality in atom transfer radical polymerization. *Macromol. Chem. Phys.* **2002,** 203, (10-11), 1385-1395.

16. Ballard, N.; Salsamendi, M.; Santos, J. I.; Ruipérez, F.; Leiza, J. R.; Asua, J. M. Experimental Evidence Shedding Light on the Origin of the Reduction of Branching of Acrylates in ATRP. *Macromolecules* **2014,** 47, (3), 964-972.

17. Nicolas, J.; Guillaneuf, Y.; Lefay, C.; Bertin, D.; Gigmes, D.; Charleux, B. Nitroxide-mediated polymerization. *Progress in Polymer Science* **2013,** 38, (1), 63-235.

18. Moad, G.; Rizzardo, E.; Solomon, D. H. A product study of the nitroxide inhibited thermal polymerization of styrene. *Polym. Bull.* **1982,** 6, (11-1), 589-593.

19. Georges, M. K.; Veregin, R. P. N.; Kazmaier, P. M.; Hamer, G. K. Narrow molecular-weight resins by a free-radical polymerization process. *Macromolecules* **1993,** 26, (11), 2987-2988.

20. Hawker, C. J. Molecular Weight Control by a "Living" Free-Radical Polymerization Process. *J. Am. Chem. Soc.* **1994,** 116, (24), 11185-11186.

21. Hawker, C. J.; Barclay, G. G.; Orellana, A.; Dao, J.; Devonport, W. Initiating Systems for Nitroxide-Mediated "Living" Free Radical Polymerizations: Synthesis and Evaluation. *Macromolecules* **1996,** 29, (16), 5245-5254.

22. Fischer, H. The Persistent Radical Effect In "Living" Radical Polymerization. *Macromolecules* **1997,** 30, (19), 5666-5672.

23. Fischer, H. The persistent radical effect in controlled radical polymerizations. *J. Polym. Sci. Pol. Chem.* **1999,** 37, (13), 1885-1901.

24. Tang, W.; Tsarevsky, N. V.; Matyjaszewski, K. Determination of equilibrium constants for atom transfer radical polymerization. *J. Am. Chem. Soc.* **2006,** 128, (5), 1598-1604.

25. Toloza Porras, C.; D'hooge, D. R.; Van Steenberge, P. H. M.; Reyniers, M.-F.; Marin, G. B. A Theoretical Exploration of the Potential of ICAR ATRP for One- and Two-Pot Synthesis of Well-Defined Diblock Copolymers. *Macromol. React. Eng.* **2013,** 7, (7), 311-326.

26. Jakubowski, W.; Matyjaszewski, K. Activator Generated by Electron Transfer for Atom Transfer Radical Polymerization. *Macromolecules* **2005,** 38, (10), 4139-4146.

27. Jakubowski, W.; Min, K.; Matyjaszewski, K. Activators Regenerated by Electron Transfer for Atom Transfer Radical Polymerization of Styrene. *Macromolecules* **2005,** 39, (1), 39-45.

28. D'hooge, D. R.; Konkolewicz, D.; Reyniers, M.-F.; Marin, G. B.; Matyjaszewski, K. Kinetic Modeling of ICAR ATRP. *Macromol. Theory Simul.* **2012,** 21, (1), 52-69.

29. Mohammad Rabea, A.; Zhu, S. Achieving High-Conversion Bulk ATRP with Good Livingness and Well Controlled by Design and Optimization of Polymerization Temperature Profile. *Macromol. React. Eng.* **2014,** 8, (11), 771-776.

30. Van Steenberge, P. H. M.; D'hooge, D. R.; Wang, Y.; Zhong, M. J.; Reyniers, M. F.; Konkolewicz, D.; Matyjaszewski, K.; Marin, G. B. Linear Gradient Quality of ATRP Copolymers. *Macromolecules* **2012,** 45, (21), 8519-8531.

31. Toloza Porras, C.; D'hooge, D. R.; Reyniers, M. F.; Marin, G. B. Computer-Aided Optimization of Conditions for Fast and Controlled ICAR ATRP of n-Butyl Acrylate. *Macromol. Theory Simul.* **2013,** 22, (2), 136-149.

32. D'hooge, D. R.; Van Steenberge, P. H. M.; Reyniers, M.-F.; Marin, G. B. Fed-Batch Control and Visualization of Monomer Sequences of Individual ICAR ATRP Gradient Copolymer Chains. *Polymers* **2014,** 6, (4), 1074-1095.

33. Chan, N.; Cunningham, M. F.; Hutchinson, R. A. Copper mediated controlled radical polymerization of methyl acrylate in the presence of ascorbic acid in a continuous tubular reactor. *Polymer Chemistry* **2012,** 3, (5), 1322-1333.

34. Chan, N.; Meuldijk, J.; Cunningham, M. F.; Hutchinson, R. A. Continuous ARGET ATRP of Methyl Methacrylate and Butyl Acrylate in a Stirred Tank Reactor. *Industrial & Engineering Chemistry Research* **2013,** 52, (34), 11931-11942.

35. Greszta, D.; Matyjaszewski, K. Mechanism of controlled/"living" radical polymerization of styrene in the presence of nitroxyl radicals. Kinetics and simulations. *Macromolecules* **1996,** 29, (24), 7661-7670.

36. Solomon, D. H., Rizzardo E., Cacioli P. Polymerization process and polymers produced thereby. 1986.

37. Bertin, D.; Gigmes, D.; Marque, S. R. A.; Tordo, P. Kinetic subtleties of nitroxide mediated polymerization. *Chem. Soc. Rev.* **2011,** 40, (5), 2189-2198.

38. Fukuda, T.; Goto, A.; Ohno, K. Mechanisms and kinetics of living radical polymerizations. *Macromol. Rapid Commun.* **2000,** 21, (4), 151-165.

39. Gigmes, D.; Bertin, D.; Lefay, C.; Guillaneuf, Y. Kinetic Modeling of Nitroxide-Mediated Polymerization: Conditions for Living and Controlled Polymerization. *Macromol. Theory Simul.* **2009,** 18, (7-8), 402-419.

40. Lutz, J. F.; Lacroix-Desmazes, P.; Boutevin, B. The persistent radical effect in nitroxide mediated polymerization: Experimental validity. *Macromol. Rapid Commun.* **2001,** 22, (3), 189-193.

41. Hernandez-Ortiz, J. C.; Vivaldo-Lima, E.; Lona, L. M. F.; McManus, N. T.; Penlidis, A. Modeling of the Nitroxide-Mediated Radical Copolymerization of Styrene and Divinylbenzene. *Macromol. React. Eng.* **2009,** 3, (5-6), 288-311.

42. Saldívar-Guerra, E.; Bonilla, J.; Becerril, F.; Zacahua, G.; Albores-Velasco, M.; Alexander-Katz, R.; Flores-Santos, L.; Alexandrova, L. On the Nitroxide Quasi-Equilibrium in the Alkoxyamine-Mediated Radical Polymerization of Styrene. *Macromol. Theory Simul.* **2006,** 15, (2), 163-175.

43. Tang, W.; Fukuda, T.; Matyjaszewski, K. Reevaluation of persistent radical effect in NMP. *Macromolecules* **2006,** 39, (13), 4332-4337.

44. Benoit, D.; Chaplinski, V.; Braslau, R.; Hawker, C. J. Development of a Universal Alkoxyamine for "Living" Free Radical Polymerizations. *J. Am. Chem. Soc.* **1999,** 121, (16), 3904-3920.

45. Grimaldi, S.; Finet, J.-P.; Le Moigne, F.; Zeghdaoui, A.; Tordo, P.; Benoit, D.; Fontanille, M.; Gnanou, Y. Acyclic β-Phosphonylated Nitroxides: A New Series of Counter-Radicals for "Living"/Controlled Free Radical Polymerization. *Macromolecules* **2000,** 33, (4), 1141-1147.

46. Greszta, D.; Matyjaszewski, K. TEMPO-mediated polymerization of styrene: Rate enhancement with dicumyl peroxide. *Journal of Polymer Science Part A: Polymer Chemistry* **1997,** 35, (9), 1857-1861.

47. He, J. P.; Chen, J. M.; Li, L.; Pan, J. Y.; Li, C. M.; Cao, J. Z.; Tao, Y. F.; Hua, F. J.; Yang, Y. L.; McKee, G. E.; Brinkmann, S. Rate enhancement of nitroxide-mediated living free-radical polymerization by continuous addition of initiator. *Polymer* **2000,** 41, (12), 4573-4577.

48. Malmström, E.; Miller, R. D.; Hawker, C. J. Development of a new class of rate-accelerating additives for nitroxide-mediated 'living' free radical polymerization. *Tetrahedron* **1997,** 53, (45), 15225-15236.

49. Grubbs, R. B. Nitroxide-Mediated Radical Polymerization: Limitations and Versatility. *Polymer Reviews* **2011,** 51, (2), 104-137.

50. Nayak, A.; Gupta, S. K. Multi-Objective Optimization of Semi-Batch Copolymerization Reactors Using Adaptations of Genetic Algorithm. *Macromol. Theory Simul.* **2004,** 13, (1), 73-85.

51. Deb, K.; Kalyanmoy, D., *Multi-Objective Optimization Using Evolutionary Algorithms*. John Wiley \& Sons, Inc.: 2001; p 518.

52. Coello Coello, C. A. Evolutionary multi-objective optimization: a historical view of the field. *Computational Intelligence Magazine, IEEE* **2006,** 1, (1), 28-36.

53. Srinivas, N.; Deb, K. Muiltiobjective Optimization Using Nondominated Sorting in Genetic Algorithms. *Evolutionary Computation* **1994,** 2, (3), 221-248.

54. Deb, K.; Pratap, A.; Agarwal, S.; Meyarivan, T. A fast and elitist multiobjective genetic algorithm: NSGA-II. *IEEE Trans. Evol. Comput.* **2002,** 6, (2), 182-197.

55. Mitra, K.; Deb, K.; Gupta, S. K. Multiobjective dynamic optimization of an industrial nylon 6 semibatch reactor using genetic algorithm. *J. Appl. Polym. Sci.* **1998,** 69, (1), 69-87.

56. Bhaskar, V.; Gupta, S. K.; Ray, A. K. Multiobjective optimization of an industrial wiped film poly(ethylene terephthalate) reactor: some further insights. *Computers & Chemical Engineering* **2001,** 25, (2–3), 391-407.

57. Mitra, K.; Majumdar, S.; Raha, S. Multiobjective dynamic optimization of a semi-batch epoxy polymerization process. *Computers & Chemical Engineering* **2004,** 28, (12), 2583-2594.

58. Garg, S.; Gupta, S. K. Multiobjective optimization of a free radical bulk polymerization reactor using genetic algorithm. *Macromol. Theory Simul.* **1999,** 8, (1), 46-53.

59. Benyahia, B.; Latifi, M. A.; Fonteix, C.; Pla, F. Multicriteria dynamic optimization of an emulsion copolymerization reactor. *Computers & Chemical Engineering* **2011,** 35, (12), 2886-2895.

60. Massebeuf, S.; Fonteix, C.; Hoppe, S.; Pla, F. Development of new concepts for the control of polymerization processes: Multiobjective optimization and decision engineering. I. Application to emulsion homopolymerization of styrene. *J. Appl. Polym. Sci.* **2003,** 87, (14), 2383-2396.

61. Fierens, S. K.; D'hooge, D. R.; Van Steenberge, P. H. M.; Reyniers, M.-F.; Marin, G. B. MAMA-SG1 initiated nitroxide mediated polymerization of styrene: From Arrhenius parameters to model-based design. *Chem. Eng. J.* in press doi:10.1016/j.cej.2014.09.024.

62. Bentein, L.; D'hooge, D. R.; Reyniers, M. F.; Marin, G. B. Kinetic Modeling as a Tool to Understand and Improve the Nitroxide Mediated Polymerization of Styrene. *Macromol. Theory Simul.* **2011,** 20, (4), 238-265.

63. Petzold, L. Automatic selection of methods for solving stiff and nonstiff systems of ordinary differential-equations. *Siam Journal on Scientific and Statistical Computing* **1983,** 4, (1), 136-148.

64. Payne, K. A.; D'hooge, D. R.; van Steenberge, P. H. M.; Reyniers, M. F.; Cunningham, M. F.; Hutchinson, R. A.; Marin, G. B. ARGET ATRP of Butyl Methacrylate: Utilizing Kinetic Modeling To Understand Experimental Trends. *Macromolecules* **2013,** 46, (10), 3828-3840.

65. Derboven, P.; D'hooge, D. R.; Reyniers, M.-F.; Marin, G. B.; Barner-Kowollik, C. The Long and the Short of Radical Polymerization. *Macromolecules* **2015,** 48, (3), 492-501.

66. Tang, W.; Matyjaszewski, K. Kinetic Modeling of Normal ATRP, Normal ATRP with Cu-II (o), Reverse ATRP and SR&NI ATRP. *Macromol. Theory Simul.* **2008,** 17, (7-8), 359-375.

67. Mayo, F. R. Chain Transfer in the Polymerization of Styrene. VIII. Chain Transfer with Bromobenzene and Mechanism of Thermal Initiation1. *J. Am. Chem. Soc.* **1953,** 75, (24), 6133-6141.

68. Zetterlund, P. B.; Saka, Y.; McHale, R.; Nakamura, T.; Aldabbagh, F.; Okubo, M. Nitroxide-mediated radical polymerization of styrene: Experimental evidence of chain transfer to monomer. *Polymer* **2006,** 47, (23), 7900-7908.

69. Johnston-Hall, G.; Monteiro, M. J. Bimolecular radical termination: New perspectives and insights. *J. Polym. Sci. Pol. Chem.* **2008,** 46, (10), 3155-3173.

70. Johnston-Hall, G.; Monteiro, M. J. Kinetic Simulations of Atom Transfer Radical Polymerization (ATRP) in Light of Chain Length Dependent Termination. *Macromol. Theory Simul.* **2010,** 19, (7), 387-393.

71. Matyjaszewski, K. Mechanistic and Synthetic Aspects of Atom Transfer Radical Polymerization. *Journal of Macromolecular Science, Part A* **1997,** 34, (10), 1785-1801.

72. Goto, A.; Fukuda, T. Kinetics of living radical polymerization. *Prog. Polym. Sci.* **2004,** 29, (4), 329-385.

73. Zhong, M. J.; Matyjaszewski, K. How Fast Can a CRP Be Conducted with Preserved Chain End Functionality? *Macromolecules* **2011,** 44, (8), 2668-2677.

74. Woloszyn, J. D.; McAuley, K. B. Application of Parameter Selection and Estimation Techniques in a Thermal Styrene Polymerization Model. *Macromol. React. Eng.* **2011,** 5, 453-466.

75. Belincanta-Ximenes, J.; Mesa, P. V. R.; Lona, L. M. F.; Vivaldo-Lima, E.; McManus, N. T.; Penlidis, A. Simulation of styrene polymerization by monomolecular and bimolecular nitroxide-mediated radical processes over a range of reaction conditions. *Macromol. Theory Simul.* **2007,** 16, (2), 194-208.

Chapter 5. Model-based design to push the boundaries of sequence-control

Summary

An innovative model-based design strategy to synthesize well-defined sequence-controlled polymers is presented, enabling selection of both the most appropriate mediating agent and reaction conditions. In combination with experimental analysis, advanced kinetic Monte Carlo simulations are conducted allowing a visualization of the connectivity of all monomer units of *ca.* 10^5 individual copolymer chains. The product quality can therefore be uniquely and unambiguously predicted for the first time at the molecular level, explicitly accounting for chain-to-chain deviations. The strategy is illustrated for BlocBuilder MA initiated nitroxide mediated polymerization, with styrene and N-benzyl maleimide as comomomers, and is generally applicable for all reversible deactivation radical polymerization (RDRP) techniques. Further design of the nitroxide mediating capabilities and the reaction conditions allows the realization of a targeted (multi)functionalization pattern, including an increase of the contribution of trifunctionalized chains above 75%. The reported results are interpreted in terms of the individual activation-growth-deactivation cycles and provide an unprecedented mechanistic understanding of RDRP in general. This work was published in *Macromolecules* 2016, 49, 9336-9344.

5.1 Introduction

One of the key challenges for future polymer synthesis is the capability to place functional monomer units according to a specific pattern in each chain.[1-6] Such precision control opens the way for the design of highly organized structured materials that can be folded or self-assembled into well-defined nanoscale morphologies.[1, 3, 4, 7-9] In particular, sequence-controlled polymers in which functionality is incorporated at specific local regions (*e.g.* blue, red, and green region in Figure 5.1a) have already permitted advanced macromolecular engineering opportunities, ultimately leading to enhanced macroscopic properties of the final polymeric materials.[10-12]

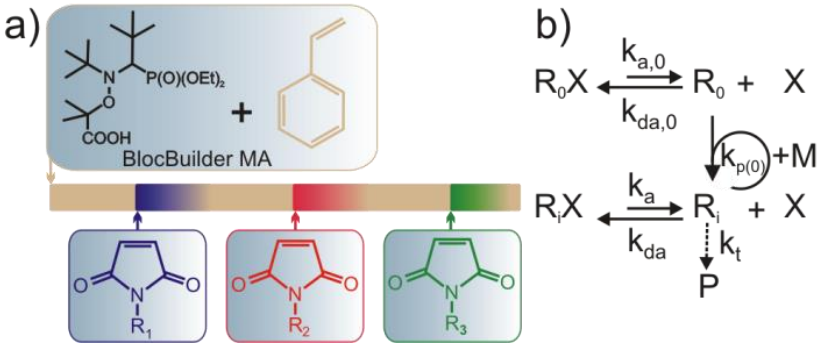

Figure 5.1. *a) Synthesis strategy for sequence-controlled polymers: sequential addition of three functional N-substituted maleimides via BlocBuilder MA initiated nitroxide mediated polymerization (NMP) of styrene; b) Principle of NMP with R_0X as initiator; (d)a,p,t: (de)activation, propagation, termination; 0: NMP initiator related.*

With the advent of reversible deactivation radical polymerization (RDRP)[13-20] or controlled radical polymerization (CRP) it has become possible to synthesize a wide range of sequence-controlled polymers by selecting appropriate comonomer pairs, consisting of an electron-donor and -acceptor comonomer.[1, 21-23] Such pairs strongly facilitate cross-propagation and therefore allow the local functionalization of copolymer chains via a variety of RDRP agents, including transitional metal complexes as in atom transfer radical polymerization (ATRP), nitroxides as in

nitroxide mediated polymerization (NMP), and thiocarbonylthio moieties as in reversible addition fragmentation chain transfer (RAFT) polymerization.[21, 23-26] Specifically, for NMP significant focus has been on BlocBuilder MA initiated polymerization of styrene with small amounts of *N*-substituted maleimides.[15, 27, 28] The principle of NMP is depicted in Figure 5.1b. Upon activation of alkoxyamine dormant species (R_iX; $i \geq 0$, NMP initiator: i=0), active (macro)radicals (R_i; $i \geq 0$) and persistent nitroxide radicals (X) are released. The formed (macro)radicals take up a controlled number of monomer units before they are quickly deactivated to their dormant form upon reversible recombination with X species. Thanks to the persistent radical effect,[29-31] in which a substantial accumulation of X species takes place at very low reaction times, the impact of unwanted termination reactions is minimized and thus a high end-group functionality can be ensured.[32-35] For a fast NMP initiation, the dispersity ($Đ$) can be brought well below 1.3 with a number average chain length (x_n) determined by the initial NMP initiator amount.

Based on comonomer conversion data, Pfeifer *et al.*[21] have shown that N-substituted maleimides can be successfully incorporated at specific regions during RDRP of styrene, at least on an *average* basis. The natural and paramount question that arises is whether this excellent average microstructural control can also be realized for all *individual* polymer chains. Since RDRP techniques are stochastic processes, it can be expected that significant intermolecular deviations exist, as already highlighted theoretically for ideal chain-growth mechanisms, assuming *e.g.* the absence of termination reactions.[36] In contrast, for detailed RDRP reaction schemes, no kinetic studies have been conducted aiming at the characterization of the monomer placement in each individual chain of a sequence controlled polymer.

In the present work, it is demonstrated that combining advanced kinetic Monte Carlo (*k*MC) simulations and experimental analysis, is the recommended tool to (*i*) unambiguously evaluate

the product quality of sequence-controlled polymers and (*ii*) to facilitate the screening of the most suited reaction conditions and reactants for the synthesis of high quality sequence-controlled polymers. The presented combined modeling and experimental design strategy is exemplified for NMP of styrene with small amounts of N-benzylmaleimide (BzMI), including a successful model-based design for the nitroxide choice and comonomer addition programs. The results are interpreted for the first time based on the individual activation-growth-deactivation cycles along the NMP and allow to conclude that currently SG1 is the most suited nitroxide for NMP synthesized sequence-controlled polymers.

5.2 Experimental procedure and analysis

5.2.1 Materials

BlocBuilder MA (Arkema, 97%; aka MAMA-SG1), *N*-benzylmaleimide (Alfa Aesar, 99%), anisole (Sigma Aldrich, 99%), tetrahydrofuran (Sigma Aldrich, 99.8% HPLC, stabilizer-free), and chloroform-d (Sigma Aldrich, 99.8%) were all used as received. Styrene (Sigma Aldrich, > 99%) was distilled over CaH_2 (90-95%) under reduced pressure and stored under argon atmosphere at -15°C.

5.2.2 NMP synthesis and analysis

The desired amount of BlocBuilder MA (R_0X) was weighed into a 25 mL flask, after which a magnetic stirrer was added and the flask was sealed off using a septum, degassed, and filled with argon. Next, deoxygenated inhibitor-free styrene (5 mL) was added to the flask using a degassed syringe, after which the mixture was purged with argon for 30 minutes. The flask was then submerged into a preheated oil bath thermostated at the reaction temperature (120°C). At a given

time, 0.5 mL BzMI solution (1 eq. with respect to R_0X; solvent: anisole) was added, using a degassed syringe. This solution was previously purged with argon for 30 minutes.

Samples were withdrawn periodically, using a degassed syringe and analyzed with size exclusion chromatography (SEC) and ^{1}H nuclear magnetic resonance (NMR; further details see Appendix).

5.3 Kinetic model

For MAMA-SG1 initiated NMP of styrene and BzMI (R_0X: BlocBuilder; 120 °C), the incorporation of all comonomer units for *each* individual chain of a representative polymer sample (*e.g.* 100,000 chains) is explicitly tracked v*ia* advanced matrix-based kinetic Monte Carlo (*k*MC) simulations.[37-39] Hence, the exact location of the styrene and functional BzMI monomer units in each chain is known at any time, allowing an unbiased quality labeling for precision control and in particular a quantification of the functionalization efficiency. The *k*MC model has been validated by benchmarking with measurable average NMP characteristics such as comonomer conversion and *Đ* data (see further).

To properly represent the NMP kinetics, a detailed reaction scheme (full details provided in Appendix) is considered with NMP (de)activation, propagation, and termination by recombination as the core reactions. Thermal self-initiation, according to the Mayo-mechanism,[40] and chain transfer to monomer and dimer are also included, as they can affect the microstructural control at high temperature (> 100 °C) and for the higher chain lenghts.[41-43] Transfer reactions with the SG1 nitroxide and chain transfer to polymer are neglected based on previous kinetic studies.[44, 45]

To calculate the rate coefficients a terminal model is used. At first sight it could although be expected that a penultimate model is necessary. For example, Klumperman *et al.*[46, 47] have

indicated a penultimate unit effect for the conventional copolymerization of styrene and maleic anhydride, which is also a donor-acceptor comonomer pair displaying high cross-propagation rate coefficients. However, as shown in detail in the Appendix, for the typical conditions for the synthesis of sequence controlled polymers and the considered comonomer pair in the present work, the deviations between the terminal and penultimate model are very limited, both for the average properties and those for each individual chain. Hence, to a first approximation, it is afforded to consider a terminal model. Furthermore, (de)activation reactions involving macrospecies with terminal BzMI units have been neglected as these are kinetically insignificant under the typically applied sequence-controlled polymerization conditions (see Figure C.2 in Appendix). All rate coefficients are based on literature data (see Appendix), as obtained via dedicated experimental analysis, further highlighting the accuracy of the *k*MC simulations.

The simulations fundamentally account for the viscosity change along the polymerization, leading to diffusional limitations on termination and thus lower observed termination reactivities at higher reaction times (diffusion parameters: see Appendix).[48-51] Only by explicitly accounting for this viscosity change, a joint accurate simulation of the comonomer conversion profiles as well as the preservation of end-group functionality becomes possible.[35, 49] Diffusional limitations on the NMP activation deactivation process can be ignored, as the regime of very high viscosities is not considered.[49]

5.4 Results and discussion

5.4.1 Model validation

The strength of the presented model-based design strategy relies on the accurate representation of the NMP kinetics for the synthesis of sequence-controlled polymers. This not only requires the

consideration of a detailed kinetic model, properly reflecting the complex interplay between chemical and diffusion phenomena, but also a validation with experimental data wherever possible.

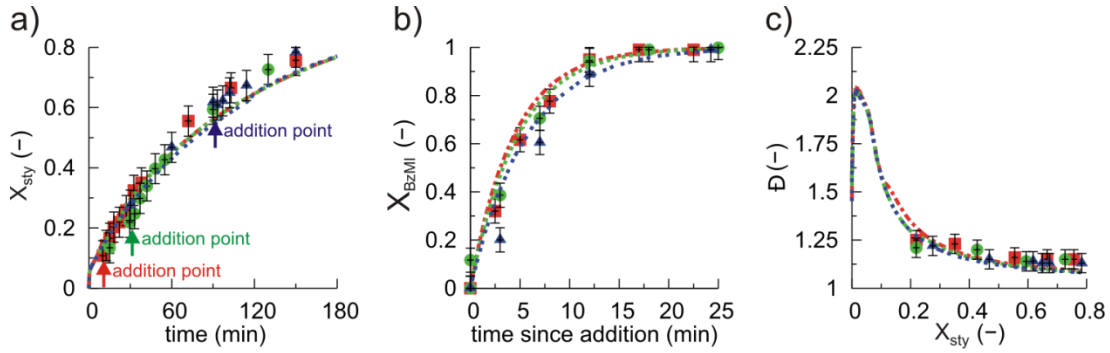

Figure 5.2. *Experimental (points) and simulated (lines) a) styrene conversion (X_{sty}) as a function of time, b) benzylmaleimide conversion (X_{BzMI}) as a function of time elapsed since addition point of BzMI (addition points: see arrows in a)), c) dispersity (Đ) as a function of X_{sty}; NMP of styrene and BzMI initiated by BlocBuilder MA at 120°C with $[Sty]_0:[R_0X]_0:[BzMI]_{addition\ point}$ = 50:1:1.*

Therefore, a series of NMP experiments has been first conducted with different BzMI addition points (Figure 5.2a: arrows at styrene conversion (X_{sty}) of 0.11, 0.22, and 0.62). A polymerization temperature of 120°C has been selected to ensure a high polymer yield for sufficiently low reaction times (< 3 hours). One equivalent of BzMl, as defined with respect to the NMP initiator (BlocBuilder MA), has been used, based on the first experimental studies.[21]

To allow for a reliable NMR integration for the measurement of the comonomer conversions the initial molar amount of styrene has been limited ($[Sty]_0:[R_0X]_0$=50:1). Figure 5.2 shows a comparison of the experimental and simulations results, considering the comonomer conversion profiles and the evolution of *Đ* with increasing X_{sty}. Clearly, the description of the experimental data is excellent. Importantly, the BzMI consumptions, which are limited to small time spans (*ca.* 25 minutes), are well-described (X_{BzMI} profiles; Figure 5.2b). Also for the dispersities a good

match between the simulated and experimental results (Figure 5.2c) is obtained. The latter is an important prerequisite to accurately describe the BzMI placement in the individual polymer chains (see further). Hence, the *k*MC model can be reliably used to obtain additional microstructural information on the molecular level and to perform model-based design (see next subsections), keeping in mind that its parameters have been reliably determined via dedicated kinetic analysis (see Appendix).

5.4.2 Placement and distribution of the functionalities along individual chains

Figure 5.3a displays, at X_{sty}=0.8, the actual positions at which BzMI units (blue rectangles) are incorporated in the chains, for a random selection of *ca.* 500 macrospecies out of a representative polymer sample of *ca.* 100,000 chains. BzMI (still 1 eq.) has been injected at X_{sty}=0.4. To allow for an easy and direct interpretation of the simulation results, $[Sty]_0$:$[R_0X]_0$ is now doubled to 100:1, implying that ideally every chain should possess a BzMI unit at an absolute position of 41. This design target is also represented by the blue dashed line in Figure 5.3a with for the sake of comparison a beige dashed line indicating the targeted x_n of 81 for the final X_{sty} of 0.8. At the top part of Figure 5.3a, the dead polymer chains, mainly formed due to inevitable terminations, are displayed separately.[33] Their impact on the overall NMP characteristics is however limited, as they form the minority of the chain population (end-group functionality of 0.93).

The majority of the chains are thus dormant, although their actual composition strongly varies from chain to chain. First, both too short and too long dormant chains exist (Figure 5.3a), despite that the dispersity (*Đ*) amounts to 1.10. Next to that a significant amount of dormant chains does not contain any functional monomer unit (no blue rectangle) or possesses several of those units (multiple blue rectangles). The latter becomes more clear upon post-processing of the computational results, in which the performance of each chain of the entire polymer sample (*ca.*

100,000 chains) can be explicitly evaluated. As shown in Figure 5.3b (blue bars), *ca.* 45% of the chains lack functionality, whereas *ca.* 30% of the chains contain only 1 BzMl unit. Thus, the remaining *ca.* 25% of the chains can be considered as overfunctionalized, *i.e.* they contain more than 1 BzMI unit. A mean average (μ) value of 1.03 BzMI units per chain results, indicating a reasonable average degree of functionalization for the selected NMP system and conditions. Note that these observations somewhat differ from previously reported results for RDRP synthesized BzMI functionalized polystyrene. For example, based on matrix-assisted laser desorption/ionization-time of flight mass spectroscopy (MALDI-TOF MS), it has been reported that only 10% of the polymer chains is nonfunctionalized under ATRP conditions (catalyst: Cu(I)Br/dNbipy (dNbipy: 4,4'-di-5-nonyl-2,2'-bipyridine)) with similar comonomer molar ratios as in this work.[23, 52] However, as previously underlined and also confirmed via theoretical calculations,[23, 36] these MALDI-TOF measurements probably underestimate the contribution of nonfunctionalized chains, due to the effect of the polar maleimide unit on the ionization selectivity of the sample.

As shown in Figure 5.3c (blue line), a reasonable microstructural control is obtained over the actual BzMl placement(s) per macrospecies, *i.e.* the absolute position(s) of the functional monomer unit(s) in the chains, as most conveniently defined with respect to the NMP initiator fragment (α-functionalization). This absolute control is one of the most stringent design criteria in precision polymer synthesis. It can be seen in Figure 5.3c that the BzMI-unit is on average incorporated at an absolute position equal to 48. This is higher than the expected value of 41, due to parallel styrene consumption during the incorporation period of the BzMI monomer (*cf.* Figure 5.2b). A relatively broad distribution of the functional monomer unit placement (standard deviation (σ) = 15 monomer units) is obtained, with 90% of the functional monomer incorporated

in the chains between an absolute position of 26 and 75 (non-colored region for blue line in Figure 5.3c).

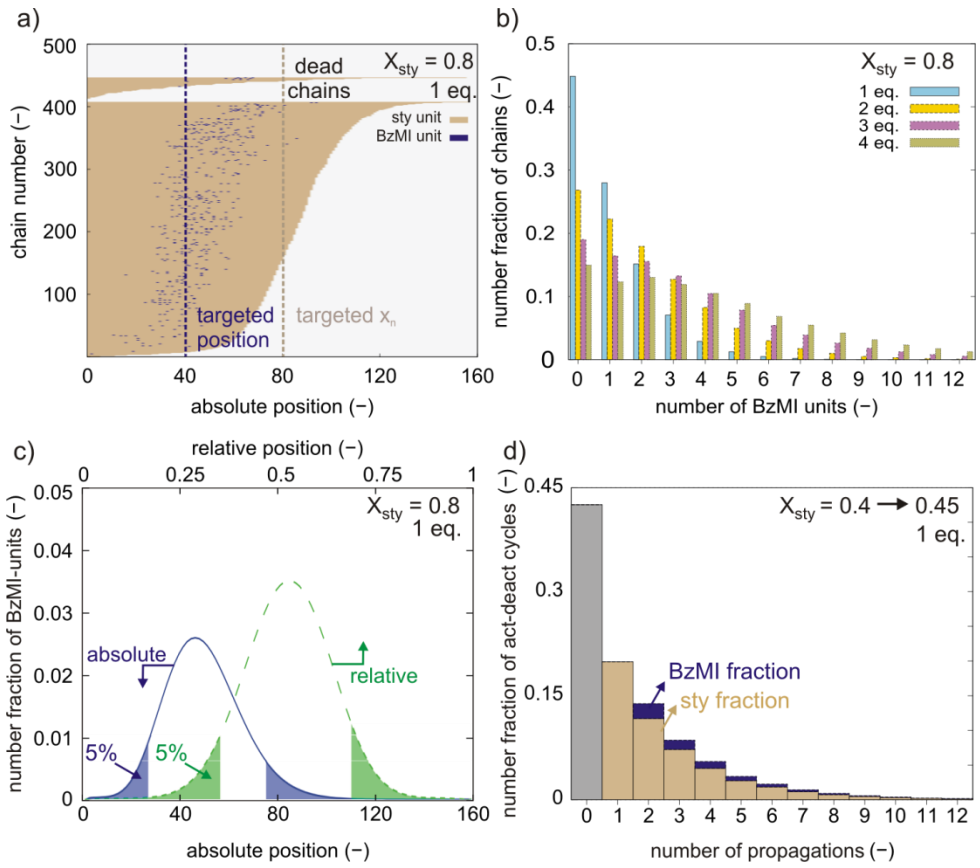

Figure 5.3. *a) Explicit in silico visualization of microstructure for each individual copolymer chain (ca. 500 out a representative polymer sample of 100,000 chains), b) number fraction of chains with a given number BzMI units, c) number fraction of BzMI units at absolute (blue line) and relative (green dashed line) positions in the chain, d) number fraction of activation-deactivation cycles as a function of number of propagations with relative contribution of styrene and BzMI indicated for X_{sty} interval from 0.40 to 0.45; NMP of styrene and BzMI initiated by BlocBuilder MA (R_0X) at 120°C ($[Sty]_0$:$[R_0X]_0$:$[BzMI]_{addition\ point}$=100:1:eq.;eq. defined with respect to R_0X; addition point: X_{sty}=0.4); x_n: number average chain length; targeted relative position of 0.51; average chain length characteristics benchmarked via experimental data (cf. Figure 5.2).*

Part of the mismatch with the targeted value is due to the unavoidable presence of non-identical macrospecies at the moment of BzMI addition, as reflected by the corresponding $Đ$ of 1.13 (X_{sty}=0.4). This is a direct consequence of the NMP mechanism (Figure 5.1b), in which the activation and deactivation rate can only reach (pseudo-)equilibrium once NMP initiation is finished (here at X_{sty}=0.05). Note that for a lower $[Sty]_0$:$[R_0X]_0$ and a lower X_{sty} at which the functional monomer is added less microstructural control is inherently obtained as such conditions lead to a slower NMP consumption as a function of X_{sty}.[53]

Another design criterion for the monomer placement is to demand only control over the relative position of the functional monomer unit with respect to the length of the polymer chain it is incorporated in. By focusing only on the relative position the variation with respect to the chain length is less important, making this design criterion less stringent. Ideally, a relative position of 0.51 needs to be realized, following from dividing the targeted absolute position of 41 by the targeted x_n of 81. The results (Figure 5.3c; green line) show that the BzMI unit is on average at a relative position of 0.53 (σ = 0.11), with 90% of the functional monomers incorporated between a relative position of 0.35 and 0.69 (non-colored region for green line). A narrower distribution for the relative positioning is obtained compared to the absolute positioning, as can be deduced from the coefficients of variation (ratio of standard deviations and mean values): 0.22 (relative) *vs.* 0.30 (absolute). This confirms that a well-defined absolute placement is more tedious, which can be understood by the less pronounced impact of non-instantaneous NMP initiation upon an inspection of the product quality (Figure 5.3c) in the case of normalization by the chain length. Hence, the model can be used to quantify the polymer product quality in various ways, including the specification of the allowed maximal deviation of the targeted monomer incorporation pattern.

The above discussed results for the functionalization degree and monomer placement as obtained with the detailed *k*MC model (Figure 5.3b-c; BzMI = 1 eq.) differ considerably from the theoretically derived values for ideal living polymerizations, as previously explored by Gody *et al.*[36] As shown in Appendix (Figure C.3), the use of an idealized reaction scheme leads to an underestimation of the non-functionalized chains and consequently to an overestimation of the mono- and difunctionalized chains which constitutes, together with the non-functionalized ones, the majority of the chain population (*ca.* 90%). These mismatches are due to an alteration of the number of comonomer units incorporated per activation-deactivation cycle upon the consideration of a detailed NMP reaction scheme. For the *k*MC model, *in Figure 5.3d*, the simulated distribution of the number of activation-deactivation cycles with a given number or propagation steps is displayed for a X_{sty} interval between 0.40 and 0.45. During this interval the majority of the added BzMI is converted (conversion of *ca.* 0.80) and therefore it is representative to study the functionalization at this stage of the NMP process. A further distinction is made in this figure according to the monomer type being incorporated on an average basis (styrene fraction: beige; BzMI fraction: blue). It should be stressed that this is the first time that a complete and explicit mapping of the diversity in activation-deactivation cycles is realized for RDRP. Since in the selected model approach the reaction event history is completely tracked, post-processing allows a dedicated kinetic and microstructural analysis according to user-defined specifications, in this case the efficiency of BzMl incorporation per activation-deactivation cycle.

As can be seen in Figure 5.3d, the majority of the activation-deactivation cycles (*ca.* 40%) does not contribute to the "growth" of the dormant polymer chains, whereas in only 20% of the cycles 1 monomer unit is incorporated. A large fraction of the cycles therefore incorporates more than one monomer unit, leading to deviations from the theoretical predictions based on idealized

monomer incorporation (see Figure C.3 in Appendix). It should be further noted that for a copolymerization in which cross-propagation is strongly favored, which is the case with styrene and BzMI, the average number of propagation steps during an activation-deactivation cycle inherently shifts to higher values, leading to amplified deviations from the idealized case. This follows from comparing Figure 5.3d with the results for styrene homopolymerization (Figure C.4 in Appendix).

5.4.3 Design of added BzMI amount

From the previous discussion it is clear that employing one equivalent of functional monomer with respect to the NMP initiator does not lead to the desired incorporation of one BzMI in each polymer chain. A solution previously put forward to enhance the fraction of functionalized chains is to use more than one equivalent of BzMI.[21, 23] The results considering up to 4 equivalents are shown in Figure 5.3b (blue: 1 eq. (already discussed before), yellow: 2 eq., purple: 3 eq., and green: 4 eq.).

Upon inspection of this figure it follows that the number fraction of nonfunctionalized chains decreases from 45% to 27%, upon increasing the number of equivalents from 1 to 2. The fraction of singly functionalized chains however decreases from 28% to 22% and the fraction of largely overfunctionalized chains (> 5 functionalizations) increases with a factor of 9 from 0.8 to 7%. Further increasing the number of equivalents has a smaller impact on the decrease of the number of nonfunctionalized chains. Due to the persistent radical effect, a small fraction of styrene homopolymer dead chains is formed at the start of the NMP, which implies a limiting value for the contribution of nonfunctionalization chains, since BzMI is added at the later stages of the NMP (X_{sty}=0.4). In contrast, the formation of overfunctionalized chains is strongly amplified. For instance, adding four equivalents of BzMI reduces the fraction of non-functionalized chains to

15%, but increases the fractions of largely overfunctionalized chains (> 5 functionalizations) to *ca.* 40%.

It can thus be concluded that too high BzMl amounts should be avoided, as they are associated with the formation of too high amounts of strongly overfunctionalized polymer chains. Hence, further design including a variation of other process parameters is recommended, which is explored in the next subsections.

5.4.4 Design of comonomer addition programs

To improve the positioning of the functional monomer units along the polymer chains, again defined with respect to the NMP initiator fragment, to follow the most strict definition of precision control, sequential additions of both the donor and acceptor comonomer have been previously proposed to enable ultra-precision control.[54] On average, a better functionalization was obtained compared to the conventional approach, which can now also be verified at the level of the individual polymer chains, using the matrix-based visualization tool as put forward in the present work.

For example, Figure 5.4a depicts the detailed microstructure per chain still aiming, as before, at the placement of the BzMl unit at an absolute position of 41 for a targeted chain length of 100. Half of the total styrene amount is added initially and converted until X_{sty}=0.80, upon which all of the BzMl is added. When X_{sty} becomes 0.90 the remaining amount of styrene is added. The absolute and relative positions of the BzMI-units, as obtained by post-processing, are shown in Figure 5.4b. On an absolute basis, the functional monomer is incorporated at an average position of 46. A slight improvement compared to the conventional approach (absolute position of 48; Figure 5.3c) is thus achieved, which can be attributed to the lower styrene concentration during the interval in which BzMI is consumed upon the use of a comonomer addition program. The

standard deviation of the absolute BzMI location improves more significantly with a change from 15 to 11 monomer units and 90% of the functional monomers incorporated between position 29 and 64, as opposed to 26 and 75 in the reference case (Figure 5.3c), thus conforming previous experimental observations.[54]

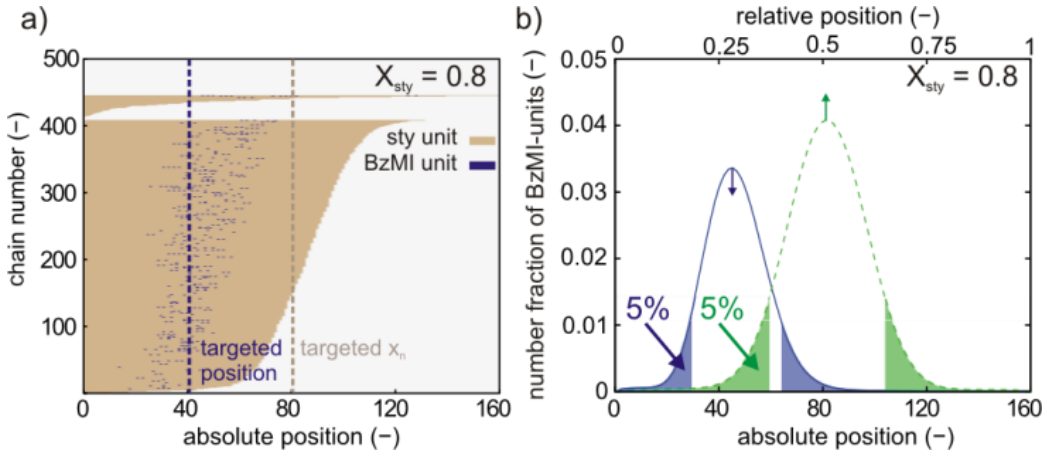

Figure 5.4. *Positive influence of fed-batch styrene program for improved microstructural control: a) In silico visualization of microstructure for each individual copolymer chain (ca. 500 chains out of a representative polymer sample of 10^5 chains), b) number fraction of BzMI units at absolute and relative positions of BzMI units in the chain; NMP of styrene and BzMI initiated by BlocBuilder MA at 120°C ($[Sty]_0$:$[BzMI]_{AP1}$:$[Sty]_{AP2}$:$[R_0X]_0$ = 50:1:50:1); with addition point (AP) 1 and 2 at X_{sty} = 0.8 and 0.9.*

This improvement is mainly due to a lower dispersity at the moment of addition (1.09 vs. 1.14), *i.e.* a higher NMP initiation efficiency is achieved, and thus not due to a significant change in end-group functionality. A similar end-group functionality is obtained as before, as for both the reference and present case most termination reactions take place at low monomer conversions at which the same apparent termination reactivities result. On the other hand, upon the use of comonomer addition programs, a small influence of diffusional limitations on the activation-deactivation process can be expected, as high viscosity regimes are more easily reached. As indicated above, in the present work, the latter diffusional limitations are ignored for simplicity

and, hence, a slightly less controlled monomer incorporation is expected at the higher monomer positions than visualized in Figure 5.4.[49, 55] The relative position of the BzMI units also improves (mean (μ) = 0.51 and σ = 0.09) with 90% of the functional monomers contained between 0.37 and 0.65, as opposed to 0.35 and 0.69 for the conventional case (Figure 5.3c). Note that this improvement is less pronounced than for the absolute position, which is consistent with the above explanation of a reduced impact of changes of the NMP initiation efficiency upon normalization with the chain length.

5.4.5 Design of NMP activation-deactivation reactivities

Up to now, model-based design has only been used to optimize reaction conditions, for a given NMP initiator, *i.e.* the SG1-based alkoxyamine BlocBuilder MA. This initiator is typically considered in experimental studies for sequence controlled polymers via the NMP technique, taking into account that SG1 possesses excellent mediating properties for reasonable reaction times.[56, 57] Hence, it is worthwhile to verify if another nitroxide would perform better, which has only been explored to a limited extend in previous kinetic studies.

For this purpose, the impact of the nitroxide mediating capabilities on the microstructural control has been theoretically evaluated at fixed reaction conditions. As shown in Figure 5.5, for this study, grid simulations for bicomponent NMP of styrene and BzMl with benzoyl peroxide (BPO) as conventional radical initiator have been performed. Taking into account the conventional initiator efficiency of 0.7,[58] the nitroxide is added in a stoichiometric amount with respect to BPO: $[BPO]_0$:$[X]_0$ = 0.71:1.

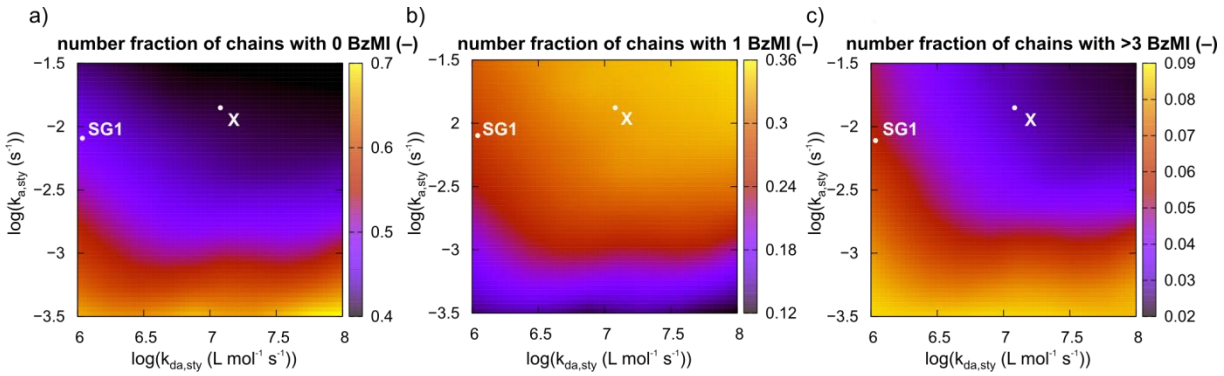

Figure 5.5. *Model-based identification of the most suited nitroxide via a screening of (k_a, k_{da}) combinations for (bicomponent) NMP synthesis of sequence controlled polymers, ignoring side reactions with the theoretical nitroxides for simplicity; number fraction of chains with a) 0 BzMI units, b) 1 BzMI unit, and c) more than 3 BzMI units; conditions: bicomponent NMP of styrene and BzMI initiated with BPO at 120°C ($[Sty]_0$:$[BzMI]_{addition\ point}$:$[X]_0$:$[BPO]_0$=100:1:1:0.71); with $2f[BPO]_0 = [X]_0$; f: initiator efficiency); results shown for X_{sty} = 0.8 and addition point X_{sty}=0.4; white circles: SG1 for which side reactions can be ignored*[28, 59] *and experimental validation has been successfully performed (cf. Figure 5.2) and ideal nitroxide X used for the combined optimized approach in Figure 5.6.*

Bicomponent NMP is considered to obtain an unbiased kinetic modeling analysis, since a lower number of NMP initiation related rate coefficients are required (see Appendix), as compared to the conventional (monocomponent) NMP initiation considered before. Due to the lack of kinetic parameters, for simplicity, side reactions with all the theoretical nitroxides have been ignored. On the other hand, styrene specific side reactions, such as thermal initiation, are still incorporated in the *k*MC model. For the grid simulations, the activation and deactivation rate coefficient for styryl macroradicals (k_a and k_{da}) are allowed to freely vary within physically relevant ranges: k_a: $10^{-3.5}$ and $10^{-1.5}$ s^{-1} and k_{da}: 10^6 and 10^8 L mol^{-1} s^{-1}. Based on literature data (see Table S3 in Appendix),[32, 60-63] this scanning range includes the most commonly used nitroxides, *i.e.* SG1

(white circles; safely no side reactions [28, 59]), 2,2,5-trimethyl-4-phenyl-3-azahexane-3 oxyl (TIPNO), di-tert-butyl nitroxide (DBNO), and 2,2,6,6-tetramethylpiperidinyl-1-oxy (TEMPO).

Three microstructural properties, *i.e.* the number fraction of nonfunctionalized (Figure 5.5a), monofunctionalized (Figure 5.5b), and overfunctionalized (more than three functionalizations; Figure 5.5c) chains are considered to evaluate the relevance of chain-to-chain deviations. It can be observed that for minimization of the number fraction of nonfunctionalized chains (Figure 5.5a) and tuning toward monofunctionalization (Figure 5.5b-c), a nitroxide with both a high k_a and k_{da} (top right region) should be used. Upon the addition of BzMl, ideally all dormant chains need to participate for incorporation of this functional monomer, explaining the need for a high k_a. Once a dormant chain is activated, it should ideally only add to 1 BzMI unit - next to some inevitable styrene units - in order to avoid overfunctionalization. The selected nitroxide should therefore also possess an as high as possible k_{da}.

It should be noted that thermal self-initiation is also affecting the trends in Figure 5.5. For nitroxides possessing a low k_a and/or a high k_{da}, the number of radicals generated by thermal self-initiation is no longer negligible with respect to the number of radicals formed by BPO dissociation. This leads to an imbalance for deactivation and, hence, deteriorates the synthesis of the targeted sequence-controlled polymers. This can be better understood by comparing Figure 5.5 with Figure C.5 in Appendix, in which the corresponding results are given if thermal self-initiation is neglected.

Upon further analysis of Figure 5.5 it follows that SG1 (white circles), despite its successful use for the synthesis of well-defined sequence-controlled polymers (see above), does not possess mediating capabilities in the preferred top right (k_a, k_{da}) region. Hence, theoretically room for improvement exists for the design of the nitroxide. At first sight, DBNO seems a better candidate

as it is characterized by a higher NMP (de)activation reactivity than SG1.[61, 62] However, as indicated by Catala *et al.*[64] and also confirmed experimentally in this work DBNO side reactions cannot be ignored, as was done for the construction of Figure 5.5.

It should be clear that the model-based screening of (k_a, k_{da}) combinations and the development of novel nitroxides with mediating capabilities in the top right region of Figure 5.5 - and a limited impact of side reactions - will allow a full exploitation of the NMP technique for the synthesis of well-defined sequence-controlled polymers. The latter observation can be generalized to other RDRP techniques, further highlighting the relevance of model-based design for precision control and the relevance of future research in which various RDRP agents beyond the SG1 nitroxide can be tested, including a variation of the polymerization temperature to further tune the efficiency of activation-growth-deactivation cycles.

5.4.6 Combined design for optimal performance

Previously, monofunctionalized polymer chains have been targeted and several separate model-based design strategies have been applied. In this section, the model-based design strategy is extended to sequence-controlled polymers containing three distinct functionalizations, *i.e.* multifunctionalization. The aforementioned design strategies are combined to achieve the best performance for the functionality placements.

The aim is that each polymer chain contains 150 styrene units at full styrene conversion and 3 functional monomer units at an absolute position of 38, 75, and 113 (Figure 5.6a; X_{sty} =0.9). For simplicity, BzMI is employed three times as the functional monomer unit, further referred to as BzMI-1 (blue), BzMI-2 (red), and BzMI-3 (green). The results for the combined multi-based design strategy are depicted in Figure 5.6a-b. For illustration purposes, a theoretical alkoxyamine with high quality mediating capabilities is selected ((k_a, k_{da})=(1.4 10^{-2} s^{-1}, 1.2 10^{7} L mol^{-1} s^{-1}); no

side reactions with the nitroxide; top right region in Figure 5.5). Sequential additions of BzMI and styrene are also performed per functionalization step, taking X_{sty} equal to 0.8 and 0.9 (*cf.* Figure 5.4). For each functionalization, 2 eq. of BzMI is considered, taking into account that too high equivalents easily lead to overfunctionalization, as explained above (*cf.* Figure 5.3). In Appendix (Figure C.6), for comparison, the corresponding results using the SG1 nitroxide are considered, assuming only an addition program for the functional monomer unit.

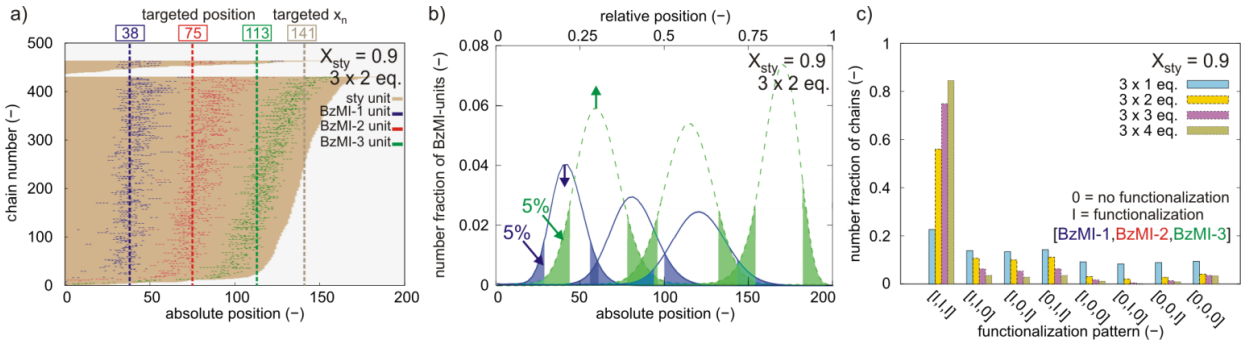

Figure 5.6. *Model-based design for sequence-controlled polymer synthesis by combining all previous design strategies: a) Explicit in silico visualization of microstructure for each individual copolymer chain (ca. 500 chains of a representative polymer sample of 100.000 chains), b) number fraction of BzMI units at absolute and relative positions in the chain, c) number fraction of chains depending on the functionalization pattern (target: [I,I,I]); NMP styrene with 3 BzMI additions with* (k_a,k_{da})*= (1.4* 10^{-2} s^{-1}*,* $1.2\ 10^{7}$ $L\ mol^{-1}\ s^{-1}$*; no side reactions with nitroxide); 120°C;* $[Sty]_0:[R_0X]_0:[BzMI\text{-}1]_{AP1}:[Sty]_{AP2}:[BzMI\text{-}2]_{AP3}:[Sty]_{AP4}:[BzMI\text{-}3]_{AP5}:[Sty]_{AP6}$ *= 47:1:eq.:45:eq.:45:eq.:13; eq. each time 2 for a) and b) but parameter for c); defined with respect to* R_0X*; addition point (AP) 1,3 and 5 at* X_{sty} *= 0.8 and addition point 2, 4 and 6 at* X_{sty} *= 0.9; Figure C.6 comparative figure upon use of SG1 nitroxide.*

It follows from Figure 5.6a that an excellent control over the copolymerization kinetics is obtained, although for a small part of the chains an overlap exists for the absolute positions (blue regions Figure 5.6b). The three distributions are characterized by mean positions of 42, 79, and 116 for BzMI-1, BzMI-2, and BzMI-3, which are very close the targeted ones of 38, 75, and 113.

The standard deviations are all lower than in Figure C.6 (SG1 counter case) and given by 10, 13, and 18 monomer units with corresponding coefficients of variation equal to 0.24, 0.17, and 0.16. On a relative position basis, an even better performance results with a low overlap (green regions in Figure 5.6b). The mean values are all close to the targeted values and given by 0.30 (BzMI-1), 0.56 (BzMI-2), and 0.82 (BzMI-3). Based on the standard deviations of 0.073, 0.071, and 0.065, the coefficients of variation become 0.24, 0.13, and 0.08. Hence, the broadness of the relative positioning of BzMI units considerably improves if the addition occurs at higher chain lengths, taking also into account that the average number of propagation steps in the activation-deactivation cycles during the functionalization stages decreases with decreasing styrene concentration.

Further model-based analysis allows to map the complete functionalization pattern for each individual chain. If a single functionalization is successful the label ‘I’ is considered, as opposed to the label ‘0’ for an unsuccessful one. This convention gives rise to eight possibilities for the multifunctionalization with perfect, *i.e.* threefold, functionalization reflected by the functionalization pattern [I,I,I]. In Figure 5.6c, the results from the post-processing are shown for different equivalents of each BzMI addition (reference case (yellow bars): each time 2 eq; direct link to Figure 5.6a-b). Upon the use of one equivalent (blue bars), a poor result is obtained with only 23% of the chains possessing all three functionalizations, whereas 9% remains nonfunctionalized. Upon increasing the number of equivalents, the functionalization efficiency rapidly improves. Using two equivalents (yellow bars), the number fraction of tri-functionalized chains increases already to 56%, decreasing the number of non-functionalized chains to a very low amount of 4%, following initial assumptions.[23, 26] Further increasing the number of equivalents to three (purple bars) or four (green bars) further increases the number fraction of tri-

functionalized chains even to 75%, and 85%, whereas the amount of non-functionalized chains remains around 4%. The latter can be attributed to unavoidable nonfunctionalized dead polymer formation at low reaction times due to the persistent radical effect, as explained above.

In addition, the improvements for the multifunctionalization pattern with the combined model-based design strategy can also be deduced by comparison with the corresponding pattern as obtained with the SG1-nitroxide and considering only an addition program for the functional monomer (Figure C.6c in Appendix). In particular, an increase of *ca.* 15% (2 eq.) is obtained for the chains with threefold functionalization using the combined design strategy.

Hence, upon a careful selection of the RDRP mediating agent and the reactions conditions, it has been theoretically illustrated that well-defined sequence controlled polymers can be obtained, according to a predetermined multifunctionalization pattern.

5.5 Conclusions

A full design of the NMP synthesis procedure for sequence-controlled polymers has been successfully performed using matrix-based kinetic Monte Carlo simulations, in which chain-to-chain microstructural deviations are explicitly mapped. Such detailed model-based characterization of the polymer microstructure – for each individual copolymer chain – allows an unambiguous product quality labeling with respect to a targeted functionalization pattern, including multifunctionalizations.

To obtain a high product quality an excellent control over the individual activation-growth-deactivation cycles, which can be visualized and tuned with the developed simulation tool, is required. This microstructural control can be established by (*i*) selecting a nitroxide/ alkoxyamine characterized by a sufficiently high NMP (de)activation reactivity and a minimal impact of side

reactions, (*ii*) adding the correct overall amount of the functional monomer(s), and (*iii*) applying an addition program for all comonomers to ensure low styrene concentrations during the addition of the functional monomer. To support the application of these three control strategies, both separately and jointly, model-based design is a powerful and indispensable tool.

Currently, in agreement with experimental results on the average chain length characteristics, the highest NMP copolymer product quality is obtained with the SG1 nitroxide in case the number of BzMl equivalents is sufficiently increased and the comonomers are added along the NMP at high styrene conversion.

Moreover, the proposed model-based design strategy is of a generic nature and can also be considered for the design of other functionalization processes aiming at precision control, provided that reliable model parameters are available or determined. In particular, the model allows to map the differences of the sequence-controlled quality between different RDRP techniques in order to identify the most suitable reaction conditions for the synthesis of well-defined sequence-controlled polymers consisting of a given comonomer pair.

References

1. Lutz, J.-F.; Ouchi, M.; Liu, D. R.; Sawamoto, M. Sequence-Controlled Polymers. *Science* **2013,** 341, (6146), 628-637.

2. Badi, N.; Chan-Seng, D.; Lutz, J.-F. Microstructure Control: An Underestimated Parameter in Recent Polymer Design. *Macromol. Chem. Phys.* **2013,** 214, (2), 135-142.

3. Lutz, J.-F.; Lehn, J.-M.; Meijer, E. W.; Matyjaszewski, K. From precision polymers to complex materials and systems. *Nat. Rev. Mater.* **2016,** 1, 16024.

4. Matyjaszewski, K. Architecturally Complex Polymers with Controlled Heterogeneity. *Science* **2011,** 333, (6046), 1104-1105.

5. Gody, G.; Maschmeyer, T.; Zetterlund, P. B.; Perrier, S. Rapid and quantitative one-pot synthesis of sequence-controlled polymers by radical polymerization. *Nat Commun* **2013,** 4.

6. Gutekunst, W. R.; Hawker, C. J. A General Approach to Sequence-Controlled Polymers Using Macrocyclic Ring Opening Metathesis Polymerization. *J. Am. Chem. Soc.* **2015,** 137, (25), 8038-8041.

7. Lehn, J.-M. Perspectives in Chemistry—Steps towards Complex Matter. *Angew. Chem. Int. Ed.* **2013,** 52, (10), 2836-2850.

8. Schmidt, B. V. K. J.; Fechler, N.; Falkenhagen, J.; Lutz, J.-F. Controlled folding of synthetic polymer chains through the formation of positionable covalent bridges. *Nat Chem* **2011,** 3, (3), 234-238.

9. Jiang, Y.; Golder, M. R.; Nguyen, H. V. T.; Wang, Y.; Zhong, M.; Barnes, J. C.; Ehrlich, D. J. C.; Johnson, J. A. Iterative Exponential Growth Synthesis and Assembly of Uniform Diblock Copolymers. *J. Am. Chem. Soc.* **2016**, 9369–9372.

10. Hadjichristidis, N.; Iatrou, H.; Pitsikalis, M.; Mays, J. Macromolecular architectures by living and controlled/living polymerizations. *Prog. Polym. Sci.* **2006,** 31, (12), 1068-1132.

11. Badi, N.; Lutz, J.-F. Sequence control in polymer synthesis. *Chem. Soc. Rev.* **2009,** 38, (12), 3383-3390.

12. Srichan, S.; Kayunkid, N.; Oswald, L.; Lotz, B.; Lutz, J.-F. Synthesis and Characterization of Sequence-Controlled Semicrystalline Comb Copolymers: Influence of Primary Structure on Materials Properties. *Macromolecules* **2014,** 47, (5), 1570-1577.

13. Pyun, J.; Matyjaszewski, K. Synthesis of Nanocomposite Organic/Inorganic Hybrid Materials Using Controlled/"Living" Radical Polymerization. *Chemistry of Materials* **2001,** 13, (10), 3436-3448.

14. Matyjaszewski, K.; Tsarevsky, N. V. Macromolecular Engineering by Atom Transfer Radical Polymerization. *J. Am. Chem. Soc.* **2014,** 136, (18), 6513-6533.

15. Braunecker, W. A.; Matyjaszewski, K. Controlled/living radical polymerization: Features, developments, and perspectives. *Prog. Polym. Sci.* **2007,** 32, (1), 93-146.

16. Chiefari, J.; Chong, Y. K.; Ercole, F.; Krstina, J.; Jeffery, J.; Le, T. P. T.; Mayadunne, R. T. A.; Meijs, G. F.; Moad, C. L.; Moad, G.; Rizzardo, E.; Thang, S. H. Living free-radical polymerization by

reversible addition-fragmentation chain transfer: The RAFT process. *Macromolecules* **1998,** 31, (16), 5559-5562.

17. Ouchi, M.; Terashima, T.; Sawamoto, M. Transition Metal-Catalyzed Living Radical Polymerization: Toward Perfection in Catalysis and Precision Polymer Synthesis. *Chem. Rev.* **2009,** 109, (11), 4963-5050.

18. Bertin, D.; Gigmes, D.; Marque, S. R. A.; Tordo, P. Kinetic subtleties of nitroxide mediated polymerization. *Chem. Soc. Rev.* **2011,** 40, (5), 2189-2198.

19. Delaittre, G.; Rieger, J.; Charleux, B. Nitroxide-Mediated Living/Controlled Radical Polymerization of N,N-Diethylacrylamide. *Macromolecules* **2011,** 44, (3), 462-470.

20. Akeroyd, N.; Klumperman, B. The combination of living radical polymerization and click chemistry for the synthesis of advanced macromolecular architectures. *Eur. Polym. J.* **2011,** 47, (6), 1207-1231.

21. Pfeifer, S.; Lutz, J.-F. A Facile Procedure for Controlling Monomer Sequence Distribution in Radical Chain Polymerizations. *J. Am. Chem. Soc.* **2007,** 129, (31), 9542-9543.

22. Lutz, J.-F. Writing on Polymer Chains. *Acc. Chem. Res.* **2013,** 46, (11), 2696-2705.

23. Lutz, J.-F.; Schmidt, B. V. K. J.; Pfeifer, S. Tailored Polymer Microstructures Prepared by Atom Transfer Radical Copolymerization of Styrene and N-substituted Maleimides. *Macromol. Rapid Commun.* **2011,** 32, (2), 127-135.

24. Lutz, J.-F. Sequence-controlled polymerizations: the next Holy Grail in polymer science? *Polym. Chem.* **2010,** 1, (1), 55-62.

25. Klumperman, B., The Rationale Behind Sequence-Controlled Maleimide Copolymers. In *Sequence-Controlled Polymers: Synthesis, Self-Assembly, and Properties*, American Chemical Society: 2014; Vol. 1170, pp 213-221.

26. Chan-Seng, D.; Zamfir, M.; Lutz, J.-F. Polymer-Chain Encoding: Synthesis of Highly Complex Monomer Sequence Patterns by Using Automated Protocols. *Angew. Chem. Int. Ed.* **2012,** 51, (49), 12254-12257.

27. Hawker, C. J.; Bosman, A. W.; Harth, E. New Polymer Synthesis by Nitroxide Mediated Living Radical Polymerizations. *Chem. Rev.* **2001,** 101, (12), 3661-3688.

28. Nicolas, J.; Guillaneuf, Y.; Lefay, C.; Bertin, D.; Gigmes, D.; Charleux, B. Nitroxide-mediated polymerization. *Progress in Polymer Science* **2013,** 38, (1), 63-235.

29. Fischer, H. The Persistent Radical Effect In "Living" Radical Polymerization. *Macromolecules* **1997,** 30, (19), 5666-5672.

30. Tang, W.; Fukuda, T.; Matyjaszewski, K. Reevaluation of persistent radical effect in NMP. *Macromolecules* **2006,** 39, (13), 4332-4337.

31. Lutz, J. F.; Lacroix-Desmazes, P.; Boutevin, B. The persistent radical effect in nitroxide mediated polymerization: Experimental validity. *Macromol. Rapid Commun.* **2001,** 22, (3), 189-193.

32. Goto, A.; Fukuda, T. Kinetics of living radical polymerization. *Prog. Polym. Sci.* **2004,** 29, (4), 329-385.

33. Zhong, M. J.; Matyjaszewski, K. How Fast Can a CRP Be Conducted with Preserved Chain End Functionality? *Macromolecules* **2011,** 44, (8), 2668-2677.

34. Konkolewicz, D.; Krys, P.; Matyjaszewski, K. Explaining Unexpected Data via Competitive Equilibria and Processes in Radical Reactions with Reversible Deactivation. *Acc. Chem. Res.* **2014,** 47, (10), 3028-3036.

35. Johnston-Hall, G.; Monteiro, M. J. Kinetic Simulations of Atom Transfer Radical Polymerization (ATRP) in Light of Chain Length Dependent Termination. *Macromol. Theory Simul.* **2010,** 19, (7), 387-393.

36. Gody, G.; Zetterlund, P. B.; Perrier, S.; Harrisson, S. The limits of precision monomer placement in chain growth polymerization. *Nat Commun* **2016,** 7.

37. Van Steenberge, P. H. M.; D'hooge, D. R.; Wang, Y.; Zhong, M. J.; Reyniers, M. F.; Konkolewicz, D.; Matyjaszewski, K.; Marin, G. B. Linear Gradient Quality of ATRP Copolymers. *Macromolecules* **2012,** 45, (21), 8519-8531.

38. Payne, K. A.; D'hooge, D. R.; van Steenberge, P. H. M.; Reyniers, M. F.; Cunningham, M. F.; Hutchinson, R. A.; Marin, G. B. ARGET ATRP of Butyl Methacrylate: Utilizing Kinetic Modeling To Understand Experimental Trends. *Macromolecules* **2013,** 46, (10), 3828-3840.

39. Van Steenberge, P. H. M.; D'hooge, D. R.; Reyniers, M. F.; Marin, G. B. Improved kinetic Monte Carlo simulation of chemical composition-chain length distributions in polymerization processes. *Chem. Eng. Sci.* **2014,** 110, 185-199.

40. Mayo, F. R. Chain Transfer in the Polymerization of Styrene. VIII. Chain Transfer with Bromobenzene and Mechanism of Thermal Initiation1. *J. Am. Chem. Soc.* **1953,** 75, (24), 6133-6141.

41. Bentein, L.; D'hooge, D. R.; Reyniers, M. F.; Marin, G. B. Kinetic Modeling as a Tool to Understand and Improve the Nitroxide Mediated Polymerization of Styrene. *Macromol. Theory Simul.* **2011,** 20, (4), 238-265.

42. Yao, F.; Michael, F. C.; Robin, A. H. Modeling of Nitroxide-Mediated Semibatch Radical Polymerization. *Macromol. React. Eng.* **2007,** 1.

43. Payne, K. A.; Nesvadba, P.; Debling, J.; Cunningham, M. F.; Hutchinson, R. A. Nitroxide-Mediated Polymerization at Elevated Temperatures. *ACS Macro Letters* **2015,** 4, (3), 280-283.

44. Ananchenko, G. S.; Souaille, M.; Fischer, H.; Le Mercier, C.; Tordo, P. Decomposition of model alkoxyamines in simple and polymerizing systems. II. Diastereomeric N-(2-methylpropyl)-N-(1-diethyl-phosphono-2,2-dimethylpropyl)-aminoxyl-b ased compounds. *J. Polym. Sci. Pol. Chem.* **2002,** 40, (19), 3264-3283.

45. Skene, W. G.; Scaiano, J. C.; Yap, G. P. A. An Improved Mimetic Compound for Styrene "Living" Free Radical Polymerization. An Initiator Containing the "Penultimate" Unit. *Macromolecules* **2000,** 33, (10), 3536-3542.

46. Klumperman, B.; O'Driscoll, K. F. Interpreting the copolymerization of styrene with maleic anhydride and with methyl methacrylate in terms of the bootstrap model. *Polymer* **1993,** 34, (5), 1032-1037.

47. Klumperman, B. Mechanistic considerations on styrene-maleic anhydride copolymerization reactions. *Polymer Chemistry* **2010,** 1, (5), 558-562.

48. Johnston-Hall, G.; Monteiro, M. J. Bimolecular radical termination: New perspectives and insights. *J. Polym. Sci. Pol. Chem.* **2008,** 46, (10), 3155-3173.

49. D'hooge, D. R.; Reyniers, M.-F.; Marin, G. B. The Crucial Role of Diffusional Limitations in Controlled Radical Polymerization. *Macromol. React. Eng.* **2013,** 7, (8), 362-379.

50. Barner-Kowollik, C.; Russell, G. T. Chain-length-dependent termination in radical polymerization: Subtle revolution in tackling a long-standing challenge. *Prog. Polym. Sci.* **2009,** 34, (11), 1211-1259.

51. Derboven, P.; D'hooge, D. R.; Reyniers, M.-F.; Marin, G. B.; Barner-Kowollik, C. The Long and the Short of Radical Polymerization. *Macromolecules* **2015,** 48, (3), 492-501.

52. Pfeifer, S.; Lutz, J. F. Development of a library of N-substituted maleimides for the local functionalization of linear polymer chains. *Chemistry* **2008,** 14, (35), 10949-57.

53. Bentein, L.; D'hooge, D. R.; Reyniers, M. F.; Marin, G. B. Kinetic modeling of miniemulsion nitroxide mediated polymerization of styrene: Effect of particle diameter and nitroxide partitioning up to high conversion. *Polymer* **2012,** 53, (3), 681-693.

54. Zamfir, M.; Lutz, J.-F. Ultra-precise insertion of functional monomers in chain-growth polymerizations. *Nat Commun* **2012**, 1138.

55. Zetterlund, P. B. Compartmentalization in Atom Transfer Radical Polymerization to High Conversion in Dispersed Systems: Effects of Diffusion-Controlled Reactions. *Macromolecules* **2010,** 43, (3), 1387-1395.

56. Grimaldi, S.; Finet, J.-P.; Le Moigne, F.; Zeghdaoui, A.; Tordo, P.; Benoit, D.; Fontanille, M.; Gnanou, Y. Acyclic β-Phosphonylated Nitroxides: A New Series of Counter-Radicals for "Living"/Controlled Free Radical Polymerization. *Macromolecules* **2000,** 33, (4), 1141-1147.

57. Benoit, D.; Chaplinski, V.; Braslau, R.; Hawker, C. J. Development of a universal alkoxyamine for "living" free radical polymerizations. *J. Am. Chem. Soc.* **1999,** 121, (16), 3904-3920.

58. Moad, G.; Rizzardo, E.; Solomon, D. H. A product study of the nitroxide inhibited thermal polymerization of styrene. *Polym. Bull.* **1982,** 6, (11-1), 589-593.

59. Gryn'ova, G.; Lin, C. Y.; Coote, M. L. Which side-reactions compromise nitroxide mediated polymerization? *Polym. Chem.* **2013,** 4, (13), 3744-3754.

60. Kruse, T. M.; Souleimonova, R.; Cho, A.; Gray, M. K.; Torkelson, J. M.; Broadbelt, L. J. Limitations in the Synthesis of High Molecular Weight Polymers via Nitroxide-Mediated Controlled Radical Polymerization: Modeling Studies. *Macromolecules* **2003,** 36, (20), 7812-7823.

61. Marque, S.; Le Mercier, C.; Tordo, P.; Fischer, H. Factors influencing the C-O-bond homolysis of trialkylhydroxylamines. *Macromolecules* **2000,** 33, (12), 4403-4410.

62. Drockenmuller, E.; Catala, J.-M. Synthesis of a New Stable β-Sulfinyl Nitroxide and the Corresponding Alkoxyamine for Living/Controlled Radical Polymerization of Styrene: Kinetic and ESR Studies. *Macromolecules* **2002,** 35, (7), 2461-2466.

63. Sobek, J.; Martschke, R.; Fischer, H. Entropy Control of the Cross-Reaction between Carbon-Centered and Nitroxide Radicals. *J. Am. Chem. Soc.* **2001,** 123, (12), 2849-2857.

64. Catala, J. M.; Bubel, F.; Hammouch, S. O. Living Radical Polymerization: Kinetic Results. *Macromolecules* **1995,** 28, (24), 8441-8443.

Chapter 6. How penultimate monomer unit effects and initiator choice influence ICAR ATRP of n-butyl acrylate and methyl methacrylate

Summary

The relevance of penultimate monomer unit (PMU) effects and the selection of the correct initiator species under typical reversible deactivation radical copolymerization conditions is illustrated, using matrix-based kinetic Monte Carlo simulations allowing the visualization of all monomer sequences along individual chains. Initiators for continuous activator regeneration atom transfer radical polymerization (ICAR ATRP) is selected as illustrative polymerization technique with *n*-butyl acrylate and methyl methacrylate as comonomers, aiming at the synthesis of well-defined gradient copolymers. Using literature based model parameters, in particular temperature dependent monomer and radical reactivity ratios, it is demonstrated that PMU effects on propagation and ATRP (de)activation cannot be ignored to identify the most suited ICAR ATRP reactants (*e.g.* tertiary ATRP initiator) and reaction conditions (*e.g.* feeding rates under fed-batch conditions). The formulated insights highlight the need for further research on PMU effects on all reaction steps in radical polymerization. This work was published in *AIChE Journal* 2017, DOI: 10.1002/aic.15851

6.1 Introduction

Radical polymerization is a powerful synthesis technique, allowing upon processing of the produced grades the realization of both commodity materials (*e.g.* household goods and construction items) and more specialized applications (*e.g.* coatings and paints).[1, 2] In many cases a copolymerization is conducted to combine several properties in one polymer product. Important commercial copolymers are for instance poly(acrylonitrile-butadiene-styrene), poly(styrene-acrylonitrile), and copolymers based on (meth)acrylates and acrylamides.

Under batch free radical polymerization (FRP) conditions, as shown in Figure 6.1, conventional radical initiator molecules (I_2; *e.g.* azobisisobutyronitrile (AIBN)) dissociate into *I* radicals that take up many (*e.g.* 10^3) comonomer molecules (*M*) to form macroradicals R_i (*i*: chain length). These R_i species live only for milliseconds before they are transformed into dead polymer molecules *P* via either termination or chain transfer reactions. As the I_2 and *M* concentrations continuously decrease and the observed reaction rates can depend on the viscosity and hence on the monomer conversion, a polymer product with a broad chain length distribution (CLD) results. For example, at low to intermediate overall monomer conversions (X_m=0.20-0.70) diffusional limitations on termination lead to a gel-effect so that longer chains are formed, as propagation is relatively favored.[3] On the other hand, at high overall monomer conversions (X_m > 0.90) or thus low monomer concentrations propagation is less likely and shorter chains are again formed, with an even further reduction of the chain length for a diffusion-controlled propagation.[4]

For batch copolymerization, the situation is even more complex with a drifting composition for the formed chains with increasing reaction time.[5-7] This drifting is due to the difference in chemical structure of the comonomers and a favoritism toward the incorporation of the more reactive monomer at low reaction times and thus depletion of this comonomer already at

intermediate X_m. Hence, in conventional batch radical copolymerization not only a wide range of chain lengths are formed, leading to highly disperse polymers ($Đ > 1.5$), but also the comonomer sequences or even simply the overall amounts of comonomer per chain can be strongly different. To partially compensate for this heterogeneous character of the copolymer composition fed-batch (or semi-batch) procedures are typically applied.[8, 9] The monomer feed composition is kept constant by continuously adding comonomer(s) so that the instantaneous average copolymer compositions, *i.e.* the average incorporated amounts of each comonomer over all chains, remains on target. A differentiation in the comonomer sequences is however still obtained upon comparison of the monomer sequences of individual chains.[10] By applying a fed-batch procedure compositional drift on an average basis is avoided, however, the monomer sequences of individual macrospecies and thus the individual copolymer compositions cannot be made identical.[11] It should be further realized that even under fed-batch conditions a broad CLD results and therefore FRP has its inherent limitations for the synthesis of more advanced copolymers such as for instance block and gradient copolymers for self-assembly applications.[12]

More recently so-called controlled radical copolymerization (CRP) or reversible deactivation radical copolymerization (RDRP) techniques have been developed that allow a much better intermolecular homogeneity of the polymer microstructure, both with respect to the control over chain length and comonomer incorporation.[12-16] In these techniques, a (mediating) agent is added which allows the temporarily deactivation of R_i into dormant species (R_iX), as shown in Figure 6.1, taking (“normal") atom transfer radical polymerization (ATRP) as illustrative CRP technique. In ATRP, mostly a Cu-based catalyst or activator (M_t^nL/X) allows the activation of dormant (macro)species by taking up the X (halogen) moiety and becoming deactivator ($M_t^{n+1}L/X_2$). After a couple of propagations this moiety can be transferred back via deactivation,

as this reaction is characterized by a high intrinsic reactivity (> *ca.* 10^6 L mol^{-1} s^{-1}). This also leads to the regeneration of the activator, highlighting the catalytic nature of the ATRP process.[14, 17, 18] Under well-defined reaction conditions, activation-propagation-deactivation cycles are dominant so that R_iX species are mostly formed and, hence, in contrast to FRP a functional polymer product is obtained. Moreover, for a sufficiently fast CRP initiation, a low dispersity polymer ($Đ$ < 1.5) can be made as well.[19]

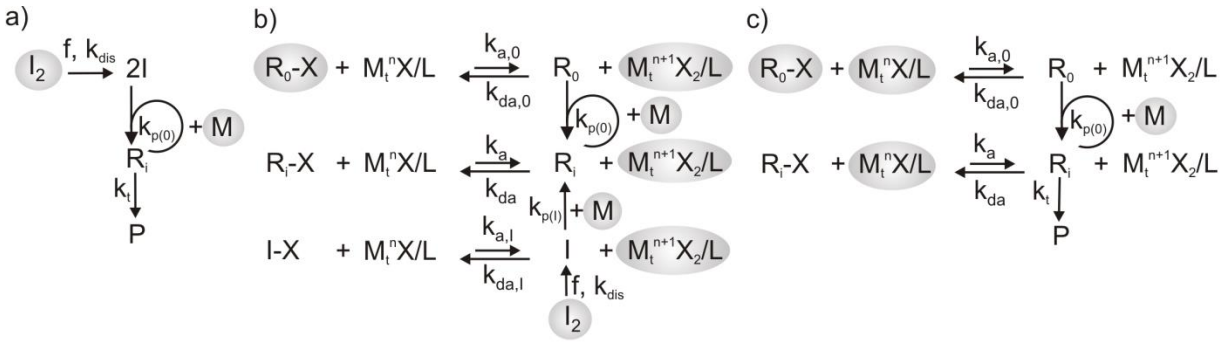

Figure 6.1. *Principle of (a) conventional free radical polymerization (FRP), (b) initiators for continuous activators regeneration (ICAR) ATRP and (c) "normal" atom transfer radical polymerization (ATRP);* k_a, k_{da}, k_p, k_t, k_{dis}*: rate coefficient for ATRP activation, ATRP deactivation, propagation, termination, dissociation; f: conventional initiator efficiency; subscript 0: ATRP initiator, subscript i: chain length;* M_t^nX/L*: activator,* $M_t^{n+1}X_2/L$*: deactivator; starting compounds: grey circles; for ICAR ATRP termination is not explicitly shown for simplicity.*

In general, CRP allows to gradually incorporate monomer units along individual (co)polymer chains in an almost identical way, since each "growing" dormant species experiences the same reaction conditions, as opposed to FRP, in which the radical lifetime is only in the order of milliseconds.[20] This implies the possibility of intermolecular homogeneity for the monomer sequences, which is a characteristic as good as unachievable via FRP as explained above. On the other hand, CRP often suffers from low polymerization rates, making it less industrially attractive as compared to the well-established FRP technique.[12, 21, 22] For ATRP this issue has been greatly

resolved by developing modified ATRP systems[23-29] such as initiators for continuous activators regeneration (ICAR) ATRP of which the principle is shown in Figure 6.1. In ICAR ATRP, the polymerization is started with small amounts of the oxygen insensitive deactivator (< 50 ppm; molar with respect to monomer) and I_2. Hence, a FRP (Figure 6.1) and "normal" ATRP (Figure 6.1) procedure are mixed to ensure simultaneously a high polymerization rate and an excellent microstructural control. It should be further stressed that CRP remains a radical polymerization technique and therefore as in FRP a complex interplay between chemistry and diffusional limitations exist, which can only be properly mapped via kinetic modeling due to the high number of parameters involved.[30-32] This complexity is specifically increased in case copolymerizations are studied in which both comonomers are sufficiently present. So-called penultimate monomer unit (PMU) effects can exist, implying that the intrinsic reactivities are determined by the last two monomer units of the macroreactants and not only by the last one.[33]

For example, if the PMU effect is relevant for the propagation reactivity, 8 propagation rate coefficients need to be distinguished for kinetic modeling studies in contrast to the conventional 4 of the terminal model with only the last monomer unit determining the propagation reactivity. At first, only terminal propagation models have been used, which were rarely critically tested against both polymer composition and monomer conversion experimental data.[34] Later on, a more profound testing indicated a general failure of the terminal propagation model which led to the development of several penultimate models.[35, 36] The two most successfully applied PMU propagation models under both FRP and CRP conditions are the so-called implicit and explicit penultimate model.[33] The former assumes an influence of both the terminal and penultimate monomer unit on the individual propagation reactivities, in combination with only an influence of the terminal monomer unit on the propagation selectivity ($\frac{k_{pii,i}^{chem}}{k_{pii,j}^{chem}} = \frac{k_{pji,i}^{chem}}{k_{pji,j}^{chem}}$). On the other hand, for

an explicit PMU model, also the propagation selectivity is influenced by the penultimate monomer unit.[34, 35, 37] Currently, the implicit propagation model is most frequently used, although in general the true nature of the PMU effect is more likely of an explicit nature.[38-40] The kinetic relevance of the PMU effect further depends on the reactions conditions and nature of the comonomer pair.[41, 42] In addition, the PMU effect can also be relevant for the intrinsic (chemical) CRP activation and deactivation reactivities, giving rise to 4 extra intrinsic (penultimate) rate coefficients.[43-45] For example, Nanda *et. al.*[45] experimentally highlighted PMU effects for ATRP activation rate coefficients comparing the reactivities of mono- and dimeric (meth)acrylate Br-capped species, using a trapping procedure with a persistent radical. A computational study by Lin *et al.*[46] confirmed this PMU effect on the equilibrium coefficient for the related bond dissociation step. Moreover, the recent progress in theoretical or *ab initio* calculations will very likely lead in the near future to an additional pathway to further map the impact of PMU effects on intrinsic rate coefficients.[5, 33, 47-49]

To reduce the complexity and taking into account the limited knowledge on penultimate rate coefficients most CRP kinetic modeling studies resort to the use of the simplified terminal model to calculate the intrinsic reactivities.[50-54] In case a PMU model is used, it only relates to the propagation reactivity - thus not to the CRP (de)activation reactivity - and this almost exclusively in an implicit way.[55-57] Moreover, the temperature dependency of the reactivity ratios is rarely taken into account and often values are employed which have been obtained at a different temperature than the actual polymerization temperature considered in the kinetic modeling study. In general, it can be expected that this is a too strong simplification, in particular for reactions with a wide range of activation energies.[13, 58]

In the present work, matrix-based kinetic Monte Carlo (*k*MC) simulations[4] are used to highlight the relevance of PMU effects in CRP, selecting ICAR ATRP as reference technique and *n*-butyl acrylate (*n*BuA) and methyl methacrylate (MMA) as comonomers. A distinction is made between PMU effects on propagation and ATRP (de)activation, considering literature data to calculate the Arrhenius parameters for the associated monomer and radical reactivity ratios. For the first time, the monomer sequences of individual polymer chains are visualized while accounting for PMU effects and a comparison is made with model simulations according to the approximate but typically applied terminal model. It is also demonstrated that the temperature dependency of the monomer and radical reactivity ratios cannot be ignored, a simplification which is frequently made in previous kinetic modeling studies as mentioned above. A broad window of polymerization conditions is considered, including a variation of the temperature and operation mode (batch *vs.* fed-batch). Model-based design is also applied to explore the influence of the PMU effect on the identification of optimal reaction conditions for the synthesis of well-defined gradient copolymers. The formulated kinetic insights contribute greatly to the improved understanding of radical copolymerization in general and emphasize the need for further research and quantification of PMU effects on the propagation and CRP (de)activation reactivity.

6.2 Kinetic model

In the present work, a detailed kinetic model is constructed for ICAR ATRP of *n*-butyl acrylate (*n*BuA; M_1) and methyl methacrylate (MMA; M_2), employing Cu(II)Br_2/PMDETA (*N*,*N*,*N*′,*N*″,*N*″-pentamethyldiethylenetriamine) as deactivator and considering penultimate monomer unit (PMU) effects on all relevant reaction steps. This RDRP system is selected to allow for a direct comparison with previous kinetic modeling results employing a terminal

model[54] and taking into account that the model parameters can be derived from literature. The kinetic model considers dissociation, chain initiation, propagation, ATRP (de)activation, and termination. Backbiting could be ignored based on preliminary simulations (see Section S.1 of the Appendix), taking into account that a maximal and reference temperature of 363 K is used.

In a first stage, grid simulations are performed at 363 K to identify a suited ICAR ATRP initiation system to ensure a sufficiently high batch polymerization rate and control over the polymer properties with an acceptable Cu ppm level. These simulations involve the consideration of several ATRP initiators (R_0X) with reported ATRP activation rate coefficients (k_{a0}^{chem}) ranging from 3.0×10^{-1} to 4.1×10^{2} L mol^{-1} s^{-1} and several conventional radical initiators (I_2) for which the reported dissociation rate coefficient (k_{dis}^{chem}) varies between 6.3×10^{-6} and 2.5×10^{-4} s^{-1}.[58, 59] For simplicity the corresponding deactivation rate coefficients (k_{da0}^{chem}) are not altered, as preliminary simulations showed that this parameter is kinetically less significant (see Appendix). In a second stage, a detailed understanding and design of the copolymerization process is targeted for the optimized initiation system determined in the first stage. This includes evaluation of the effect of a variation of the temperature and reactor operation mode (batch *vs.* fed-batch) and ultimately aims at the relatively fast synthesis of well-defined gradient copolymers.

6.2.1 Kinetic parameters

The monomer and radical reactivity ratios reported in the study of Yu *et al.*[60] (Table 6.1: left) are used together with the well-known homopropagation coefficients.[61, 62] to calculate the 8 penultimate propagation kinetic parameters (*i.e.* $k_{pXY,Z}^{chem}$ *with X,Y,Z = 1,2)* , of which the two first indeces of the subscript relate to the penultimate and terminal monomer unit of the macroradical, and the third one to the monomer involved in the propagation reaction.. These ratios, as defined

in Equation (6.1), relate to the copolymerization of methyl acrylate and MMA, of which the former is taken as a representative for *n*BuA, the selected acrylate monomer in the present work.

$$r_1 = \frac{k_{p11,1}^{chem}}{k_{p11,2}^{chem}};\ r_2 = \frac{k_{p22,2}^{chem}}{k_{p22,1}^{chem}};\ r_1{}' = \frac{k_{p21,1}^{chem}}{k_{p21,2}^{chem}};\ r_2{}' = \frac{k_{p12,2}^{chem}}{k_{p12,1}^{chem}};\ s_1 = \frac{k_{p21,1}^{chem}}{k_{p11,1}^{chem}};\ s_2 = \frac{k_{p12,2}^{chem}}{k_{p22,2}^{chem}} \qquad (6.1)$$

Yu *et al.*[60] calculated from first principles both terminal and penultimate propagation reactivity ratios, using mono-, dimeric, and trimeric radicals as model compounds and considering different temperatures so that Arrhenius type of relations could be calculated for the reactivity ratios (Table 6.1; left). For the terminal model, in which the propagation reactivities are retrieved from *ab initio* calculations with mono-radicals, it follows by definition that $r_1 = r_1{}'$, $r_2 = r_2{}'$, and $s_1 = s_2 = 1$. A comparison of the terminal reactivity ratios at 293 and 363 K in Table 6.1 and the corresponding reactivity ratios via the penultimate model allows to conclude that PMU effects cannot be ignored for the selected comonomer pair but are not equally relevant for all propagation reactions. Most deviations with respect to the terminal model are related to the *s* values as still rather similar *r* and *r'* values are obtained, highlighting that a so-called implicit PMU is very likely active with most significant PMU effects upon on evaluation of the ICAR ATRP process on a time basis. [10, 34] Nevertheless at a given monomer conversion microstructural changes, *e.g.* compositional heterogeneity, can also be expected taking into account that in practice often fed-batch procedures are applied for radical copolymerization processes for which the feeding rate profiles need to be defined as a function of the reaction time.[53, 63]

Table 6.1. *Arrhenius relations for the reactivity ratios for propagation/ATRP (de)activation (Equation (6.1)/(6.2)) in the copolymerization of n-butyl acrylate (M_1) and methyl methacrylate (M_2) with Cu(II)Br2/PMDETA; terminal (T) and penultimate (PMU); values at 293 and 363 K also specified.*[45, 46, 60]

		propagation[(a)]						(de)activation[(a)]			
		r_1	r_2	r_1'	r_2'	s_1	s_2	$s_{a,1}$	$s_{a,2}$	$s_{da,1}$	$s_{da,2}$
T	*A* (-)	1.72	0.90	1.72	0.90	1.00	1.00	1.00	1.00	1.00	1.00
	E_a (kJ mol^{-1})	3.71	-2.97	3.71	-2.97	0.00	0.00	0.00	0.00	0.00	0.00
	r/s(293K)	0.38	3.05	0.38	3.05	1.00	1.00	1.00	1.00	1.00	1.00
	r/s(363K)	0.49	2.47	0.49	2.47	1.00	1.00	1.00	1.00	1.00	1.00
PMU	*A* (-)	2.48	1.08	1.34	0.74	0.70	1.03	4.72	84.44	1.23	0.59
	E_a (kJ mol^{-1})	4.69	-2.36	3.10	-3.58	1.43	-1.25	0.00	15.48	0.00	0.00
	r/s(293K)	0.36	2.85	0.38	3.22	0.39	1.72	4.72	0.15	1.23	0.59
	r/s(363K)	0.50	2.41	0.47	2.50	0.43	1.58	4.72	0.43	1.23	0.59

[(a)] values of $k_{p11,1}^{chem}$, $k_{p22,2}^{chem}$, $k_{(d)a11}^{chem}$, and $k_{(d)a22}^{chem}$ can be found in Table S.1 (Appendix)

For ATRP (de)activation PMU effects are also taken into account, despite that typically terminal values are considered in CRP kinetic modeling studies as explained above.[45, 46] Only a few kinetic studies[45] are devoted to the quantification of the PMU effect for ATRP (de)activation, explaining the lack of fully penultimate (ICAR) ATRP kinetic models. In analogy with the propagation radical reactivity ratios, following (de)activation radical reactivity ratios can be defined using the eight penultimate (de)activation rate coefficients (*i.e.* $k_{(d)aXY}^{chem}$ with X,Y = 1,2 related to the penultimate and terminal monomer unit of the macrospecies involved):

$$s_{a,1} = \frac{k_{a21}^{chem}}{k_{a11}^{chem}}; s_{a,2} = \frac{k_{a12}^{chem}}{k_{a22}^{chem}};\ s_{da,1} = \frac{k_{da21}^{chem}}{k_{da11}^{chem}}; s_{da,2} = \frac{k_{da12}^{chem}}{k_{da22}^{chem}} \quad (6.2)$$

Due to the limited availability of Arrhenius parameters for ATRP (de)activation, and the illustrative nature of the present work, the homopolymerization Arrhenius parameters, *i.e.* $k_{(d)a11}^{chem}$and $k_{(d)a22}^{chem}$, have been approximated by those reported for isobornyl acrylate and butyl methacrylate.[64, 65] As explained in detail in Appendix, the other activation penultimate Arrhenius parameters can be assessed by considering the s_a values from the experimental study by Kumar *et al.* at 308 K[45] and Evans-Polanyi-type relationships based on literature bond dissociation energies (BDEs) for the homolytic cleavage of the Br group. As also explained in Appendix, the corresponding s_{da} values can be assessed by ignoring temperature dependencies and using thermodynamic BDE data.[45, 46] The resulting Arrhenius parameters for the (de)activation radical reactivity ratios and the corresponding values at 293 and 363 K are specified in Table 6.1 (right).

For termination, in agreement with literature data, no PMU effects are taken into account.[5] The termination reactivities are described based on the terminal monomer units of the participating radicals, correcting for diffusional limitations. In other words, apparent termination rate coefficients are used in agreement with previous kinetic studies.[66-69] To account for the different diffusivity of homopolymer and copolymer chains an averaging according to the overall copolymer composition is performed, as explained in Appendix. The homopolymer apparent termination rate coefficients are taken from the work of Johnston-Hall *et al.* who applied the so-called reversible addition fragmentation chain transfer- chain length dependent- termination technique to measure the chain length and monomer conversion dependencies.[67, 70] Diffusional limitations on the (de)activation process can be ignored to a first approximation as the conversion remains below 0.80.[66]

An overview of the Arrhenius parameters of all the reactions is provided in Table S.1 in the Appendix. For simplicity and again reminding the illustrative nature of the present work, the dissociation activation energy is taking equal to the one reported for AIBN.[59] The chain initiation steps (CI1 to CI12 in Table S.1) comprise all monomer additions until a chain length of two is reached, since a penultimate model is used. Depending on the nature of the initiator radical, *i.e.* secondary or tertiary, and the monomer which is being incorporated, the Arrhenius parameters are approximated by those for the corresponding propagation. In Table S.1 in the Appendix the corresponding values at 363 K are also included. Anoverview of the intrinsic propagation and ATRP (de)activation reaction coefficients is given in Table S.3 of the Appendix.

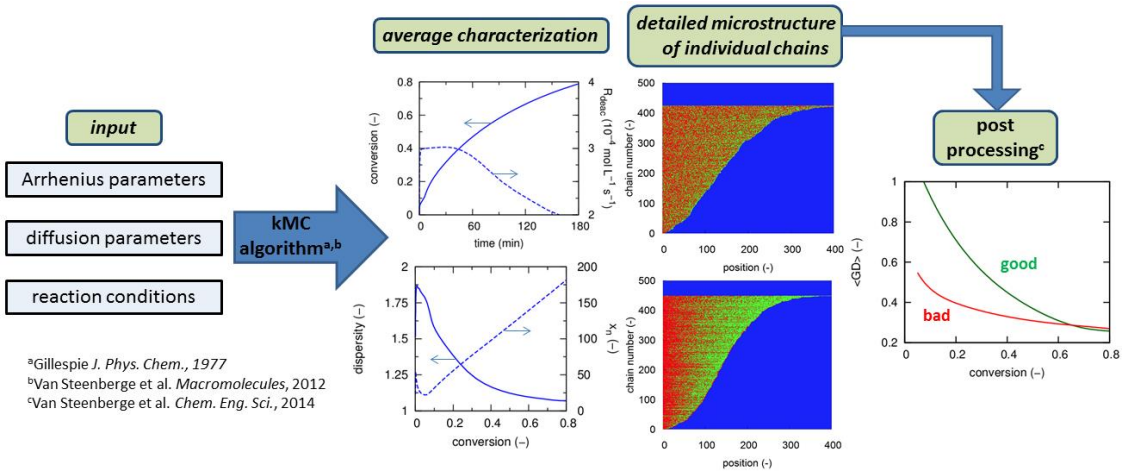

Figure 6.2. *Outcome of the penultimate kMC model, focusing both on an average characterization and a detailed microstructural description of individual chains;* R_{deac}*: ATRP deactivation rate.*

6.2.2 Model output

The *k*MC modeling strategy is the same as the one introduced by Van Steenberge *et al.*[4] and allows not only the calculation of average ICAR ATRP characteristics such as the dispersity and deactivation reaction rate (second to minute scale) but also the explicit microstructure of a representative copolymer sample (Figure 6.2; middle; minute to hour scale; single core). The latter refers to the visualization of the monomer sequence for each of the chains in this sample.

Note that with deterministic solvers such level of microstructural detail is extremely challenging as this is associated with a too high number of differential equations and thus an unrealistic computational cost. A direct average calculation is also not suited, taking into account the lack of a uniform chain length.

Particularly with the selected *k*MC strategy for gradient copolymers an unbiased product quality labeling can made by *a posteriori* calculation of the so-called gradient deviation (<GD>; Figure 6.2 (right)).[20] Each chain in the sample is compared to the analogous 'perfect' (linear) gradient copolymer chain and <GD> results upon averaging over all chains and normalization toward a worst-case scenario of homopolymerization (normalization factor: 0.166). Theoretically a perfect (linear) gradient thus corresponds to a <GD> of 0. In practice, deviations always exist (*e.g.* due to unavoidable termination) and low <GD> values can be related to a high quality gradient copolymer.[71] Earlier CRP kinetic modeling studies have indicated that a high quality gradient copolymer requires, at high X_m, a <GD> lower than 0.3 and a steep decrease for <GD> from low to high X_m. The latter is reflected by the difference between the green line in Figure 6.2 (right; good gradient) and the red line in Figure 6.2 (right) corresponding to a more poorly defined gradient copolymer.[20, 54]

6.3 Results and Discussion

In this section, the strength of *k*MC modeling to understand and design ICAR ATRP of MMA and *n*BuA toward the synthesis of well-defined gradient copolymers is illustrated. Attention is first focused on the identification of the correct initiator species types and the relevance of PMU effects under batch conditions. Subsequently attention is paid to the importance of the reaction

temperature and the reactor operation mode by comparing the gradient synthesis under batch and fed-batch conditions.

6.3.1 Selection of initiator species types under batch conditions

One of the key challenges for ICAR ATRP is the identification of a suited R_0X and I_2 pair, allowing on the one hand a reasonable polymerization rate so that a high monomer conversion can be easily reached and on the other hand an acceptable control over the polymer microstructure, *i.e.* a low dispersity and a high EGF. This identification is not straightforward as it also depends on the reaction conditions. [24, 26, 65, 72, 73] Overall many ICAR ATRP characteristics play a role and grid simulations need to be ideally performed over a wide range of reaction conditions and initiator kinetic parameters to avoid or at least minimize a biased identification of suited ICAR ATRP process characteristics.

In Appendix, it is shown via such grid simulations that an intermediate Cu level (*e.g.* 40 ppm) and targeted chain length (*e.g.* TCL=200; initial molar ratio of monomer to ATRP initiator) are required to obtain a successful ICAR ATRP process. From Figure 6.3, in which grid simulation results for the initiator reactivities with respect to the polymerization time and dispersity are depicted (fixed X_m of 0.8; TCL of 200; 40 ppm Cu; 363 K), it follows that k_{dis}^{chem} needs to possess an intermediate value and ATRP initiators with a sufficiently high k_{a0}^{chem} are needed. A k_{dis}^{chem} of 5×10^{-5} s^{-1} is selected in the present work in good correspondence with commercially available initiators.[59] A threshold value for k_{a0}^{chem} corresponding to *ca.* 1 L mol^{-1} s^{-1} can be identified in Figure 3 in order to achieve a good microstructural control, *i.e.* a good control over dispersity and EGF, while still maintaining a reasonable polymerization rate. Therefore, a tertiary R_0X (yellow spheres) such as methyl 2-bromoisobutyrate is put forward in the present work to be most suited (k_{a0}^{chem} = 4.1×10^2 L mol^{-1} s^{-1}).[58, 65] In contrast, a secondary R_0X (white crosses in Figure 6.3(a)-

(b); k_{a0}^{chem} = 3.0 × 10^{-1} L mol^{-1} s^{-1})[64] leads to too high dispersities (> 1.6) despite that the polymerization time is significantly reduced (< 8 hours).

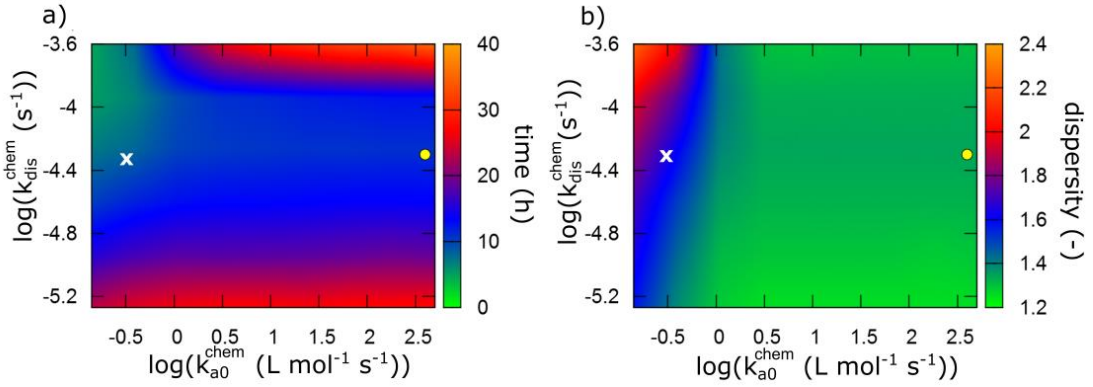

Figure 6.3*. Mapping of the impact of dissociation rate coefficient* k_{dis}^{chem} *and ATRP initiator (*R_0X*) activation rate coefficient (*k_{a0}^{chem}*) on (a) the polymerization time and (b) dispersity at an overall conversion of* X_m *= 0.80 for ICAR ATRP of n-butyl acrylate (*M_1*) and methyl methacrylate (*M_2*) at 363K with* $[M_1]_0 = [M_2]_0$*; yellow dots: optimized batch system with tertiary ATRP initiator (*k_{a0}^{chem} *=4.1 ×* 10^2 *L* mol^{-1} s^{-1}*) and* $[M]_0:[R_0X]:[I_2]_0$ *= 200:1:0.03 and initial Cu(II) ppm level = 40 ppm; white "x": results for unsuited secondary ATRP initiator (*k_{a0}^{chem} *=3.0 ×* 10^{-1} *L* mol^{-1} s^{-1}*); parameters: Table D.1 (Appendix); similar grid simulation results for reaction conditions in the Appendix.*

This different behavior of the secondary and tertiary R_0X with respect to the polymerization time and dispersity is even more clear in Figure 6.4, the focus is now on both low and high reaction times or X_m values (full/dotted lines: tertiary/secondary R_0X). For the secondary R_0X, except at very low reaction times, the ICAR ATRP is always significantly faster. In agreement with the results in Figure 6.3(a) an overall polymerization time of *ca.* 8 hours is sufficient to reach a X_m of 0.8 (dotted line in Figure 6.4(a)). On the other hand, for the tertiary R_0X, the ICAR ATRP is slower with an increased polymerization time of *ca.* 11 hours. It should be noted that on an X_m basis the relative consumptions of both comonomers are independent of the R_0X type as coinciding instantaneous copolymer composition fractions ($F_{1,inst}$; $d[M_1]/d[M_1 + M_2]$) are

obtained (green lines Figure 6.4(f) ; cumulative copolymer composition fractions can be found in Figure D.11. of the Appendix).

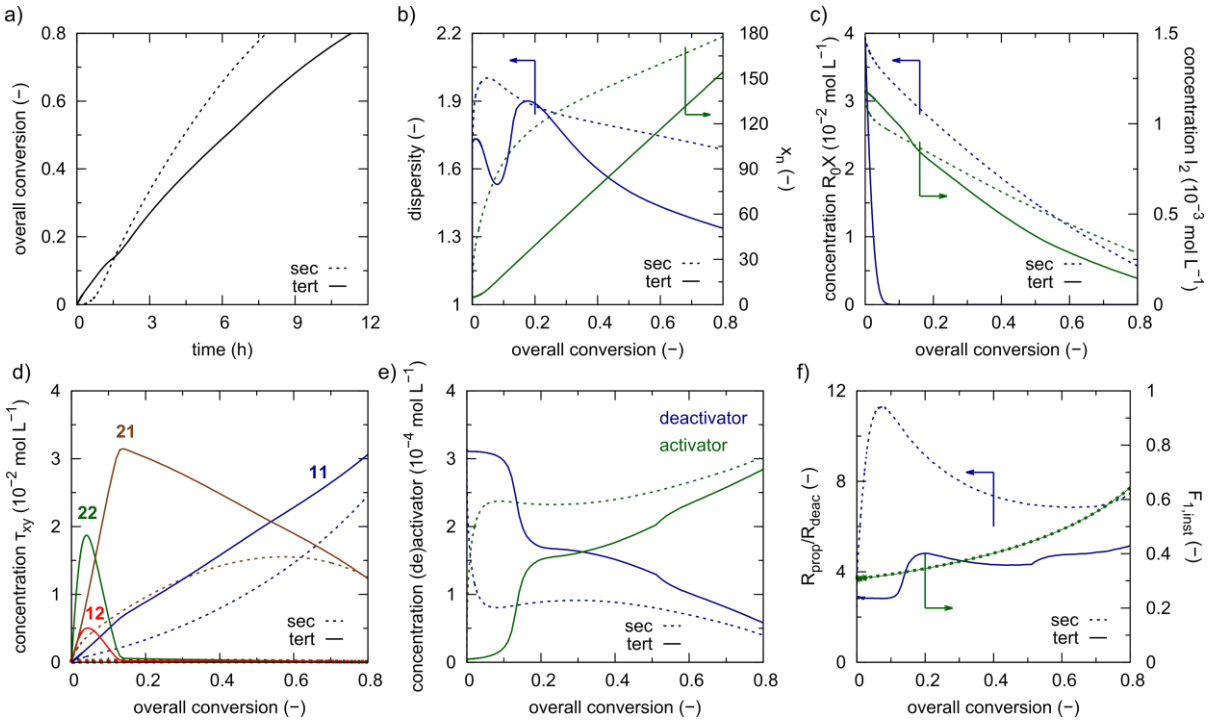

Figure 6.4. *(a) Overall monomer conversion as a function of time, (b) dispersity (Đ, blue) and number averaged chain length (x_n, green), (c) concentration of R_0X (blue) and I_2 (green), (d) concentration of dormant macrospecies (τ_{11}, blue; τ_{22}, green; τ_{12}, red; τ_{21}, brown; xy penultimate units), (e) concentration of deactivator (blue) and activator (green), (f) ratio of propagation to deactivation and instantaneous copolymer composition ($F_{1,inst}$, green) as a function of the overall monomer conversion for batch ICAR ATRP of n-butyl acrylate (M_1) and methyl methacrylate (M_2) at 363K ($[M]_0$:$[R_0X]_0$:$[I_2]_0$ = 200:1:0.03; $[M_1]_0 = [M_2]_0$; initial Cu(II) ppm level = 40 ppm) using a secondary ($k_{a0}^{chem} = k_{a11}^{chem}$; dotted lines) and a tertiary ($k_{a0}^{chem} = k_{a22}^{chem}$; full lines) ATRP initiator (white crosses/yellow spheres in Figure 6.3); parameters: Table D.1 (Appendix).*

Furthermore, the dispersity and x_n profiles (Figure 6.4(b), blue and green lines) indicate a very different degree of microstructural control depending on the R_0X type. The secondary R_0X displays a strong non-linear evolution of the x_n profile and leads to high dispersities (> 1.7)

throughout the whole ICAR ATRP, indicating a lack of control over the chain growth and suggesting a slow ATRP initiation, in agreement with experimental findings of Ziegler *et al.*[74] In contrast, the tertiary R_0X displays an almost perfect linear evolution of x_n (Figure 6.4(b)) and a relatively low final dispersity (*ca*. 1.3), indicative of a much better ATRP initiation. Indeed, Figure 6.4(c) (green lines) shows that on an X_m basis the tertiary ATRP initiation (full line) is much more effective, highlighting a better control over chain length.[19, 75]

A closer inspection of the dispersity profile in Figure 6.4(b) for the tertiary R_0X shows the presence of two local maxima, one at a very low X_m of *ca.* 0.05 and one at a low X_m of *ca.* 0.2. In contrast, for the secondary R_0X only one maximum can be identified at a very low X_m of *ca.* 0.06. The existence of two maxima for the tertiary ATRP initiator can be related to a "two-stage initiation", as can be deduced from an analysis of the dormant polymer concentrations in Figure 6.4(d) (full lines). At the start of the ICAR ATRP, tertiary R_0X consumption by activator is dominant (first initiation stage), as these dormant R_0X species possess the highest concentration and ATRP activation reactivity. The generated tertiary R_0 radicals are transformed into macroradicals (Figure D.6 in Appendix) but are quickly deactivated into novel dormant species, *i.e.* *RX*, with still a too low concentration and/or too low ATRP activation reactivity to significantly participate in further activation-growth-deactivation cycles. In particular, at very low X_m, increases in concentrations for the dormant macrospecies with a terminal M_2 (MMA) unit can be seen in Figure 6.4(d) (full green and red line). Once the tertiary R_0X species are depleted (X_m of *ca*. 0.05; Figure 6.4(c); blue full line) these terminal M_2 dormant macrospecies, which thus no longer suffer from competition for ATRP activation and which possess a high ATRP activation reactivity, behave as macroinitiator species. The latter phenomenon explains the second initiation stage and thus the second maximum in the dispersity profile in Figure 6.4(b). In contrast, for the

secondary R_0X with a much lower k_{a0}^{chem} a much slower consumption of the R_0X species takes place (Figure 6.4(c); dashed blue line) and the M_2 terminal dormant macrospecies, possessing high ATRP activation reactivities, can be easily consumed at low X_m (no maxima in Figure 6.4(d)), explaining the absence of the second initiation stage and dispersity maximum. Note that at high X_m, the differences between both ATRP initiator types become less relevant, which can be related to the diminished effect of the initiation process on the copolymerization kinetics.

Figure 6.4(e) shows that the first initiation stage with a tertiary R_0X is occurring with a high deactivator concentration very close to the initial one. This implies that the (re)generated amount of activator is directly employed for R_0X activation, consistent with the appearance of the initial maxima in Figure 6.4(d) and resulting in a very low ratio of the propagation to ATRP deactivation rate (R_{prop} to R_{deac}; Figure 6.4(f); blue full line). After the first initiation stage, the activation process becomes slower and the deactivator concentration decreases significantly, as on the one hand the I_2 concentration (Figure 4(c)) is still high enough to provide for activator regeneration and on the other hand the monomer mixture becomes richer in *n*BuA (M_1), leading to a shift of the (de)activation equilibrium to the dormant side. As can be derived from Table S.3 in the Appendix, the activation/deactivation equilibrium coefficient for macrospecies with two M_1 units near the radical chain end is lower than the one with a penultimate M_2 and a terminal M_1 unit. Since dormant "11" macrospecies are dominant over dormant "12" macrospecies at higher X_m (Figure 4(d)) the system becomes therefore less prone to ATRP activation as these species possess a much lower k_a^{chem} contributing to the aforementioned buildup of activator. For the secondary R_0X, at low X_m, the activator concentration is already high as secondary ATRP initiation can only commence with a much stronger initial activator generation. Consequently, the actual chain-growth takes place with lower deactivator amounts and thus a higher ratio of R_{prop} to

R_{deac} compared to the tertiary case (Figure 6.4(f)). In other words, the degree of microstructural control can be easily linked to the evolution of the ratio of R_{prop} to R_{deac} with lower values being beneficial, in agreement with earlier work,[42, 76] and as also further illustrated in Figure D.4 in Appendix, selecting some representative additional batch reactions conditions in Figure D.2. (all tertiary R_0X).

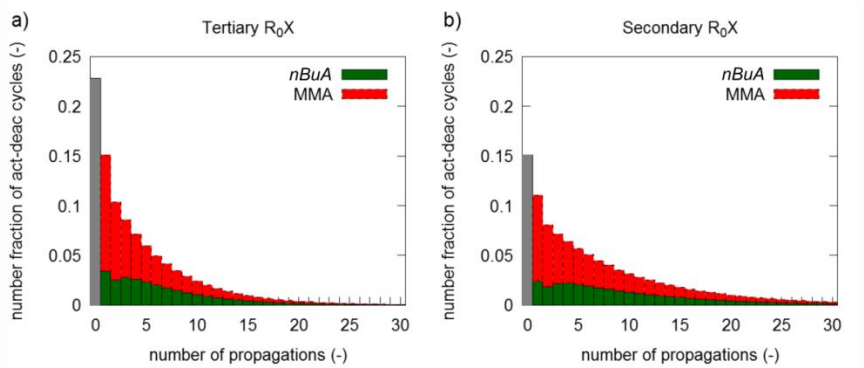

Figure 6.5. *Number fraction of activation-deactivation cycles as a function of number of propagations with relative contribution of nBuA (M_1; green) and MMA (M_2; red); batch ICAR ATRP at 363 K ($[M]_0$:$[R_0X]_0$:$[I_2]_0$ = 200:1:0.03; $[M_1]_0 = [M_2]_0$; initial Cu(II) ppm level = 40 ppm) using a tertiary (a) and secondary (b) ATRP initiator (R_0X) (yellow spheres/white crosses in Figure 6.3). during X_M = [0.40-0.45]; relative contribution allows to calculate the absolute amounts of both comonomers for a given number of propagations; parameters: Table D.1 (Appendix); grey bar represent subsequent activation-deactivation steps.*

Finally, as explained above, the *k*MC model allows to track all monomer sequences of individual copolymer chains. The results for the secondary and tertiary R_0X at a X_m of 0.8 are shown in Figure 6.6(a)-(b), selecting *ca.* 400 chains out of a representative polymer sample of 150000 chains. For clarity, the chains are ranked from small to large, except the dead polymer chains who are included at the top but again ranked from small to large. In agreement with the discussion of Figure 6.3-5 the copolymer with the tertiary R_0X is better defined. A better transition from MMA

(red) to *n*BuA (green) units can be observed per chain from "left" to "right", which is required for the production of gradient copolymers. Due to slow ATRP initiation with the secondary R_0X (Figure 6.4(c)), the later formed ATRP initiator radicals are created in a more *n*BuA rich feed, and, hence, the associated dormant chains possess a too low amount of initial MMA units, as visible at the bottom of Figure 6.6(b).

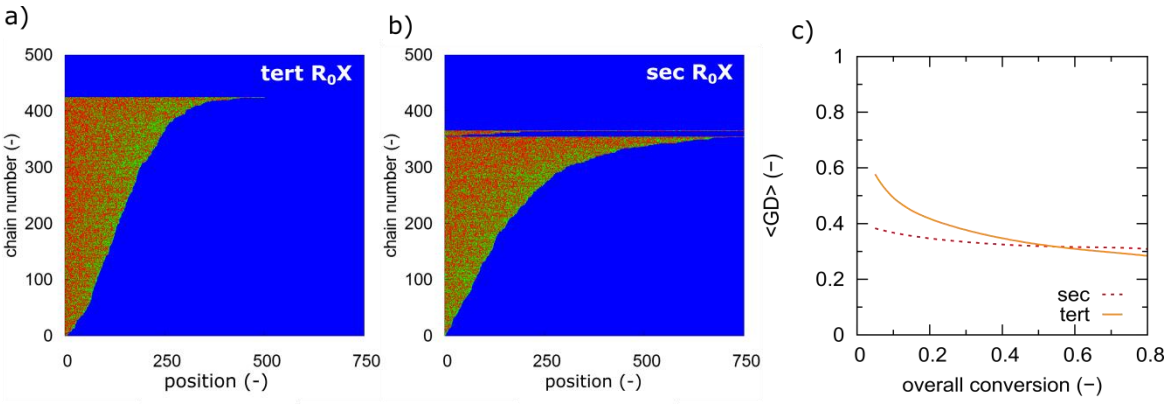

Figure 6.6. *(a-b) Explicit copolymer composition of ca. 400 chains out of a representative polymer sample of 150000 chains at an overall monomer conversion of 0.8 and (c) evolution of gradient quality (<GD>) for batch ICAR ATRP of n-butyl acrylate (M_1; red) and methyl methacrylate (M_2; green) at 363 K ($[M]_0$:$[R_0X]_0$:$[I_2]_0$ = 200:1:0.03; $[M_1]_0 = [M_2]_0$; initial Cu(II) ppm level = 40 ppm), using a tertiary ((a), full orange line in (c)) and secondary ((b), dotted red line in (c)) ATRP initiator (R_0X); parameters: Table D.1 (Appendix).*

The latter is also reflected in the <GD> profile (Figure 6.6(c)), which is more flat for the secondary R_0X (red color, indicating a bad gradient quality). As explained above, previous modeling studies have shown that to ensure an excellent gradient quality steeply decreasing <GD> profiles are needed with final values well below 0.30.[20, 54] Only by using a tertiary R_0X a certain steepness for <GD> can be obtained. However, the final <GD> value is still relatively high (*ca.* 0.30), highlighting an intermediate gradient quality (orange color) under the selected

batch conditions, even with the tertiary R_0X. The latter is consistent with the claim of Chuang *et al.*[77] who indicated a difficult ATRP microstructural control with the selected comonomer pair.

6.3.2 Relevance of PMU effects under batch conditions

As indicated above (*cf.* Table 6.1), for propagation and ATRP (de)activation penultimate rate coefficients are considered . A natural question that arises is the relevance of these PMU effects on the evolution of the ICAR ATRP characteristics from a fundamental point view and thus ignoring the possible usefulness of the less parameterized terminal model in view of basic process design. In this subsection, it is demonstrated that these effects can become highly relevant due to their influence on the polymerization kinetics. The discussion is limited to the tertiary R_0X, which appeared as the most suited ATRP initiator in the previous subsection. Attention is focused on the optimal ICAR ATRP batch conditions, as defined by the yellow spheres in Figure 6.3, again with a final X_m of 0.80.

For the study of the relevance of the PMU effect, a distinction is made between all relevant combinations of reactivity ratio assumptions: (i) a complete penultimate model thus considering a PMU effect for both propagation and ATRP (de)activation; (ii) a model with only a PMU effect for ATRP (de)activation, which is a very hypothetical case; (iii) a model with only a PMU effect for propagation, which is currently the most commonly used model if PMU effects are accounted for in CRP; (iv) a complete terminal model, thus without any PMU effect as mostly applied in current kinetic modeling studies. In what follows, these models are referred to as Model 1-4, respectively.

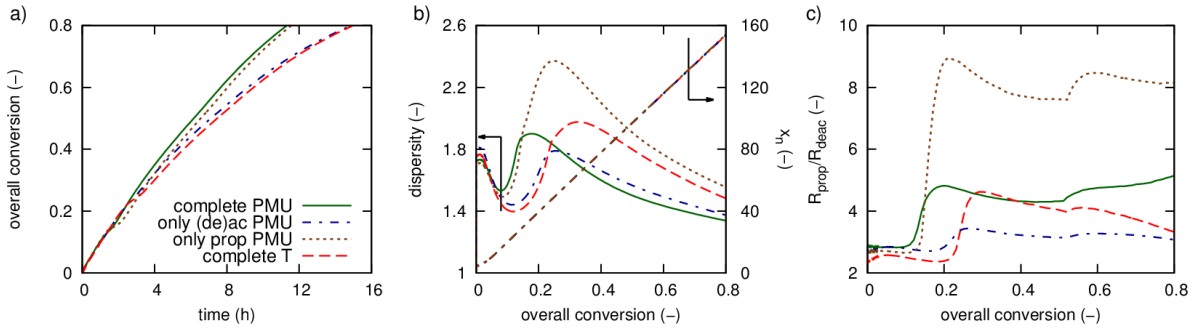

Figure 6.7. *Effect of penultimate unit (PMU) effects on the (a) overall monomer conversion as a function of time, (b) dispersity (left y-axis) and x_n (right y-axis), (c) ratio of propagation rate to deactivation rate as a function of overall conversion for batch ICAR ATRP of n-butyl acrylate (M_1) and methyl methacrylate (M_2) at 363K ($[M]_0$:$[R_0X]_0$:$[I_2]_0$ = 200:1:0.03; $[M_1]_0 = [M_2]_0$; initial Cu(II) ppm level = 40 ppm) using a tertiary ATRP initiator (yellow spheres in Figure 6.3); full green lines: complete penultimate model (propagation and ATRP (de)activation; model 1); dashed-dotted blue lines: only PMU effects on ATRP (de)activation (model 2); dotted brown lines: only PMU effects on propagation (model 3); dashed red lines: complete terminal model (model 4); parameters: Table D.1 (Appendix).*

As can be seen in Figure 6.7(a), the polymerization rate is strongly affected by a PMU for propagation. Similar X_m profiles result with the complete penultimate model (full green line; model 1) and the one with only a PMU effect for propagation (dotted brown line; model 3), whereas significantly slower polymerizations are simulated with a model with only a PMU for ATRP (de)activation (dashed-dotted blue line; model 2) and a terminal model (dashed red line; model 4).

In contrast, the dispersity profile (Figure 6.7(b)) has a more complex interpretation with respect to the relevance of the PMU effect. Initially, all four models give rise to same dispersity change, which corresponds to the dominance of R_0X consumption and the limited chain growth at very low X_m, as explained above (first initiation stage in Figure 6.4). During the second initiation stage, as for the X_m profile (Figure 6.7(a)), PMU effects on propagation are relevant, as witnessed

by the coinciding full green line (complete penultimate; model 1) and dotted brown line (PMU effect for propagation only; model 3) but different lines for the other two models. From intermediate X_m onwards, however, a model with only a PMU effect for propagation is incorrect and clearly the PMU on ATRP (de)activation becomes very relevant (almost coinciding full green line and short dashed blue line; model 1 and 2).

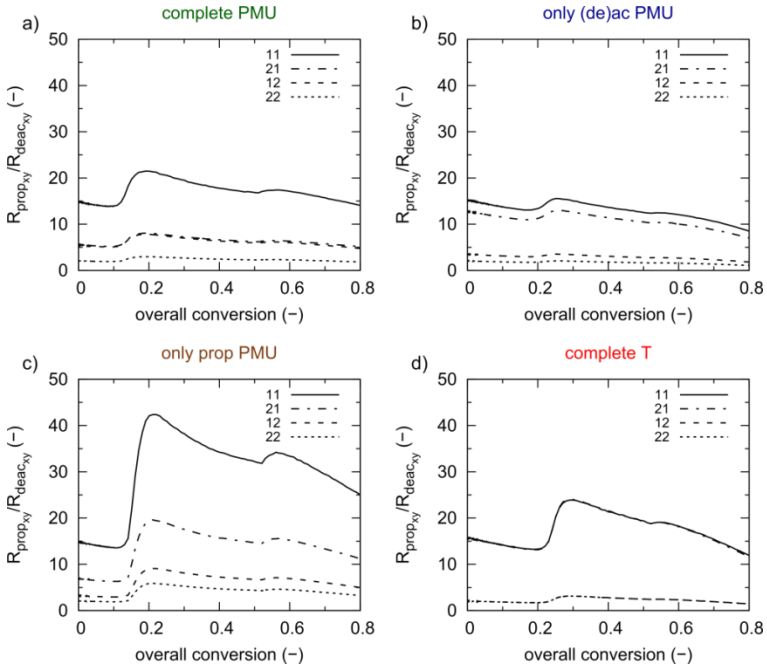

Figure 6.8. *Ratio of propagation rate to deactivation rate for the different macroradicals (ij: penultimate units) full: 11, dash-dot: 21, dashed: 12, dotted: 22 for batch ICAR ATRP of n-butyl acrylate (M_1) and methyl methacrylate (M_2) at 363K ($[M]_0$:$[R_0X]_0$:$[I_2]_0$ = 200:1:0.03; $[M_1]_0$ = $[M_2]_0$; initial Cu(II) ppm level = 40 ppm) using a tertiary ATRP initiator (yellow spheres in Figure 6.3); (a): complete penultimate model (model 1), (b): only PMU effects on ATRP (de)activation (model 2), (c): only PMU effects on propagation (model 3), (d): complete terminal model (model 4); for complete terminal model 4 lines are appearing as it is a simplification of the PMU model, parameters: Table D.1 (Appendix).*

Overall the commonly used terminal model (model 4) results thus in an incorrect increase of the polymerization time from 11 to 15 hours with an incorrect increased final dispersity (1.3 vs. 1.5).

An understanding of the trends observed in Figure 6.7(b) is facilitated by an analysis of the ratios of the evolution of the propagation to deactivation rates with the overall monomer conversion. Figure 6.7(c) shows the ratios with the total rates (R_{prop}/R_{deac}) for the 4 rate coefficient models, whereas Figure 6.8(a)-(d) is more detailed with a differentiation for each rate coefficient model according to the 4 individual penultimate ratios ($R_{prop,ij}/R_{deac,ij}$; i,j=1,2). Note that the ratio with the "22" macrospecies is the lowest in Figure 6.8 and thus crucial for the level of microstructural control, in particular at lower X_m as explained above. All profiles in Figure 6.7(c) and Figure 6.8 also reflect the two-stage initiation for a tertiary R_0X (*cf.* Figure 3(f) full blue line). However, the onset of the second-stage and thus the settlement of the main activation-growth-deactivation process occurs at a different X_m, depending on the selected rate coefficient model. The sooner this onset takes place the better the expected microstructural control. Furthermore as explained above, low R_{prop} to R_{deac} values are needed to ensure a good microstructural control.

Inspection of Figure 6.7(c) and Figure 6.8 shows that with the complete penultimate model (model 1) the onset for the second initiation stage is fast and globally low R_{prop} to R_{deac} ratios are obtained, explaining why this model predicts the best microstructural control. In contrast, the model with only a PMU effect for propagation (model 3) predicts a fast onset but is characterized by much too high R_{prop} to R_{deac} ratios, explaining the high dispersities in Figure 6.7(b). The differentiation between model 1 and 3 can be related to the drop in k_{a21}^{chem} for the latter model (Table S.3 in the Appendix; factor 5 as terminal model for ATRP activation). As this rate coefficient does not play a major role in the initiation mechanism, no noticeable effect is initially present. However, once the initiation stage is over the smaller k_{a21}^{chem} value in model 3 leads to a loss in control. A smaller k_{a21}^{chem} leads to a larger concentration for dormant "21" macrospecies (Figure D.7 in Appendix) and thus a lower deactivator concentration (Figure D.8 in Appendix).

This in turn leads to a much lower deactivation rate of terminal M_2 macroradicals, which directly influences the microstructural control being the largest contributor as explained above. Hence, a higher ratio of the propagation to the deactivation rate results, explaining the much higher dispersity for model 3 compared to model 1. As can be seen in Figure 6.7(c), the other two models (both no PMU for propagation; model 2 and 4) have low R_{prop} to R_{deac} ratios but their onsets are rather late, resulting in a reasonable microstructural control at high X_m but still less than with the complete PMU model. These slower onsets of the second initiation stage can be understood by comparing the propagation rate coefficients. The terminal propagation model results in a more pronounced build-up of dormant "12" macrospecies at the early stages of the ICAR ATRP, which can be mainly attributed to the much larger $k_{p,212}^{chem}$ rate coefficient for the terminal model (Table S.3 in Appendix). As such, during the second initiation stage, a larger amount of these dormant macrospecies needs to be "initiated", *i.e.* activated, thus delaying the onset of the actual activation-growth-deactivation process.

Finally, Figure 6.9 shows the evolutions of the <GD> profile for the 4 rate coefficient models (model 1-4) with the complete explicit microstructures at X_m=0.80 given in Figure D.9 in the Appendix. It follows that these profiles all possess a similar steepness corresponding to an intermediate gradient quality (*cf.* the discussion of Figure 6.6(c); full orange line). Closer inspection shows that the complete penultimate model predicts somewhat lower <GD> values at high X_m. Since the *in silico* <GD> property is rather sensitive to changes in monomer sequences, this implies that the best gradient quality is simulated with this model (model 1). Hence, even with the complete penultimate model in the present work with rather implicit penultimate effects (Table 6.1; similar r values; different s values), and thus coinciding $F_{1,inst}$ profiles as a function of conversion (Figure 6.7(c); cumulative copolymer composition fractions can be found in Figure

D.11. of the Appendix), changes for the microstructural control at a given overall monomer conversion can be observed. It can be expected that for a comonomer pair displaying stronger explicit PMU effects, an even more pronounced impact exists, as in that case also the instantaneous copolymer compositions as predicted by a terminal and penultimate model strongly deviate. Hence, penultimate models are not only needed to accurately describe time dependencies but also the microstructural control as a function of the overall monomer conversion. It should however be noted that the latter statement can only be fully confirmed in case in the future more reliable reactivity ratios for general comonomer pairs become available.

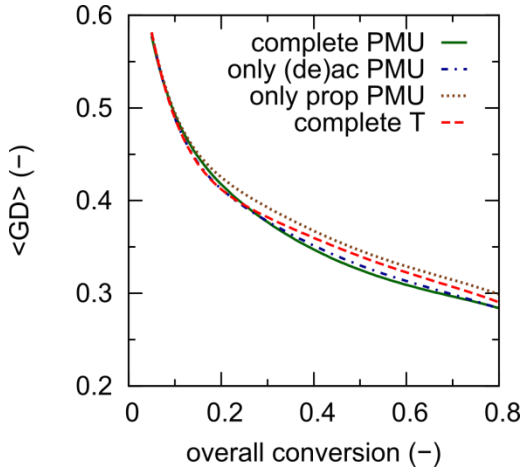

Figure 6.9. *Effect of penultimate unit (PMU) effects on the gradient quality (<GD>) at an overall monomer conversion of 0.8 for batch ICAR ATRP of n-butyl acrylate (M_1) and methyl methacrylate (M_2) at 363K ($[M]_0$:$[R_0X]_0$:$[I_2]_0$ = 200:1:0.03; $[M_1]_0$ = $[M_2]_0$; initial Cu(II) ppm level = 40 ppm) using a tertiary ATRP initiator (yellow spheres in Figure 6.3); full green lines: complete penultimate model (model 1); dashed-dotted blue lines: only PMU effects on ATRP (de)activation (model 2); dotted brown lines: only PMU effects on propagation (model 3); dashed red lines: complete terminal model (model 4); parameters: Table D.1 (Appendix).*

6.3.3 Relevance of temperature effects

In this subsection, the influence of the reaction temperature on the batch ICAR ATRP characteristics is investigated. In Figure 6.10(a)-(b), the results are shown for the evolution of X_m and the control over chain length applying a complete penultimate model at three temperatures, *i.e.* 343, 353, and 363 K, and keeping the other initial concentrations as specified before. It follows that a lower temperature results in a longer reaction time and a lower dispersity. This can be attributed to a lower R_{prop}/R_{deac} (Figure 6.10(c); blue lines), reminding that ATRP deactivation can be seen as non-activated (Table S.1 in the Appendix).

Making the trade-off between a sufficiently high polymerization rate and control over chain length, it follows that a high temperature is needed based on the literature parameters employed in the present work. By decreasing the temperature with only 20 K a too slow ICAR ATRP results and the gain in microstructural control cannot compensate this fully. The latter is partially a consequence of the still similar $F_{1,inst}$ values upon such a small temperature change (Figure 6.10(c); green lines; cumulative copolymer composition fractions can be found in Figure D.11. of the Appendix). Furthermore, the gradient quality (see Figure D.10(a) in Appendix) is influenced only to a limited extent by changing the reaction temperature.

It should be further stressed that it is crucial to account for the temperature dependency of the reactivity ratios. Typically in literature reactivity ratios determined at one temperature are input values in kinetic models applied at different temperatures. To illustrate the approximate nature of such implementation Figure 6.10(d-e) compares the simulation results at the reference temperature of 363 K (full lines) with those of simulations substituting the correct reactivity ratios by those at 293 K (dashed lines). As can be seen from the X_m profiles, the incorrect use of the reactivity ratios at 293 K leads to a slower polymerization (11 vs. 13 hours) and lower

dispersities (Figure 6.10(e)). The changes in propagation reactivity ratios are now also large enough to result in different $F_{1,inst}$ profiles (Figure 6.10(f) ; cumulative copolymer composition fractions can be found in Figure D.11. of the Appendix) and thus different instantaneous copolymer microstructures. This is further illustrated in Figure D.10(b) of the Appendix, which shows significant changes in the obtained gradient qualities for both cases.

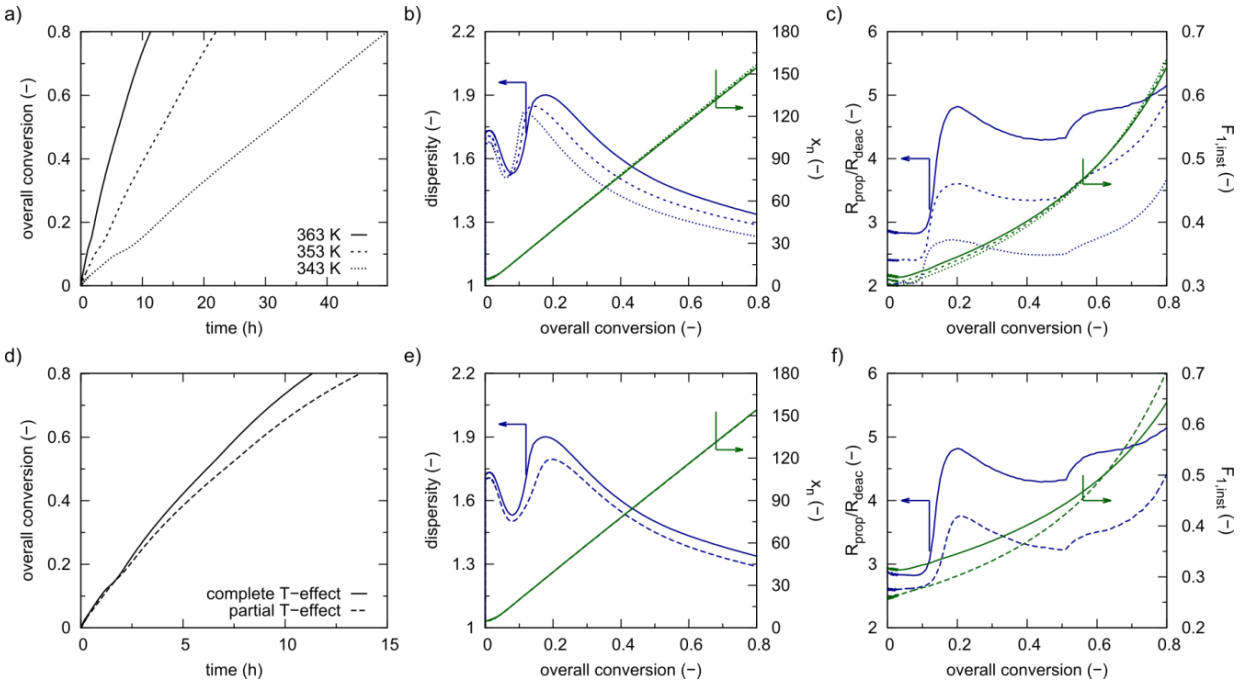

Figure 6.10. *Influence of temperature on (a and d) overall monomer conversion as a function of time, (b and e) dispersity (dotted lines) and x_n (full lines), (c and f) ratio of propagation rate to deactivation rate as a function of overall monomer conversion for batch ICAR ATRP of n-butyl acrylate (M_1) and methyl methacrylate (M_2) ($[M]_0$:$[R_0X]_0$:$[I_2]_0$ = 200:1:0.03; $[M_1]_0 = [M_2]_0$; Cu(II) ppm level = 40 ppm) using a tertiary initiator (Figure 6.3 yellow spheres at 363 K); (a-c) full PMU model at 363 K (full lines), 353 K (dashed lines), 343 K (dotted lines), (d-f) full PMU model at 363K using correct reactivity ratios at 363 K (full lines), complete PMU model at 363 K but using the typical literature values for the reactivity ratios at 293 K; parameters: Table D.1 (Appendix).*

6.3.4 Effect of operation mode: batch vs. fed-batch operation

Under the batch conditions explored before, $F_{1,inst}$ is not varying linearly with X_m (*e.g.* Figure 6.4(f) and Figure 6.7(c)) and, hence, it is inherently difficult to obtain a high (linear) gradient quality. The naturally occurring gradient under batch conditions with only an increase of $F_{1,inst}$ at higher X_m is insufficient and thus fed-batch monomer feeding programs need to be applied in order to force a well-defined gradient into the copolymer product.[78-82] In the case of ICAR ATRP, the situation is complicated due to the complex interplay between ATRP and conventional initiation, ATRP (de)activation, and propagation. As such not only the comonomers have to be gradually added but also the conventional radical initiator and ATRP deactivator in order to assure a good microstructural control. For the selected comonomer pair in the present work, this multicomponent fed-batch strategy was for instance illustrated by D'hooge *et al.*[54] using for simplicity a terminal model. A key question that arises is whether the effectiveness of the fed-batch multicomponent strategy strongly depends on the use of a terminal or penultimate model.

Figure 6.11 compares the key results of a terminal (dashed lines) and complete penultimate (full lines) model under fed-batch conditions, using a similar feeding strategy as introduced by D'hooge *et al.*[54] The ICAR ATRP is started with the total R_0X batch amount and 5 mol% of the batch amount of one of the monomers (M_1=*n*BuA), employing the same initial deactivator and I_2 concentrations as for the batch reference case. At an *in situ* monomer conversion of 0.8 minute amounts of both comonomers are each time added in pulsed manner in order to realize a linear relation between $F_{1,inst}$ and X_m, which is defined with respect to the batch amount (Figure 6.11(f); green lines) whilst at the same time adding deactivator and I_2 in the same ratio as initially for the batch reference case. Note that this relation for $F_{1,inst}$ is a linear decrease (except at very high X_m) as a fed-batch strategy against the natural gradient (MMA to *n*BuA) is selected. As illustrated in

Table S.5 in the Appendix, other analogous starting procedures lead to unrealisticly high polymerization times or a loss of microstructural control, explaining the aforementioned multi-component fed-batch strategy.

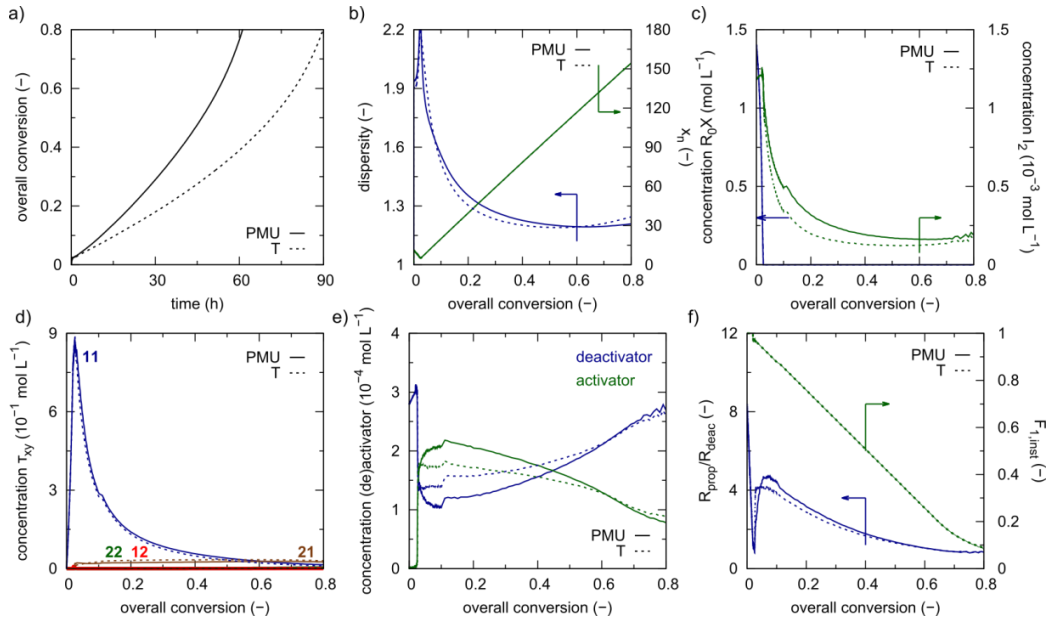

Figure 6.11. *(a) Overall monomer conversion (defined with respect to the batch amount) as a function of time, (b) dispersity (Đ, blue) and number averaged chain length (x_n, green), (c) concentration of R_0X (blue) and I_2 (green), (d) concentration of dormant macrospecies (τ_{11}, blue; τ_{22}, green; τ_{12}, red; τ_{21}, brown; xy penultimate units), (e) concentration of deactivator (blue) and activator (green), (f) ratio of propagation to deactivation and instantaneous copolymer composition ($F_{1,inst}$, green) as a function of the overall monomer conversion for ICAR ATRP of n-butyl acrylate (M_1) and methyl methacrylate (M_2) at 363K using a fed-batch program with initially all batch R_0X, 5 mol% of the batch nBuA amount and I_2 and Cu(II) in the same concentration as the batch case; addition of both monomers at an in situ monomer conversion of 0.80 so that a linear decrease of $F_{1,inst}$ is obtained as a function of the overall monomer conversion with I_2 and Cu(II) co-added in the feed with the same concentration as the initial batch case; batch reference conditions: $[M]_0:[R_0X]_0:[I_2]_0$ = 200:1:0.03; $[M_1]_0=[M_2]_0$; initial Cu(II) ppm level = 40 ppm) for a full PMU (full lines) and terminal (dashed lines) model; parameters: Table D.1 (Appendix).*

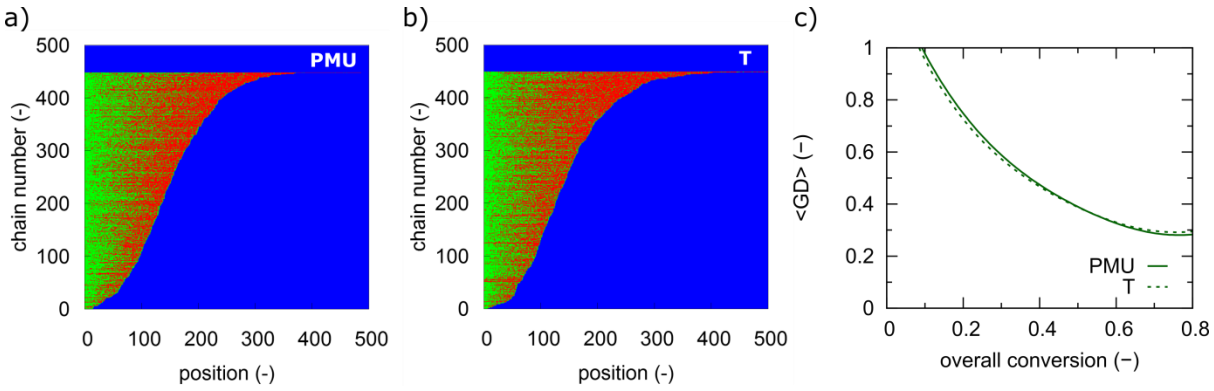

Figure 6.12. *(a-b) Explicit copolymer composition of ca. 400 chains out of a representative polymer sample of 150000 chains at an overall monomer conversion (with respect to the batch amount) of 0.8 with (a) the complete PMU model (model 1), (b) the complete T model (model 4), and (c) gradient quality as a function of the overall monomer conversion; corresponding to Figure 6.11; parameters: Table D.1 (Appendix).*

It follows from Figure 6.11(a) that with both models the fed-batch approach is very slow as compared to the corresponding batch cases (Figure 6.7(a); green complete (penultimate) and red dashed (terminal) line). High *in situ* monomer conversions are always requested under fed-batch conditions which require high reaction times between new monomer additions. On the other hand, the dispersities are lower and display a different steepness as a function of conversion (Figure 6.11(b) vs. Figure 6.7(b)), which can be related to the faster R_0X consumption on a X_m basis (*e.g.* Figure 6.11(c) vs. Figure 6.4(c); penultimate model) and the lower R_{prop}/R_{deac} values (Figure 6.11(f) vs. Figure 6.7(c)) compared to the batch counter case. Further inspection allows to conclude that in agreement with the batch case the terminal model cannot be used, as it reflects the wrong time dependencies (Figure 11(a)). However, on a X_m basis similar results are obtained for both models as witnessed by the similar dependencies for the dispersity (Figure 6.11(b)), dormant species concentrations (Figure 6.11(d)), Cu(II) concentrations (Figure 6.11(e)), and R_{prop}/R_{deac} (Figure 6.11(f)) as a function of X_m.

The latter is also reflected in the plots for the explicit microstructure of the gradient copolymer products at a fixed X_m of 0.80, as shown in Figure 6.12(a)-(b). Clearly much better gradients compared to the batch reference cases are obtained (Figure 6.6(a-b)) but only a limited differentiation can be made between the terminal and penultimate model. Similar conclusions can be formulated for the <GD> evolution as function of X_m in Figure 6.12(c). Compared to the batch cases (Figure 9; full green line (penultimate) and red dashed line (terminal)), a much steeper decline as a function of X_m is obtained, indicative of a higher gradient quality. On the other hand, the differences between both models are very limited.

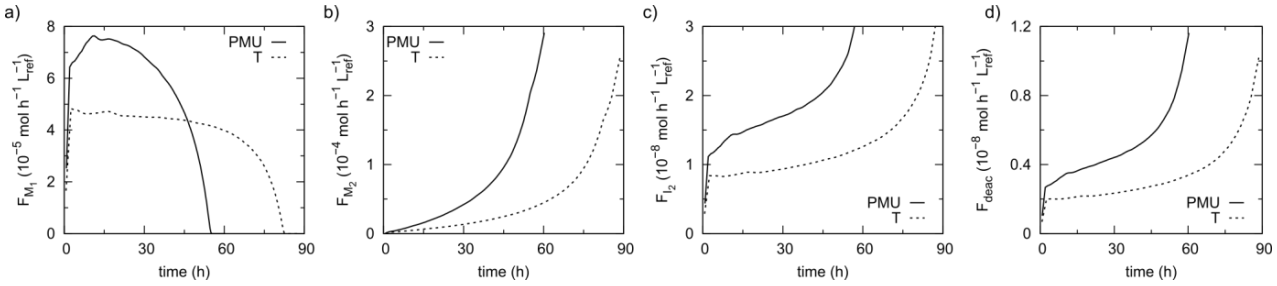

Figure 6.13. *Feeding rates of (a) n-butyl acrylate (M_1), (b) methyl methacrylate (M_2), (c) conventional radical initiation (I_2), and (d) ATRP deactivator corresponding to Figure 6.11; parameters: Table D.1 (Appendix).*

It should however be emphasized that an evaluation of the ICAR ATRP process on an X_m basis is purely theoretical and in practice of less added value. In practice, feeding rates need to be defined on a time basis, as for instance shown in Figure 6.13 for the studied fed-batch strategies in Figure 6.11 (full lines: penultimate model; dashed lines: terminal model). Clearly different time dependencies are observed with both models under fed-batch conditions. A terminal model predicts too slow addition rates, highlighting that upon the existence of a PMU effect the correct fed-batch feeding rates cannot be approximated by the ones predicted via the commonly applied

terminal model. It is thus clear that penultimate models are highly recommended to guarantee a correct copolymer production.

6.4 Conclusions

Using matrix based kinetic Monte Carlo (*k*MC) simulations and literature kinetic parameters, it has been demonstrated that ICAR ATRP of *n*-butyl acrylate and methyl methacrylate cannot be accurately described and designed using the conventional terminal model but instead a penultimate model should be used for both the calculation of the propagation and ATRP (de)activation rate coefficients.

Grid *k*MC simulations, covering both a variation of the batch reaction conditions and the conventional radical and ATRP initiator type, are of high added value to fully map the potential of the ICAR ATRP technique and to identify a suitable reaction system capable of a fast polymerization and acceptable degree of microstructural control. The nature of the ATRP initiator was shown to have a profound effect on the main ICAR ATRP characteristics. A secondary ATRP initiator leads to a slow initiation as a function of the overall monomer conversion, deteriorating the microstructural control. A tertiary ATRP initiator resolves this issue at the cost of an increase of the polymerization time. Due to the penultimate nature of the polymerization process the relative contributions of the dormant species types is different under batch conditions, with even a two-stage initiation involving a first disappearance of the tertiary ATRP initiator and a second disappearance of MMA terminal dormant oligomeric species. Furthermore, intermediate Cu ppm levels and initial molar ratios of monomer to ATRP initiator are beneficial and the optimal polymerization temperature should be as high as 363 K. Under such premises, the aforementioned two-stage initiation is sufficiently fast and the ratio of the propagation rate to the

ATRP deactivation rate (R_{prop}/R_{deac}) is sufficiently low. Under these optimized batch conditions only an intermediate gradient quality is obtained, as deducible upon a visual inspection of the explicit polymer microstructure of the individual chains and as reflected in the non-steep <GD> profile.

Upon a comparison of the batch simulations accounting for PMU effects and those using a terminal model it becomes clear that both PMU effects for propagation and ATRP (de)activation are crucial. The former are more relevant at lower overall monomer conversions and the latter at higher. The degree of microstructural control could again be linked to the efficiency of the two-stage initiation and R_{prop}/R_{deac}. Notably a terminal model predicts a too slow polymerization process and too low microstructural control. The *k*MC model has also been successfully applied to demonstrate that the temperature dependency of the penultimate reactivity ratios needs to be taken into account. It is thus not afforded to plug in fixed values as a determined at room temperature, as is typically done in kinetic studies on copolymerization, is to be avoided. The instantaneous copolymer compositions deviate strongly, resulting in different individual monomer sequences and <GD> values.

Finally, it has been demonstrated that multicomponent fed-batch strategies allow to increase the gradient quality. In particular a much steeper <GD> profile is obtained, although accompanied by a strong increase of the reaction time. In agreement with the batch simulation results, a terminal model fails in the identification of the most appropriate feeding rates as a function of the reaction time. Too low addition rates are predicted, resulting in an incorrect model-based design.

Overall the present work suggests that future kinetic copolymerization modeling studies should evaluate whether penultimate rate coefficients are needed. As a corollary, attention should be paid to the determination of such rate coefficients in order to improve the fundamental understanding

of radical polymerization processes in general and to fully develop the potential of RDRP techniques in particular.

References

1. Asua, J., *Polymer Reaction Engineering*. Wiley: 2008.

2. Nesvadba, P., Radical Polymerization in Industry. In *Encyclopedia of Radicals in Chemistry, Biology and Materials*, John Wiley & Sons, Ltd: 2012.

3. Flory, P., *Principles of Polymer Chemistry*. 1953.

4. Van Steenberge, P. H. M.; D'hooge, D. R.; Reyniers, M. F.; Marin, G. B. Improved kinetic Monte Carlo simulation of chemical composition-chain length distributions in polymerization processes. *Chem. Eng. Sci.* **2014,** 110, 185-199.

5. D'hooge, D. R.; Van Steenberge, P. H. M.; Reyniers, M.-F.; Marin, G. B. The strength of multi-scale modeling to unveil the complexity of radical polymerization. *Progress in Polymer Science* **2016,** 58, 59-89.

6. Montaudo, M. S. Determination of the compositional distribution and compositional drift in styrene/maleic anhydride copolymers. *Macromolecules* **2001,** 34, (9), 2792-2797.

7. Rudin, A.; Choi, P., Chapter 9 - Copolymerization. In *The Elements of Polymer Science & Engineering (Third Edition)*, Academic Press: Boston, 2013; pp 391-425.

8. Hamielec, A. E.; MacGregor, J. F.; Penlidis, A. Multicomponent free-radical polymerization in batch, semi- batch and continuous reactors. *Makromolekulare Chemie. Macromolecular Symposia* **1987,** 10-11, (1), 521-570.

9. Dubé, M. A.; Soares, J. B. P.; Penlidis, A.; Hamielec, A. E. Mathematical Modeling of Multicomponent Chain-Growth Polymerizations in Batch, Semibatch, and Continuous Reactors: A Review. *Industrial & Engineering Chemistry Research* **1997,** 36, (4), 966-1015.

10. D'hooge, D. R.; Van Steenberge, P. H. M.; Reyniers, M. F.; Marin, G. B., Modeling of Monomer Sequences in Chain-Growth Copolymerization. In *Reference Module in Chemistry, Molecular Sciences and Chemical Engineering*, Elsevier: 2016.

11. Fujisawa, T.; Penlidis, A. Copolymer Composition Control Policies: Characteristics and Applications. *Journal of Macromolecular Science, Part A* **2008,** 45, (2), 115-132.

12. Braunecker, W. A.; Matyjaszewski, K. Controlled/living radical polymerization: Features, developments, and perspectives. *Prog. Polym. Sci.* **2007,** 32, (1), 93-146.

13. Nicolas, J.; Guillaneuf, Y.; Lefay, C.; Bertin, D.; Gigmes, D.; Charleux, B. Nitroxide-mediated polymerization. *Progress in Polymer Science* **2013,** 38, (1), 63-235.

14. Wang, J. S.; Matyjaszewski, K. Controlled living radical polymerization - atom-transfer radical polymerization in the presence of transition-metal complexes. *J. Am. Chem. Soc.* **1995,** 117, (20), 5614-5615.

15. Zapata-González, I.; Hutchinson, R. A.; Payne, K. A.; Saldívar-Guerra, E. Mathematical modeling of the full molecular weight distribution in ATRP techniques. *AIChE Journal* **2016,** 62, (8), 2762-2777.

16. Guo, J.-K.; Zhou, Y.-N.; Luo, Z.-H. Kinetic insight into electrochemically mediated ATRP gained through modeling. *AIChE Journal* **2015,** 61, (12), 4347-4357.

17. Matyjaszewski, K.; Xia, J. H. Atom transfer radical polymerization. *Chem. Rev.* **2001,** 101, (9), 2921-2990.

18. Kamigaito, M.; Ando, T.; Sawamoto, M. Metal-catalyzed living radical polymerization. *Chem. Rev.* **2001,** 101, (12), 3689-3745.

19. Bentein, L.; D'hooge, D. R.; Reyniers, M. F.; Marin, G. B. Kinetic modeling of miniemulsion nitroxide mediated polymerization of styrene: Effect of particle diameter and nitroxide partitioning up to high conversion. *Polymer* **2012,** 53, (3), 681-693.

20. Van Steenberge, P. H. M.; D'hooge, D. R.; Wang, Y.; Zhong, M. J.; Reyniers, M. F.; Konkolewicz, D.; Matyjaszewski, K.; Marin, G. B. Linear Gradient Quality of ATRP Copolymers. *Macromolecules* **2012,** 45, (21), 8519-8531.

21. Barner-Kowollik, C.; Buback, M.; Charleux, B.; Coote, M. L.; Drache, M.; Fukuda, T.; Goto, A.; Klumperman, B.; Lowe, A. B.; McLeary, J. B.; Moad, G.; Monteiro, M. J.; Sanderson, R. D.; Tonge, M. P.; Vana, P. Mechanism and kinetics of dithiobenzoate-mediated RAFT polymerization. I. The current situation. *Journal of Polymer Science Part A: Polymer Chemistry* **2006,** 44, (20), 5809-5831.

22. De Rybel, N.; Van Steenberge, P. H. M.; Reyniers, M.-F.; Barner-Kowollik, C.; D'hooge, D. R.; Marin, G. B. An Update on the Pivotal Role of Kinetic Modeling for the Mechanistic Understanding and Design of Bulk and Solution RAFT Polymerization. *Macromol. Theory Simul.* **2016**, n/a-n/a.

23. Matyjaszewski, K.; Jakubowski, W.; Min, K.; Tang, W.; Huang, J. Y.; Braunecker, W. A.; Tsarevsky, N. V. Diminishing catalyst concentration in atom transfer radical polymerization with reducing agents. *Proc. Natl. Acad. Sci. U. S. A.* **2006,** 103, (42), 15309-15314.

24. D'hooge, D. R.; Konkolewicz, D.; Reyniers, M.-F.; Marin, G. B.; Matyjaszewski, K. Kinetic Modeling of ICAR ATRP. *Macromol. Theory Simul.* **2012,** 21, (1), 52-69.

25. Konkolewicz, D.; Magenau, A. J. D.; Averick, S. E.; Simakova, A.; He, H.; Matyjaszewski, K. ICAR ATRP with ppm Cu Catalyst in Water. *Macromolecules* **2012,** 45, (11), 4461-4468.

26. Krys, P.; Schroeder, H.; Buback, J.; Buback, M.; Matyjaszewski, K. The Borderline between Simultaneous Reverse and Normal Initiation and Initiators for Continuous Activator Regeneration ATRP. *Macromolecules* **2016,** 49, (20), 7793-7803.

27. Magenau, A. J. D.; Bortolamei, N.; Frick, E.; Park, S.; Gennaro, A.; Matyjaszewski, K. Investigation of Electrochemically Mediated Atom Transfer Radical Polymerization. *Macromolecules* **2013,** 46, (11), 4346-4353.

28. Konkolewicz, D.; Wang, Y.; Zhong, M. J.; Krys, P.; Isse, A. A.; Gennaro, A.; Matyjaszewski, K. Reversible-Deactivation Radical Polymerization in the Presence of Metallic Copper. A Critical Assessment of the SARA ATRP and SET-LRP Mechanisms. *Macromolecules* **2013,** 46, (22), 8749-8772.

29. Treat, N. J.; Sprafke, H.; Kramer, J. W.; Clark, P. G.; Barton, B. E.; Read de Alaniz, J.; Fors, B. P.; Hawker, C. J. Metal-Free Atom Transfer Radical Polymerization. *J. Am. Chem. Soc.* **2014,** 136, (45), 16096-16101.

30. D'hooge, D. R.; Van Steenberge, P. H. M.; Derboven, P.; Reyniers, M.-F.; Marin, G. B. Model-based design of the polymer microstructure: bridging the gap between polymer chemistry and engineering. *Polymer Chemistry* **2015,** 6, (40), 7081-7096.

31. Mastan, E.; Li, X.; Zhu, S. Modeling and theoretical development in controlled radical polymerization. *Progress in Polymer Science* **2015,** 45, 71-101.

32. Zhou, Y.-N.; Luo, Z.-H. State-of-the-Art and Progress in Method of Moments for the Model-Based Reversible-Deactivation Radical Polymerization. *Macromol. React. Eng.* **2016,** 10, (6), 516-534.

33. Coote, M. L.; Davis, T. P. The mechanism of the propagation step in free-radical copolymerisation. *Progress in Polymer Science* **1999,** 24, (9), 1217-1251.

34. Fukuda, T.; Ma, Y.-D.; Inagaki, H. Free-radical copolymerization, 6. New interpretation for the propagation rate versus composition curve. *Die Makromolekulare Chemie, Rapid Communications* **1987,** 8, (10), 495-499.

35. Fukuda, T.; Ma, Y. D.; Inagaki, H. Free-radical copolymerization. 3. Determination of rate constants of propagation and termination for styrene/methyl methacrylate system. A critical test of terminal-model kinetics. *Macromolecules* **1985,** 18, (1), 17-26.

36. Odian, G., *Principles of Polymerization*. 4th ed.; 2004.

37. Merz, E.; Alfrey, T.; Goldfinger, G. Intramolecular reactions in vinyl polymers as a means of investigation of the propagation step. *Journal of Polymer Science* **1946,** 1, (2), 75-82.

38. Coote, M. L.; Davis, T. P.; Radom, L. Effect of the Penultimate Unit on Radical Stability and Reactivity in Free-Radical Polymerization. *Macromolecules* **1999,** 32, (9), 2935-2940.

39. Coote, M. L.; Davis, T. P.; Radom, L. Conformational Dependence of the Penultimate Unit Effect in Free-Radical Copolymerization. *Macromolecules* **1999,** 32, (16), 5270-5276.

40. Coote, M. L.; Davis, T. P. Copolymerization Propagation Kinetics of Para-Substituted Styrenes: A Critical Test of the Implicit Penultimate Model. *Macromolecules* **1999,** 32, (11), 3626-3636.

41. Klumperman, B. Mechanistic considerations on styrene-maleic anhydride copolymerization reactions. *Polymer Chemistry* **2010,** 1, (5), 558-562.

42. Fierens, S. K.; Telitel, S.; Van Steenberge, P. H. M.; Reyniers, M.-F.; Marin, G. B.; Lutz, J.-F.; D'hooge, D. R. Model-Based Design To Push the Boundaries of Sequence Control. *Macromolecules* **2016,** 49, (24), 9336-9344.

43. Heuts, J. P. A.; Davis, T. P. Atom transfer radical copolymerization kinetics. *Macromol. Rapid Commun.* **1998,** 19, (7), 371-375.

44. Charleux, B.; Nicolas, J.; Guerret, O. Theoretical Expression of the Average Activation−Deactivation Equilibrium Constant in Controlled/Living Free-Radical Copolymerization Operating via Reversible Termination. Application to a Strongly Improved Control in Nitroxide-Mediated Polymerization of Methyl Methacrylate. *Macromolecules* **2005,** 38, (13), 5485-5492.

45. Nanda, A. K.; Matyjaszewski, K. Effect of Penultimate Unit on the Activation Process in ATRP. *Macromolecules* **2003,** 36, (22), 8222-8224.

46. Lin, C. Y.; Coote, M. L.; Petit, A.; Richard, P.; Poli, R.; Matyjaszewski, K. Ab Initio Study of the Penultimate Effect for the ATRP Activation Step Using Propylene, Methyl Acrylate, and Methyl Methacrylate Monomers. *Macromolecules* **2007,** 40, (16), 5985-5994.

47. Noble, B. B.; Coote, M. L. First principles modelling of free-radical polymerisation kinetics. *International Reviews in Physical Chemistry* **2013,** 32, (3), 467-513.

48. Dossi, M.; Moscatelli, D. A QM Approach to the Calculation of Reactivity Ratios in Free-Radical Copolymerization. *Macromol. React. Eng.* **2012,** 6, (2-3), 74-84.

49. Mavroudakis, E.; Cuccato, D.; Moscatelli, D. On the Use of Quantum Chemistry for the Determination of Propagation, Copolymerization, and Secondary Reaction Kinetics in Free Radical Polymerization. *Polymers* **2015,** 7, (9), 1483.

50. Fortunatti, C.; Sarmoria, C.; Brandolin, A.; Asteasuain, M. Theoretical Analysis of Nitroxide-Mediated Copolymerization of Styrene and α-Methyl-Styrene under Different Operating Policies and Reactor Designs. *Macromol. React. Eng.* **2014,** 8, (4), 260-281.

51. Al-Harthi, M.; Soares, J. B. P.; Simon, L. C. Mathematical Modeling of Atom-Transfer Radical Copolymerization. *Macromol. React. Eng.* **2007,** 1, (4), 468-479.

52. Ye, Y.; Schork, F. J. Modeling of Sequence Length and Distribution for the NM-CRP of Styrene and 4-Methylstyrene in Batch and Semi-Batch Reactors. *Macromol. React. Eng.* **2010,** 4, (3-4), 197-209.

53. Wang, R.; Luo, Y.; Li, B.; Sun, X.; Zhu, S. Design and Control of Copolymer Composition Distribution in Living Radical Polymerization Using Semi-Batch Feeding Policies: A Model Simulation. *Macromol. Theory Simul.* **2006,** 15, (4), 356-368.

54. D'hooge, D. R.; Van Steenberge, P. H. M.; Reyniers, M.-F.; Marin, G. B. Fed-Batch Control and Visualization of Monomer Sequences of Individual ICAR ATRP Gradient Copolymer Chains. *Polymers* **2014,** 6, (4), 1074-1095.

55. Demirel Özçam, D.; Teymour, F. Chain-by-Chain Monte Carlo Simulation: A Novel Hybrid Method for Modeling Polymerization. Part I. Linear Controlled Radical Polymerization Systems. *Macromol. React. Eng.* **2016**, n/a-n/a.

56. Regatte, V. R.; Gao, H.; Konstantinov, I. A.; Arturo, S. G.; Broadbelt, L. J. Design of Copolymers Based on Sequence Distribution for a Targeted Molecular Weight and Conversion. *Macromol. Theory Simul.* **2014,** 23, (9), 564-574.

57. Nicolas, J.; Mueller, L.; Dire, C.; Matyjaszewski, K.; Charleux, B. Comprehensive Modeling Study of Nitroxide-Mediated Controlled/Living Radical Copolymerization of Methyl Methacrylate with a Small Amount of Styrene. *Macromolecules* **2009,** 42, (13), 4470-4478.

58. Seeliger, F.; Matyjaszewski, K. Temperature Effect on Activation Rate Constants in ATRP: New Mechanistic Insights into the Activation Process. *Macromolecules* **2009,** 42, (16), 6050-6055.

59. AkzoNobel https://www.akzonobel.com/polymer/our_products/polymerization_initiators/.

60. Yu, X.; Levine, S. E.; Broadbelt, L. J. Kinetic Study of the Copolymerization of Methyl Methacrylate and Methyl Acrylate Using Quantum Chemistry. *Macromolecules* **2008,** 41, (21), 8242-8251.

61. Buback, M.; Kurz, C. H.; Schmaltz, C. Pressure dependence of propagation rate coefficients in free-radical homopolymerizations of methyl acrylate and dodecyl acrylate. *Macromol. Chem. Phys.* **1998,** 199, (8), 1721-1727.

62. Beuermann, S.; Buback, M.; Davis, T. P.; Gilbert, R. G.; Hutchinson, R. A.; Olaj, O. F.; Russell, G. T.; Schweer, J.; van Herk, A. M. Critically evaluated rate coefficients for free-radical polymerization, 2.. Propagation rate coefficients for methyl methacrylate. *Macromol. Chem. Phys.* **1997,** 198, (5), 1545-1560.

63. Roberto, L.-N.; Antonio, F.-T.; Enrique, S.-G. Optimal Operating Policies for the Nitroxide-Mediated Radical Polymerization of Styrene in a Semibatch Reactor. *Industrial & Engineering Chemistry Research* **2006,** 45.

64. Toloza Porras, C.; D'hooge, D. R.; Van Steenberge, P. H. M.; Reyniers, M.-F.; Marin, G. B. A Theoretical Exploration of the Potential of ICAR ATRP for One- and Two-Pot Synthesis of Well-Defined Diblock Copolymers. *Macromol. React. Eng.* **2013,** 7, (7), 311-326.

65. Payne, K. A.; D'hooge, D. R.; van Steenberge, P. H. M.; Reyniers, M. F.; Cunningham, M. F.; Hutchinson, R. A.; Marin, G. B. ARGET ATRP of Butyl Methacrylate: Utilizing Kinetic Modeling To Understand Experimental Trends. *Macromolecules* **2013,** 46, (10), 3828-3840.

66. D'hooge, D. R.; Reyniers, M.-F.; Marin, G. B. The Crucial Role of Diffusional Limitations in Controlled Radical Polymerization. *Macromol. React. Eng.* **2013,** 7, (8), 362-379.

67. Johnston-Hall, G.; Monteiro, M. J. Bimolecular radical termination: New perspectives and insights. *J. Polym. Sci. Pol. Chem.* **2008,** 46, (10), 3155-3173.

68. Barner-Kowollik, C.; Russell, G. T. Chain-length-dependent termination in radical polymerization: Subtle revolution in tackling a long-standing challenge. *Prog. Polym. Sci.* **2009,** 34, (11), 1211-1259.

69. Delgadillo-Velázquez, O.; Vivaldo-Lima, E.; Quintero-Ortega, I. A.; Zhu, S. Effects of diffusion-controlled reactions on atom-transfer radical polymerization. *AIChE Journal* **2002,** 48, (11), 2597-2608.

70. Derboven, P.; D'hooge, D. R.; Reyniers, M.-F.; Marin, G. B.; Barner-Kowollik, C. The Long and the Short of Radical Polymerization. *Macromolecules* **2015,** 48, (3), 492-501.

71. Zhong, M. J.; Matyjaszewski, K. How Fast Can a CRP Be Conducted with Preserved Chain End Functionality? *Macromolecules* **2011,** 44, (8), 2668-2677.

72. Payne, K. A.; Van Steenberge, P. H. M.; D'Hooge, D. R.; Reyniers, M.-F.; Marin, G. B.; Hutchinson, R. A.; Cunningham, M. F. Controlled synthesis of poly[(butyl methacrylate)-co-(butyl acrylate)] via activator regenerated by electron transfer atom transfer radical polymerization: insights and improvement. *Polym. Int.* **2014,** 63, (5), 848-857.

73. Toloza Porras, C.; D'hooge, D. R.; Reyniers, M. F.; Marin, G. B. Computer-Aided Optimization of Conditions for Fast and Controlled ICAR ATRP of n-Butyl Acrylate. *Macromol. Theory Simul.* **2013,** 22, (2), 136-149.

74. Ziegler, M. J.; Matyjaszewski, K. Atom Transfer Radical Copolymerization of Methyl Methacrylate and n-Butyl Acrylate. *Macromolecules* **2001,** 34, (3), 415-424.

75. Bentein, L.; D'hooge, D. R.; Reyniers, M. F.; Marin, G. B. Kinetic Modeling as a Tool to Understand and Improve the Nitroxide Mediated Polymerization of Styrene. *Macromol. Theory Simul.* **2011,** 20, (4), 238-265.

76. Fierens, S. K.; D'hooge, D. R.; Van Steenberge, P. H. M.; Reyniers, M.-F.; Marin, G. B. Exploring the Full Potential of Reversible Deactivation Radical Polymerization Using Pareto-Optimal Fronts. *Polymers* **2015,** 7, (4), 655.

77. Chuang, Y.-M.; Wenn, B.; Gielen, S.; Ethirajan, A.; Junkers, T. Ligand switch in photoinduced copper-mediated polymerization: synthesis of methacrylate-acrylate block copolymers. *Polymer Chemistry* **2015,** 6, (36), 6488-6497.

78. Sun, X.; Luo, Y.; Wang, R.; Li, B.-G.; Liu, B.; Zhu, S. Programmed Synthesis of Copolymer with Controlled Chain Composition Distribution via Semibatch RAFT Copolymerization. *Macromolecules* **2007,** 40, (4), 849-859.

79. Sun, X.; Luo, Y.; Wang, R.; Li, B.-G.; Zhu, S. Semibatch RAFT polymerization for producing ST/BA copolymers with controlled gradient composition profiles. *AIChE Journal* **2008,** 54, (4), 1073-1087.

80. Li, X.; Liang, S.; Wang, W.-J.; Li, B.-G.; Luo, Y.; Zhu, S. Model-Based Production of Polymer Chains Having Precisely Designed End-to-End Gradient Copolymer Composition and Chain Topology

Distributions in Controlled Radical Polymerization, A Review. *Macromol. React. Eng.* **2015,** 9, (5), 409-417.

81. Zhou, Y.-N.; Li, J.-J.; Luo, Z.-H. Synthesis of gradient copolymers with simultaneously tailor-made chain composition distribution and glass transition temperature by semibatch ATRP: From modeling to application. *Journal of Polymer Science Part A: Polymer Chemistry* **2012,** 50, (15), 3052-3066.

82. Zhao, Y.; Luo, Y.-W.; Ye, C.; Li, B.-G.; Zhu, S. Model-based design and synthesis of gradient MMA/tBMA copolymers by computer-programmed semibatch atom transfer radical copolymerization. *Journal of Polymer Science Part A: Polymer Chemistry* **2009,** 47, (1), 69-79.

Chapter 7. A qualitative evaluation of the impact of SG1 disproportionation and the addition of styrene in nitroxide mediated polymerization of methyl methacrylate

Summary

A detailed kinetic study, employing a kinetic Monte Carlo (*k*MC) model, is presented for batch nitroxide mediated polymerization (NMP) of methyl methacrylate (MMA; nitroxide: N-*tert*-butyl-N-[1-diethylphosphono-(2,2-dimethylpropyl)] (SG1)), focusing on the improved quantification of the effect of SG1 disproportionation in the absence and presence of styrene (up to 10 mol%). Arrhenius parameters for this SG1 disproportionation ($A = 1.4\ 10^7$ L mol^{-1} s^{-1}; E_a = 23 kJ mol^{-1}) are reported, based on MMA homopolymerization data accounting for unavoidable temperature variations with increasing reaction time, *i.e.* non-isothermicity. For low targeted chain lengths (TCLs ≤ 300), this non-isothermicity also affects the copolymerization kinetics if a small amount of styrene is added to improve the microstructural control by lowering the average (de)activation equilibrium and the relevance of SG1 disproportionation. Parameter tuning to an extensive set of comonomer conversion, number average chain length and dispersity data indicates a penultimate monomer unit effect for NMP activation ($s_{a2} = k_{a21}/k_{a22}$=6.7; 363 K). To obtain, for a broad range of TCLs (up to 800), a dispersity well below 1.3 an initial styrene mass fraction of *ca.* 10% is required. The *k*MC model allows to visualize the monomer sequences of individual chains and indicates that the dormant macrospecies possess a terminal styrene unit. An interpretation of the comonomer incorporation is further performed by calculating the fractions of activation-growth-deactivation cycles with a given amount of monomer units and the fractions of chains with a given % of styrene units. This work will be submitted in Macromolecules (envisioned)

7.1 Introduction

The advent of reversible deactivation radical polymerization (RDRP) techniques has allowed the polymerization of many monomer families with a level of microstructural control unachievable using conventional free radical polymerization (FRP).[1-7] This microstructural control relates to a low dispersity ($Đ$ < 1.3) and a high end-group functionality (EGF > 0.9). Among the developed RDRP techniques, nitroxide mediated polymerization (NMP) is one of the oldest and most frequently employed,[8-12] along with atom transfer radical polymerization (ATRP),[13-15] single electron transfer – living radical polymerization (SET-LRP),[16, 17] and reversible addition-fragmentation chain transfer (RAFT) polymerization.[18, 19]

The principle of NMP, as illustrated in Figure **7.1**(a) for a copolymerization with the comonomers methyl methacrylate (MMA) and styrene, relies on the reversible deactivation of (macro)radicals into dormant (macro)species (R_iX; $i \geq 0$) by a nitroxide X ($k_{da(0)}$). The latter species, originally (2,2,6,6-tetramethylpiperidin-1-yl)oxyl (TEMPO), is initially released upon the activation of an alkoxyamine initiator (R_0X; k_{a0}) and undergoes accumulation via the so-called persistent radical effect, due to unavoidable termination ($k_{tc/td}$).[20, 21] The dormant macrospecies are temporarily activated (k_a) into macroradicals that can increase ideally their chain length by addition of a limited number of (co)monomer units before being deactivated again into the resulting longer macrospecies. Under well-chosen conditions, the final number average chain length (x_n) is given by the initial molar ratio of monomer to R_0X, which is also known as the targeted chain length (TCL).

The mechanistic simplicity and catalyst-free nature of NMP can be considered as major benefits in comparison with other RDRP techniques. On the other hand, NMP typically suffers from several drawbacks, such as long reaction times (over several hours), high reaction temperatures

(> 100 °C), side-reactions and, probably most importantly, a limited monomer range allowing only sufficient microstructural control for styrenics and acrylates.[8] Part of these disadvantages have been resolved by the development of novel nitroxides and alkoxyamines, which lead to more active NMP systems and are expected to be less prone to side reactions. The most popular and successfully applied second-generation nitroxide is N-*tert*-butyl-N-[1-diethylphosphono-(2,2-dimethylpropyl)] (SG1) with the most commonly associated R_0X being N-(2-methyl-2-propyl)-N-(1-diethylphosphono-2,2-dimethylpropyl)-O-(2-carboxyprop-2-yl) hydroxylamide (BlocBuilder MA or MAMA-SG1; Figure **7.1**(b)).[22, 23]

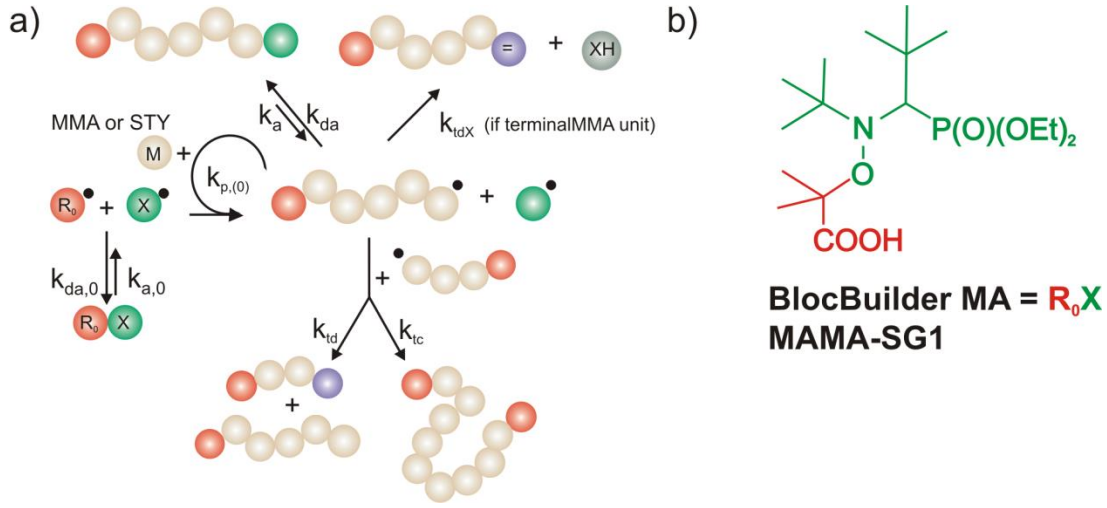

Figure 7.1. *(a) Principle of nitroxide mediated copolymerization (NMP) of methyl methacrylate (MMA) and styrene using an alkoxyamine (R_0X) as initiator; k rate coefficient, neglecting for simplicity the copolymerization aspect; (d)a, p, tdX, td, tc: (de)activation, propagation, termination via disproportionation involving a nitroxide, termination via disproportionation involving macroradicals, termination via recombination involving macroradicals; 0: NMP initiator related; M: monomer, XH: hydroxylamine, = to denote unsaturated double bond; targeted product with number average chain length equal to initial molar ratio of monomer to R_0X: top left; (b) chemical structure of BlocBuilder MA, the R_0X used in the present work.*

NMP of methacrylates with well-defined microstructural control remains a challenge, even with these second generation nitroxides. The reason for this failure is a too high activation/deactivation equilibrium coefficient ($K_{eq}=k_a/k_{da}$) and the dominant occurrence of disproportionation reactions involving nitroxide species. These reactions are β-hydrogen transfer reactions, leading to the formation of hydroxylamines (XH in Figure 7.1(a)) and polymer chains with an unsaturated chain-end ($k_{td,X}$ in Figure 7.1(a)).[24, 25] Both an intra- and intermolecular pathway (k_{tdX} in Figure **7.1**(a)) have been put forward.[26-28] For the SG1 nitroxide and the MMA monomer, the intermolecular pathway has been put in forward in most studies as the most plausible one.[25, 29, 30]

A breakthrough for controlling NMP of methacrylate monomers was realized with the so-called copolymerization approach.[31, 32] This approach relies on the addition of a small amount of comonomer that under homopolymerization conditions leads to a NMP with a much lower K_{eq} than the one for MMA homopolymerization. For the copolymerization, the formally observed (de)activation equilibrium coefficient ($<K_{eq}>$), as theoretically introduced by Charleux *et al.*[31], becomes thus lower than the K_{eq} for MMA. The actual $<K_{eq}>$ value depends on factors, including the NMP activation/deactivation and propagation rate coefficients of both comonomers and the initial monomer molar fractions.[31] Nicolas *et al.*[33] explored this aspect in their isothermal and intrinsic kinetic modelling study to identify suited copolymerization conditions.[33] Initially, the controlling comonomer was mostly a styrenic monomer.[23, 32, 34] In a later stage, also other controlling comonomers have been considered such as acrylonitrile and 9-(4-vinylbenzyl)-9H-carbazole.[35, 36]

Even though for the SG1 nitroxide promising results have been obtained using the copolymerization approach, reasonable microstructural control was only obtained for rather low chain lengths (TCL < 500) and for relatively high initial controlling comonomer amounts (> 8

mol %), implying microstructural deviations from the targeted homopolymerization product. These constraints indicate that even with the copolymerization approach $k_{td,X}$ is still a kinetic parameter affecting the microstructural control, and encouraged further research into so-called third-generation nitroxides. Focus has been on (i) minimizing the nitroxide disproportionation reaction rate for active NMP systems and (ii) further lowering $<K_{eq}>$. Several nitroxides have been investigated as reviewed by Nicolas *et al.*,[24] who concluded that 2,2-diphenyl-3-phenylimino-2,3-dihydroindol-1-yloxyl (DPAIO) could be a promising nitroxide for NMP of MMA. However, DPAIO displays limitations towards NMP of styrenic and acrylate monomers. More recently, novel alkoxyamines bearing cyanopropyl groups have been developed by Ballard *et al.*[37] These alkoxyamines can be employed to acceptably control methacrylates (*Đ* of *ca.* 1.3), which was mainly attributed to a lowering of $k_{td,X}$. Moreover, some of these alkoxyamines were also able to successfully control the homopolymerization of styrene, an important prerequisite for the synthesis of block copolymers.[38]

It should be realized that active radical polymerization systems leading to high polymerization rates can induce, even at lab-scale, non-isothermicity and thus a temperature variation with increasing reaction time. Typically such non-isothermal conditions are associated with bulk free radical polymerization (FRP) of exothermic monomers such as vinyl chloride and *n*-butyl acrylate (*n*BuA).[39-42] Recent research has shown that for *n*BuA radical polymerization in solution and even under RDRP conditions temperature spikes can be obtained, complicating the kinetic description and promoting side reactions.[40, 42, 43] For RDRP of less reactive monomers such as styrene and MMA it is often taken for granted that isothermicity can be assumed.[35, 44-46] It should be noted that microreactors has shown to be beneficial to ensure isothermicity. However, they do

require diluted conditions and limited conversions, taking into account practical pressure drops. Hence, in general solvent effects cannot be avoided.[40, 47]

In the present work, it is demonstrated that for typical lab-scale experiments for bulk NMP of MMA initiated by BlocBuilder a strong non-isothermicity is obtained with increasing time, despite temperature control and therefore the use of set-point. The non-isothermicity complicates the $k_{td,SG1}$ parameter determination and requires the use of Arrhenius parameters to describe the polymerization kinetics, even if a single set temperature is considered. It is further demonstrated that non-isothermicity can also be still present upon the addition of small amount of styrene as comonomer, in particular at low TCLs. For NMP with MMA and styrene as comonomers, a large set of experimental data is reported to fully understand the comonomer incorporation kinetics and to map the impact of disproportionation with SG1. For this purpose, a kinetic Monte Carlo (*k*MC) model is employed capable of visualizing the monomer sequences of individual copolymer chains.[48-50] Attention is focused on the efficiency of the activation-growth-deactivation cycles and the identification of optimal reaction conditions in view of a minimization of the amount of styrene comonomer units.

7.2 Experimental

7.2.1 Materials

Alkoxyamine NMP initiator N-(2-methyl-2-propyl)-N-(1-diethylphosphono-2,2-dimethylpropyl)-O-(2-carboxyprop-2-yl) hydroxylamide (BlocBuilder MA or MAMA-SG1; Arkema; 97%) is used without further purification. Methyl methacrylate (MMA; M_1, ≥99%, Sigma Aldrich) and styrene (M_2, ≥99%, Sigma Aldrich) were passed through a column filled with basic aluminum oxide to remove the inhibitor monomethyl ether hydroquinone and the stabilizer 4-tert-

butylcatechol. Dichloromethane (DCM, ≥99,8%, Sigma-Aldrich), *n*-decane (≥99%, Sigma-Aldrich), deuterated chloroform ($CDCl_3$, ≥99.8%, Euroiso-top), and tetrahydrofuran (THF, ≥99.9%, Sigma-Aldrich) were used as received.

7.2.2 NMP synthesis and analysis

For batch bulk NMP of MMA with or without a small amount of styrene, the desired amount of BlocBuilder was weighted and added to a 100 mL three-neck Schlenk flask (batch reactor) containing a magnetic stirrer. The desired amount of styrene was added using a micropipette together with 30 mL of MMA. In case of GC analysis in view of the determination of comonomer conversions, the internal standard *n*-decane (6.25 vol%) was added using a micropipette after which a stopcock was attached to the upper neck and the other necks were sealed off using silicon septa. In a next step, three freeze-pump-thaw cycles were performed to degas the solution, after which an argon atmosphere was created inside the flask using a balloon attached to the stopcock. A thermocouple was inserted through one of the septa in order to monitor the actual reaction temperature. The flask was submerged into a pre-heated oil bath thermostated at the desired reaction temperature, which was defined as the set-point (T_{set}). Samples (0.3 mL) were withdrawn using degassed syringes. For the copolymerization the set-point was always taken as 363 K to ensure a sufficiently high polymerization rate.

For homopolymerization, the MMA conversion was determined using ^1H nuclear magnetic resonance (NMR). The spectra were recorded at 400 MHz and ambient temperature with $CDCl_3$ as solvent, using a Bruker Avance II spectrometer equipped with a Broadband Observe probe. For copolymerization, the conversions of both comonomers were determined using a trace-GC ultra-Gas Chromatograph equipped with an AS3000 auto sampler, flame ionization detector, and a CP Wax 52 CB 30 m capillary column. The injector and detector temperature were set at

275°C. Helium (flow rate: 1.3 mL min^{-1}) was used as carrier gas and a stepwise temperature program was set as follows: 40 °C during 4 min, followed by a heating ramp of 20 °C min^{-1} until a temperature of 145 °C was reached, which was maintained for 2 minutes. *n*-Decane was used as internal standard and dichloromethane (DCM) as solvent to prepare the samples. Data acquisition and processing were performed with Chrom-Card Trace-Focus GC software.

Size exclusion chromatography (SEC) analysis was performed using a PL-GPC50 plus instrument equipped with a PL-AS RT auto sampler and a refractive index (RI) detector. Following columns were connected in series: one Resipore 50 7.5 mm guard column and two Resipore 300 7.5 mm columns. THF is used as eluent (1 mL min^{-1}) at a temperature of 30°C. Calibration was based on *p*MMA standards (Medium EasiVials kit, Agilent Technologies) respectively ranging from 5.5 10^2 to 2.1 10^6 g mol^{-1} and correcting for the copolymer nature based on Mark-Houwink parameters. Data acquisition and processing was performed using PL Cirrus GPC/SEC software. Error bar assessment is explained in Section S.4 of the Appendix, based on data of typical polymerization experiments. An overview of all experiments can be found in Appendix (Section S.1.). End-group functionality (EGF) data have not been recorded as they are tedious and error sensitive based on previous experimental NMP studies.[29, 32]

7.2.3 Kinetic model

The kinetic Monte Carlo (*k*MC) model as previously developed for RDRP copolymerization is considered, denoting MMA as monomer 1 (M_1) and styrene as monomer 2 (M_2).[48-50] It enables to follow the temporal evolution of the explicit microstructure of individual polymer chains as well as the tracking of the individual reaction events. The list of all homo- and copolymerization reactions and the Arrhenius parameters can be found in the Appendix (Table S.2). Rate coefficients have in principle two indices with the first one referring to the penultimate unit and

the second one to the terminal unit. All NMP non-specific and most of the NMP specific parameters are based on literature data.[32, 33, 50-52] Only for the disproportionation reaction involving nitroxide and one of the NMP cross-activation rate coefficients (k_{a12}) parameter tuning to the experimental data is performed: homopolymerizaiton data for the former and copolymerization data for the latter.

A penultimate monomer unit (PMU) effect on both the propagation and NMP activation reactivity is accounted for in the copolymerization simulations. Hence, for these reactions the reactivity can depend on the last two monomer units next to the radical center. The penultimate propagation rate coefficients are based on literature data.[53, 54] For MMA and styrene as comonomer pair, the so-called implicit PMU propagation model is used, as it has shown to provide an adequate description of both copolymer composition and polymerization rate data over a broad range of monomer feeding compositions.[33, 54, 55] For NMP activation, also PMU literature data are used.[33] Only the NMP cross-activation rate coefficient for dormant species with as penultimate unit MMA and as terminal unit styrene (k_{a12}) is tuned, based on the copolymerization data in the present work. In practice, this comes down to a tuning of the reactivity ratio s_{a2} (= k_{a21}/k_{a22}), as k_{a22} is taken from literature.[33] The reactivity ratios for propagation and NMP activation are assumed to be temperature independent, taking into account that no Arrhenius parameters have been reported and typically the activation energies are between 0 and 10 kJ mol^{-1}.[56] As shown in Section S.2 of the Appendix, indeed, the use of Arrhenius parameters in this range has a negligible effect on the simulation outcome. The NMP deactivation rate coefficients are assumed to be dependent only on the terminal unit, in accordance with the kinetic study of Nicolas *et al.*[33] For the actual rate coefficients literature data[51] are used, except for NMP of MMA for which preliminary model screening indicated that an increase of the

literature k_{da11} with a factor 10 leads to a better qualitative description of the experimental homopolymerization trends as reported in the present work.

Furthermore, if the terminal monomer unit of macroradical is a MMA unit, disproportionation with SG1 ($k_{td,SG1}$; k_{tdX} in Figure **7.1**) is considered. It is assumed that an intermolecular H-transfer takes place, in accordance with the majority of experimental and kinetic studies.[25, 29, 30] The Arrhenius parameters have been determined in this work while accounting for non-isothermicity and focusing only on the MMA homopolymerization experiments. Preliminary simulations indicated the negligible impact of macropropagation after a disproportionation step (see Figure E.2 Appendix).

To accurately describe conventional termination ($k_{td/tc}$ in Figure **7.1**(a)), conversion and chain length dependent apparent rate coefficients are used.[57] As MMA is in excess with respect to styrene, it is assumed that the apparent copolymerization termination is affected by diffusional limitations to the extent as for the homopolymerization of MMA. The empirical expression for MMA determined by Derboven *et al.*[58] is used. The contributions of the mode of termination, *i.e.* disproportionation versus recombination, are calculated based on the nature of the terminal units of the participating radicals. For the other reaction steps, diffusional limitations can be ignored at least to a first approximation.[57] More details can be found in the Appendix.

For a reliable comparison with experimental data, the integration ranges of the experimental SEC analyses were explicitly used for the calculation of the x_n and $Đ$ evolutions and the related simulated chain length distributions (CLDs).

7.3 Results and discussion

A *k*MC model-based design of NMP of MMA with small amounts of styrene and initiated by BlocBuilder (MAMA-SG1) is presented, focusing on the incorporation of the latter comonomer at the level of the individual macromolecule. To allow for a reliable design of the copolymerization, NMP with only MMA, thus the homopolymerization, is studied first and it is shown that non-isothermicity must be accounted for to fully understand the relevance of $k_{td,SG1}$.

7.3.1 BlocBuilder initiated NMP of MMA

NMP of MMA with SG1 is characterized by a strong loss of microstructural control leading to low final monomer conversions. The three pathways toward the formation of dead polymer molecules (no X moiety), as shown in Figure **7.1**(a), are (i) termination by recombination between two macroradicals (k_{tc}); (ii) termination by disproportionation between two macroradicals (k_{td}); and (iii) disproportionation of a macroradical with SG1 (k_{tdX}).[25, 29] The latter was shown in previous studies to be the main contributor, especially if free SG1 is initially added.[25, 30] A good estimate of the associated $k_{td,SG1}$ is not only paramount for the accurate description of the homopolymerization data but also for the description of NMP of MMA with a small amount of styrene.[33]

A first attempt for quantifying $k_{td,SG1}$ has been made by Dire *et al.*[29] using a Predici© kinetic model to describe experimental data with a set point of 343 K for various initial levels of free nitroxide. However, several assumptions were made during this study adding a high degree of uncertainty to the reported value ($k_{td,SG1}$ = 1.7 10^3 L mol^{-1} s^{-1}). A first implicit assumption is the isothermicity of the experiments, which for active radical polymerization systems can be difficult to achieve. Diffusional limitations on conventional termination, *i.e.* termination between macroradicals, which are known to be strong in MMA radical polymerization, have also been

neglected.[58, 59] As conventional termination and disproportionation with SG1 are in direct competition (see Figure **7.1**(a)), this simplification is expected to lead to a biased $k_{td,SG1}$ parameter assessment. A more recent experimental study by Edeleva *et al.* focusing on small molecule analogues and based on ^{1}H and ^{31}P NMR spectroscopy also quantified $k_{td,SG1}$ at 343 K as $1.7\ 10^{3}$ L mol^{-1} s^{-1}.[25] However, the kinetic study has not been performed under bulk polymerization conditions and at the same time (de)activation rate coefficients related to MMA-SG1 had to be tuned based on a limited data set.

In the present work, MMA homopolymerization experiments at three different set temperatures (333, 343 and 353 K; red lines in Figure 7.2(a-c)) are considered. Temperature monitoring in the reaction mixture is performed to (i) quantify possible non-isothermicity and (ii) provide the temperature evolutions as a direct input for the kinetic model used for the $k_{td,SG1}$ determination. As can be seen from the measured temperature evolutions (Figure 7.2 (a-c); green lines) strong non-isothermal conditions are established as a function of time with maximum temperature overshoots of respectively 13, 21, and 23 K with respect to the set temperatures. Moreover, looking at the measured MMA conversion profiles (Figure 7.2 (d-f)), it can be seen that the majority of the MMA conversion occurs during the non-isothermal time period. Hence, it follows from Figure 7.2 that it is of utmost importance to describe the experimental data with a kinetic model including Arrhenius parameters, as more activated reactions will gain in relative importance at an increased temperature.

Using literature data[33, 58, 60] for the other reaction steps, parameter adjustment to monomer conversion (symbols in Figure 2) and average chain length data (symbols in Figure 3) allows to deduce that:

$$k_{td,SG1}(\mathrm{L\ mol^{-1}s^{-1}}) = 1.40\ 10^{7}\ \exp\left(\frac{-22.5\ 10^{3}}{R\ T}\right) \quad (3)$$

in which R is the universal gas constant and T the temperature. The simulation results for the MMA conversion profiles, using Equation (3), are provided as green lines in Figure 7.2 (d-f) with the corresponding evolutions for x_n and $Đ$ given in Figure 7.3. A good agreement with the experimental data is obtained. In Figure 7.2 and Figure 7.3, the simulation results are also included if isothermicity is incorrectly assumed (red lines; temperature directly and always at T_{set}). A very different MMA conversion evolution results and the experimentally observed cessation of the polymerization cannot be captured in Figure 7.2, clearly showing that the isothermal model cannot be applied. Furthermore, both the experimental and simulated data in Figure 7.3 indicate that non-isothermicity leads to much higher initial x_n and $Đ$ values, whereas at higher MMA conversions more similar profiles are obtained. The EGF profiles are given in Appendix (Figure E.3).

The observed trends and the differences between the non-isothermal (green lines) and isothermal (red lines) simulations can be explained by an analysis of the reaction rates. As shown in previous modeling studies on NMP[56, 61] it is recommended to focus on (i) the ratio of the propagation to deactivation rate (R_{prop}/R_{deac}), (ii) the (conventional) termination rate probability (P_{term}), and (iii) the probabilities for additional side reactions, which is in this case restricted to the probability for disproportionation involving nitroxide ($P_{td,X}$). Figure E.4 (a-c) in the Appendix show that R_{prop}/R_{deac} has very high initial values for the non-isothermal case. Since deactivation is non-activated in contrast to propagation, temperatures above the set-point as encountered in the non-isothermal case result in more uncontrolled NMP kinetics and thus a faster monomer incorporation. Due to the initial temperature spike, a more pronounced loss of control over chain length also results at low reaction times, explaining the deviations between the isothermal and

non-isothermal case in Figure 7.2 and Figure 7.3 at low MMA conversions. On the other hand, R_{prop}/R_{deac} (Figure E.4 (a-c) in the Appendix) decreases significantly towards higher MMA conversions as a build-up of nitroxide is obtained (Figure E.3 (d-f) in the Appendix). Differences between non-isothermal and isothermal conditions become thus somewhat less important, explaining for instance the more similar green and red lines in Figure 7.3 at the higher MMA conversions.

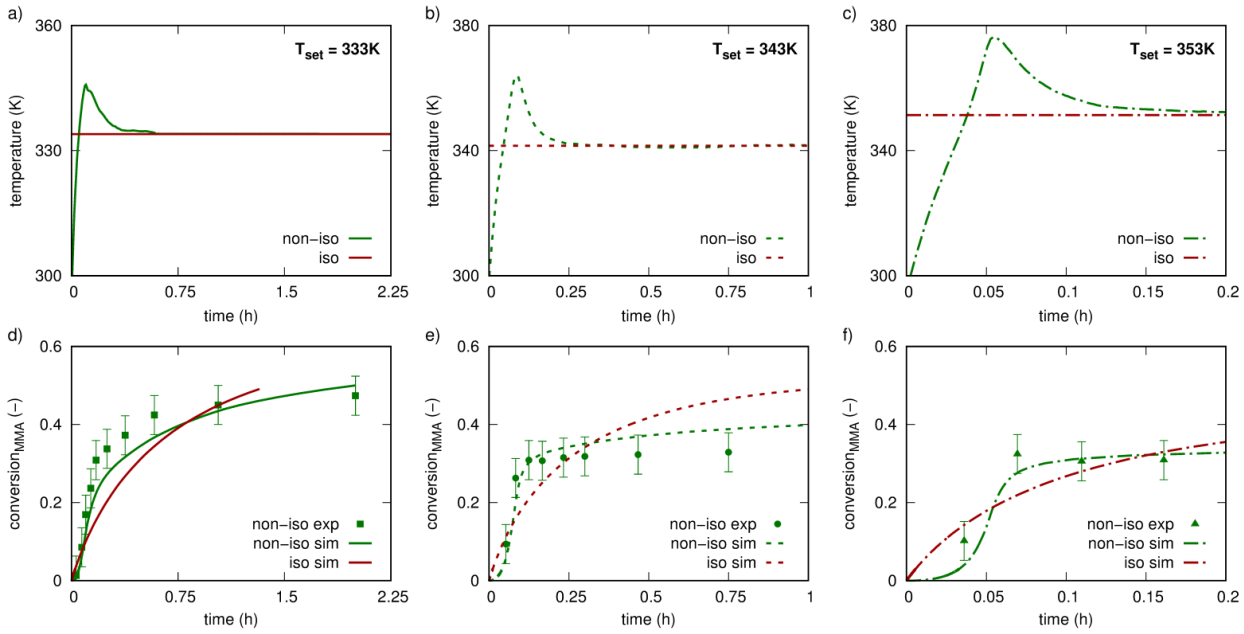

Figure 7.2. *Effect of non-isothermicity for NMP of MMA (TCL = 200) initiated by BlocBuilder; (a-c): experimentally recorded temperature (green lines) and targeted set temperature (red lines); (d-f): corresponding experimental (points) and simulated (lines) MMA conversion profiles for T_{set}: 333 K (a, d; full lines and squares), 343 K (b, e; dashed lines and circles) , 353 K (b, e; dashed-dotted lines and triangles); red lines correspond to simulation outcome if an isothermicity is incorrectly assumed; parameters: Table S.2 (Appendix) and Equation (1); initially: room temperature; bars: typical experimental error.*

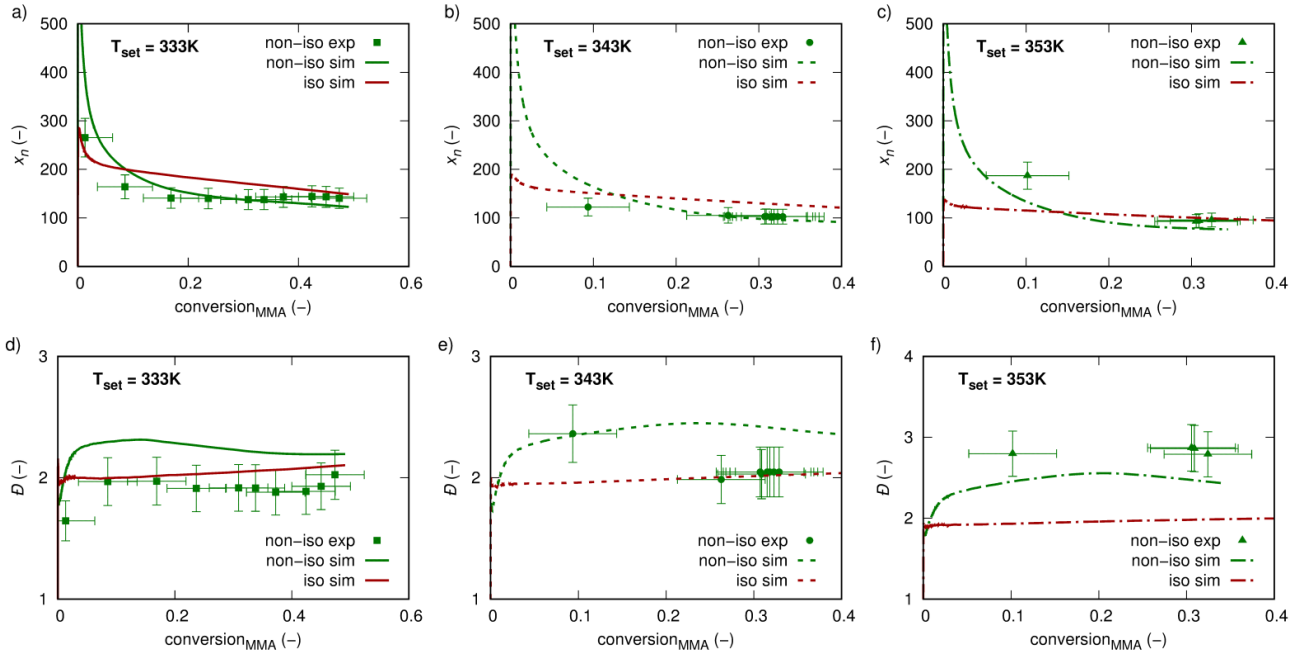

Figure 7.3. *Corresponding results to Figure 7.2 for (a-c) number average chain length (x_n) and (d-f) dispersity (Đ) as a function of MMA conversion (points: experiments, lines: simulations).*

P_{term} (Figure E.4 (d-f) in the Appendix) also shows high initial values and this more pronounced under non-isothermal conditions, reflecting the high K_{eq} specifically at increased temperatures. Low EGF values (EGF < 0.5) thus result at low MMA conversions, as confirmed in Figure E.3 in the Appendix. In agreement with the trend for R_{prop}/R_{deac}, under both isothermal and non-isothermal conditions P_{term} almost approaches zero towards higher MMA conversions. This is caused by the strong impact of diffusional limitations on conventional termination, contributing to a lower apparent termination reactivity and therefore conventional termination rate. Furthermore, lower macroradical concentrations are present at these higher conversion due to R_0X depletion (Figure E.3(d-f) in the Appendix). Again at higher batch times the relevance of the non-isothermicity is thus somewhat suppressed.

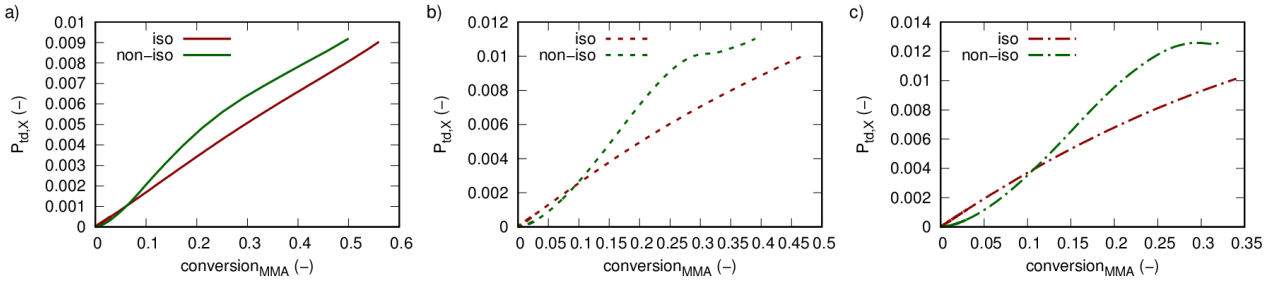

Figure 7.4. *Evolution of probabilities for termination by disproportionation as a function of MMA conversion related to Figure 7.2 and 7.*

$P_{td,X}$ (Figure 7.4 (a-c)) is initially very low, since almost no nitroxide is present. As the nitroxide builds up due to conventional termination as highlighted above, a clear increase in $P_{td,X}$ occurs at higher batch times and this more clearly for the non-isothermal case. The fraction of dead polymer formed by disproportionation to nitroxide (Figure E.3 (g-i) in the Appendix) thus increases toward higher MMA conversions and even accounts in the end for more than 60% of the formed dead polymer chains. Since diffusional limitations can be ignored for this disproportionation reaction due to a too low intrinsic reactivity, a full transition to a dead polymer system (EGF of zero) can be obtained through this reaction pathway. Towards high MMA conversions, the polymerization rate is also strongly reduced, in particular for the non-isothermal case. Figure E.3(a-c) in the Appendix shows how EGF indeed approaches zero, thereby lowering the radical concentration as soon the NMP initiator is completely consumed, as highlighted above. This further confirms the importance of the homopolymerization experiments in view of the $k_{td,SG1}$ determination.

Figure 7.5 displays the mass CLDs at a given MMA conversion (*ca.* 0.35) for the three set temperatures, again differentiating between the experimental results (black lines), the simulated results with the non-isothermal model (green lines), and the simulated results with the isothermal model (red lines). The latter model globally performs worse as the tail of the CLD is less well-

described, *i.e.* too high chain lengths are simulated. The non-isothermal model leads on average to a higher contribution of shorter chains due to the enhanced termination probability which is reflected in the better description of the tail of the CLDs.

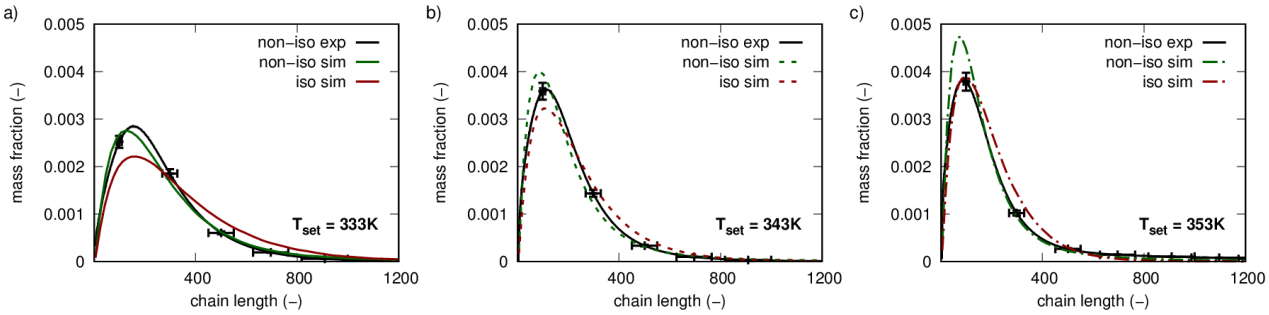

Figure 7.5. *Mass chain length distribution (CLD) via SEC measurements (black lines) and via non-isothermal (green lines) and incorrect isothermal (red lines) simulations corresponding to Figure 7.2 at (a)* T_{set} *= 333 K and* X_{MMA} *= 0.37 (full lines), (b)* T_{set} *= 343 K and* X_{MMA} *= 0.31 (dashed lines), (c)* T_{set} *= 353 K and* X_{MMA} *= 0.31 (dashed-dotted lines).*

Using Equation (3), at 343 K, a value of 5.3 10^3 L mol^{-1} s^{-1} is obtained, *i.e.* an increase with *ca.* a factor 3 compared to previous studies ($k_{td,SG1}$ = 1.7 10^3 L mol^{-1} s^{-1}).[25, 29] Figure E.4 in the Appendix shows the description of the conditions in Figure 7.2 and 7 using this literature value, assuming isothermicity in agreement with the kinetic modeling work of Dire *et al.*[29] Significant deviations are obtained with the simulation results of Figure 7.2 and Figure 7.3 (green lines), further highlighting the approximate nature of the isothermal model.

7.3.2 BlocBuilder initiated NMP of methyl methacrylate with a small amount of styrene

For NMP of MMA and styrene, a large experimental data set for various TCLs (200-750) and initial styrene amounts (up to 10 m%) has been collected (Figure 7.6). The set temperature is taken equal to 363 K in order to ensure a fast polymerization even for the higher TCLs. The overall monomer conversion, *i.e.* of both monomers jointly, is denoted as X_M. Temperature recording showed that only for the lower TCLs non-isothermicity is relevant. In particular, at a

TCL of 200, an overshoot of 3.5, 8, and 10 K is measured for an initial styrene mass fraction of 10, 5 and 2.5 m% (Section S.7 of the Appendix).

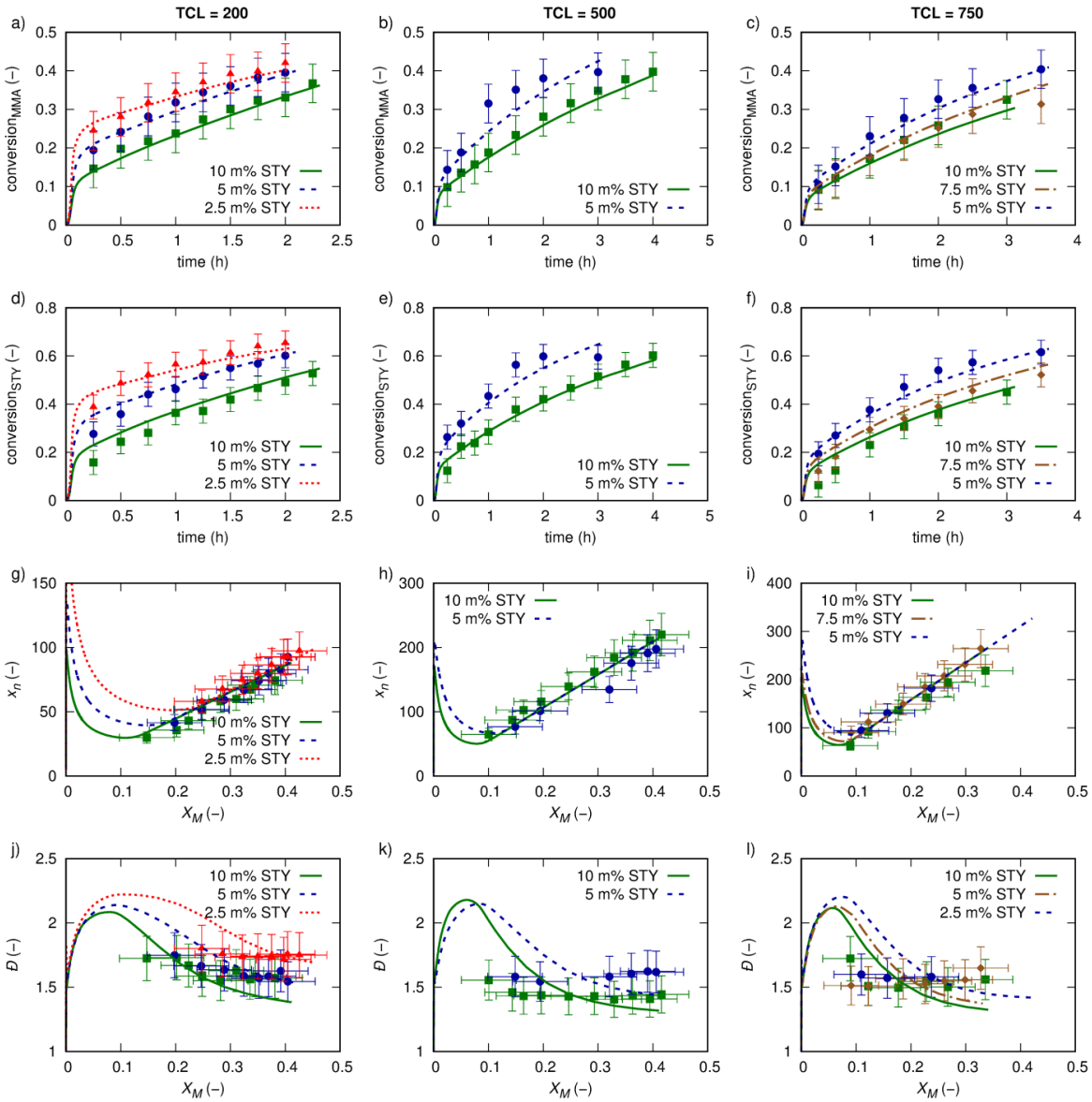

Figure 7.6. *Comparison between simulation (lines) and experiments (points) for NMP of MMA and styrene initiated by BlocBuilder for a T_{set} of 363 K: (a-c) MMA conversion, (d-f) styrene conversion as a function of time, (g-i) number average chain length, (j-l) dispersity as a function of overall conversion (X_M) for a TCL of 200 (left), 500 (middle), and 750 (right) for distinct initial mass fractions of styrene: 10 (green full lines/squares), 7.5 (brown dashed-dotted lines/diamonds), 5 (blue dashed lines/circles), and 2.5*

(red dotted lines/triangles). Recorded temperature evolution and comparison with isothermal simulations can be found in the Appendix (Figure E.6-E.7). Only at low TCLs non-isothermicity is relevant; model parameters see Section E.2-3 (Appendix)

For the simulation results in Figure 5, the only parameter that has been adjusted in order to obtain an adequate description of all experimental copolymerization data is s_{a2} (= k_{a21}/k_{a22}; k_{a22} according to literature[50]). A constant value of 6.7 is put forward in the presented work. This value is slightly smaller than the one published in literature and as such this work predicts a slightly weaker PMU effect on activation of terminal styrene macrospecies.[33, 62] Note that for terminal MMA macrospecies (s_{a1}) a literature value was used.[33] The use of constant value is defendable reminding that a large part of the data points in Figure 5 are obtained under isothermal conditions. Preliminary simulations (Section E.2 of the Appendix) additionally showed the limited impact of temperature dependencies on the reactivity ratios, highlighting that the determination of their activation energies is not needed from a kinetic point of view and recommendable from a parameter estimation point of view. Since the s_{a2} value is higher than 1, the presence of a MMA unit before a terminal styrene unit enhances the NMP activation, in line with the MMA homopolymerization results. Figure E.17 in the Appendix also demonstrates that neglecting the PMU effect on activation (s_{a2} =1) leads to a very approximate kinetic description. Furthermore, Figure 7.7 shows that also a good agreement between the experimental and simulated CLDs (TCL=200) is obtained.

For every condition in Figure 7.6 a steep initial increase of both comonomer conversions is obtained as for the homopolymerization case (Figure 7.2), which then levels off to a quasi-linear increase later on. These quasi-linearities can be understood by considering the comonomer fraction profiles (Figure E.9 in Appendix), which show a depletion of styrene with respect to the

initial content as the NMP proceeds. As styrene functions as the controlling monomer, the typical NMP rate retardation due to a well-established persistent radical effect, is less relevant at higher batch times. A typical downward curvature for the comonomer conversion profiles is thus compensated for ultimately resulting in a quasi-linearity. For the lowest TCL (first column in Figure 7.6) and the lower initial styrene amounts (red (2.5 m%) and blue (5 m%) lines), the initial comonomer conversion increases are even very steep. As NMPs with a lower TCL are inherently faster due to a higher initial R_0X concentration, it can be expected that they are more prone to temperature variations. This is specifically true if they have low initial styrene contents and thus resemble more the homopolymerization process. Indeed as shown in the Appendix, isothermal simulations cannot predict the experimental observations at for instance a TCL of 200 and for an initial styrene amount of 2.5 m%.

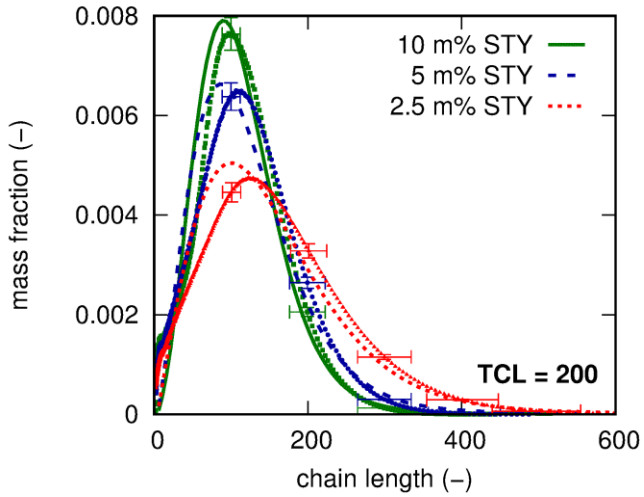

Figure 7.7. *Mass chain length distribution (CLD) via SEC measurements (dots) and simulations (lines) corresponding to Figure 7.6 (TCL = 200) for an initial mass fraction of styrene of 10 (green full lines; X_M = 0.38), 5 (blue dashed lines; X_M = 0.37) and 2.5 (red dotted lines; X_M = 0.42).*

The deleterious effect of a lower initial styrene amount can also be seen in the $Đ$ profiles in Figure 7.6. As shown in the Appendix (Figure E.7-E.8), the reduced control over chain length is

also accompanied by a stronger decrease in EGF, which is more pronounced for higher TCLs. As for the homopolymerization these trends for the control over chain length and livingness can be related to variations for R_{prop}/R_{deac}, P_{term}, (Figure E.10). Moreover, $P_{td,X}$ (Figure 7.8) specifically shows that the relevance of the side reaction is significantly lowered by the presence of styrene and this more pronounced for a lower TCL.

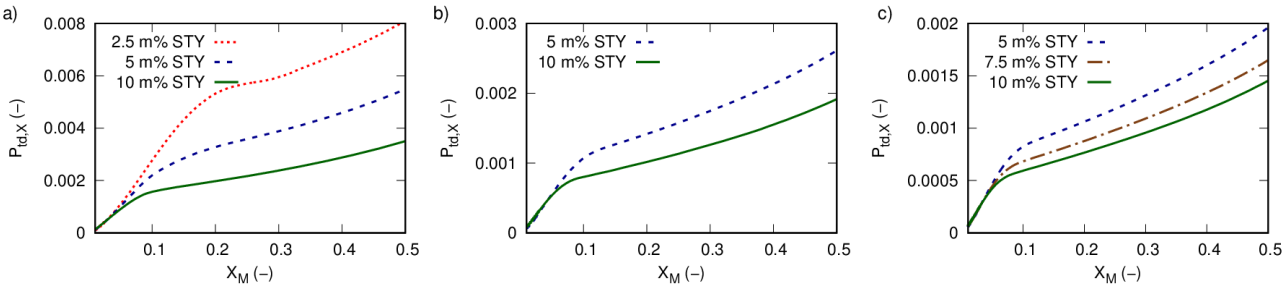

Figure 7.8. *Probabilities for disproportionation involving SG1 nitroxide corresponding to Figure 7.6.*

With the model parameters being validated (Figure 7.6-8), the effect of the reaction times and levels of microstructural control can be mapped *in silico* over a broad range of TCLs and initial mass fractions of styrene. This is done in Figure 7.9 with the focus on the region of at most a very limited effect of non-isothermicity (TCL ≥ 300; initial styrene mass fraction ≥ 0.03) and selecting a X_M of 0.50. It follows from this figure that low dispersities can be obtained ($Đ$ < 1.3) for the entire TCL range, provided that the initial styrene fraction is sufficiently high (> 9 m%). A reasonable EGF (> 0.7) is however limited to TCLs below 500, even for high initial styrene contents.

Furthermore, an advantage of the *k*MC model is the possibility to track the chain growth of every single molecule for a representative polymer sample, *e.g.* starting with $2\,10^5$ NMP initiator molecules. With the convention to color MMA units in beige and styrene units in blue, Figure 7.10 shows for two different initial mass fractions of styrene (5 and 10 m%) the monomer sequences for a TCL of 200 at an X_M of 0.5. To facilitate the interpretation dead and dormant

polymer molecules are separated and both ranked from low to high chain length. It can be seen that a rather large fraction of dead polymer product is formed in both cases but for the higher styrene initial amount this fraction is smaller. The latter is related to a better suppression of termination reactions (Figure E.10 (d-f)).

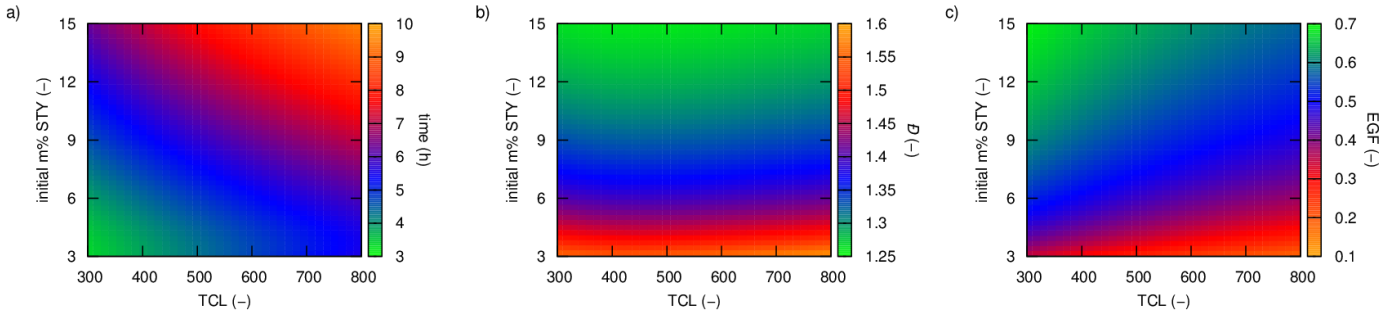

Figure 7.9. *Mapping of the impact of TCL and initial mass fraction of styrene on (a) polymerization time, (b) dispersity (Đ), and (c) end-group functionality (EGF) at X_M = 0.5 for NMP of MMA and styrene initiated by BlocBuilder for at 363 K*

For the chain lengths in Figure 7.10, a large rather broad distribution is further obtained with a dispersity of 1.47 and 1.33 for the 5 and 10 m% case, respectively. Note that for a sufficiently high initial styrene amount thus similar degrees of microstructural control, at least based on *Đ*, are obtained as for the third generation nitroxides (*ca. Đ* of 1.3).[37] The incorporation of styrene (blue units) can also be clearly seen in the chains in Figure 7.10. In the dormant copolymer product, the terminal unit is always a styrene unit, reflecting the working principle of the copolymerization approach as introduced by Charleux *et al.*[31] By the presence of styrene a much higher deactivation probability (Figure E.13 in the Appendix) is obtained if the terminal unit of a macroradical is styrene thereby lowering the formally observed activation/deactivation equilibrium coefficient $<K_{eq}>$.

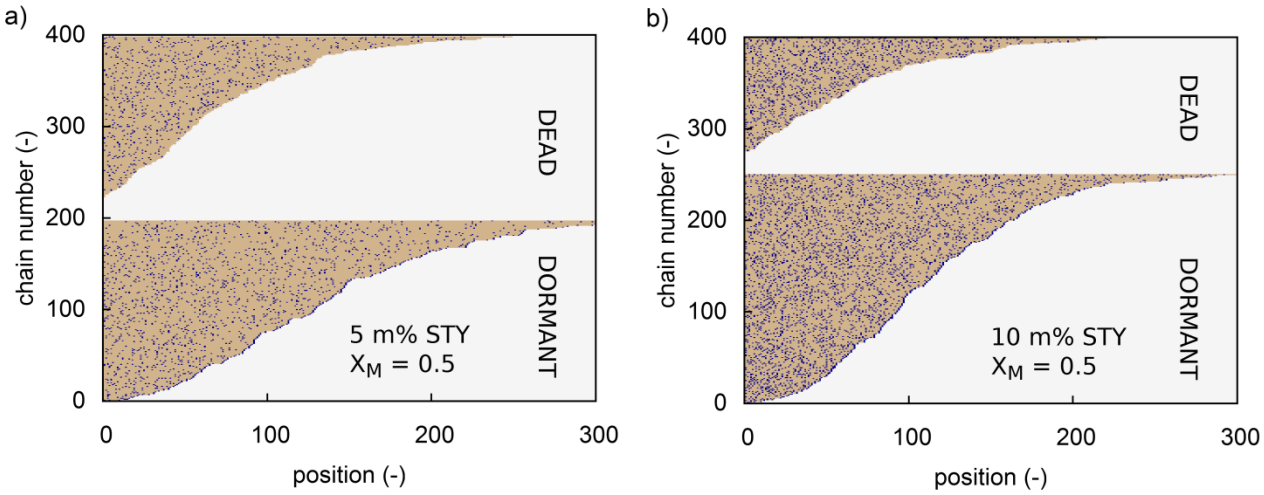

Figure 7.10. *In silico visualization of copolymer microstructure for each individual copolymer chain for NMP of MMA (beige) and styrene (blue) (TCL = 200) initiated by BlocBuilder for a* T_{set} *of 363 K with an initial mass fraction of styrene of (a) 5m% styrene, and (b) 10m% styrene.*

Another advantage of the *k*MC model is the calculation of the amount and type of monomer units that is incorporated per activation-growth-deactivation cycle.[49, 56] Upon normalization a distribution can be constructed, as for example shown in Figure 7.11 for a TCL of 200 and again an initial mass fraction of styrene equal to 5 and 10 m%, focusing on a X_M interval between 0.4 and 0.5. Note that the relative fraction of both monomer types is indicated in beige (MMA) and blue (styrene). Compared with other RDRP processes, for which a tracking of activation-growth-deactivation cycles was performed,[49, 56] a rather unusual distribution results. It follows that there is a large number fraction of zero growth activation-deactivation cycles (no propagation during cycle) which amounts to 0.45 and 0.48 for a 5 and 10 initial styrene mass fraction, respectively. Further inspection allows to deduce that for cycles with the incorporation of monomer units the fraction of those of limited propagation is rather low. For instance, a fraction of only 0.24 is obtained in both cases for cycles with 1 to 5 monomer units. This observation is also reflected in the pronounced tail formation in Figure 7.11, indicative of the significant contribution of cycles with incorporation of a very high number of monomer units (> 5).

The contribution of zero-growth cycles is mainly coming from terminal styrene dormant macrospecies, which can undergo a direct deactivation after they are activated. The latter is confirmed in the Appendix (Figure E.13) in which the R_{prop}/R_{deac} per radical type is shown. For terminal styrene radicals much lower ratios are obtained than for terminal MMA macroradicals, indicating that the zero-growth contribution is mainly originating from the former radicals. Moreover, if the deactivation rate coefficient for macroradicals with a terminal styrene unit is formally assumed 10 times smaller, the fraction of zero growth cycles is reduced to 0.18 (Figure E.14 in the Appendix) and thus the more typical RDRP distributions are obtained. Similarly, the tail in Figure 7.11 can be related to the slow deactivation of terminal MMA radicals. Several MMA units are incorporated before the dormant species is formed.

It further follows from Figure 7.11 that the difference between 5 m% and 10 m% of initial styrene fraction is mainly reflected in the tail of the distribution, as very similar fractions are obtained for cycles with a limited amount of propagation steps. For activation-growth-deactivation cycles with a larger number of propagation steps (> 25), a number fraction of 0.03 and 0.02 is obtained for an initial styrene mass fraction of 5 m% and 10 m%, respectively. This seems at first sight a small difference, however, the associated fraction of monomer units incorporated are 0.28 vs. 0.23. Note that for cycles with 1 propagation step a rather large fraction of MMA incorporation occurs. This means that despite the large K_{eq}, MMA terminal chains still participate in the deactivation process. They undergo however very fast activation so that the concentration of terminal MMA dormant species is still low (Figure E.16 in the Appendix).

An additional advantage of the *k*MC model is the a posteriori calculation of the fraction of styrene comonomer units per chain. The aim of the copolymerization approach is to use as little as possible styrene to allow a good microstructural control but still to obtain a copolymer product

close to *p*MMA, as it can be expected that even a small amount of styrene will influence the final properties. Focusing on a TCL of 200 and an X_M of 0.5, the distribution of the fraction of styrene units among the polymer chains is shown in Figure 7.12 for an initial styrene mass fraction of 2.5, 5 and 10 %, with the corresponding figure without normalization for chain length provided in the Appendix (Figure E.15). For the lower initial styrene amounts, two very clear extrema can be identified, indicating a bimodality. For the highest initial styrene fraction, a quasi-unimodal distribution results with the fraction of pure MMA homopolymer chains being only 0.01 in contrast to above 0.10 for the lower initial amounts.

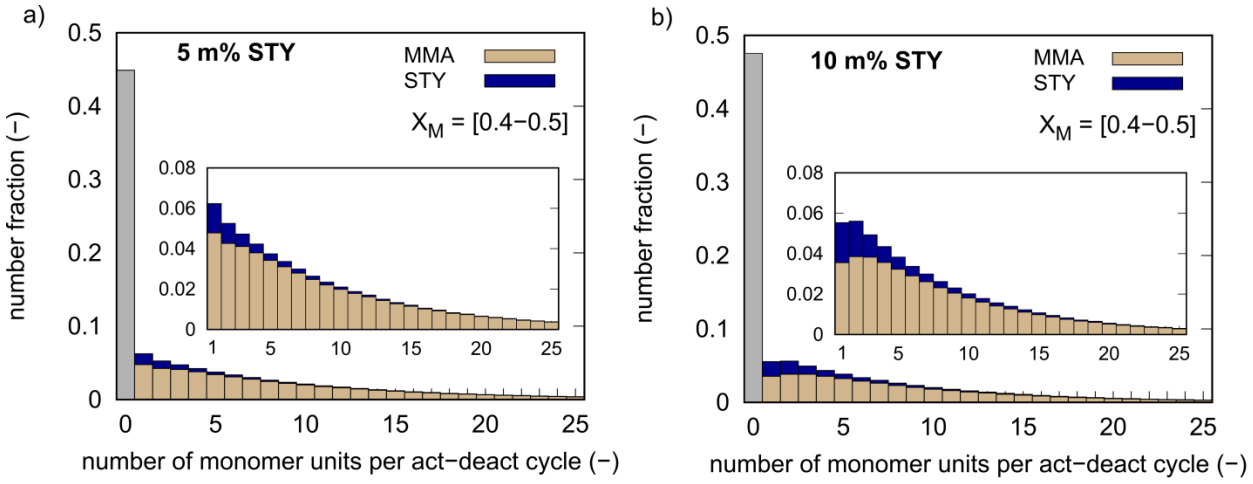

Figure 7.11. *Number fraction of activation-deactivation cycles as a function of the number of propagation steps with the relative contribution of MMA (beige) and styrene (blue) indicated for X_M interval from 0.4-0.5 (grey referring to zero-growth activation-deactivation cycles) for the NMP of MMA and styrene (TCL = 200) initiated by BlocBuilder for a T_{set} of 363 K using (a) 5 m% and (b) 10 m% of styrene.*

At the selected X_M of 0.5, typical average properties can be also calculated *a posteriori*. For example, an average number styrene fraction or mean value of 0.04, 0.07, and 0.14 are calculated for an initial styrene amount of 2.5, 5, and 10 m%, respectively. The molar fractions of styrene units in the chains are thus at that X_M higher than the initial styrene molar monomer fractions,

which are very similar to the initial mass fractions. This preferential styrene incorporation is a consequence of the values of the monomer reactivity ratios (Table S.2 in Appendix). A second average parameters is the width of the distribution, which to limit bias can be reflected best by the coefficient of variation. The latter is defined as the ratio of the standard deviation and the aforementioned mean value. For an initial styrene amount of 2.5, 5, and 10 m%, values of 0.79, 0.51, and 0.31 result, respectively.

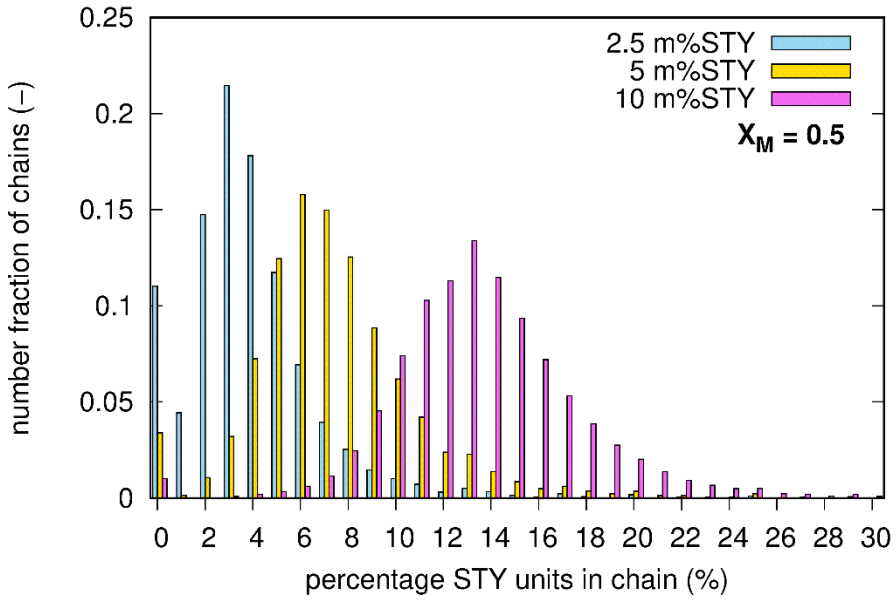

Figure 7.12. *Number fraction of chains with a given percentage of styrene units for NMP of MMA and styrene (TCL = 200) initiated by BlocBuilder at X_M = 0.5 for a T_{set} of 363 K using an initial mass fraction of styrene of 2.5 m%(blue), 5 m% (yellow) and 10 m% (fuchsia) of styrene.*

7.4 Conclusions

Both for NMP of MMA and the related copolymerization with small amounts of styrene, a combined experimental and *k*MC modeling study has shown to be beneficial for an improved understanding of the evolution of the polymerization rate and control over chain length. It is demonstrated that a temperature recording in the reaction mixture is indispensable with non-

isothermicity strongly affecting the aforementioned evolutions. This impact is very large for the homopolymerization and relevant for the copolymerization up to TCLs of 300.

By accounting for this non-isothermicity Arrhenius parameters for disproportionation with SG1 are reported for the first time ($A = 1.4\ 10^7$ L mol^{-1} s^{-1}; $E_a = 23$ kJ mol^{-1}). The negative impact of this reaction is also shown to be higher than previously anticipated based on simplified kinetic descriptions, with at 343 K an increase with a factor 3. For the copolymerization, parameter tuning shows a penultimate monomer effect for NMP activation (styrene terminal unit), with a 6.7 times faster activation at 363 K in case the penultimate unit is changed from styrene to MMA.

Model-based design demonstrates that a minimum amount of 9 m% initial styrene is necessary for achieving a low $Đ$ (<1.3). If a relatively high EGF (> 0.7) is also aimed at, a successful NMP is limited to low TCLs below 500, even for relatively high initial styrene amounts (> 10 m%).

Moreover, the *k*MC model allows to fully understand the comonomer incorporation kinetics. Not only are the monomer sequences visualized for the chains in a representative polymer sample but also it is known how much and which type of comonomer is incorporated per activation-growth-deactivation cycle and how many styrene units are present in a copolymer chain. For the MMA/styrene copolymerization, atypical RDRP distributions result, with in particular a large amount of zero-growth activation-growth-deactivation cycles and dormant copolymer chains with only a terminal styrene unit.

References

1. Braunecker, W. A.; Matyjaszewski, K. Controlled/living radical polymerization: Features, developments, and perspectives. *Prog. Polym. Sci.* **2007,** 32, (1), 93-146.

2. Matyjaszewski, K.; Davis, T. P., *Handbook of Radical Polymerization*. Wiley: 2002.

3. Matyjaszewski, K. Macromolecular engineering: From rational design through precise macromolecular synthesis and processing to targeted macroscopic material properties. *Progress in Polymer Science* **2005,** 30, (8-9), 858-875.

4. Lessard, B. H.; Ling, E. J. Y.; Marić, M. Fluorescent, Thermoresponsive Oligo(ethylene glycol) Methacrylate/9-(4-Vinylbenzyl)-9H-carbazole Copolymers Designed with Multiple LCSTs via Nitroxide Mediated Controlled Radical Polymerization. *Macromolecules* **2012,** 45, (4), 1879-1891.

5. Lessard, B.; Tervo, C.; De Wahl, S.; Clerveaux, F. J.; Tang, K. K.; Yasmine, S.; Andjelić, S.; D'Alessandro, A.; Marić, M. Poly(tert-butyl methacrylate/styrene) Macroinitiators as Precursors for Organo- and Water-Soluble Functional Copolymers Using Nitroxide-Mediated Controlled Radical Polymerization. *Macromolecules* **2010,** 43, (2), 868-878.

6. Zhou, Y.-N.; Luo, Z.-H. State-of-the-Art and Progress in Method of Moments for the Model-Based Reversible-Deactivation Radical Polymerization. *Macromol. React. Eng.* **2016,** 10, (6), 516-534.

7. Li, X.; Liang, S.; Wang, W.-J.; Li, B.-G.; Luo, Y.; Zhu, S. Model-Based Production of Polymer Chains Having Precisely Designed End-to-End Gradient Copolymer Composition and Chain Topology Distributions in Controlled Radical Polymerization, A Review. *Macromol. React. Eng.* **2015,** 9, (5), 409-417.

8. Nicolas, J.; Guillaneuf, Y.; Lefay, C.; Bertin, D.; Gigmes, D.; Charleux, B. Nitroxide-mediated polymerization. *Progress in Polymer Science* **2013,** 38, (1), 63-235.

9. Greszta, D.; Matyjaszewski, K. Mechanism of controlled/"living" radical polymerization of styrene in the presence of nitroxyl radicals. Kinetics and simulations. *Macromolecules* **1996,** 29, (24), 7661-7670.

10. Hawker, C. J.; Bosman, A. W.; Harth, E. New Polymer Synthesis by Nitroxide Mediated Living Radical Polymerizations. *Chem. Rev.* **2001,** 101, (12), 3661-3688.

11. Wang, L.; Broadbelt, L. J. Factors Affecting the Formation of the Monomer Sequence along Styrene/Methyl Methacrylate Gradient Copolymer Chains. *Macromolecules* **2009,** 42, (21), 8118-8128.

12. Wang, L.; Broadbelt, L. J. Kinetics of Segment Formation in Nitroxide-Mediated Controlled Radical Polymerization: Comparison with Classic Theory. *Macromolecules* **2010,** 43, (5), 2228-2235.

13. Ouchi, M.; Terashima, T.; Sawamoto, M. Transition Metal-Catalyzed Living Radical Polymerization: Toward Perfection in Catalysis and Precision Polymer Synthesis. *Chem. Rev.* **2009,** 109, (11), 4963-5050.

14. Wang, J. S.; Matyjaszewski, K. Controlled living radical polymerization - atom-transfer radical polymerization in the presence of transition-metal complexes. *J. Am. Chem. Soc.* **1995,** 117, (20), 5614-5615.

15. Magenau, A. J. D.; Kwak, Y.; Matyjaszewski, K. ATRP of Methacrylates Utilizing CuIIX2/L and Copper Wire. *Macromolecules* **2010,** 43, (23), 9682-9689.

16. Rosen, B. M.; Percec, V. Single-Electron Transfer and Single-Electron Transfer Degenerative Chain Transfer Living Radical Polymerization. *Chem. Rev.* **2009,** 109, (11), 5069-5119.

17. Nguyen, N. H.; Kulis, J.; Sun, H. J.; Jia, Z. F.; Van Beusekom, B.; Levere, M. E.; Wilson, D. A.; Monteiro, M. J.; Percec, V. A comparative study of the SET-LRP of oligo(ethylene oxide) methyl ether acrylate in DMSO and in H2O. *Polymer Chemistry* **2013,** 4, (1), 144-155.

18. Chiefari, J.; Chong, Y. K.; Ercole, F.; Krstina, J.; Jeffery, J.; Le, T. P. T.; Mayadunne, R. T. A.; Meijs, G. F.; Moad, C. L.; Moad, G.; Rizzardo, E.; Thang, S. H. Living free-radical polymerization by reversible addition-fragmentation chain transfer: The RAFT process. *Macromolecules* **1998,** 31, (16), 5559-5562.

19. Moad, G.; Rizzardo, E.; Thang, S. H. Living Radical Polymerization by the RAFT Process – A Third Update. *Aust. J. Chem.* **2012,** 65, (8), 985-1076.

20. Fischer, H. The persistent radical effect in controlled radical polymerizations. *J. Polym. Sci. Pol. Chem.* **1999,** 37, (13), 1885-1901.

21. Lutz, J. F.; Lacroix-Desmazes, P.; Boutevin, B. The persistent radical effect in nitroxide mediated polymerization: Experimental validity. *Macromol. Rapid Commun.* **2001,** 22, (3), 189-193.

22. Benoit, D.; Grimaldi, S.; Robin, S.; Finet, J. P.; Tordo, P.; Gnanou, Y. Kinetics and mechanism of controlled free-radical polymerization of styrene and n-butyl acrylate in the presence of an acyclic beta-phosphonylated nitroxide. *J. Am. Chem. Soc.* **2000,** 122, (25), 5929-5939.

23. Benoit, D.; Chaplinski, V.; Braslau, R.; Hawker, C. J. Development of a universal alkoxyamine for "living" free radical polymerizations. *J. Am. Chem. Soc.* **1999,** 121, (16), 3904-3920.

24. Guégain, E.; Guillaneuf, Y.; Nicolas, J. Nitroxide-Mediated Polymerization of Methacrylic Esters: Insights and Solutions to a Long-Standing Problem. *Macromol. Rapid Commun.* **2015,** 36, (13), 1227-1247.

25. Edeleva, M.; Marque, S. R. A.; Kabytaev, K.; Guillaneuf, Y.; Gigmes, D.; Bagryanskaya, E. H-transfer reaction during decomposition of N-(2-methylpropyl)- N-(1-diethylphosphono-2,2-dimethylpropyl)-N-oxyl (SG1)-based alkoxyamines. *Journal of Polymer Science Part A: Polymer Chemistry* **2013,** 51, (6), 1323-1336.

26. Edeleva, M. V.; Kirilyuk, I. A.; Zubenko, D. P.; Zhurko, I. F.; Marque, S. R. A.; Gigmes, D.; Guillaneuf, Y.; Bagryanskaya, E. G. Kinetic Study of H-Atom Transfer in Imidazoline-, Imidazolidine-, and Pyrrolidine-Based Alkoxyamines: Consequences for Nitroxide-Mediated Polymerization. *J. Polym. Sci. Pol. Chem.* **2009,** 47, (23), 6579-6595.

27. Edeleva, M.; Marque, S. R. A.; Bertin, D.; Gigmes, D.; Guillaneuf, Y.; Morozov, S. V.; Bagryanskaya, E. G. Hydrogen-Transfer Reaction in Nitroxide Mediated Polymerization of Methyl Methacrylate: 2.2-Diphenyl-3-phenylimino-2,3-dihydroindol-1-yloxyl Nitroxide (DPAIO) vs. TEMPO. *J. Polym. Sci. Pol. Chem.* **2008,** 46, (20), 6828-6842.

28. Gryn'ova, G.; Lin, C. Y.; Coote, M. L. Which side-reactions compromise nitroxide mediated polymerization? *Polym. Chem.* **2013,** 4, (13), 3744-3754.

29. Dire, C.; Belleney, J.; Nicolas, J.; Bertin, D.; Magnet, S.; Charleux, B. beta-hydrogen transfer from poly(methyl methacrylate) propagating radicals to the nitroxide SG1: Analysis of the chain-end and determination of the rate constant. *J. Polym. Sci. Pol. Chem.* **2008,** 46, (18), 6333-6345.

30. McHale, R.; Aldabbagh, F.; Zetterlund, P. B. The role of excess nitroxide in the SG1 (N-tert-butyl-N-[1-diethylphosphono-(2,2-dimethylpropyl)] nitroxide)-mediated polymerization of methyl methacrylate. *Journal of Polymer Science Part A: Polymer Chemistry* **2007,** 45, (11), 2194-2203.

31. Charleux, B.; Nicolas, J.; Guerret, O. Theoretical Expression of the Average Activation−Deactivation Equilibrium Constant in Controlled/Living Free-Radical Copolymerization Operating via Reversible Termination. Application to a Strongly Improved Control in Nitroxide-Mediated Polymerization of Methyl Methacrylate. *Macromolecules* **2005,** 38, (13), 5485-5492.

32. Nicolas, J.; Dire, C.; Mueller, L.; Belleney, J.; Charleux, B.; Marque, S. R. A.; Bertin, D.; Magnet, S.; Couvreur, L. Living character of polymer chains prepared via nitroxide-mediated controlled free-radical polymerization of methyl methacrylate in the presence of a small amount of styrene at low temperature. *Macromolecules* **2006,** 39, (24), 8274-8282.

33. Nicolas, J.; Mueller, L.; Dire, C.; Matyjaszewski, K.; Charleux, B. Comprehensive Modeling Study of Nitroxide-Mediated Controlled/Living Radical Copolymerization of Methyl Methacrylate with a Small Amount of Styrene. *Macromolecules* **2009,** 42, (13), 4470-4478.

34. Hawker, C. J.; Elce, E.; Dao, J.; Volksen, W.; Russell, T. P.; Barclay, G. G. Well-Defined Random Copolymers by a "Living" Free-Radical Polymerization Process. *Macromolecules* **1996,** 29, (7), 2686-2688.

35. Lessard, B. H.; Guillaneuf, Y.; Mathew, M.; Liang, K.; Clement, J.-L.; Gigmes, D.; Hutchinson, R. A.; Marić, M. Understanding the Controlled Polymerization of Methyl Methacrylate with Low Concentrations of 9-(4-Vinylbenzyl)-9H-carbazole Comonomer by Nitroxide-Mediated Polymerization: The Pivotal Role of Reactivity Ratios. *Macromolecules* **2013,** 46, (3), 805-813.

36. Nicolas, J.; Brusseau, S.; Charleux, B. A minimal amount of acrylonitrile turns the nitroxide-mediated polymerization of methyl methacrylate into an almost ideal controlled/living system. *Journal of Polymer Science Part A: Polymer Chemistry* **2010,** 48, (1), 34-47.

37. Ballard, N.; Aguirre, M.; Simula, A.; Agirre, A.; Leiza, J. R.; Asua, J. M.; van Es, S. New Class of Alkoxyamines for Efficient Controlled Homopolymerization of Methacrylates. *ACS Macro Letters* **2016,** 5, (9), 1019-1022.

38. Simula, A.; Aguirre, M.; Ballard, N.; Veloso, A.; Leiza, J. R.; van Es, S.; Asua, J. M. Novel alkoxyamines for the successful controlled polymerization of styrene and methacrylates. *Polymer Chemistry* **2017,** 8, (10), 1728-1736.

39. Wieme, J.; D'hooge, D. R.; Reyniers, M. F.; Marin, G. B. Importance of Radical Transfer in Precipitation Polymerization: The Case of Vinyl Chloride Suspension Polymerization. *Macromol. React. Eng*. **2009,** 3, (1), 16-35.

40. Derboven, P.; Van Steenberge, P. H. M.; Vandenbergh, J.; Reyniers, M.-F.; Junkers, T.; D'hooge, D. R.; Marin, G. B. Improved Livingness and Control over Branching in RAFT Polymerization of Acrylates: Could Microflow Synthesis Make the Difference? *Macromol. Rapid Commun.* **2015,** 36, (24), 2149-2155.

41. Kiparissides, C.; Daskalakis, G.; Achilias, D. S.; Sidiropoulou, E. Dynamic Simulation of Industrial Poly(vinyl chloride) Batch Suspension Polymerization Reactors. *Industrial & Engineering Chemistry Research* **1997,** 36, (4), 1253-1267.

42. Hamzehlou, S.; Ballard, N.; Reyes, Y.; Aguirre, A.; Asua, J. M.; Leiza, J. R. Analyzing the discrepancies in the activation energies of the backbiting and beta-scission reactions in the radical polymerization of n-butyl acrylate. *Polymer Chemistry* **2016,** 7, (11), 2069-2077.

43. Yu, X.; Broadbelt, L. J. Kinetic Study of 1,5-Hydrogen Transfer Reactions of Methyl Acrylate and Butyl Acrylate Using Quantum Chemistry. *Macromol. Theory Simul.* **2012,** 21, (7), 461-469.

44. Yao, F.; Michael, F. C.; Robin, A. H. Modeling of Nitroxide-Mediated Semibatch Radical Polymerization. *Macromol. React. Eng.* **2007,** 1.

45. Payne, K. A.; Nesvadba, P.; Debling, J.; Cunningham, M. F.; Hutchinson, R. A. Nitroxide-Mediated Polymerization at Elevated Temperatures. *ACS Macro Letters* **2015,** 4, (3), 280-283.

46. Bentein, L.; D'hooge, D. R.; Reyniers, M. F.; Marin, G. B. Kinetic Modeling as a Tool to Understand and Improve the Nitroxide Mediated Polymerization of Styrene. *Macromol. Theory Simul.* **2011,** 20, (4), 238-265.

47. Junkers, T. Precision Polymer Design in Microstructured Flow Reactors: Improved Control and First Upscale at Once. *Macromol. Chem. Phys.* **2017,** 218, (2), 1600421-n/a.

48. Van Steenberge, P. H. M.; D'hooge, D. R.; Reyniers, M. F.; Marin, G. B. Improved kinetic Monte Carlo simulation of chemical composition-chain length distributions in polymerization processes. *Chem. Eng. Sci.* **2014,** 110, 185-199.

49. Fierens, S. K.; Telitel, S.; Van Steenberge, P. H. M.; Reyniers, M.-F.; Marin, G. B.; Lutz, J.-F.; D'hooge, D. R. Model-Based Design To Push the Boundaries of Sequence Control. *Macromolecules* **2016,** 49, (24), 9336-9344.

50. Fierens, S. K.; D'hooge, D. R.; Van Steenberge, P. H. M.; Reyniers, M.-F.; Marin, G. B. MAMA-SG1 initiated nitroxide mediated polymerization of styrene: From Arrhenius parameters to model-based design. *Chem. Eng. J.* **2015,** 278, 407-420.

51. Guillaneuf, Y.; Gigmes, D.; Marque, S. R. A.; Tordo, P.; Bertin, D. Nitroxide-Mediated Polymerization of Methyl Methacrylate Using an SG1-Based Alkoxyamine: How the Penultimate Effect Could Lead to Uncontrolled and Unliving Polymerization. *Macromol. Chem. Phys.* **2006,** 207, (14), 1278-1288.

52. Beaudoin, E.; Bertin, D.; Gigmes, D.; Marque, S. R. A.; Siri, D.; Tordo, P. Alkoxyamine C–ON Bond Homolysis: Stereoelectronic Effects. *European Journal of Organic Chemistry* **2006,** 2006, (7), 1755-1768.

53. Coote, M. L.; Davis, T. P. The mechanism of the propagation step in free-radical copolymerisation. *Progress in Polymer Science* **1999,** 24, (9), 1217-1251.

54. Coote, M. L.; Johnston, L. P. M.; Davis, T. P. Copolymerization Propagation Kinetics of Styrene and Methyl Methacrylate-Revisited. 2. Kinetic Analysis. *Macromolecules* **1997,** 30, (26), 8191-8204.

55. Dossi, M.; Moscatelli, D. A QM Approach to the Calculation of Reactivity Ratios in Free-Radical Copolymerization. *Macromol. React. Eng.* **2012,** 6, (2-3), 74-84.

56. Fierens, S. K.; D'hooge, D. R.; Van Steenberge, P. H. M.; Reyniers, M.-F.; Marin, G. B. How penultimate monomer unit effects and initiator choice influence ICAR ATRP of n-butyl acrylate and methyl methacrylate. *AIChE Journal* **2017**, DOI: 10.1002/aic.15851.

57. D'hooge, D. R.; Reyniers, M.-F.; Marin, G. B. The Crucial Role of Diffusional Limitations in Controlled Radical Polymerization. *Macromol. React. Eng.* **2013,** 7, (8), 362-379.

58. Derboven, P.; D'hooge, D. R.; Reyniers, M.-F.; Marin, G. B.; Barner-Kowollik, C. The Long and the Short of Radical Polymerization. *Macromolecules* **2015,** 48, (3), 492-501.

59. Johnston-Hall, G.; Monteiro, M. J. Bimolecular radical termination: New perspectives and insights. *J. Polym. Sci. Pol. Chem.* **2008,** 46, (10), 3155-3173.

60. Beuermann, S.; Buback, M.; Davis, T. P.; Gilbert, R. G.; Hutchinson, R. A.; Olaj, O. F.; Russell, G. T.; Schweer, J.; van Herk, A. M. Critically evaluated rate coefficients for free-radical polymerization, 2.. Propagation rate coefficients for methyl methacrylate. *Macromol. Chem. Phys.* **1997,** 198, (5), 1545-1560.

61. Fierens, S. K.; D'hooge, D. R.; Van Steenberge, P. H. M.; Reyniers, M.-F.; Marin, G. B. Exploring the Full Potential of Reversible Deactivation Radical Polymerization Using Pareto-Optimal Fronts. *Polymers* **2015,** 7, (4), 655.

62. Bertin, D.; Dufils, P. E.; Durand, I.; Gigmes, D.; Giovanetti, B.; Guillaneuf, Y.; Marque, S. R. A.; Phan, T.; Tordo, P. Effect of the penultimate unit on the C-ON bond homolysis in SGi-based alkoxyamines. *Macromol. Chem. Phys.* **2008,** 209, (2), 220-224.

Chapter 8. General conclusions and future outlook

8.1 General conclusions

In this PhD thesis, a synergistic combination of experimental study and kinetic modeling is applied to obtain fundamental insights in and formulate optimization strategies for several well-established reversible deactivation radical polymerization (RDRP) techniques. Therefore, the generic LCT modeling platform is extended. This platform consists out of a fast deterministic simulation method which will be used for estimation of rate coefficients and, for the first time, Pareto optimization of RDRPs. The second simulation method is a matrix-based kinetic Monte Carlo technique (stochastic) which allows highly detailed kinetic and microstructural insights albeit at a higher computational cost. This allows tracking of the time evolution of the explicit microstructure and *a posteriori* calculation of novel distributions. The complex interplay between intrinsic reaction kinetics and physical phenomena, such as diffusional limitations due to the viscosity increase inherently present in polymerization reactions, is always accounted for.

Chapter 1 provides a general introduction of RDRP techniques focusing mainly on the techniques applied in this PhD thesis, *i.e.* nitroxide mediated polymerization and two modified atom transfer radical polymerization (ATRP) techniques, namely initiators for continuous activator regeneration (ICAR) ATRP and activators regenerated by electron transfer (ARGET) ATRP. These kinetic features of these techniques are briefly discussed after which the scope of this PhD thesis is clarified.

In **Chapter 2**, an in-depth discussion of the state-of-the art copolymer models is provided focusing on both kinetic, such as the propagation rate, and microstructural properties, *e.g.* sequence length distribution. Both analytically derived and numerical models are discussed. A

discussion is provided according to the level of detail provided by the model starting with models describing only average properties such as for example the instantaneous copolymer composition. Next, models that allow the description of uni- and bivariate distributions are discussed. From these discussions, it can be concluded that the aforementioned models require assumptions resulting in a loss of detail. By using explicit models, based on stochastic *k*MC codes, no such assumptions are needed and the entire reaction history and polymer microstructure can be tracked. This allows the *a posteriori* calculation of several novel (multi)variate distributions as has been done in various chapters of this PhD thesis.

In **Chapter 3** a combined experimental and modeling study into the NMP of styrene initiated by MAMA-SG1. A large experimental data set is obtained for a wide range of temperatures (90-120°C) and targeted chain lengths (TCL; 100-1000). From this experimental data, a loss of control for the higher TCLs can be observed based on the evolution of the dispersity (*Đ*). Based on this experimental data set, multi-response regression analysis based on conversion, number-averaged chain length (x_n) and *Đ* data was performed using the Levenberg-Marquardt algorithm (ODR-pack) combined with a deterministic model. This allowed to estimate values for the 4 NMP specific Arrhenius parameters in a statistically sound manner. These values are in line with experimentally determined values in literature. Subsequently, these values are used in a *k*MC code for more advanced predictions of the microstructure. For example, the predicted complete molar mass distribution (MMD) is tested against the experimentally obtained MMD and displays a good fit. For the first time, the microstructure of the polymer chains is visualized while at the same time differentiating according to their initiation or termination mechanism. From these results, it can be concluded that the chain transfer to dimer reaction is the main deteriorating factor resulting in a loss of control for higher TCLs. Finally, the beneficial use of a simple

stepwise temperature program is demonstrated *in silico* and verified experimentally. Simulations allowed to conclude that a more efficient initiation phase is the underlying reason for the improvement in the polymer microstructure.

In **Chapter 4**, the beneficial use of multi-objective optimization algorithms is demonstrated, for the first time, for the optimization of RDRP techniques. These algorithms allow the optimization of design problems with conflicting attributes resulting in the identification of the Pareto-optimal front. The widely applied NSGA-II algorithm was implemented into FORTRAN and used for the optimization of the ARGET ATRP of butyl methacrylate and NMP of styrene. For ARGET ATRP two objectives, *i.e.* batch time (for an overall conversion (X_M) of 0.75) and final $Đ$, are considered. Temperature, monomer addition, and reducing agent addition programs and the combinations thereof as optimization strategies are considered. A Pareto-optimal front for all three individual strategies was identified with a monomer addition as the most promising one. Combinations of individual strategies display synergistic effects leading to a more improved Pareto-optimal front. Explanation of the optimization strategies is provided based on the kinetic significance of several key reactions, such as the termination probability and the ratio of propagation to deactivation probability (P_{prop}/P_{deac}). The optimization of NMP of styrene included 3 objectives: time (X_M = 0.75), $Đ$, and end-group functionality (EGF) including temperature -, monomer addition -, and initial nitroxide amount programs. The NSGA-II algorithm identified Pareto optimal fronts for all individual strategies, showing that a temperature program is most promising. Again, a kinetic explanation of the obtained optimization pathways is provided by considering the termination probability and P_{prop}/P_{deac}, as well as the reaction probability for the transfer to dimer reaction.

Chapter 5 considers the synthesis of sequence-controlled copolymers via NMP. These systems allow the incorporation of functional monomer at desired positions in the polymer chain by using an electron-donor and an electron-acceptor comonomer which display strongly alternating propagation behavior. First, an experimental data set, using BlocBuilder as NMP initiator and styrene and *N*-benzyl maleimide (BzMI) is gathered. This experimental data, including comonomer conversion and dispersity, is successfully predicted by the developed kinetic Monte Carlo model. Subsequently, the *k*MC model is used for explicit visualization of the copolymer chains from which novel insights into the precision of the functional monomer placement in the chains can be *a posteriori* extracted. A rather broad distribution of the functional monomer placement results, around both its absolute and relative position along the polymer chain. The incorporation of the number of functional monomers per polymer chain is also far from ideal, displaying a broad distribution. Upon using 1 equivalent BzMI with respect to the initial monomer concentration, a number fraction of approx. 0.45 of the polymer chains remains non-functionalized. For the first time, a quantification of the distribution of activation-growth-deactivation cycles with respect to their number of propagation steps is extracted from the *k*MC simulations. *In silico* model-based optimization allowed to identify fed-batch monomer programs which result in an improved position of the BzMI functionality. Grid simulations varying the activation (k_a) and deactivation rate coefficient (k_{da}) were performed to identify the optimal reactivity of the mediating agent. It is concluded that the SG1 nitroxide does not possess optimal mediating qualities toward sequence-controlled polymer synthesis. A nitroxide possessing a higher k_{da} results in a better distribution of the functional monomer units among the polymer chains. Finally, the model-based optimized strategy is demonstrated for a trifunctionalized sequence-controlled poly(styrene) product.

The importance of penultimate monomer unit (PMU) effects are demonstrated in **Chapter 6** for the ICAR ATRP of *n*-butyl acrylate (*n*BA) and methyl methacrylate (MMA), which yields a gradient copolymer. A literature based kinetic model is implemented in the *k*MC code and grid simulations allowed to identify a suitable ATRP initiator. It is shown that a tertiary ATRP initiator is preferred over a secondary ATRP initiator as the latter leads to too slow initiation, thereby deteriorating the microstructural control. A two-step initiation stage is present for the tertiary initiator, due to strong differences in the reactivities of the different macrospecies. The importance of PMU effects on propagation and (de)activation show to be crucial for an accurate description of the copolymerization kinetics. The former are more relevant for the initiation stage whereas the latter mostly influence the (de)activation equilibrium at higher conversions. The temperature dependence of the reactivity ratios, an often overlooked aspect, proves to be non-negligible. Finally, the naturally occurring gradient is improved by applying a fed-batch monomer addition program resulting in a better gradient quality (<*GD*>). It is demonstrated how the PMU affects the <*GD*> in the *in silico* determination of ideal monomer feeding programs. In conclusion, this chapter is a strong message towards the polymer community that the effect of the PMU should always be considered in kinetic modeling studies for copolymerizations as it can have a large effect on the kinetics and microstructure. As a corollary, attention should be paid to the determination of such rate coefficients since for many systems reactivity ratios are lacking and a large scatter on the reported values exists.

In **Chapter 7** a combined experimental and modelling study for NMP of MMA with and without a small amount of styrene is presented. The importance of non-isothermal conditions, leading to a temperature overshoot with respect to the set temperature, is demonstrated in view of accurate description of the experimental data. The NMP of MMA fails due to a too large (de)activation

equilibrium and the occurrence of disproportionation of the nitroxide SG1 may with MMA macroradicals. For the latter, an updated Arrhenius rate coefficient is reported based on dedicated homopolymerization experiments for 3 distinct temperatures. By using the comonomer approach, *i.e.* adding a small amount of monomer (styrene) with a much smaller (de)activation equilibrium coefficient, control over the NMP can be improved. A large set of experimental data is adequately described by adjusting only the activation radical reactivity ratio (for macrospecies with styrene terminal unit). The *k*MC code is applied to map the influence of the initial styrene content and identify thresholds for acceptable control which shows that an initial styrene content of approx. 10 m% is needed for acceptable control and that control is lost for higher TCLs. Insights into the explicit copolymer microstructure are provided as well as into the individual activation-growth-deactivation cycles, which display atypical distributions for RDRP processes, as the zero-growth cycles are promoted by the presence of a small styrene amount.

Additionally, the state of the art of explicit kinetic Monte Carlo modeling of polymerizations has been advanced. It has been demonstrated that explicit modeling allows to extract novel and useful distributions: the distribution of (relative and absolute) positions of functionalities along polymer chains (Chapter 5), the distribution of functionalities over the polymer chains (Chapter 5) and the distribution of activation-growth-deactivation cycles with respect to their propagation steps (Chapter 5-7).

8.2 Future outlook

In the research presented in this thesis, the synergetic effects originating from reagent addition and temperature programs (Chapter 4) have been determined *in silico* and an experimental verification of these results would benefit the development of NMP and ARGET ATRP towards improved control within reasonable reaction times. Applying MOO-algorithms towards other

RDRP techniques and more complex macromolecular architecture such as gradient, graft and star copolymers, not only in homogeneous but also heterogeneous media, can be expected to lead to interesting insights and improved understanding in for example optimization of the droplet size distribution.

In general, understanding how adjusting macroscopic variables (temperature, concentrations, reactant feeding) affect polymer microstructure on the microscale is crucial to improve our capability to synthesize next-generation polymers. One pre-requisite is that rate coefficients must be accurately determined. Systematic approaches as presented in Chapter 3, wherein a large set of experimental data is fitted using regression analysis, are important to characterize the reactivity of novel mediating agents, which are still being discovered and developed. Reversely, the model-based design of sequence-controlled polymers allows the identification of the required reactivity of an (as yet) unknown mediating agent, which may aid in the synthesis of tailor-made mediating agents (Chapter 5).

A second pre-requisite is to advance the state-of-the-art of kinetic modeling. Explicit kinetic Monte Carlo modeling has proven to be an indispensable tool when a high level of detail into the kinetics and microstructure is needed. Many (co)polymerizations remain unexplored and could benefit from the novel distributions used in this thesis. More complex architectures are of interest: branched polymers can be investigated to gain insight in the position of branches along the polymer chains, possibly combined with monomer feeding to tune the average distance between branches. For network copolymers, segment length distributions and pore size distributions will become accessible via simulation, further aiding model-based design of complex macromolecular architectures.

Such complex macromolecular architectures should, at least in principle, display different diffusion behavior compared to linear polymer chains. Hence, diffusion behavior can be more precisely defined and modeled if the chain architecture is explicitly accounted for in kinetic models.

A third resource for the synthesis of next-generation polymers are the ever-increasing computer resources. These will allow computational chemists to investigate increasingly larger molecules, which are necessary for the accurate determination of the monomer and radical reactivity ratios in copolymerizations where PMU effects play a major role. These effects have shown to play an important role for the microstructure of the final polymer product.

Such developments will positively affect the model-based design of next-generation polymers.

Appendix A. MAMA-SG1 initiated nitroxide mediated polymerization of styrene: from Arrhenius parameters to model-based design

A.1 Overview experimental conditions

Table A.1. *Overview of polymerization conditions covered in the experimental study of NMP of styrene initiated by BlocBuilder MA; 6% decane was added on a volume basis (with respect to monomer) to allow for GC analysis; TCL: targeted chain length: initial molar ratio of monomer to NMP initiator.*

Entry	Temperature (°C)	TCL (-)	Nr. of exp. points
1	90	100	8
2	90	300	10
3	100	100	8
4	100	500	10
5	100	1000	10
6	110	300	10
7	110	500	10
8	110	1000	10
9	120	100	10
10	120	500	10
11	120	1000	10
12	100	300	10
13	100	750	10
14	110	750	10
15	120	300	10
16	120	750	10
17[(a)]	103-118	1000	6

[(a)] Experiment performed with step-wise temperature profile as obtained via model-based design (103°C for first 30 minutes, 118°C for the remainder of the polymerization). Not included in estimation procedure (only use of isothermal conditions: entry 1-16).

A.2 Consistency check of gravimetrical and gas chromatography data on conversion data

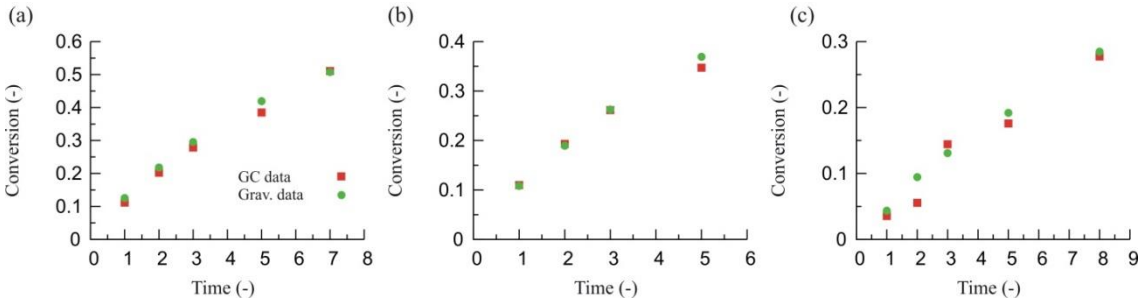

Figure A.1. *Comparison of monomer conversion date obtained via gravimetrical (●, green) and GC analysis (■, red) for NMP of styrene initiated by BlocBuilder MA: (a) T=110 °C; TCL: 500 (Table S.1 Entry 7); (b) T=110 °C; TCL: 750 (Table A.1 Entry 14); (c) T=100 °C; TCL: 300 (Table A.1 Entry 12).*

Clearly, a good agreement is obtained. For the regression analysis, the monomer conversions as obtained with gravimetric analysis are used.

A.3 Reproducibility check of data used for multi-response regression analysis

Figure A.2 shows for two polymerization conditions the results concerning the reproducibility. Clearly, the reproducibility is good. Based on all reproducibility experiments, average errors could be calculated for the conversion (X_m), number averaged chain length (x_n), and dispersity ($Đ$). This gave a relative error of 5% for the the conversion (X_m) and number averaged chain length (x_n). On dispersity ($Đ$) an absolute error of 0.05 is obtained.

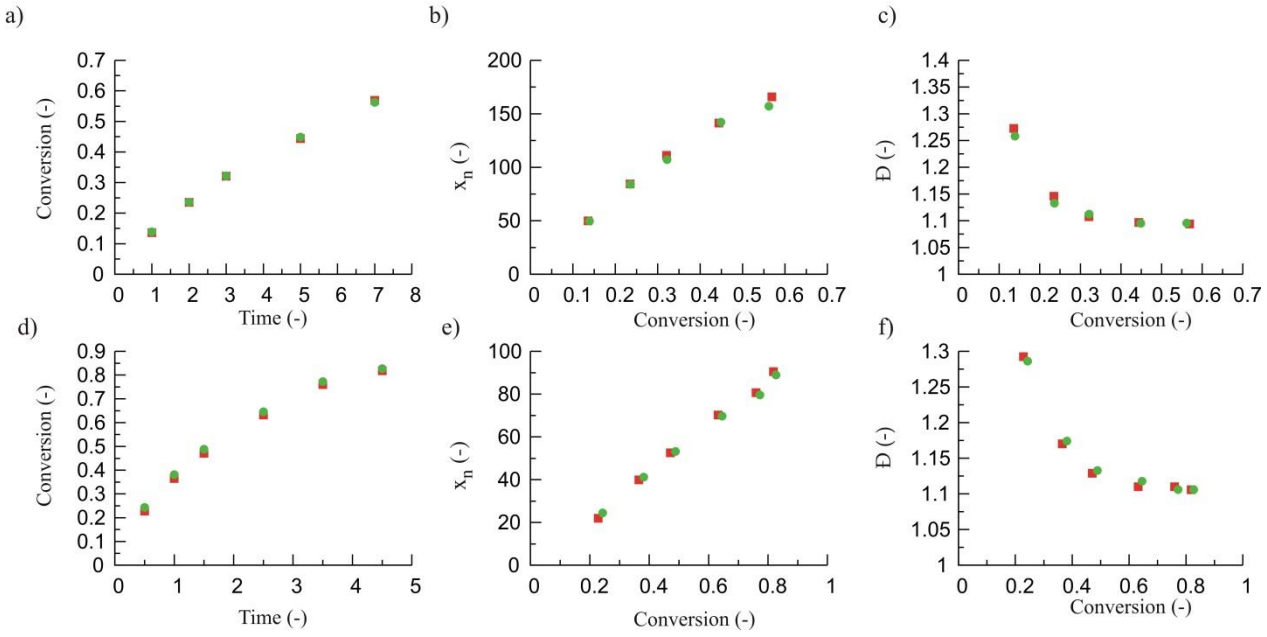

Figure A.2. *Reproducibility measurements for NMP of styrene initiated by BlocBuilder MA at (a)-(c): 110 (TCL 300) (Table A.1 Entry 6) correspond to the two repeated experiments; (d)-(e) 120 °C (TCL 100) (Table A.1 Entry 9); (●, green) and (●, red) correspond to two reproducibility experiments; (a),(d) Conversion as a function of time, (b),(e) and number-averaged chain length, and (c),(f) dispersity as a function of conversion.*

A.4 Apparent termination rate coefficients

Apparent "homo-termination" rate coefficients (equal (average) chain lengths) as determined with the so-called composite k_t model are used as a function of polymer mass fraction w_p, as also done in the recent work of Toloza Porras *et al.* [1]. The corresponding equations are given below:

$$\text{for } i < i_{\text{gel}} \text{ and } i < i_{\text{SL}}\text{: } k_{\text{t,ii}}^{\text{app}} = k_{\text{t,11}}^{\text{app}} i^{-\alpha_{\text{s}}}$$

$$\text{for } i < i_{\text{gel}} \text{ and } i \geq i_{\text{SL}}\text{: } k_{\text{t,ii}}^{\text{app}} = k_{\text{t,11}}^{\text{app}} i_{\text{SL}}^{\alpha_{\text{l}}-\alpha_{\text{s}}} i^{-\alpha_{\text{l}}}$$

$$\text{for } i \geq i_{\text{gel}} \text{ and } i < i_{\text{SL}}\text{: } k_{\text{t,ii}}^{\text{app}} = k_{\text{t,11}}^{\text{app}} i_{\text{gel}}^{\alpha_{\text{gel}}-\alpha_{\text{s}}} i^{-\alpha_{\text{gel}}}$$

$$\text{for } i \geq i_{\text{gel}} \text{ and } i < i_{\text{SL}}\text{: } k_{\text{t,ii}}^{\text{app}} = k_{\text{t,11}}^{\text{app}} i_{\text{SL}}^{\alpha_{\text{l}}-\alpha_{\text{s}}} i_{\text{gel}}^{\alpha_{\text{gel}}-\alpha_{\text{l}}} i^{-\alpha_{\text{gel}}}$$

Table A.2. *Parameters used for the composite k_t model to simulate the NMP of styrene initiated by BlocBuilder MA; w_p = weight fraction of polymer.*

α_s	α_l	α_{gel}	i_{SL}	i_{gel}	$k_{t,11}^{app}$
0.55	0.15	$(1.22\times w_p) - 0.11$	30	$3.3 \times w_p^{-2.13}$	$5.11\times10^9\exp(-7\times10^3/R/T)$

The parameters of the corresponding correlations are taken from reversible addition-fragmentation chain transfer chain length dependent termination (RAFT-CLD-T) measurements at 90°C [2]. The value of k_t^{11} was however extrapolated from the value reported to a value at the desired temperature using the activation energy determined by Hui *et al.* [3].

A.5 Consistency check deterministic and kinetic Monte Carlo code

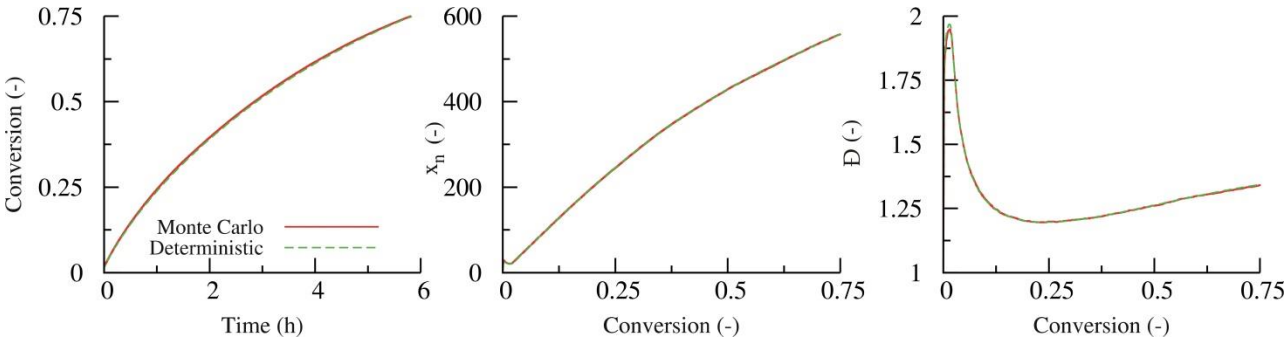

Figure A.3. *Comparison between the simulation results of the deterministic code for the NMP initiated by BlocBuilder MA at 120°C (TCL = 1000) (green dashed line) and the kinetic Monte Carlo code (red full line). (a) conversion as a function of time; (b) number averaged chain length as a function of conversion; (c) Dispersity as a function of conversion.*

Clearly, a perfect match is obtained.

A.6 Correlation matrix

Table A.3. *Correlation matrix for the 6 estimated parameters obtained in this work*

	$A*_{a0}$	$A*_{a}$	A_{da0}	A_{da}	$E_{a,a0}$	$E_{a,a}$
$A*_{a0}$	1.00					
$A*_{a}$	0.36	1.00				
A_{da0}	-0.14	-0.35	1.00			
A_{da}	-0.23	0.66	-0.02	1.00		
$E_{a,a0}$	-0.14	-0.10	-0.36	-0.25	1.00	
$E_{a,a}$	0.15	0.62	-0.30	0.21	0.19	1.00

Clearly, the absolute values are much lower then 0.95, indicative a very weak correlation and thus a very reliable parameter estimation.[4]

A.7 Experimental vs. simulation results for the excluded conditions in the main text

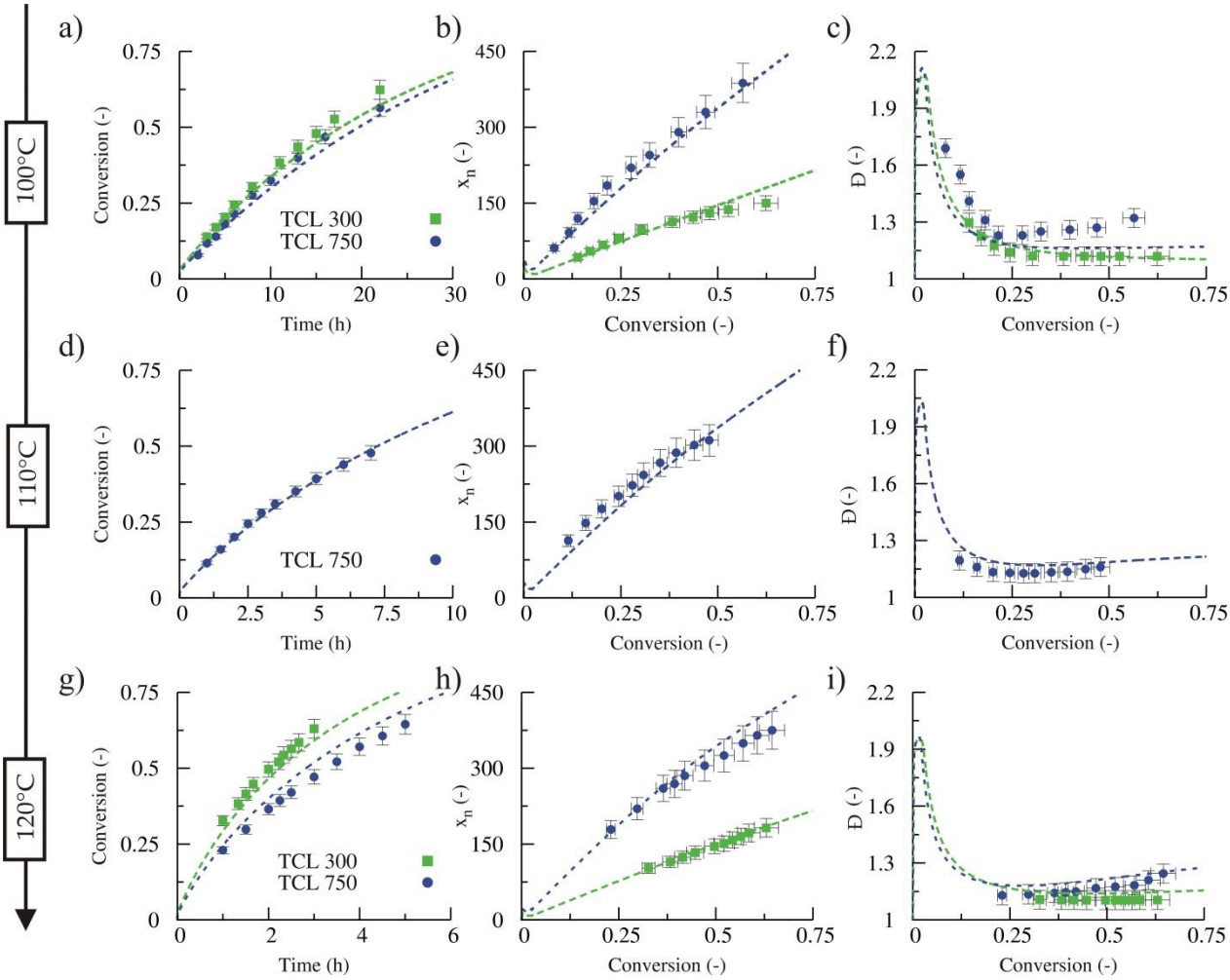

Figure A.4. *Comparison between simulations and experiments: effect of temperature for different TCLs (a),(d),(g) Conversion as a function of time; (b),(e),(h) number-average chain length (x_n), (c),(f),(i) dispersity (Đ) as a function of conversion for the NMP of styrene initiated by BlocBuilder MA at 100°C, 110°C, and 120°C. From the top row to the bottom row, respectively. (■, green) corresponds to a TCL of 300; (●, blue) corresponds to a TCL of 750; points correspond to experimental data; lines correspond to calculated values with set of parameters given in Table A.2; deterministic solver used; entries 12-16 in Table A.1 in Supporting Information.*

A.8 Comparison of simulated and measured SEC profiles for different conversions at a TCL of 300

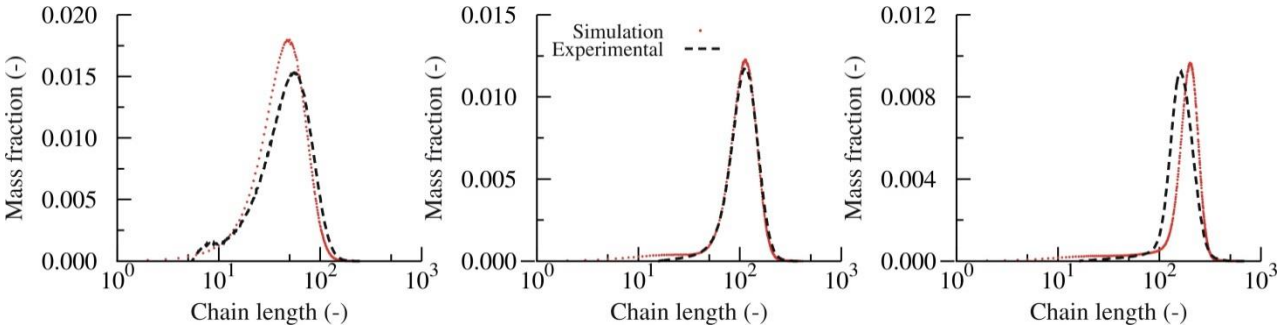

Figure A.5. *Chain length distributions (CLDs) obtained via SEC measurements (black dashed line) and via kMC simulation results (red points) for a TCL of 300 at a temperature of 110°C at a conversion of 0.15 (a), X_m = 0.15, (b) X_m = 0.35, (c) X_m = 0.60.*

As for the effect of the TCL in the main text, a relatively good agreement is obtained. Deviations at the lower chain lengths can be partially attributed to the difficult calibration in this region of the CLD [5].

References

1. Toloza Porras, C.; D'hooge, D. R.; Van Steenberge, P. H. M.; Reyniers, M.-F.; Marin, G. B. ICAR ATRP for Estimation of Intrinsic Macro-Activation/Deactivation Arrhenius Parameters under Polymerization Conditions. *Industrial & Engineering Chemistry Research* **2014**.

2. Johnston-Hall, G.; Monteiro, M. J. Bimolecular radical termination: New perspectives and insights. *J. Polym. Sci. Pol. Chem.* **2008,** 46, (10), 3155-3173.

3. Hui, A. W.; Hamielec, A. E. Thermal polymerization of styrene at high conversions and temperatures. An experimental study. *J. Appl. Polym. Sci.* **1972,** 16, (3), 749-769.

4. Heynderickx, P. M.; Thybaut, J. W.; Poelman, H.; Poelman, D.; Marin, G. B. The total oxidation of propane over supported Cu and Ce oxides: A comparison of single and binary metal oxides. *J. Catal.* **2010,** 272, (1), 109-120.

5. Payne, K. A.; D'hooge, D. R.; van Steenberge, P. H. M.; Reyniers, M. F.; Cunningham, M. F.; Hutchinson, R. A.; Marin, G. B. ARGET ATRP of Butyl Methacrylate: Utilizing Kinetic Modeling To Understand Experimental Trends. *Macromolecules* **2013,** 46, (10), 3828-3840.

Appendix B. Exploring the full potential of reversible deactivation radical polymerization using Pareto-optimal fronts

In this Appendix addition Tables, Schemes, and Figures are given relating to the discussion of following subjects in the main text:

(i) a brief description of the mathematical model based on the method of moments

(ii) the genetic optimization algorithm NSGA-II

(iii) the multi-objective optimization results for ARGET ATRP of BMA

(iv) the multi-objective optimization results for NMP of styrene

B.1 Description of the mathematical model

In this work, a deterministic modeling approach is considered for the description of the evolution of polymerization kinetics . For simplicity, the method of moments is applied in which the chain length distribution (CLD) is described by a limited number of characteristic points. The CLD is namely represented by a discrete number of *s*-th (s >0) order averages:

$$x_s = \frac{\sum_i i^s([R_i] + [P_i] + [R_iX])}{\sum_i i^{s-1}([R_i] + [P_i] + [R_iX])}$$

In this equation, $[R_i]$,$[P_i]$, and $[R_iX]$ are, respectively, the concentration of radicals, dead polymer molecules, and dormant polymer molecules with chain length i. Typically for RDRP processes the calculation is limited to the first and second (s = 1,2) order average. These two averages are also known as the number-, mass-averaged chain length (x_n and x_m). The relative position of these averages can be reflected by the dispersity which allows to assess the broadness of the CLD:

$$Đ = \frac{x_m}{x_n}$$

For more details on the method of moments, the reader is referred to specialized literature [1, 2].

B.2 Genetic optimization algorithm NSGA-II

In this work, several preliminary simulations were performed in order to select the optimal NSGA-II parameters and every simulation was performed multiple times using different random numbers sequences and checked for convergence.

Table B.1. *NSGA-II GA parameter values used.* [3]

Parent population size[(a)]	200*/400**
Selection strategy	Binary tournament
Crossover type	Simulated binary crossover
Mutation type	Polynomial mutation
Crossover probability	0.9
Mutation probability (real)	0.05
Distribution index crossover	5
Distribution index mutation	1
Numbers of generations	125*/150**

(a) *Parent population size equal to offspring population size; * relates to single variation optimization studies, ** relates to multiple variation (combinations of individual optimization pathways) optimization studies*

Table B.2. *Overview of upper and lower boundaries of the variables used in the MOO-optimizations. For simultaneous variation of process conditions identical boundaries were used is in the single variation studies; in all cases the final (overall) conversion is 0.75.*

Type of optimization		Lower-upper boundary
ARGET ATRP temperature profile		
	Var1-7	60-90 °C
ARGET ATRP monomer addition*		
	Var1	0.15-1 (-)
	Var2-7	0-1 (-)
ARGET ATRP reducing agent addition*		
	Var1-7	0-1 (-)
NMP temperature profile		
	Var1-7	80-120°C
NMP monomer addition*		
	Var1	0.1-1 (-)
	Var2-7	0-1 (-)
NMP initial nitroxide loading		
	Var1	0-0.5 (-)

*sum of fractions equal to 1.

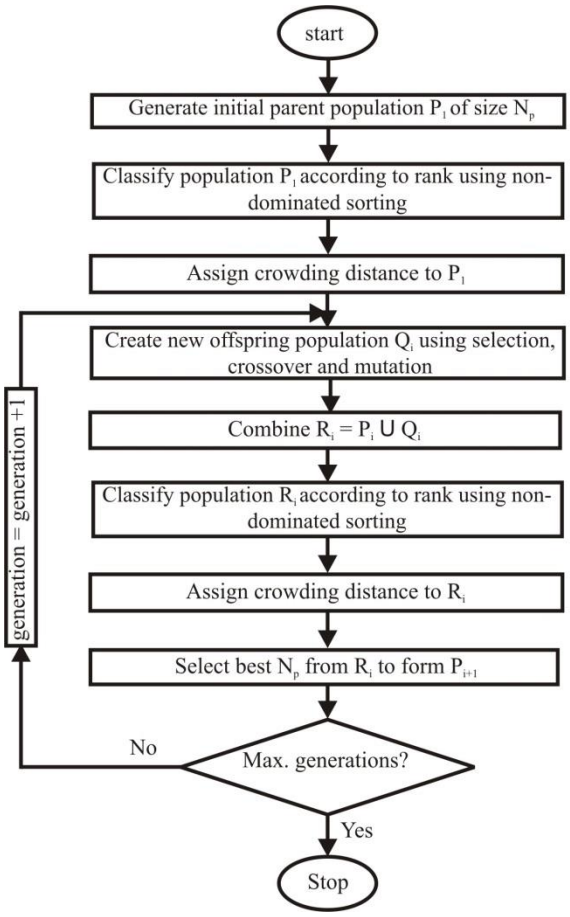

Figure B.1. Flowchart of the NSGA-II algorithm

B.3 Multi-objective optimization results for ARGET ATRP of BMA

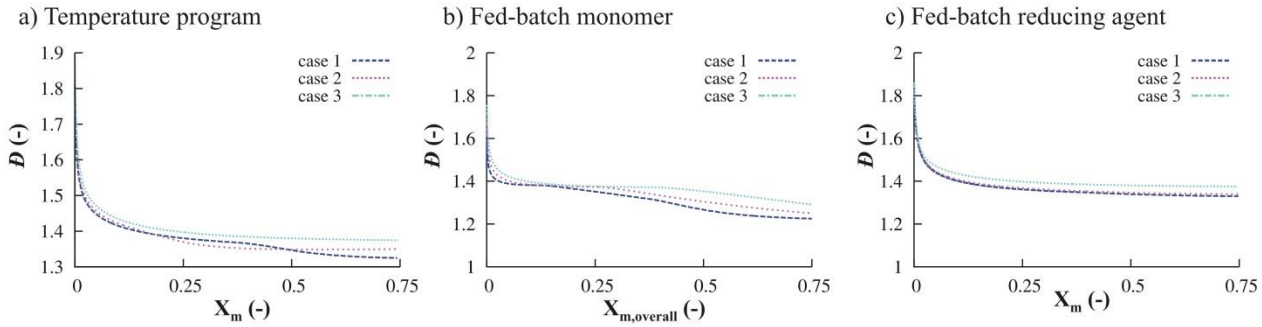

Figure B.2. *Dispersity (Đ) profiles as a function of conversion for the 3 selected cases for the MOO-studies of the ARGET ATRP of BMA using (a) a piecewise linear temperature program (Figure 4.2; Main text); (b) a fed-batch monomer program (Figure 4.4; Main text); (c) a fed-batch reducing agent program (Figure 4.5; Main text).*

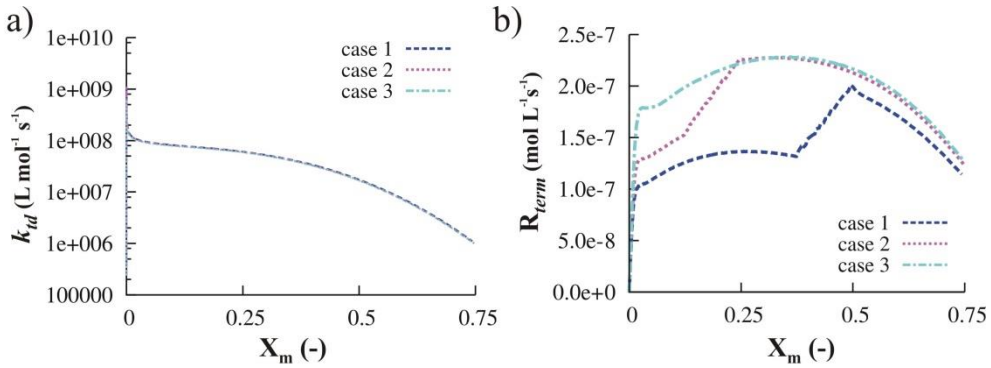

Figure B.3. *(a) Apparent rate coefficient for termination by disproportionation (recombination similar profile) as a function of conversion and (b) Termination rate as a function of conversion for the 3 selected cases for the MOO-studies of the ARGET ATRP of BMA using a piecewise linear temperature program (Figure 4.2; Main text).*

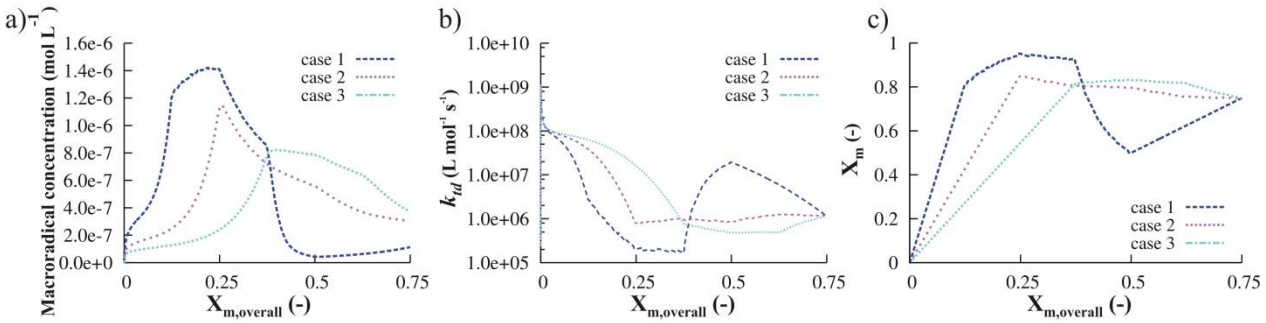

Figure B.4. *(a) Macroradical concentration as a function of the overall conversion (b) Apparent rate coefficient for termination by disproportionation (recombination similar profile) as a function of the overall conversion (c) in situ conversion as a function of the overall conversion for the 3 selected cases for the MOO-studies of the ARGET ATRP of BMA using a fed-batch monomer program (Figure 4.4; Main text).*

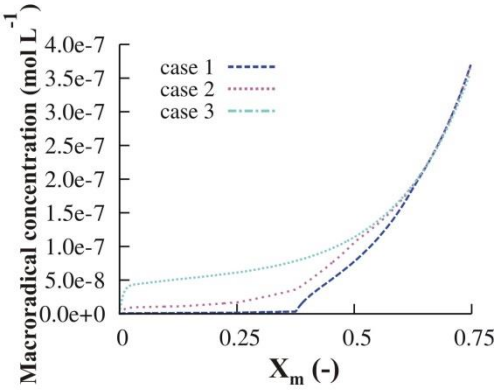

Figure B.5. *Macroradical concentration as a function of conversion for the 3 selected cases for the MOO-studies of the ARGET ATRP of BMA using a fed-batch reducing agent program (Figure 4.5; Main text).*

B.4 Multi-objective optimization results for NMP of styrene

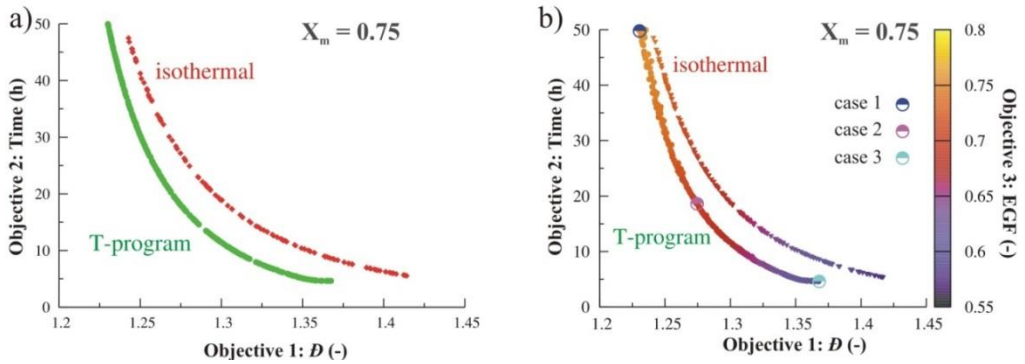

Figure B.6. *Multi-objective optimization (MOO) results for NMP of styrene using a piecewise linear temperature program with: (a) 2 objectives (i.e. dispersity (Đ) and time to reach X_m = 0.75; (b) 3 objectives (i.e. dispersity (Đ), time to reach X_m = 0.75, and end-group functionality (EGF).*

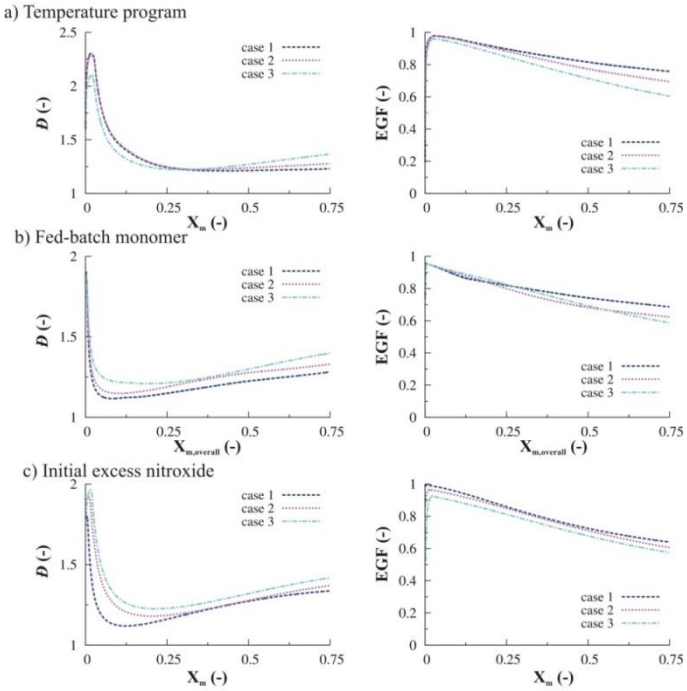

Figure B.7. *Dispersity (Đ) profiles as a function of conversion (left chart) and end-group functionality (EGF) profiles as a function of conversion (right chart) for the 3 selected cases for the MOO-studies of the NMP of styrene using: (a) a piecewise linear temperature program (Figure 4.7; Main text); (b) a fed-batch monomer program (Figure 4.8; Main text); (c) an excess initial nitroxide loading (Figure 4.9; Main text).*

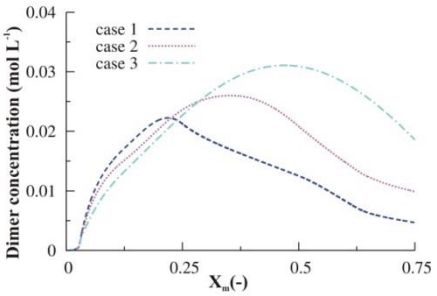

Figure B.8. *Dimer concentration profiles as a function of conversion for the 3 selected cases of the MOO of styrene using a piecewise linear temperature program (Figure 4.7; Main text).*

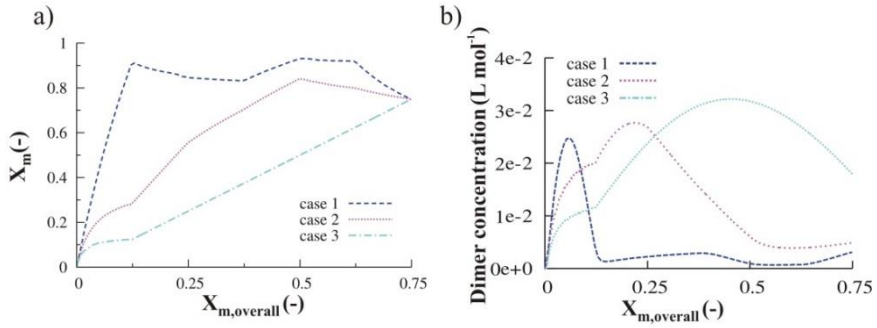

Figure B.9. *In situ conversion (X_m) as a function of the overall conversion ($X_{m,overall}$) for the 3 selected cases and (b) dimer concentration as a function of $X_{m,overall}$ for the MOO of NMP of styrene using a fed-batch monomer program (Figure 4.8; Main text).*

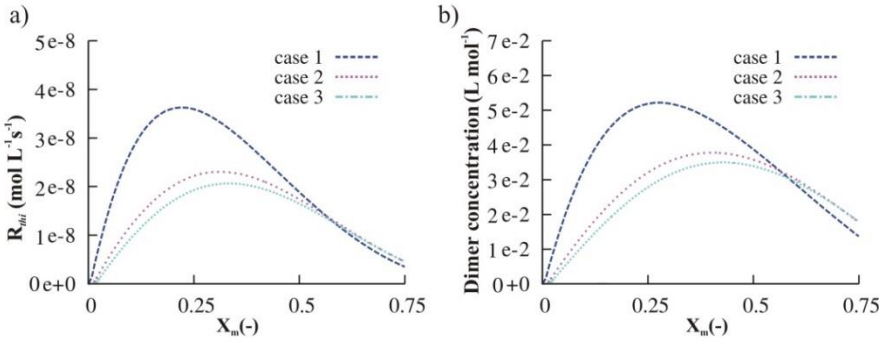

Figure B.10. *Thermal initiation rate (R_{thi}) as a function of conversion (X_m) and (b) dimer concentration as a function of X_m for the 3 selected cases for the MOO of NMP of styrene using excess initial nitroxide (Figure 4.9; Main text).*

References

1. Wang, A. R.; Zhu, S. P. Modeling the reversible addition-fragmentation transfer polymerization process. *J. Polym. Sci. Pol. Chem.* **2003,** 41, (11), 1553-1566.

2. Mastan, E.; Li, X.; Zhu, S. Modeling and theoretical development in controlled radical polymerization. *Progress in Polymer Science* **2015,** 45, 71-101.

3. Deb, K.; Pratap, A.; Agarwal, S.; Meyarivan, T. A fast and elitist multiobjective genetic algorithm: NSGA-II. *IEEE Trans. Evol. Comput.* **2002,** 6, (2), 182-197.

Appendix C. Model-based design to push the boundaries of sequence-control

C.1 Details on experimental analysis for NMP of styrene and BzMI initiated by BlocBuilder MA

^{1}H NMR spectra to measure the comonomer conversions to simulate and design BlocBuilder MA (or 2-methyl-2-[Ntert-butyl-N-(1-diethoxyphosphoryl-2,2-dimethylpropyl)aminoxy]propionic acid (MAMA-SG1)) initiated NMP of styrene (M_1) with additions of small amounts of N-benzylmaleimide (BzMI; M_2; Figure 5.2-5.4 in the main text) were recorded in $CDCl_3$ (d = 7.26 ppm), using a Bruker Avance 400 MHz spectrometer equipped with an Ultrashield magnet. Conversion of styrene was determined from the ^{1}H NMR spectra by comparing the integrated signals of one of the vinyl protons of the styrene monomer at 5.69 ppm to those of the protons in the 6.25-7.25 ppm region, corresponding to 2 aromatic protons of the formed copolymer, 1 methine proton of the unreacted styrene, and 2 protons of to the BzMI. If the functional monomer had already been added also five aromatic protons of anisole, which was used as solvent, and five protons of the polymerized BzMI are included in this region requiring a further correction. The conversion of the functional monomer BzMI was determined from the ^{1}H NMR spectra by following the signal at 4.67 ppm and the formation of the polymer at 4.6-4.1 ppm.[1]

Molar mass distributions were determined with size exclusion chromatography (SEC) analysis, taking tetrahydrofuran as eluent (flow rate: 1 ml min^{-1}), using a Shimadzu LC20AD pump. A SEC instrument was used, which is equipped with four PLGel Mixed C columns (5 mm, 30 cm, diameter = 7.5 mm), a Wyatt Viscostar-II viscometer, a Wyatt TREOS light scattering detector, a Shimadzu SPD-M20A diode array UV detector, and a Wyatt Optilab T-rEX refractometer. The

calibration was done with 15 linear polystyrene (PS) standards from Polymer Laboratories within a range of 1.35 10^3-1.95 10^6 g mol^{-1}.

C.2 Details on kinetic Monte Carlo model for simulation of (bicomponent) NMP of styrene with small amounts of BzMI

C.2.1 Reactions and intrinsic rate coefficients

In Table S1, an overview is given of the reactions and the corresponding intrinsic rate coefficients to simulate and design BlocBuilder MA initiated NMP of styrene (M_1) with additions of small amounts of BzMI (M_2; Figure 5.2-5.4 in the main text). For simplicity, a terminal model is used to describe the copolymerization kinetics, *i.e.* the impact of the penultimate monomer unit (PMU) on the reactivities is neglected. The latter is justified, at least to a first approximation, taking into account the limited information available in literature for radical polymerizations with as comonomer pair styrene and BzMI. In addition, as demonstrated below, preliminary simulations, selecting expected values for the penultimate rate coefficients (*cf.* Table C.2), indicated that the assumption of a terminal model is valid to a first approximation for the considered set of reaction conditions.

For the simulations of the (bicomponent) NMP systems with other nitroxide moieties than SG1 (Figure 5.5-5.6 in the main text; no side reactions with nitroxide), additional reactions and terminal intrinsic rate coefficients are provided in Table C.3.

In what follows, the reactions in Table C.1 and Table C.3 are discussed in detail. A distinction is made between NMP non-specific and specific reactions. The negligible impact of the PMU on the NMP kinetics is also illustrated (parameters: Table C.2).

NMP non-specific reactions

Table C.1. *Overview of reactions and their intrinsic rate coefficients at 120 °C, except termination, for modeling and design of BlocBuilder MA ($R_{0,1}X$) initiated nitroxide mediated polymerization (NMP) of styrene (M_1) with small amounts of N-benzyl maleimide (M_2); for other nitroxide moieties: Table C.3; terminal model can be used based on the results of Figure 5.1.*

	Reaction step		k at 120°C((L mol^{-1})s^{-1})	Ref.
	Thermal initiation			
TI1	Diels-Alder dimerization	$2M_1 \overset{k_d}{\rightarrow} D$	1.79×10^{-7}	2, 3
TI2	Retro Diels-Alder dimerization	$D \overset{k_{dr}}{\longrightarrow} 2M_1$	1.36×10^{-4}	2, 3
TI3	Molecule assisted homolysis	$D + M_1 \overset{k_{thi}}{\longrightarrow} R_{0,2} + R_{0,3}$	9.07×10^{-8}	2, 3
	Chain initiation[a,b]			
CI1		$R_{0,1} + M_1 \overset{k_p^{0,1}}{\longrightarrow} R_1^1$	1.00×10^4	4
CI2		$R_{0,2} + M_1 \overset{k_p^{0,2}}{\longrightarrow} R_1^1$	2.04×10^3	5
CI3		$R_{0,3} + M_1 \overset{k_p^{0,3}}{\longrightarrow} R_1^1$	2.04×10^3	5
CI4		$R_{0,4} + M_1 \overset{k_p^{0,4}}{\longrightarrow} R_1^1$	2.04×10^3	5
	Propagation[c]			
P1		$R_i^1 + M_1 \overset{k_p^{11}}{\longrightarrow} R_{i+1}^1$	2.04×10^3	5
P2		$R_i^1 + M_2 \overset{k_p^{12}}{\longrightarrow} R_{i+1}^2$	5.10×10^4	this work
P3		$R_i^2 + M_1 \overset{k_p^{21}}{\longrightarrow} R_{i+1}^1$	5.82×10^4	6
P4		$R_i^2 + M_2 \overset{k_p^{22}}{\longrightarrow} R_{i+1}^2$	7.57×10^2	7
	Termination[d]			
T1		$R_{0,y} + R_{0,z} \overset{k_{tc,app}^{0,y;0,z}}{\longrightarrow} R_0R_0$	composite k_t model	8, 9
T2		$R_{0,y} + R_i^1 \overset{k_{tc,app}^{0,y;i}}{\longrightarrow} P_i$		8, 9
T3		$R_i^1 + R_j^1 \overset{k_{tc,app}^{i;j}}{\longrightarrow} P_{i+j}$		8, 9
	Chain transfer			
CT1	to monomer	$R_{0,y} + M_1 \overset{k_{trm}^{0,y}}{\longrightarrow} P_0 + R_{0,4}$	2.09×10^{-1}	8
CT2		$R_i^1 + M_1 \overset{k_{trm}^{1}}{\longrightarrow} P_i + R_{0,4}$	2.09×10^{-1}	8
CT3	to dimer	$R_{0,y} + D \overset{k_{trd}^{0,y}}{\longrightarrow} P_0 + R_{0,3}$	1.50×10^2	10, 11
CT4		$R_i^1 + D \overset{k_{trd}^{1}}{\longrightarrow} P_i + R_{0,3}$	1.50×10^2	10, 11
	NMP (de)activation[e]			
A1	Activation	$R_{0,1}X \overset{k_a^{0,1}}{\longrightarrow} R_{0,1} + X$	1.18×10^{-1}	12
A2		$R_i^1X \overset{k_a^{1}}{\rightarrow} R_i^1 + X$	7.08×10^{-3}	12
DA1	Deactivation	$R_{0,1} + X \overset{k_{da}^{0,1}}{\longrightarrow} R_{0,1}X$	2.80×10^6	12
DA2		$R_i^1 + X \overset{k_{da}^{1}}{\longrightarrow} R_i^1X$	1.09×10^6	12

[(a)]Chain initiation rate coefficient for $R_{0,1}$ is assumed to be equal to be the one of the 2-(alkoxy)carbonylprop-2-yl radical.[13] [(b)]The chain initiation reactivity of $R_{0,2}$, $R_{0,3}$ and $R_{0,4}$ is assumed to be equal.[2, 14] [(c)]Rate coefficients for cross-propagation reactions based on monomer reactivity ratios (r_1=0.040 and r_2 = 0.013) from literature with r_1 slightly adjusted.[7] [(d)]Apparent rate coefficient is used (see Table S4) with negligible contribution of R_i^2 species.[9] [(e)]Activation / deactivation of R_i^2X/R_i^2 can be neglected based on the results of Figure C.2; those with $R_{0,y}$ (y=2-4) also neglected based on previous work.[3]

For styrene radical polymerization, in agreement with previous kinetic modeling studies,[3, 12, 15] thermal self-initiation according to the Mayo-mechanism[8, 16] is considered (entry T1-3 in Table C.1). The extra radical initiator fragments besides the NMP initiator radical $R_{0,1}$ are denoted as $R_{0,2}$ and $R_{0,3}$. The impact of this thermal self-initiation can although expected to be limited in the present kinetic study, taking into account the low targeted chain lengths (TCLs) considered.[12]

In agreement with literature data, for a terminal styryl macroradical (R_i^1; i: chain length), both chain transfer to styrene (M_1) and to the dimer (D), as formed during thermal self-initiation, are considered (entry CT1-4 in Table C.1).[3, 12, 17, 18] For chain transfer to BzMI (M_2) or chain transfer involving radicals with a terminal BzMI unit (R_i^2), no literature data on intrinsic rate coefficients are available. For simplicity, these chain transfer reactions have been neglected, taking into account that the amount of propagation events can assumed to be as good as exclusive in the short time period in which such chain transfer reactions can take place. Also chain transfer reactions with polymer are neglected based on literature data.[19]

For propagation, all four intrinsic rate coefficients (entry P1-4 in Table C.1) are based on literature data.[5-7] The homopropagation rate coefficient for BzMI (k_p^{22}) is approximated by the one reported for N-cyclohexylmaleimide, since no rate coefficients for this specific maleimide are available in literature. The cross-propagation rate coefficients (k_p^{12} and k_p^{21}) are calculated based on literature data for the monomer reactivity ratios.[5-7] The first monomer reactivity ratio ($r_1 = k_p^{11}/k_p^{12}$) is slightly altered from its literature value[6] of 0.058 but within the expected

experimental error for such measurements[20] to achieve a better match between experimental and simulated data in the present work.

In general, it could be expected that more propagation rate coefficients are needed for an accurate kinetic description, due to possible existence of a PMU. No penultimate rate coefficients are although available for the selected monomer pair, as already indicated above. Klumperman *et al.*[21] reported penultimate parameters for the related styrene and maleic anhydride comonomer pair (see Table C.2) for which a penultimate unit effect has been observed under more general polymerization conditions. Using these parameters (*i.e.* the ratio of *r1 to* r_1' = 0.6 reported by Klumperman *et al.*[22] and the radical reactivity ratio s_1 of 0.85 reported by Klumperman[21] are used), in Figure C.1 (green lines) the most important NMP characteristics as considered in this work are displayed under the conditions for Figure 5.2 in the main text (also red lines for reference in Figure C.1). It follows that the impact of the PMU can be neglected, as the green and red lines coincide, both for the average properties (top) and properties based on individual chains (bottom). Also for the other conditions in the main text this statement holds. Hence, to first approximation a terminal model for the simulation of the NMP process can be selected, keeping in mind that under the specific conditions used in this work (high styrene concentrations), the penultimate unit effects can be ignored. Moreover, as for the selected comonomer pair used in this work only terminal reactivity ratios are available in literature and deviations can be expected between maleic anhydride and BzMI, the assumption of a terminal model is further justified.

Table C.2. *Overview of propagation reactions for kinetic Monte Carlo modeling and design of BlocBuilder MA initiated nitroxide mediated polymerization (NMP) of styrene (M_1) with small amounts of N-benzyl maleimide (M_2), in case penultimate monomer unit (PMU)-effects are considered; approximation via styrene and maleic anhydride comonomer pair parameters for other reactions from Table C.1.*

	Reaction step	k at 120°C((L mol^{-1})s^{-1})[(a)]	Ref.
P1'	$R_i^{11} + M_1 \xrightarrow{k_p^{111}} R_{i+1}^{11}$	2.04×10^3	5
P2'	$R_i^{11} + M_2 \xrightarrow{k_p^{112}} R_{i+1}^{12}$	5.10×10^4	5-7, 21
P3'	$R_i^{21} + M_1 \xrightarrow{k_p^{211}} R_{i+1}^{11}$	1.77×10^3	5-7, 21
P4'	$R_i^{21} + M_2 \xrightarrow{k_p^{212}} R_{i+1}^{12}$	2.61×10^4	5-7, 21
P5'	$R_i^{12} + M_1 \xrightarrow{k_p^{121}} R_{i+1}^{21}$	5.82×10^4	5-7, 21
P6'	$R_i^{12} + M_2 \xrightarrow{k_p^{122}} R_{i+1}^{22}$	7.57×10^2	5-7, 21
P7'	$R_i^{22} + M_1 \xrightarrow{k_p^{221}} R_{i+1}^{21}$	5.82×10^4	5-7, 21
P8'	$R_i^{22} + M_2 \xrightarrow{k_p^{222}} R_{i+1}^{22}$	7.57×10^2	7

[(a)] $r_1' = k_p^{211}/k_p^{212} = 1.7 \times r_1$ and $s_1 = k_p^{211}/k_p^{111} = 0.85$

For termination (entry T1-3 in Table S1), dead polymer formation both with small and macroradicals is incorporated in the kinetic model. Only termination reactions involving terminal styryl radicals (R_i^1) are taken into account, for which recombination is the dominant termination mode.[23] This simplification can be justified due to following three reasons: (*i*) termination reactions are most important in the early NMP stages ($X_{sty} < 0.05$; onset of the so-called persistent radical effect[24-26]) in which only styrene is present; (*ii*) if an R_i^2 radical is formed, due to the very k_p^{21} and high styrene concentration, this species rapidly adds to a styrene monomer molecule, leading to the fast formation of an R_i^1 radical; (*iii*) for the related N-cyclohexylmaleimide radical polymerization it has been reported that the termination rate coefficient is three orders of magnitude lower than the one for methyl-methacrylate radical

polymerization,[7] the latter being of the same order of magnitude as for styrene radical polymerization.[9]

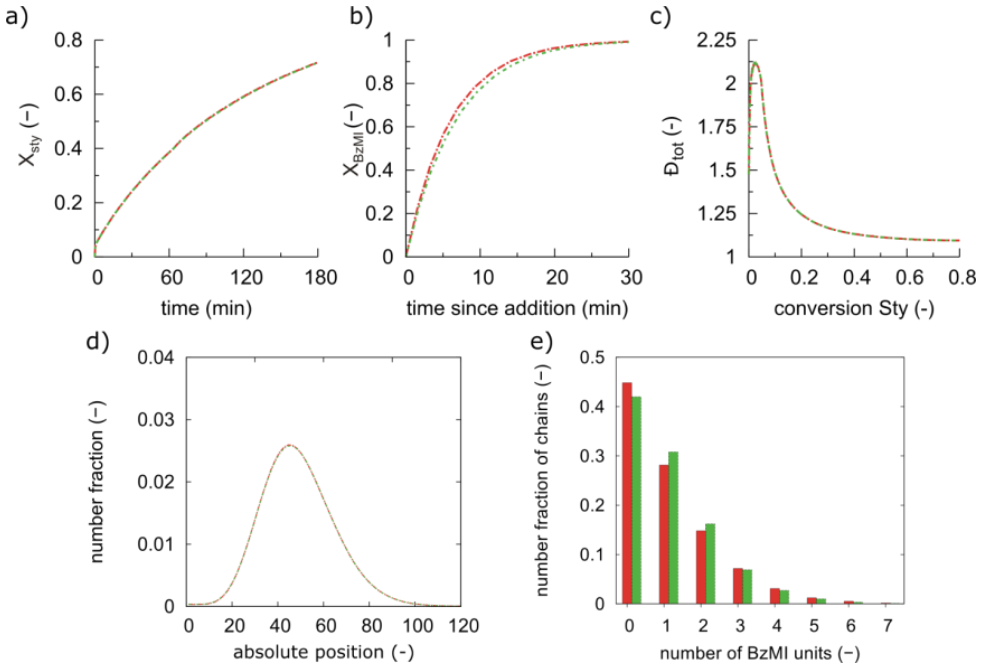

Figure C.1. *Justification of terminal model (red lines/bars; Table C.1; main text Figure 5.2) since as good as identical results with the more complex penultimate monomer unit model (green lines/bars; $r_1' = 1.7\ r_1$ and $s_1 = 0.85$ from Table C.2)[21] model for the description and design of NMP of styrene with small amounts of BzMI. A) styrene conversion (X_{sty}), b) benzylmaleimide conversion (X_{BzMI}) as a function of time, since addition of BzMI, c) dispersity (Đ) as a function of X_{sty}, d) number fraction of BzMI units as a function of absolute positions in the chain, e) number fraction of chains with a given number of BzMI units; NMP initiator: BlocBuilder MA (R_0X); 120°C ($[Sty]_0:[R_0X]_0:[BzMI]_{addition\ point}$=100:1:eq.; eq. defined with respect to R_0X; addition point: X_{sty}=0.4.*

It should be further stressed that termination rate coefficients are adapted with increasing time to reflect the impact of the viscosity increase and thus diffusional limitations on the NMP process, *i.e.* apparent termination kinetics are considered.[9, 27] The apparent termination parameters are

given in Table C.4. For more details on the actual implementation of the apparent termination kinetics the reader is referred to previous work[12] and Section C.2.2.

NMP specific reactions

The NMP (de)activation rate coefficients in Table C.1 (reactions: entry A1-2 and DA1-2; nitroxide: SG1) are based on literature data.[12] For NMP (de)activation involving the MAMA initiator fragment ($k_a^{0,1}$, $k_{da}^{0,1}$) and involving macroradicals with a terminal styrene unit (k_a^1 and k_{da}^1) accurate values have been taken from a recent kinetic modeling study for NMP of styrene, in which regression analysis was successfully performed based on an extensive set of polymerization data.[12] Importantly, these parameter values are in agreement with previously reported parameters.[28-32] The corresponding NMP activation/deactivation rate coefficients (k_a^1 and k_{da}^1) used in the simulations of the (bicomponent) NMP systems (conventional radical initiator (I_2): benzoyl peroxide (BPO)) with other nitroxide moieties than SG1 (specific points in Figure 5.5 in the main text; theoretical screening of (k_a^1 , k_{da}^1)) are provided in Table C.3 and are also based on literature data.[33-37] In this table, also the BPO related kinetic parameters are provided.

Note that for the aforementioned grid simulations, for simplicity and due to a lack of literature parameters, no side reactions with the nitroxide have been included although they are expected to occur.[38] It should h be stressed that for SG1 (key nitroxide with experimental validation in main text: Figure 5.1-5.4) these side reactions can be safely ignored.[39-41]

Table C.3. *Overview of NMP specific reactions and kinetic parameters for kinetic Monte Carlo modeling and design of (bicomponent) nitroxide mediated polymerization (NMP) of styrene (M_1) with small amounts of N-benzyl maleimide (M_2) using different nitroxide moieties compared to Table C.1 (SG1 nitroxide); f: initiator efficiency; for simplicity side reactions with the nitroxide are ignored (for SG1 (main nitroxide) this is a safe assumption, as explained in the main text), focusing on three different nitroxides for interpretation of Figure 5.5 in the main text; other kinetic parameters in Table C.1.*

	Reaction step		k at 120°C((L mol^{-1})s^{-1})	Ref.
	Initiation[(a)]			
I1'		$I_2 \xrightarrow{f,k_i} 2I$	3.6×10^{-2}	15
	Chain initiation			
CI'		$I + M_1 \xrightarrow{k_p^{0,5}} R_1^1$	2.04×10^3	5
	NMP (de)activation			
	DBNO[(b)]			
A1'		$R_{0,1}X \xrightarrow{k_a^{0,1}} R_{0,1} + X$	1.13	33
DA1'		$R_{0,1} + X \xrightarrow{k_{da}^{0,1}} R_{0,1}X$	2.47×10^8	33
A2'		$R_i^1X \xrightarrow{k_a^1} R_i^1 + X$	1.40×10^{-2}	34
DA2'		$R_i^1 + X \xrightarrow{k_{da}^1} R_i^1X$	1.20×10^7	35
	TIPNO			
A2''		$R_i^1X \xrightarrow{k_a^1} R_i^1 + X$	3.30×10^{-3}	34
DA2'		$R_i^1 + X \xrightarrow{k_{da}^1} R_i^1X$	8.00×10^6	36
	TEMPO			
A2'''		$R_i^1X \xrightarrow{k_a^1} R_i^1 + X$	5.20×10^{-4}	34
DA2'''		$R_i^1 + X \xrightarrow{k_{da}^1} R_i^1X$	7.60×10^7	37

[(a)] f = 0.7 [(b)] $R_{0,1}X$ = α-methylstyryl-di-tertbutyl nitroxide

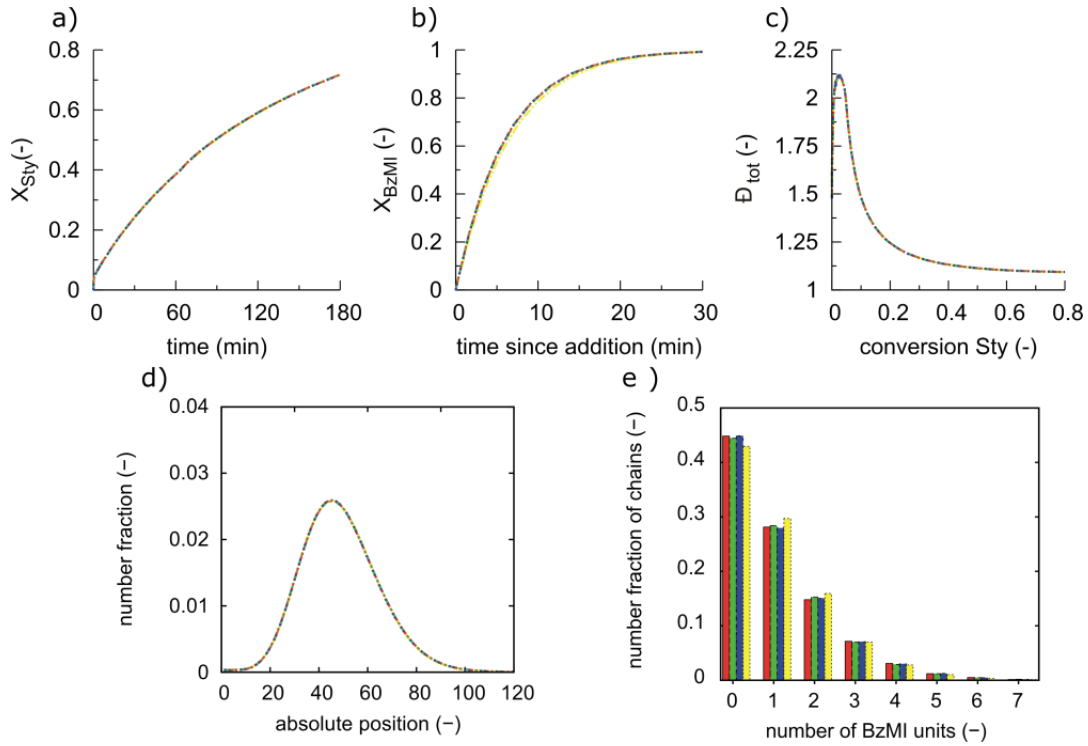

Figure C.2. *Kinetic insignificance of (de)activation involving macrospecies with terminal BzMI units; a) styrene conversion (X_{sty}), b) benzylmaleimide conversion (X_{BzMI}) as a function of time elapsed since addition point of BzMI, c) dispersity (Đ) as a function of X_{sty}, d) number fraction of BzMI units at absolute positions in the chain, e) number fraction of chains with a given number BzMI units, for NMP of styrene and BzMI initiated by BlocBuilder MA (R_0X) at 120°C ($[Sty]_0$:$[R_0X]_0$:$[BzMI]_{addition\ point}$=[100]:[1]:[eq.]; eq. defined with respect to R_0X; addition point: X_{sty}=0.4) for k_a^2 = 0 s^{-1}; k_{da}^2= 0 L mol^{-1} s^{-1} (red; main text Figure 5.2), $k_a^2 = k_a^1$ and $k_{da}^2 = k_{da}^1$ (green), $k_a^2 = 10\ k_a^1$ and $k_{da}^2 = k_{da}^1$ (blue), and $k_a^2 = k_a^1$ and $k_{da}^2 = 10\ k_{da}^1$ (blue).*

For NMP (de)activation involving macrospecies with a terminal BzMI unit (k_a^2 and k_{da}^2) no values are available. Model analysis showed that these rate coefficients can for simplicity be taken equal to zero (no entries in Table C.1). As explained above, under the conditions studied, a quick transformation from R_i^2 to R_i^1 is occurring so that deactivation of R_i^2 is kinetically insignificant. The latter is also illustrated in Figure C.2, in which focus is on the main NMP characteristics and the activation/deactivation parameters related to the second monomer are

varied. The red lines are those as used in the main text (k_a^2 = 0 s^{-1}; k_{da}^2 = 0 L mol^{-1} s^{-1}; no activation/deactivation). The green lines are for $k_a^2 = k_a^1$ and $k_{da}^2 = k_{da}^1$, the blue lines for $k_a^2 = 10\ k_a^1$ and $k_{da}^2 = k_{da}^1$, and the yellow lines for $k_a^2 = k_a^1$ and $k_{da}^2 = 10\ k_{da}^1$. It can be seen that the lines as good as coincide, highlighting the correctness of the model assumption with respect to the zero values for k_a^2 and k_{da}^2.

C.2.2 Diffusional limitations

To account for diffusional limitations on termination due to viscosity effects, apparent termination rate coefficients are considered. Since, as explained above, the dominant radicals over the complete NMP process are styryl radicals only apparent termination rate coefficients are needed for R_i^1 species. The so-called composite k_t model[9] is used, which allows to reflect the impact of the polymer mass fraction w_p and the chain length i, on the apparent homotermination rate coefficients ($k_{t,ii}^{app}$) in a piecewise manner (parameters Table C.4):

$$\text{for } i < i_{\text{gel}} \text{ and } i < i_{\text{SL}}\text{: } k_{\text{t,ii}}^{\text{app}} = k_{\text{t,11}}^{\text{app}} i^{-\alpha_{\text{s}}}$$

$$\text{for } i < i_{\text{gel}} \text{ and } i \geq i_{\text{SL}}\text{: } k_{\text{t,ii}}^{\text{app}} = k_{\text{t,11}}^{\text{app}} i_{\text{SL}}^{\alpha_{\text{l}}-\alpha_{\text{s}}} i^{-\alpha_{\text{l}}}$$

$$\text{for } i \geq i_{\text{gel}} \text{ and } i < i_{\text{SL}}\text{: } k_{\text{t,ii}}^{\text{app}} = k_{\text{t,11}}^{\text{app}} i_{\text{gel}}^{\alpha_{\text{gel}}-\alpha_{\text{s}}} i^{-\alpha_{\text{gel}}}$$

$$\text{for } i \geq i_{\text{gel}} \text{ and } i < i_{\text{SL}}\text{: } k_{\text{t,ii}}^{\text{app}} = k_{\text{t,11}}^{\text{app}} i_{\text{SL}}^{\alpha_{\text{l}}-\alpha_{\text{s}}} i_{\text{gel}}^{\alpha_{\text{gel}}-\alpha_{\text{l}}} i^{-\alpha_{\text{gel}}}$$

The parameters in these equations are taken from reversible addition-fragmentation chain transfer chain length dependent termination (RAFT-CLD-T) measurements at 363 K.[9] The value of $k_{\text{t,11}}^{\text{app}}$ is extrapolated from the value reported to a value at the polymerization temperature in this work (393 K), using the activation energy determined by Hui *et al.*[8]

Table C.4. *Parameters used for the composite k_t model to simulate NMP of styrene MA and small fraction of N-benzyl maleimide; w_p = weight fraction of polymer.*

α_s	α_l	α_{gel}	i_{SL}	i_{gel}	$k_{t,11}^{app}$
0.55	0.15	$(1.22w_p) - 0.11$	30	$3.3 \times w_p^{-2.13}$	$5.11\times10^{9}\exp(-7\ 10^{3}/R/T)$

C.3 Comparison of results with full NMP kinetic model and idealized case of living polymerization for control over monomer placement

In Figure C.3 (1 eq. BzMl), the results obtained in the main text regarding the monomer placement (full NMP kinetic model; matrix-based kinetic Monte Carlo code; green lines/bars) are compared with the recent results obtained by Gody *et al.*[42] based on ideal living polymerization kinetics (red lines/bars; x_n of 81 and targeted monomer placement at position 41). The latter corresponds with a Poisson distribution and reflects the inherent limitations purely related to the stochastic nature of radical polymerization processes.

It follows from Figure C.3 that for even for the ideal case (red lines/bars) the monomer placement follows a clear distribution, both with respect to the absolute and relative placement (left) and the frequency per chain (right). It should although be stressed that in practice non-idealities play a role and, hence, the ideal lines are only approximate, as also indicated by Gody *et al.*[42] Indeed, these distributions alter significantly upon the consideration of a full NMP kinetic model (green lines/bars). Broader distributions for the absolute and relative placement are obtained and significant changes are observed for the frequencies. For example with the ideal case the low functionalized contributions are underestimated and as a consequence the dominant higher-functionalized ones are overestimated.

The results in Figure C.3 thus highlight the relevance of the present work in order to accurately quantify the product quality for sequence-controlled polymers, as significant deviations are present with the predictions using derivations based on ideal living polymerization kinetics.

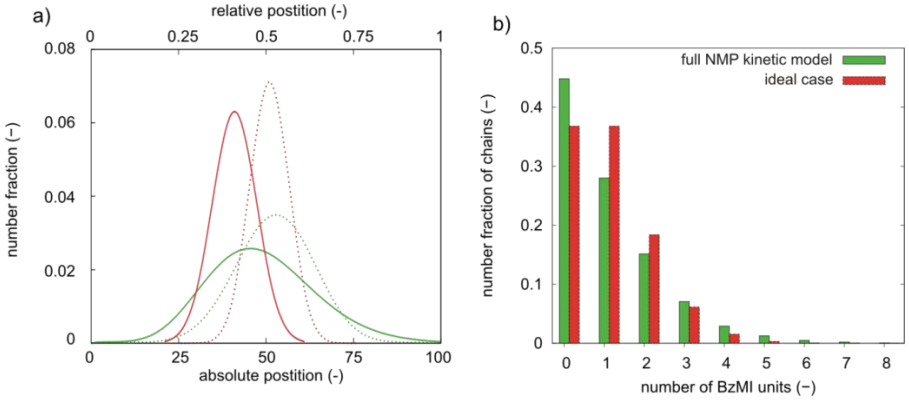

Figure C.3. *Comparison between results on microstructural control for NMP (green; X_{sty}=0.8) and idealized living case (red) a) number fraction of BzMI units at absolute positions in the chain (full lines) and relative positions in the chain (dotted lines) and b) number fraction of chains with a given number BzMI units; NMP conditions: NMP initiator = BlocBuilder MA (R_0X); 120°C ($[Sty]_0$:$[R_0X]_0$:$[BzMI]_{addition\ point}$ = 100:1:eq.; eq. defined with respect to R_0X; addition point: X_{sty}=0.4; corresponding ideal living case with as solely parameters x_n = 81 and targeted functional monomer position = 41.*

C.4 Comparison with NMP of styrene

As indicated in the main text, a sequence controlled system with strong cross-propagation is inherently more prone to deviations from the ideal case. This is illustrated in Figure C.4, in which it is shown that by an alternation from homo- to copolymerization the contribution of cycles with a higher monomer incorporation becomes more relevant (shift of the higher frequencies to the right). Figure C.4a is the analogous figure for Figure 5.3d in the main text, with for the sake of comparison a duplicate of these results (green bars). Note that for a normalization with respect to the number of monomer units instead of the number of cycles the results in Figure C.4b are

obtained. Clearly, the deviations between homo- and copolymerization are stronger, further highlighting the importance of a detailed reaction scheme for an accurate description of the copolymerization kinetics.

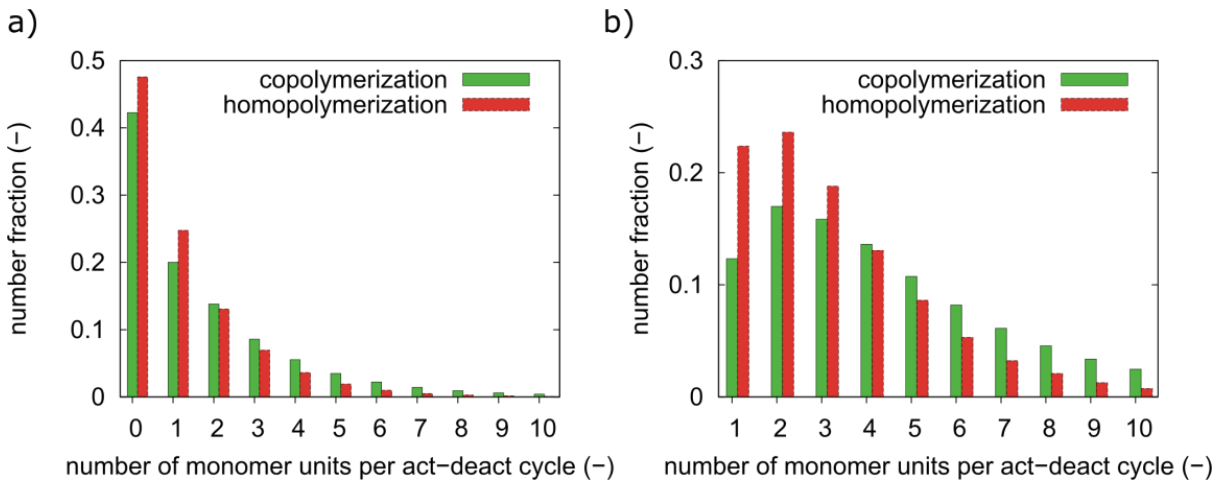

Figure C.4. *Comparison between copolymerization (green) and homopolymerization (red); (a) number fraction of activation-deactivation cycles as a function of number of propagations for X_{sty} interval from 0.40 to 0.45 (normalization with respect to the total number of activation-deactivation cycles as in Figure 5.3d in the main text); (b) alternative representation with normalization with respect to the number of monomer units; NMP of styrene and BzMI initiated by BlocBuilder MA (R_0X) at 120°C ($[Sty]_0$:$[R_0X]_0$:$[BzMI]_{addition\ point}$ =100:1:eq.; eq. defined with respect to R_0X; addition point: X_{sty}=0.4), homopolymerization: NMP of styrene initiated by BlocBuilder MA (R_0X) at 120°C ($[Sty]_0$:$[R_0X]_0$=100:1).*

C.5 Thermal self-initiation contribution for theoretical screening NMP mediating capabilities for synthesis of sequence-controlled polymers

As discussed in the main text, thermal self-initiation of styrene is no longer negligible for the whole screening range of activation and deactivation rate coefficients for styryl dormant macrospecies/macroradicals (k_a and k_{da}). This can be deduced by comparing Figure 5.5 in the main text (thermal self-initiation included) and Figure C.5 (thermal self-initiation neglected). It can be seen that for low k_a and high k_{da} values, significant deviations exist. For these parameter

ranges, the thermal self-initiation reaction deteriorates the quality of the sequence-controlled polymers. Hence, for grid simulations this reaction needs to be accounted for to ensure a reliable model-based design.

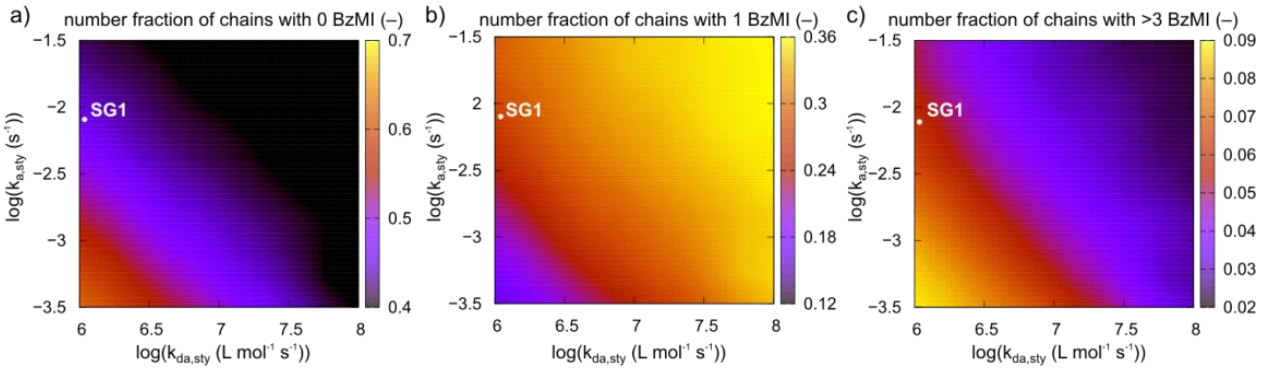

Figure C.5. *Model-based identification of the most suited nitroxide via a screening of (k_a, k_{da}) combinations for (bicomponent) NMP synthesis of sequence controlled polymers, ignoring side reactions with the nitroxides for simplicity; number fraction of chains with a) 0 BzMI units, b) 1 BzMI unit, and c) more than 3 BzMI units; conditions: bicomponent NMP of styrene and BzMI initiated with BPO at 120°C ($[Sty]_0$:$[BzMI]_{addition\ point}$:$[X]_0$:$[BPO]_0$=100:1:1:0.71); with $2f[BPO]_0 = [X]_0$; f: initiator efficiency); results shown for X_{sty} = 0.8 and addition point X_{sty}=0.4; white circles: SG1 for which side reactions can be ignored.*

C.6 Multifunctionalization in case of SG1 nitroxide and only addition program for functional monomer

In this section, the detailed microstructure for the synthesis of a sequence-controlled polymer containing three distinct functionalizations is visualized, considering the SG1 nitroxide for which a successful experimental validation has been performed (see main text). Note that only for the functional monomer an addition program is considered, *i.e.* all styrene is added at the start. The results at X_{sty} = 0.9 are depicted in Figure C.6.

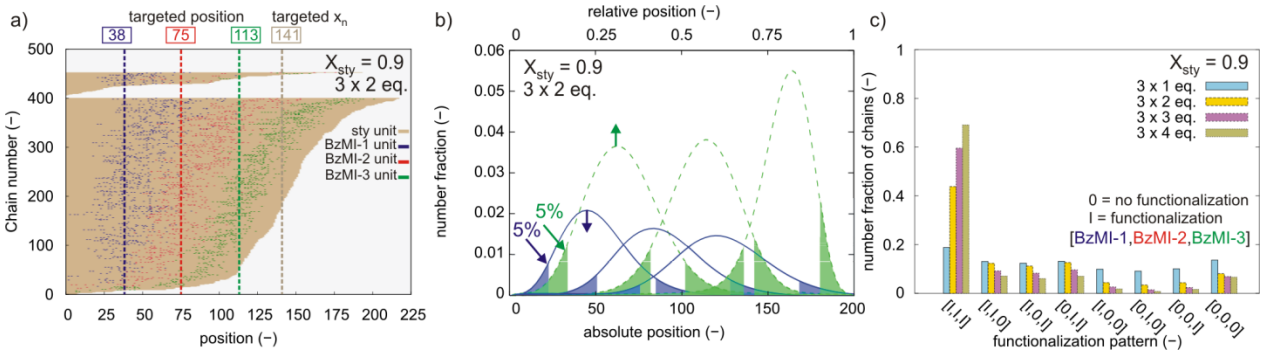

Figure C.6. *Model-based design for sequence-controlled polymer synthesis: a) Explicit in silico visualization of microstructure for each individual copolymer chain (ca. 500 chains of a representative polymer sample of 100.000 chains), b) number fraction of BzMI units at absolute and relative positions in the chain, c) number fraction of chains depending on the functionalization pattern (target: [I,I,I]); BlocBuilder initiated NMP of styrene with 3 BzMI additions; 120°C; $[Sty]_0$:$[R_0X]_0$:$[BzMI\text{-}1]_{AP1}$:$[BzMI\text{-}2]_{AP2}$:$[BzMI\text{-}3]_{AP3}$ = 150:1:eq.:eq.:eq.; eq. each time 2 for a) and b) but variable for c); defined with respect to R_0X.*

From comparing Figure C.6a with Figure 5.6a in the main text it follows already on a visual basis that an improvement of the comonomer incorporation is indeed obtained by selecting a better theoretical nitroxide and using an addition program for both comonomers. Here only an acceptable microstructural control is obtained with a reasonable positioning of the functional monomer units and a reasonable contribution of the chain-to-chain deviations. On an absolute basis, the blue three distributions of Figure C.6b are characterized by mean positions of 50, 87, and 121 for BzMI-1, BzMI-2, and BzMI-3, which are considerably further away from the targeted ones of 38, 75, and 113 compared to the mentioned values in the main text (*cf.* Figure 5.6b). The standard deviations are given by 20, 24, and 30 monomer units with corresponding coefficients of variation equal to 0.40, 0.28, and 0.24. On a relative basis, the three distributions (green lines in Figure C.6b) are characterized by mean relative positions of 0.33, 0.57 and 0.80

with standard deviations given by 0.11, 0.10, 0.09. The coefficients of variation become 0.33, 0.17, and 0.11. Upon a comparison with the respective values in the main text it is again confirmed that the microstructural control is here only reasonable and thus further model-based design as done in the main text is indeed worthwhile. Finally, it follows from Figure C.6c, which maps the complete functionalization pattern for all individual chains (analogous Figure 5.6c in main text after further model-based design) that also the fraction of chains with the preferred functionalization pattern, *i.e.* [I,I,I], can be further improved. Here a variation of the number of equivalents of each BzMI addition (1 (blue bars), 2 (yellow bars), 3 (purple bars), and 4 (green bars)) leads to number fractions of trifunctionalized chains of 0.19, 0.44, 0.60, and 0.69, which can be increased by the combined model-based design in the main text.

References

1. Zamfir, M.; Lutz, J.-F. Ultra-precise insertion of functional monomers in chain-growth polymerizations. *Nat Commun* **2012**, 1138.

2. Woloszyn, J. D.; McAuley, K. B. Application of Parameter Selection and Estimation Techniques in a Thermal Styrene Polymerization Model. *Macromol. React. Eng.* **2011,** 5, 453-466.

3. Bentein, L.; D'hooge, D. R.; Reyniers, M. F.; Marin, G. B. Kinetic Modeling as a Tool to Understand and Improve the Nitroxide Mediated Polymerization of Styrene. *Macromol. Theory Simul.* **2011,** 20, (4), 238-265.

4. Chauvin, F.; Dufils, P. E.; Gigmes, D.; Guillaneuf, Y.; Marque, S. R. A.; Tordo, P.; Bertin, D. Nitroxide-mediated polymerization: The pivotal role of the k(d) value of the initiating alkoxyamine and the importance of the experimental conditions. *Macromolecules* **2006,** 39, (16), 5238-5250.

5. Buback, M.; Gilbert, R. G.; Hutchinson, R. A.; Klumperman, B.; Kuchta, F.-D.; Manders, B. G.; O'Driscoll, K. F.; Russell, G. T.; Schweer, J. Critically evaluated rate coefficients for free-radical

polymerization, 1. Propagation rate coefficient for styrene. *Macromol. Chem. Phys.* **1995,** 196, (10), 3267-3280.

6. Oishi, T.; Kimura, T. Studies on polymerization of n-(substituted)-maleimides .3. polymerizations and copolymerizations of n-n-hexyl-maleimide, n-cyclohexyl-maleimide with n-benzyl-maleimide. *Kobunshi Ronbunshu* **1976,** 33, (11), 685-691.

7. Sato, T.; Arimoto, K.; Tanaka, H.; Ota, T.; Kato, K.; Doiuchi, K. Kinetic and ESR studies on the radical polymerization of N-cyclohexylmaleimide in benzene. *Macromolecules* **1989,** 22, (5), 2219-2223.

8. Hui, A. W.; Hamielec, A. E. Thermal polymerization of styrene at high conversions and temperatures. An experimental study. *J. Appl. Polym. Sci.* **1972,** 16, (3), 749-769.

9. Johnston-Hall, G.; Monteiro, M. J. Bimolecular radical termination: New perspectives and insights. *J. Polym. Sci. Pol. Chem.* **2008,** 46, (10), 3155-3173.

10. Fu, Y.; Mirzaei, A.; Cunningham, M. F.; Hutchinson, R. A. Atom-Transfer Radical Batch and Semibatch Polymerization of Styrene. *Macromol. React. Eng.* **2007,** 1, (4), 425-439.

11. Pryor, W. A. L. L. D. Diels-Alder and 1,4-diradical Intermediates in the. Spontaneous Polymerization of Vinyl Monomers. *Adv. Free Radic. Chem.* **1975,** 5, (27), 27-99.

12. Fierens, S. K.; D'hooge, D. R.; Van Steenberge, P. H. M.; Reyniers, M.-F.; Marin, G. B. MAMA-SG1 initiated nitroxide mediated polymerization of styrene: From Arrhenius parameters to model-based design. *Chem. Eng. J.* **2015,** 278, 407-420.

13. Zytowski, T.; Knuhl, B.; Fischer, H. Absolute rate constants for the addition of the 2-(methoxycarbonyl)propan-2-yl and the 3,3,3-trifluoracetonyl radicals to alkenes in solution. *Helv. Chim. Acta* **2000,** 83, (3), 658-675.

14. Saldivar-Guerra, E.; Bonilla, J.; Zacahua, G.; Albores-Velasco, M. Incubation period in the 2,2,4,4-tetramethyl-1-piperidinyloxy-mediated thermal autopolymerization of styrene: Kinetics and simulations. *J. Polym. Sci. Pol. Chem.* **2006,** 44, (24), 6962-6979.

15. Belincanta-Ximenes, J.; Mesa, P. V. R.; Lona, L. M. F.; Vivaldo-Lima, E.; McManus, N. T.; Penlidis, A. Simulation of styrene polymerization by monomolecular and bimolecular nitroxide-mediated radical processes over a range of reaction conditions. *Macromol. Theory Simul.* **2007,** 16, (2), 194-208.

16. Mayo, F. R. Chain Transfer in the Polymerization of Styrene. VIII. Chain Transfer with Bromobenzene and Mechanism of Thermal Initiation1. *J. Am. Chem. Soc.* **1953,** 75, (24), 6133-6141.

17. Zetterlund, P. B.; Saka, Y.; McHale, R.; Nakamura, T.; Aldabbagh, F.; Okubo, M. Nitroxide-mediated radical polymerization of styrene: Experimental evidence of chain transfer to monomer. *Polymer* **2006,** 47, (23), 7900-7908.

18. Olaj, O. F.; Kauffmann, H. F.; Breitenbach, J. W. The Diels-Alder intermediate as a chain transfer agent in spontaneous styrene polymerization 1. New evidence from the kinetic analysis of photoinitiated polymerization. *Die Makromolekulare Chemie* **1976,** 177, (10), 3065-3071.

19. Skene, W. G.; Scaiano, J. C.; Yap, G. P. A. An Improved Mimetic Compound for Styrene "Living" Free Radical Polymerization. An Initiator Containing the "Penultimate" Unit. *Macromolecules* **2000,** 33, (10), 3536-3542.

20. Burke, A. L.; Duever, T. A.; Penlidis, A. Model discrimination via designed experiments - discriminating between the terminal and penultimate models on the basis of composition data. *Macromolecules* **1994,** 27, (2), 386-399.

21. Klumperman, B. Mechanistic considerations on styrene-maleic anhydride copolymerization reactions. *Polymer Chemistry* **2010,** 1, (5), 558-562.

22. Klumperman, B.; O'Driscoll, K. F. Interpreting the copolymerization of styrene with maleic anhydride and with methyl methacrylate in terms of the bootstrap model. *Polymer* **1993,** 34, (5), 1032-1037.

23. Matyjaszewski, K.; Davis, T. P., *Handbook of Radical Polymerization*. Wiley: 2002.

24. Tang, W.; Fukuda, T.; Matyjaszewski, K. Reevaluation of persistent radical effect in NMP. *Macromolecules* **2006,** 39, (13), 4332-4337.

25. Fischer, H. The persistent radical effect in controlled radical polymerizations. *J. Polym. Sci. Pol. Chem.* **1999,** 37, (13), 1885-1901.

26. Lutz, J. F.; Lacroix-Desmazes, P.; Boutevin, B. The persistent radical effect in nitroxide mediated polymerization: Experimental validity. *Macromol. Rapid Commun.* **2001,** 22, (3), 189-193.

27. Derboven, P.; D'hooge, D. R.; Stamenovic, M. M.; Espeel, P.; Marin, G. B.; Du Prez, F. E.; Reyniers, M. F. Kinetic Modeling of Radical Thiol-Ene Chemistry for Macromolecular Design: Importance of Side Reactions and Diffusional Limitations. *Macromolecules* **2013,** 46, (5), 1732-1742.

28. Bertin, D.; Gigmes, D.; Marque, S. R. A.; Tordo, P. Polar, steric, and stabilization effects in alkoxyamines C-ON bond homolysis: A multiparameter analysis. *Macromolecules* **2005,** 38, (7), 2638-2650.

29. Goto, A.; Fukuda, T. Comparative study on activation rate constants for some styrene/nitroxide systems. *Macromol. Chem. Phys.* **2000,** 201, (16), 2138-2142.

30. Bertin, D.; Chauvin, F.; Marque, S.; Tordo, P. Lack of chain length effect on the rate of homolysis of polystyryl-SG1 alkoxyamines. *Macromolecules* **2002,** 35, (10), 3790-3791.

31. Guillaneuf, Y.; Bertin, D.; Castignolles, P.; Charleux, B. New experimental procedure to determine the recombination rate constants between nitroxides and macroradicals. *Macromolecules* **2005,** 38, (11), 4638-4646.

32. Benoit, D.; Grimaldi, S.; Robin, S.; Finet, J. P.; Tordo, P.; Gnanou, Y. Kinetics and mechanism of controlled free-radical polymerization of styrene and n-butyl acrylate in the presence of an acyclic beta-phosphonylated nitroxide. *J. Am. Chem. Soc.* **2000,** 122, (25), 5929-5939.

33. Kruse, T. M.; Souleimonova, R.; Cho, A.; Gray, M. K.; Torkelson, J. M.; Broadbelt, L. J. Limitations in the Synthesis of High Molecular Weight Polymers via Nitroxide-Mediated Controlled Radical Polymerization: Modeling Studies. *Macromolecules* **2003,** 36, (20), 7812-7823.

34. Marque, S.; Le Mercier, C.; Tordo, P.; Fischer, H. Factors influencing the C-O-bond homolysis of trialkylhydroxylamines. *Macromolecules* **2000,** 33, (12), 4403-4410.

35. Drockenmuller, E.; Catala, J.-M. Synthesis of a New Stable β-Sulfinyl Nitroxide and the Corresponding Alkoxyamine for Living/Controlled Radical Polymerization of Styrene: Kinetic and ESR Studies. *Macromolecules* **2002,** 35, (7), 2461-2466.

36. Sobek, J.; Martschke, R.; Fischer, H. Entropy Control of the Cross-Reaction between Carbon-Centered and Nitroxide Radicals. *J. Am. Chem. Soc.* **2001,** 123, (12), 2849-2857.

37. Goto, A.; Fukuda, T. Kinetics of living radical polymerization. *Prog. Polym. Sci.* **2004,** 29, (4), 329-385.

38. Catala, J. M.; Bubel, F.; Hammouch, S. O. Living Radical Polymerization: Kinetic Results. *Macromolecules* **1995,** 28, (24), 8441-8443.

39. Ananchenko, G. S.; Souaille, M.; Fischer, H.; Le Mercier, C.; Tordo, P. Decomposition of model alkoxyamines in simple and polymerizing systems. II. Diastereomeric N-(2-methylpropyl)-N-(1-diethyl-phosphono-2,2-dimethylpropyl)-aminoxyl-b ased compounds. *J. Polym. Sci. Pol. Chem.* **2002,** 40, (19), 3264-3283.

40. Gryn'ova, G.; Lin, C. Y.; Coote, M. L. Which side-reactions compromise nitroxide mediated polymerization? *Polym. Chem.* **2013,** 4, (13), 3744-3754.

41. Nicolas, J.; Guillaneuf, Y.; Lefay, C.; Bertin, D.; Gigmes, D.; Charleux, B. Nitroxide-mediated polymerization. *Progress in Polymer Science* **2013,** 38, (1), 63-235.

42. Gody, G.; Zetterlund, P. B.; Perrier, S.; Harrisson, S. The limits of precision monomer placement in chain growth polymerization. *Nat Commun* **2016,** 7.

Appendix D. How penultimate monomer unit effects and initiator influence ICAR ATRP of *n*-butyl acrylate and methyl methacrylate

D.1 Influence of backbiting reactions

As a copolymerization using *n*-butyl acrylate is performed, backbiting can occur. In order to assess the influence of backbiting on the polymerization kinetics, simulations with and without backbiting under the reference condition chosen in the main text have been first performed. It is assumed for simplicity that both R_{11} and R_{21} species can undergo backbiting with the same rate coefficient (k_{bb}^{chem} = 7.41 × 10^7 exp(-32.7 kJ mol^{-1}/R/T))[1] and this independent from the nature of the unit being present at the pen-penultimate position. The propagation rate coefficient of the formed tertiary species after a backbiting reaction is assumed to be 2 orders of magnitude lower than the respective secondary macrospecies and the activation rate coefficient and deactivation coefficient are assumed one order of magnitude higher and lower, respectively.[2, 3]

The result is shown in Figure D.1 and shows a negligible influence of backbiting on the ICAR ATRP kinetics. Since at the highest temperature already with this modeling strategy (too high backbiting reactivities for copolymerization) no effect is observed, backbiting can be safely ruled out for the simulations in the main text.

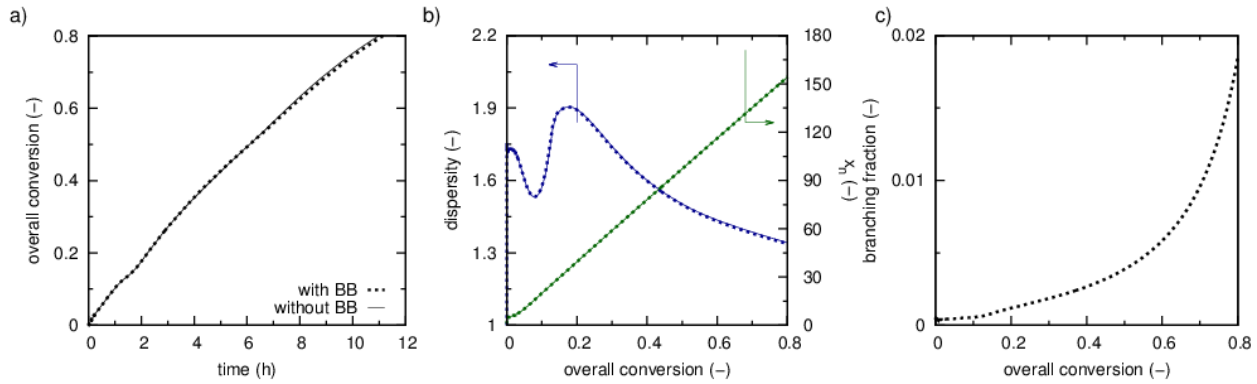

Figure D.1. *(a) Overall monomer conversion as a function of time, (b) dispersity (blue) and number averaged chain length (x_n, green), (c) branching fraction (with respect to monomer; molar) as a function of overall monomer conversion for ICAR ATRP of n-butyl acrylate (M_1) and methyl methacrylate (M_2) at 363K ($[M]_0$:$[R_0X]_0$:$[I_2]_0$ = 200:1:0.03; $[M_1]_0 = [M_2]_0$; initial Cu(II) ppm level = 40 ppm) using a tertiary ($k_{a0} = k_{a22}$; full lines) ATRP initiator with backbiting reactions (dotted line) and without (full line); parameters: see Table D.1.*

D.2 Full kinetic model

An overview of the reactions and Arrhenius parameters with the full kinetic model (all PMU effects accounted for) is given in Table D.1. Also the way of the calculation of the rate coefficients is provided. Actual values for propagation and deactivation are provided in Table D.3.

Table D.1. *Reactions and Arrhenius parameters for the simulation of ICAR ATRP of n-butyl acrylate (M_1) and methyl methacrylate (M_2) using Cu(II)Br2/PMDETA as deactivator and with the reference ATRP and conventional radical initiator (see main manuscript). Also values at 363K.*

Reaction			k_{chem} (363K) ((L mol^{-1}) s^{-1})	A ((L mol^{-1}) s^{-1})	E_a (kJ mol^{-1})	ref
Dissociation	D1[a]	$I_2 \xrightarrow{f^{chem}k_{dis}^{chem}} 2I$	5.3×10^{-5}	2.9×10^{14}	130.2	[4]
Chain initiation	CI1	$I + M_1 \xrightarrow{k_{pI1}^{chem}} IM_1$	$k_{p22,2}^{chem}/r_2$	2.4×10^{6}	24.6	[5, 6]
	CI2	$I + M_2 \xrightarrow{k_{pI2}^{chem}} IM_2$	$k_{p22,2}^{chem}$	2.6×10^{6}	22.3	[6]
	CI3	$IM_1 + M_1 \xrightarrow{k_{pIM1,1}^{chem}} R_{11}$	$k_{p11,1}^{chem} \times s_1$	1.3×10^{7}	18.8	[5, 7]
	CI4	$IM_1 + M_2 \xrightarrow{k_{pIM1,2}^{chem}} R_{12}$	$k_{p11,1}^{chem} \times s_1 / r_1'$	9.3×10^{6}	15.7	[5, 7]
	CI5	$IM_2 + M_1 \xrightarrow{k_{pIM2,1}^{chem}} R_{21}$	$k_{p22,2}^{chem}/r_2$	2.4×10^{6}	24.6	[5, 6]
	CI6	$IM_2 + M_2 \xrightarrow{k_{pIM2,2}^{chem}} R_{22}$	$k_{p22,2}^{chem}$	2.6×10^{6}	22.3	[6]
	CI7	$R_0 + M_1 \xrightarrow{k_{p01}^{chem}} R_0M_1$	$k_{p22,2}^{chem}/r_2$	2.4×10^{6}	24.6	[5, 6]
	CI8	$R_0 + M_2 \xrightarrow{k_{p02}^{chem}} R_0M_2$	$k_{p22,2}^{chem}$	2.6×10^{6}	22.3	[6]
	CI9	$R_0M_1 + M_1 \xrightarrow{k_{pR0M1,1}^{chem}} R_{11}$	$k_{p11,1}^{chem} \times s_1$	1.3×10^{7}	18.8	[5, 7]
	CI10	$R_0M_1 + M_2 \xrightarrow{k_{pR0M1,2}^{chem}} R_{12}$	$k_{p11,1}^{chem} \times s_1 / r_1'$	9.3×10^{6}	15.7	[5, 7]
	CI11	$R_0M_2 + M_1 \xrightarrow{k_{pR0M2,1}^{chem}} R_{21}$	$k_{p22,2}^{chem}/r_2$	2.4×10^{6}	24.6	[5, 6]
	CI12	$R_0M_2 + M_2 \xrightarrow{k_{pR0M2,2}^{chem}} R_{22}$	$k_{p22,2}^{chem}$	2.6×10^{6}	22.3	[6]

Table D.1. *Continued*

Propagation	P1	$R_{i,11} + M_1 \xrightarrow{k_{p11,1}^{chem}} R_{i+1,11}$	5.6×10^4	1.8×10^7	17.4	[7]
	P2	$R_{i,11} + M_2 \xrightarrow{k_{p11,2}^{chem}} R_{i+1,12}$	$k_{p11,1}^{chem}/r_1$	7.2×10^6	12.7	[5, 7]
	P3	$R_{i,21} + M_1 \xrightarrow{k_{p21,1}^{chem}} R_{i+1,11}$	$k_{p11,1}^{chem} \times s_1$	1.3×10^7	18.8	[5, 7]
	P4	$R_{i,21} + M_2 \xrightarrow{k_{p21,2}^{chem}} R_{i+1,12}$	$k_{p11,1}^{chem} \times s_1 / r_1'$	9.3×10^6	15.7	[5, 7]
	P5	$R_{i,12} + M_1 \xrightarrow{k_{p12,1}^{chem}} R_{i+1,21}$	$k_{p22,2}^{chem} \times s_2 / r_2'$	3.6×10^6	24.6	[5, 6]
	P6	$R_{i,12} + M_2 \xrightarrow{k_{p12,2}^{chem}} R_{i+1,22}$	$k_{p22,2}^{chem} \times s_2$	2.7×10^6	21.0	[5, 6]
	P7	$R_{i,22} + M_1 \xrightarrow{k_{p22,1}^{chem}} R_{i+1,21}$	$k_{p22,2}^{chem}/r_2$	2.4×10^6	24.6	[5, 6]
	P8	$R_{i,22} + M_2 \xrightarrow{k_{p22,2}^{chem}} R_{i+1,22}$	1.6×10^3	2.6×10^6	22.3	[6]

Table D.1. *Continued*

Activation	A1	$M_t^n X/L + IX \xrightarrow{k_{a,IX}^{chem}} M_t^{n+1} X_2/L + I$	k_{a22}^{chem}	4.0×10^{6}	27.7	[8]
	A2	$M_t^n X/L + R_0 X \xrightarrow{k_{a0}^{chem}} M_t^{n+1} X_2/L + R_0$	k_{a22}^{chem}	4.0×10^{6}	27.7	[8]
	A3	$M_t^n X/L + R_0 M_1 X \xrightarrow{k_{a01}^{chem}} M_t^{n+1} X_2/L + R_0 M_1$	$k_{a11}^{chem} \times s_{a,1}$	7.1×10^{5}	32.6	[9, 10]
	A4	$M_t^n X/L + R_0 M_2 X \xrightarrow{k_{a02}^{chem}} M_t^{n+1} X_2/L + R_0 M_2$	k_{a22}^{chem}	4.0×10^{6}	27.7	[8]
	A5	$M_t^n X/L + IM_1 X \xrightarrow{k_{aI1}^{chem}} M_t^{n+1} X_2/L + IM_1$	$k_{a11}^{chem} \times s_{a,1}$	7.18×10^{5}	32.6	[9, 10]
	A6	$M_t^n X/L + IM_2 X \xrightarrow{k_{aI2}^{chem}} M_t^{n+1} X_2/L + IM_2$	k_{a22}^{chem}	4.0×10^{6}	27.7	[8]
	A7	$M_t^n X/L + R_{i,11} X \xrightarrow{k_{a11}^{chem}} M_t^{n+1} X_2/L + R_{i,11}$	3.0×10^{-1}	1.5×10^{4}	32.6	[9]
	A8	$M_t^n X/L + R_{i,22} X \xrightarrow{k_{a22}^{chem}} M_t^{n+1} X_2/L + R_{i,22}$	4.1×10^{2}	4.0×10^{6}	27.7	[8]
	A9	$M_t^n X/L + R_{i,21} X \xrightarrow{k_{a21}^{chem}} M_t^{n+1} X_2/L + R_{i,21}$	$k_{a11}^{chem} \times s_{a,1}$	7.1×10^{5}	32.6	[9, 10]
	A10	$M_t^n X/L + R_{i,12} X \xrightarrow{k_{a12}^{chem}} M_t^{n+1} X_2/L + R_{i,12}$	$k_{a22}^{chem} \times s_{a,2}$	1.5×10^{8}	40.1	[8, 10]
Deactivation	DA1	$M_t^{n+1} X_2/L + I \xrightarrow{k_{da,I}^{chem}} M_t^n X/L + IX$	k_{da22}^{chem}	2.0×10^{8}	8.0	[8]
	DA2	$M_t^{n+1} X_2/L + R_0 \xrightarrow{k_{da0}^{chem}} M_t^n X/L + R_0 X$	k_{da22}^{chem}	2.0×10^{8}	8.0	[8]
	DA3	$M_t^{n+1} X_2/L + R_0 M_1 \xrightarrow{k_{da01}^{chem}} M_t^n X/L + R_0 M_1 X$	$k_{da11}^{chem} \times s_{da,1}$	1.9×10^{8}	8.0	[3]
	DA4	$M_t^{n+1} X_2/L + R_0 M_2 \xrightarrow{k_{da02}^{chem}} M_t^n X/L + R_0 M_2 X$	k_{da22}^{chem}	2.0×10^{8}	8.0	[8]
	DA5	$M_t^{n+1} X_2/L + IM_1 \xrightarrow{k_{daI1}^{chem}} M_t^n X/L + IM_1 X$	$k_{da11}^{chem} \times s_{da,1}$	1.9×10^{8}	8.0	[3]
	DA6	$M_t^{n+1} X_2/L + IM_2 \xrightarrow{k_{daI2}^{chem}} M_t^n X/L + IM_2 X$	k_{da22}^{chem}	2.0×10^{8}	8.0	[8]
	DA7	$M_t^{n+1} X_2/L + R_{i,11} \xrightarrow{k_{da11}^{chem}} M_t^n X/L + R_{i,11} X$	1.5×10^{8}	1.5×10^{8}	0.1	[3]
	DA8	$M_t^{n+1} X_2/L + R_{i,22} \xrightarrow{k_{da22}^{chem}} M_t^n X/L + R_{i,22} X$	1.4×10^{7}	2.0×10^{8}	8.0	[8]
	DA9	$M_t^{n+1} X_2/L + R_{i,21} \xrightarrow{k_{da21}^{chem}} M_t^n X/L + R_{i,21} X$	$k_{da11}^{chem} \times s_{da,1}$	1.9×10^{8}	8.0	[3]
	DA10	$M_t^{n+1} X_2/L + R_{i,12} \xrightarrow{k_{da12}^{chem}} M_t^n X/L + R_{i,12} X$	$k_{da22}^{chem} \times s_{da,2}$	1.4×10^{8}	0.1	[8]

Table D.1. *Continued*

Termination	T1	$R_0 + R_0 \xrightarrow{k_{tc,00}^{chem}/k_{td,00}^{chem}} R_0R_0/2P_0$	RAFT-CLD-T apparent kinetic parameters to account for diffusional limitations on termination; no intrinsic parameters needed
	T2	$R_0 + R_{i,1} \xrightarrow{k_{tc,0i1}^{chem}/k_{td,0i1}^{chem}} P_i/P_i + P_0$	
	T3	$R_0 + R_{i,2} \xrightarrow{k_{tc,0i2}^{chem}/k_{td,0i2}^{chem}} P_i/P_i + P_0$	
	T4	$R_{i,11} + R_{j,11} \xrightarrow{k_{tc,ij,1111}^{chem}/k_{td,ij,1111}^{chem}} P_{i+j}/P_i + P_j$	
	T5	$R_{i,11} + R_{j,12} \xrightarrow{k_{tc,ij,1112}^{chem}/k_{td,ij,1112}^{chem}} P_{i+j}/P_i + P_j$	
	T6	$R_{i,11} + R_{j,21} \xrightarrow{k_{tc,ij,1121}^{chem}/k_{td,ij,1121}^{chem}} P_{i+j}/P_i + P_j$	
	T7	$R_{i,11} + R_{j,22} \xrightarrow{k_{tc,ij,1122}^{chem}/k_{td,ij,1122}^{chem}} P_{i+j}/P_i + P_j$	
	T8	$R_{i,22} + R_{j,12} \xrightarrow{k_{tc,ij,2212}^{chem}/k_{td,ij,2212}^{chem}} P_{i+j}/P_i + P_j$	
	T9	$R_{i,22} + R_{j,21} \xrightarrow{k_{tc,ij,2221}^{chem}/k_{td,ij,2221}^{chem}} P_{i+j}/P_i + P_j$	
	T10	$R_{i,22} + R_{j,22} \xrightarrow{k_{tc,ij,2222}^{chem}/k_{td,ij,2222}^{chem}} P_{i+j}/P_i + P_j$	
	T11	$R_{i,12} + R_{j,21} \xrightarrow{k_{tc,ij,1221}^{chem}/k_{td,ij,1221}^{chem}} P_{i+j}/P_i + P_j$	
	T12	$R_{i,12} + R_{j,12} \xrightarrow{k_{tc,ij,1212}^{chem}/k_{td,ij,1212}^{chem}} P_{i+j}/P_i + P_j$	
	T13	$R_{i,21} + R_{j,21} \xrightarrow{k_{tc,ij,1221}^{chem}/k_{td,ij,1221}^{chem}} P_{i+j}/P_i + P_j$	

D.3 Determination of Arrhenius relationships for the (de)activation reactivity ratios

As described in the main text, the activation radical reactivity ratios are taken from the experimental study of Kumar *et al.* at 308 K using the TEMPO trapping method:[10]

$s_{a,1}$	$s_{a,2}$
4.72	0.20

If it is assumed that the deactivation steps are as good as not activated,[11, 12] and hence their activation energies can be assumed zero, every ATRP activation/deactivation reaction enthalpy ($\Delta_r H$) can be taken equal to the corresponding activation energy of the ATRP activation reaction. The activation energies for the ATRP activation radical reactivity ratios ($s_{a,1}$ and $s_{a,2}$) can be calculated as follow:

From the definition of the activation radical reactivity ratio (here focus on "1")

$$s_{a,1} = \frac{k_{a21}^{chem}}{k_{a11}^{chem}} = \frac{A_{a21}}{A_{a11}} \exp\left(-\frac{1}{R\,T}\left(E_{a,a21} - E_{a,a11}\right)\right) \tag{D.1}$$

and the definition

$$s_{a,1} = A\left(s_{a,1}\right) \exp\left(-\frac{E_a\left(s_{a,1}\right)}{R\,T}\right) \tag{D.2}$$

It follows:

$$E_a\left(s_{a,1}\right) = E_{a,a21} - E_{a,a11} \tag{D.3}$$

The Evans-Polanyi relationship dictates that:[13]

$$E_a = E_0 + \alpha(\Delta_r H - \Delta_r H_0) \tag{D.4}$$

in which E_0 is the activation energy of a reference reaction of the same class, α is a value between 0 and 1 which characterizes the position of the transition state along the reaction coordinate, and $\Delta_r H$ is the enthalpy of reaction.

Hence it follows that:

$$E_a(s_{a,1}) = \left(E_0 + \alpha(\Delta_r H_{21} - \Delta_r H_0)\right) - \left(E_0 + \alpha(\Delta_r H_{11} - \Delta_r H_0)\right) = \alpha(\Delta_r H_{21} - \Delta_r H_{11}) \quad \text{(D.5)}$$

Since upon a comparison of different ATRP activations the only difference is the homolytic breakage of the R-X bond, it suffices to focus on the corresponding ΔH_{BDE} only. The thermodynamic parameters related to the equilibrium coefficients for the homolytic bond rupture of M_1-X bond in H-M_2-M_1-X (or H-M_1-X for K_0) are taken from the computational study by Lin *et al.*:[14]

Table D.2. *Reported thermodynamic parameters for the homolytic bond rupture of the M_1-X Bond in H-M_2-M_1-X by Lin et al.* [14]

M_2	M_1	X	ΔH_{BDE} (kJ mol^{-1})	K/K_0
-	MA	Br	273.5	1
MA	MA	Br	281.0	0.63
MMA	MA	Br	281.1	2.37
-	MMA	Br	269.8	1
MA	MMA	Br	271.5	12.18
MMA	MMA	Br	256.1	43.77

The remaining unknown in eq. (D.5) is the value of α. Since it has been assumed that deactivation reactions are not activated, the energy levels of the transition state are very similar to the products (radical and deactivator). Taking into account Hammond's postulate[15] which dictates that a so-called "late" transition state is valid and literature data[16] it is safe to assume that α will approach 1, also keeping in mind the illustrative nature of the present work:

$$E_a(s_{a,1}) = 281.08\ kJ\ mol^{-1} - 281.04\ kJ\ mol^{-1} = 0.42\ kJ\ mol^{-1} \cong 0\ kJ\ mol^{-1} \quad \text{(D.6)}$$

$$E_a(s_{a,2}) = 271.54\ kJ\ mol^{-1} - 256.06\ kJ\ mol^{-1} = 15.48\ kJ\ mol^{-1} \quad \text{(D.7)}$$

The latter allows to calculate $s_{a,1}$ and $s_{a,2}$ at 298K. Furthermore, with the following relations the temperature independent $s_{da,1}$ and $s_{da,2}$ can be calculated:

$$\frac{\left(K/K_0\right)_{21}}{\left(K/K_0\right)_{11}} = \frac{k_{a21}^{chem}/k_{da21}^{chem}}{k_{a11}^{chem}/k_{da11}^{chem}} = \frac{s_{a,1}}{s_{da,1}} \quad \text{(D.8)}$$

$$\frac{\left(K/K_0\right)_{12}}{\left(K/K_0\right)_{22}} = \frac{k_{a12}^{chem}/k_{da12}^{chem}}{k_{a22}^{chem}/k_{da22}^{chem}} = \frac{s_{a,2}}{s_{da,2}} \quad \text{(D.9)}$$

Table D.3. *Intrinsic rate coefficients for propagation and (de)activation reactions for both the PMU and the terminal model for the ICAR ATRP of n-butyl acrylate (M_1) and methyl methacrylate (M_2) using Cu(II)Br2/PMDETA as deactivator at 363 K.*

	k (L mol^{-1} s^{-1})	PMU	T
Propagation	$k_{p11,1}^{chem}$	5.6×10^4	5.6×10^4
	$k_{p11,2}^{chem}$	1.1×10^5	1.1×10^5
	$k_{p21,1}^{chem}$	2.5×10^4	5.6×10^5
	$k_{p21,2}^{chem}$	5.1×10^4	1.1×10^5
	$k_{p12,1}^{chem}$	1.0×10^3	6.7×10^2
	$k_{p12,2}^{chem}$	2.5×10^3	1.6×10^3
	$k_{p22,1}^{chem}$	6.8×10^2	6.7×10^2
	$k_{p22,2}^{chem}$	1.6×10^3	1.6×10^3
Activation	k_{a11}^{chem}	3.0×10^{-1}	3.0×10^{-1}
	k_{a22}^{chem}	4.1×10^2	4.1×10^2
	k_{a21}^{chem}	1.5×10^0	3.0×10^{-1}
	k_{a12}^{chem}	2.1×10^2	4.1×10^2
Deactivation	k_{da11}^{chem}	1.4×10^8	1.4×10^8
	k_{da22}^{chem}	1.4×10^7	1.4×10^7
	k_{da21}^{chem}	1.7×10^8	1.4×10^8
	k_{da12}^{chem}	8.3×10^6	1.4×10^7

D.4 Calculation of apparent termination rate coefficients

The apparent homotermination rate coefficients (same chain lengths and monomer units in the present work) are calculated according to the RAFT-CLD-T method.[17] As before, RAFT-CLD-T values for methyl acrylate are used as an approximation for those of *n*BuA.

$$\begin{aligned}
&\text{for } i < i_{\mathrm{gel}} \text{ and } i < i_{\mathrm{SL}}\text{: } k_{\mathrm{t,ii}}^{\mathrm{app}} = k_{\mathrm{t,0}}^{\mathrm{app}} i^{-\alpha_{\mathrm{s}}} \\
&\text{for } i < i_{\mathrm{gel}} \text{ and } i \geq i_{\mathrm{SL}}\text{: } k_{\mathrm{t,ii}}^{\mathrm{app}} = k_{\mathrm{t,0}}^{\mathrm{app}} i_{\mathrm{SL}}^{\alpha_{\mathrm{l}}-\alpha_{\mathrm{s}}} i^{-\alpha_{\mathrm{l}}} \\
&\text{for } i \geq i_{\mathrm{gel}} \text{ and } i < i_{\mathrm{SL}}\text{: } k_{\mathrm{t,ii}}^{\mathrm{app}} = k_{\mathrm{t,0}}^{\mathrm{app}} i_{\mathrm{gel}}^{\alpha_{\mathrm{gel}}-\alpha_{\mathrm{s}}} i^{-\alpha_{\mathrm{gel}}} \\
&\text{for } i \geq i_{\mathrm{gel}} \text{ and } i < i_{\mathrm{SL}}\text{: } k_{\mathrm{t,ii}}^{\mathrm{app}} = k_{\mathrm{t,0}}^{\mathrm{app}} i_{\mathrm{SL}}^{\alpha_{\mathrm{l}}-\alpha_{\mathrm{s}}} i_{\mathrm{gel}}^{\alpha_{\mathrm{gel}}-\alpha_{\mathrm{l}}} i^{-\alpha_{\mathrm{gel}}}
\end{aligned} \tag{D.10}$$

The used RAFT-CLD-T parameters are given in Table D.4.

Table D.4. *RAFT-CLD-T parameters for n-butyl acrylate (M_1) and methyl methacrylate (M_2); data for homopolymerization.*[17]

	M_1	M_2
i_{gel}	5.40 $X_m^{-2.51}$	0.53 $X_m^{-2.5}$
i_{SL}	30	100
α_{s}	0.31	0.65
α_{l}	0.31	0.15
α_{gel}	0.81 X_m + 0.14	1.66 X_m -0.06
$\log\left(k_{t,0}^{app}\right)$	8.9	9.1

Because chain length distributions are narrow, the chain length *i* in the composite k_t model can be approximated by the average chain length of the dormant molecules, denoting the apparent homotermination rate coefficients for each monomer respectively as $k_{\mathrm{t,M1}}^{\mathrm{app}}$ and $k_{\mathrm{t,M2}}^{\mathrm{app}}$.

Based on the obtained apparent homotermination rate coefficients, a weighted rate coefficient $\langle k_t^{app} \rangle$ is calculated for the copolymerization process to take into account the chemical composition of the copolymer product, although first ignoring the nature of the terminal monomer units.

$$\langle k_{t,app} \rangle = \frac{\#M_{1,reacted}}{\#M_{1,reacted} + \#M_{2,reacted}} k_{\mathrm{t,M1}}^{\mathrm{app}} + \frac{\#M_{2,reacted}}{\#M_{1,reacted} + \#M_{2,reacted}} k_{\mathrm{t,M2}}^{\mathrm{app}} \qquad \text{(D.11)}$$

In a next step, $\langle k_t^{app} \rangle$ is corrected for the nature of the terminal units participating in the termination and the termination mode, using the fraction of recombination ($f_{rec,Mi}$) as defined for equal terminal monomer units ("11" and "22"). Acrylates most probably terminate mostly via recombination,[18] whereas it is widely accepted that methacrylates display a preference for disproportionation.[19] For methacrylates, a temperature dependent relationship between the ratio of disproportionation and recombination is available (eq. (D.12)).

$$\frac{1 - f_{rec,M2}}{f_{rec,M2}} = 0.556 \exp\left(-\frac{-1.854\ kJ\ mol^{-1}}{R\ T}\right) \qquad \text{(D.12)}$$

No such relation is available for acrylates, therefore it is assumed that for acrylates all termination happens via recombination at all temperatures ($f_{rec,M1} = 1$).

For termination between macrospecies of alike and unlike terminal nature, the apparent termination rate coefficients can thus be calculated as follows:

$$k_{tc,ij,11}^{app} = f_{rec,M1} \langle k_{t,app} \rangle;\ k_{td,ij,11}^{app} = (1 - f_{rec,M1}) \langle k_{t,app} \rangle \qquad \text{(D.13)}$$

$$k_{tc,ij,22}^{app} = f_{rec,M2}\langle k_{t,app}\rangle;\ k_{td,ij,22}^{app} = (1 - f_{rec,M2})\langle k_{t,app}\rangle \quad \text{(D.14)}$$

$$k_{tc,ij,12}^{app} = \frac{f_{rec,M1} + f_{rec,M2}}{2}\langle k_{t,app}\rangle;\ k_{td,ij,12}^{app} = \frac{(1 - f_{rec,M1}) + (1 - f_{rec,M2})}{2}\langle k_{t,app}\rangle \quad \text{(D.15)}$$

Termination between mono- or dimeric species and their termination with macrospecies are also taken into account. For termination between the small mono- and dimeric species, the secondary or tertiary nature of the species is taken into account and the corresponding $k_{t,0}^{app}$ is used as termination rate coefficient. For the termination of small or macroradicals, the apparent termination rate coefficient is determined as the square root of the product.[20]

D.5 Identification of suited batch conditions and initiator types

In this subsection, the major results of the grid simulations are discussed, considering only batch reaction conditions at a reference temperature of 363 K with for both comonomers the same initial molar amounts ($[M_1]_0 = [M_2]_0$). The grid simulations include variations of the following ICAR ATRP characteristics: (i) the targeted chain length (TCL; 100-350), which is defined as the initial molar ratio of monomer to ATRP initiator, (ii) the initial deactivator amount (10-70 ppm), (iii) the initial molar ratio of conventional radical initiator to ATRP initiator ($[I_2]_0/[R_0X]_0$; 0.015-0.05), (iv) the dissociation rate coefficient (k_{dis}^{chem}; 6.3×10^{-6} - 2.5×10^{-4} s^{-1}), and (v) the activation rate coefficient of the ATRP initiator (k_{a0}^{chem}; 3.0×10^{-1} - 4.1×10^{2} L mol^{-1} s^{-1}). For simplicity the corresponding deactivation rate coefficient (k_{da0}^{chem}) is not altered, as preliminary simulations showed that this parameter is kinetically less significant (see further this subsection).

D.5.1 Grid results for polymerization time and dispersity

In Figure D.2, the final polymerization times to reach a X_m of 0.80 and the corresponding dispersities are depicted, each time varying 2 characteristics while keeping the other ones fixed as defined by the yellow spheres in the other subplots. These spheres also relate to the optimal set of

batch ICAR ATRP characteristics as determined via the grid simulations. The corresponding average chain length (x_n) and EGF values are given for completeness in Figure D.3 of the Supporting Information. Since in all cases the control over chain length can be best represented by an inspection of the dispersity plots and the EGF values are all very high (> 0.95) this preference of Figure D.2 over Figure D.3 to identify optimal ICAR ATRP characteristics can be explained.

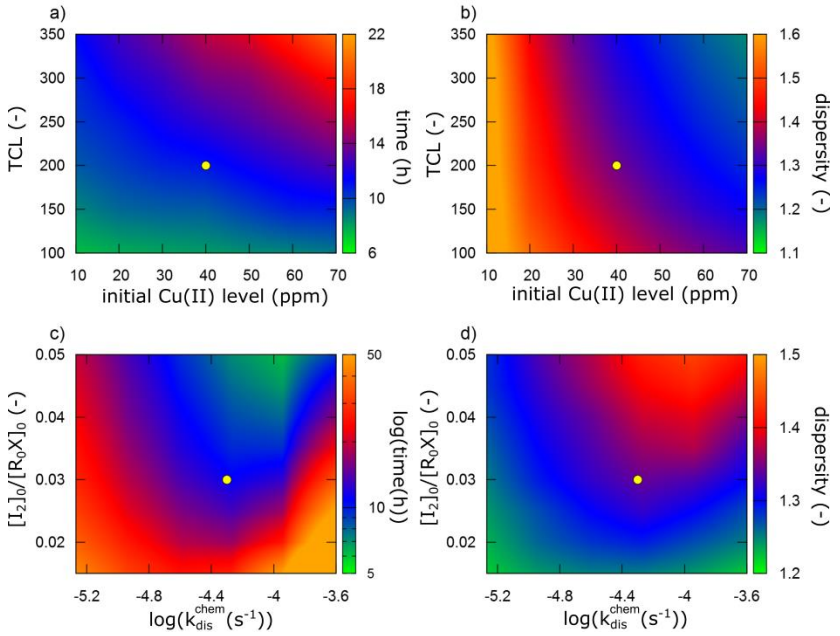

Figure D.2. *Mapping of the impact of (a-c) the targeted chain length (TCL) and initial Cu(II) level, (c-d) $[I_2]_0/[R_0X]_0$ and dissociation rate coefficient (k_{dis}^{chem}) on the polymerization time (left) and dispersity (right) (overall conversion of X_m = 0.80) for ICAR ATRP of n-butyl acrylate (M_1) and methyl methacrylate (M_2) at 363K with $[M_1]_0 = [M_2]_0$; yellow dots: optimized batch system with tertiary ATRP initiator (k_{a0}^{chem} =4.1 × 10^2 L mol^{-1} s^{-1}) and $[M]_0:[R_0X]:[I_2]_0$ = 200:1:0.03 and initial Cu(II) ppm level = 40 ppm.*

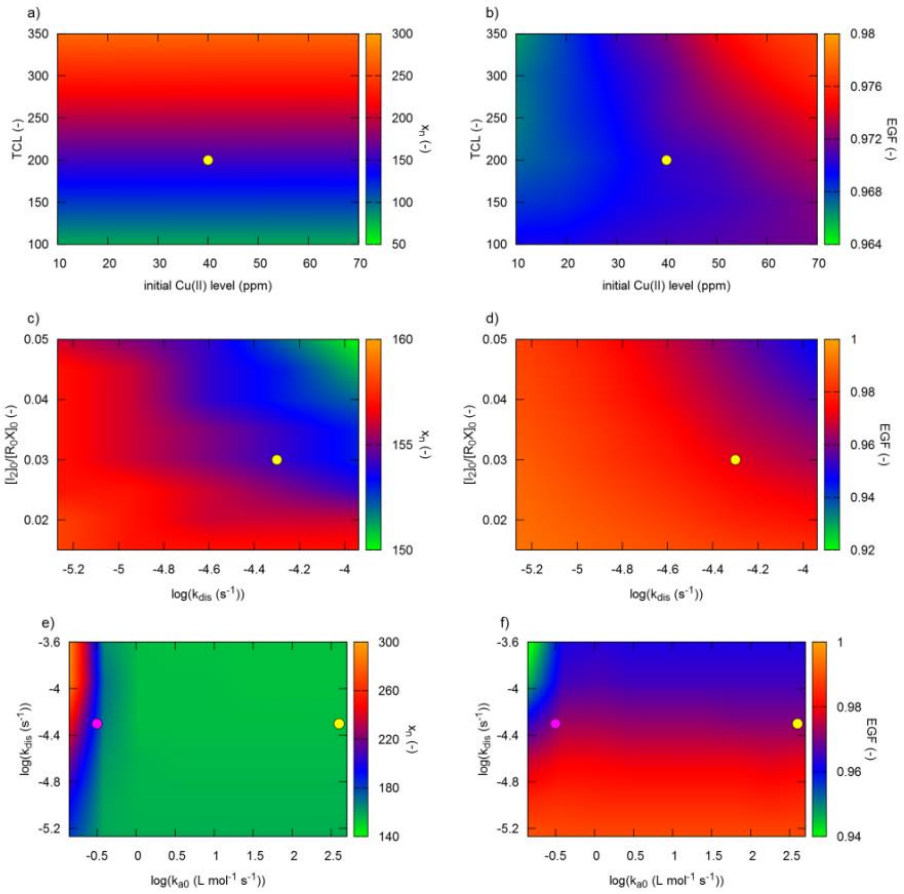

Figure D.3. *Mapping of the impact of (a) targeted chain length (TCL) and initial Cu(II) level, (b) $[I_2]/[R_0X]$ and conventional initiator dissociation rate coefficient (k_{dis}^{chem}), (c) k_{dis}^{chem} and ATRP initiator (R_0X) activation rate coefficient (k_{a0}^{chem}) for the ICAR ATRP of n-butyl acrylate (M_1) and methyl acrylate (M_2) at 363K on number averaged chain length (x_n) and the end-group functionality (EGF) at an overall monomer conversion of X_{ml} = 0.80. Yellow and pink dot: reference condition for tertiary and secondary ATRP initiator, respectively; $[M]_0:[R_0X]:[I_2]_0$ = 200:1:0.03, $[M_1]_0 = [M_2]_0$, initial Cu(II) ppm level = 40 ppm; corresponding figure for polymerization time and dispersity Figure 6.3 in the main text; parameters: see Table D.1.*

Keeping in mind that low initial deactivator amounts are preferred in ICAR ATRP,[21, 22] it can be seen in Figure D.2(a)-(b) that a trade-off between a reasonable polymerization rate and control over the polymer microstructure needs to be made, *i.e.* to reach the desired X_m of 0.80 lower

reaction times can be achieved by selecting lower initial deactivator amounts and TCLs, however these conditions result in higher dispersities. Therefore, an intermediate TCL of 200 and an initial deactivator amount of 40 ppm have been selected to define the suited batch ICAR ATRP system (yellow spheres), as these reaction conditions lead to an acceptable reaction time of *ca.* 11 hours while preserving control over the polymer microstructure with a dispersity of *ca.* 1.3. Similarly, $[I_2]_0/[R_0X]_0$ and k_{dis}^{chem} need to possess intermediate values, as illustrated in Figure D.2 (c)-(d). Optimal values of 0.03 and 5×10^{-5} s^{-1} (yellow spheres) are defined with higher values leading to fast but too uncontrolled ICAR ATRPs and lower ones resulting in a high microstructural control but a too slow polymerization. Note that the optimal k_{dis}^{chem} value is in good correspondence with commercially available conventional radical initiators.[4]

D.5.2 Grid results for number average chain length and end-group functionality

For variation of the TCL and the initial Cu(II) level it can be seen that the x_n shows a linear relationship with the TCL and is rather insensitive to the initial Cu(II) level, whereas the EGF varies only in a small range and shows in increase for higher initial Cu(II) levels. Varying k_{dis}^{chem} and $[I_2]_0/[R_0X]_0$ leads to a decrease of x_n, with higher values leading to an increased divergence from the ideal x_n profile as a higher number of $I^{\cdot}$ radicals is introduced in the system which has also been observed experimentally in previous ICAR ATRP homopolymerization studies,[23] and EGF for higher k_{dis}^{chem} and $[I_2]_0/[R_0X]_0$, which can be attributed to the higher number radicals being released. Finally, varying k_{a0}^{chem} and k_{dis}^{chem} confirms the threshold for k_{a0}^{chem} as explained in the main text and thus confirms the slow initiation for low k_{a0}^{chem} values leading to higher x_n values. The EGF is for the entire range relatively high but also confirms the loss of control for lower k_{a0}^{chem} and higher k_{dis}^{chem} values.

D.5.3 Detailed insights as a function of overall monomer conversion

In Figure D.4, some more detailed insights into the grid simulations are given by focusing on the full evolutions from low to high overall monomer conversion. A lower initial Cu(II) level leads to a slower establishment of the initiation regime (Figure D.4(b)). A higher R_{prop}/R_{deac} is also obtained along the process (Figure D.4(c)), highlighting again a less pronounced level of microstructural control.

For a given ratio of the initial amount of conventional initiator (I_2) to ATRP initiator (R_0X), a parabolic shape in both the reaction time and final dispersity appears in the main text (Figure 6.3(c)-(d)). Selecting three characteristic points of this parabolic shape, allows a more detailed kinetic understanding (Figure D.4; bottom row). A too high k_{dis}^{chem} leads to a rapid dissociation of the conventional initiator and thus also a high initial propagation rate (Figure D.4; bottom; right; blue line). However, a significant amount of termination reactions also lead to a build-up of deactivator thereby ultimately slowing down the polymerization, at the same time leading to a much lower R_{prop}/R_{deac} ratio thus resulting in an improved control at these higher conversions. A too low k_{dis}^{chem} value results in a high deactivator concentration along the whole polymerization. As a result, a long reaction time and polymerization with a good microstructural control results (red lines). Selecting a conventional initiator with an appropriate k_{dis}^{chem} value results in a dramatic decrease of polymerization time while maintaining a sufficiently low R_{prop}/R_{deac}, thus resulting in a reasonable control over the polymerization (green lines in Figure D.4; bottom row).

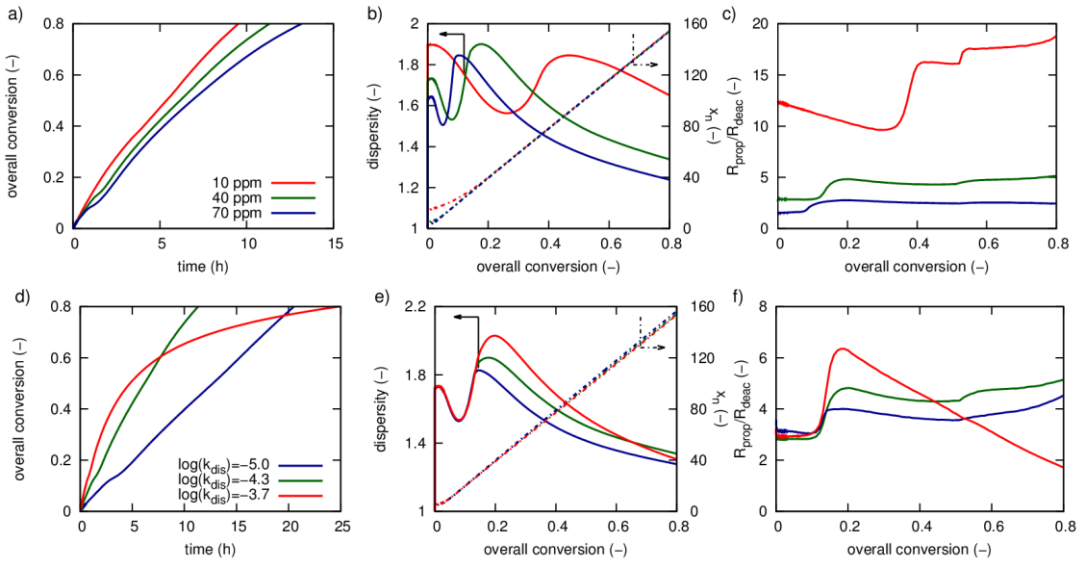

Figure D.4. *(a and d) Overall monomer conversion as a function of time, (b and e) dispersity (full lines) and number averaged chain length (dotted lines), (c and f) ratio of propagation rate to deactivation rate as a function of the overall monomer conversion for batch ICAR ATRP of n-butyl acrylate (M_1) and methyl methacrylate (M_2) at 363K ($[M]_0$:$[R_0X]_0$:$[I_2]_0$ = 200:1:0.03; $[M_1]_0 = [M_2]_0$ using a tertiary ATRP initiator for: (a-c) an initial Cu(II) level of 10 (red), 40 (green), 70 (blue) ppm; (d-f) a k_{dis}^{chem} of 1.0 × 10^{-5} (blue), 5.0 × 10^{-5} (green), and 2.0 × 10^{-4} (red) using an initial Cu(II) level of 40 ppm; parameters: see Table D.1.*

The influence of k_{a0}^{chem} has already been discussed in the main text and is mainly related to the initiation stage. Apart from the discussion secondary versus tertiary ATRP initiators, a few other peculiarities arise upon further inspection of Figure 6.3(e-f) (main text). At the reference k_{a0}^{chem}, it can be seen that an optimal k_{dis}^{chem} value exists for which a minimal reaction time can be achieved whilst having a limited influence on the dispersity. Again, this has to do with a depletion of conventional radical initiator or to slow dissociation and the corresponding effect on the deactivator concentration leading to the observed changes in the polymerization rate and R_{prop}/R_{deac}. The combination of both very low k_{a0}^{chem} and k_{dis}^{chem} values (upper left corner Figure D.3(e-f)) leads to FRP-like conditions resulting in a dispersity close to 2 and shorter reaction

times as to much initiator is released and activation of the R_0X species occurs at a slow rate resulting in low deactivator and high radical concentrations.

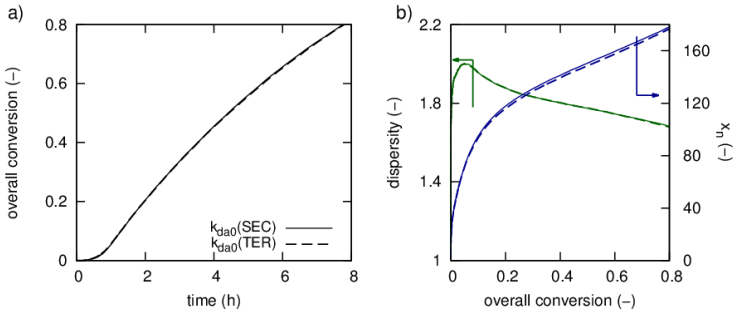

Figure D.5. *(a) Overall monomer conversion as a function of time, (b) dispersity (Đ, blue) and number averaged chain length (x_n, green) as a function of the overall monomer conversion for batch ICAR ATRP of n-butyl acrylate (M_1) and methyl methacrylate (M_2) at 363K ($[M]_0$:$[R_0X]_0$:$[I_2]_0$ = 200:1:0.03; $[M_1]_0$ = $[M_2]_0$; initial Cu(II) ppm level = 40 ppm) using a secondary (k_{a0}^{chem}= k_{a11}^{chem}) ATRP initiator with k_{da0}^{chem} = k_{da11}^{chem} (full lines; factor 10 higher) and k_{da0}^{chem} = k_{da22}^{chem} (dotted lines); parameters: see Table D.1.*

D.5.4 Validation of constant k_{da0}^{chem} for grid simulations

The grid simulation in Figure 6.3 (main text) and Figure D.3 vary k_{a0}^{chem} to find a suitable ATRP initiator which allows a good microstructural control. It is assumed that the value of k_{da0}^{chem} can be held fixed at the value of the reference tertiary R_0X species. However, it can be expected at first sight that as k_{a0}^{chem} changes, also a change in the value of k_{da0}^{chem} is needed. However preliminary simulation showed that the latter is not needed. In Figure D.5 it is demonstrated for a secondary ATRP initiator (pink dot in Figure D.3), that a negligible influence on the polymerization kinetics results upon assuming a higher rate coefficient (k_{da0}^{chem}=1.4 10^8 L mol^{-1} s^{-1}) than the one used of the grid which is strictly only representative for the tertiary case (k_{da0}^{chem}=1.4 10^7 L mol^{-1} s^{-1}). As the effect of assuming a k_{da0}^{chem} of a tertiary ATRP initiator can be expected to be most pronounced for a simulation with a secondary ATRP initiator, it is safe to say that for the entire

k_{a0}^{chem} range considered for the grid simulations the assumption made in this work (k_{da0}^{chem}=1.4 10^7 L mol^{-1} s^{-1}) is afforded.

D.5.5 Radical concentrations for the secondary and tertiary ATRP initiator type

Figure D.6 shows the concentrations for the 4 different macroradicals for a tertiary (full line) and secondary (dotted line) ATRP initiator. As terminal *n*BuA macroradicals are quickly transformed into terminal MMA macroradicals, the radical concentrations of the former are *ca.* two orders of magnitude lower than the terminal MMA macroradicals. On the other hand, the deactivation rate coefficient of terminal *n*BuA radicals is *ca.* one order of magnitude higher than for terminal MMA radicals, resulting in an rather similar initial build-up of all dormant macrospecies in the early stages of the polymerization (Figure 6.4(d) in the main text).

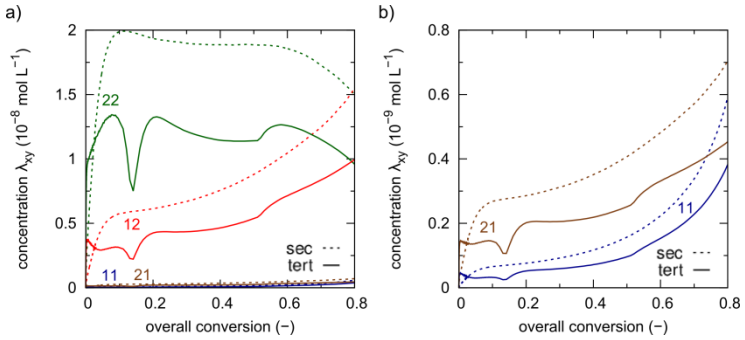

Figure D.6. *(a-b) concentration of radical macrospecies (τ_{11}, blue; τ_{22}, green; τ_{12}, red; τ_{21}, brown) as a function of overall monomer conversion for ICAR ATRP of n-butyl acrylate (M_1) and methyl methacrylate (M_2) at 363 K ($[M]_0$:$[R_0X]_0$:$[I_2]_0$ = 200:1:0.03; $[M_1]_0$ = $[M_2]_0$;Cu(II) ppm level = 40 ppm) using a secondary (dotted lines) and a tertiary (full lines) ATRP initiator; parameters: see Table D.1.*

D.6 Relevance of penultimate monomer unit effects

In Figure D.7, the influence of penultimate monomer unit effects on the concentration of dormant macrospecies is shown, as related to Figure 6.7 and 6.8 of the main text. Note the difference in the maximal concentration of the dormant τ_{12} species, as it influences the onset of the second

initiation stage, and the change in concentration of τ_{21} after the initiation stage is completed, between model 1/3 and model 2/4. The corresponding deactivator concentrations are given in Figure D.8. The influence on the explicit microstructure of the final copolymer chains is shown in Figure D.9. Similar microstructures result, but the full PMU model leads to the lowest dispersity.

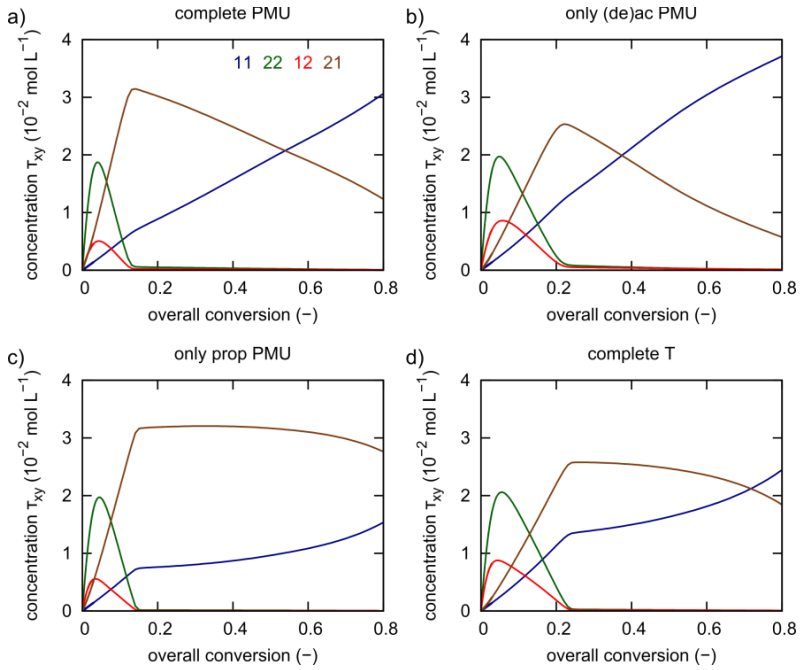

Figure D.7. *Concentration of dormant macrospecies (τ_{11}, blue; τ_{22}, green; τ_{12}, red; τ_{21}, brown) as a function of overall monomer conversion for ICAR ATRP of n-butyl acrylate (M_1) and methyl methacrylate (M_2) at 363K ($[M]_0$:$[R_0X]_0$:$[I_2]_0$ = 200:1:0.03; $[M_1]_0$ = $[M_2]_0$; Cu(II) ppm level = 40 ppm) using and a tertiary ($k_{a0}^{chem} = k_{a22}^{chem}$; full lines) ATRP initiator; (a): full PMU model (model 1), (b): only PMU effects on (de)activation reactions (model 2), (c): only PMU effects on propagation reactions (model 3), (d): full terminal model (model4); parameters: see Table D.1.*

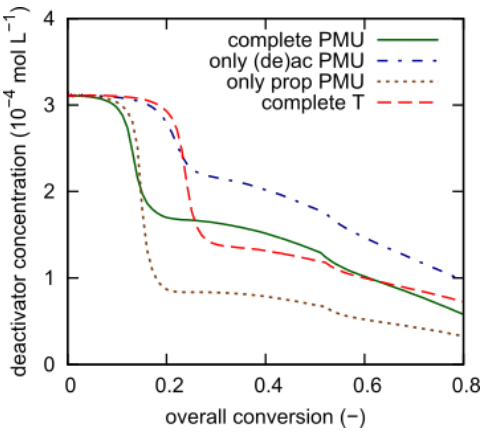

Figure D.8. *Concentration of deactivator as a function of overall monomer conversion for ICAR ATRP of n-butyl acrylate (M_1) and methyl methacrylate (M_2) at 363K ($[M]_0$:$[R_0X]_0$:$[I_2]_0$ = 200:1:0.03; $[M_1]_0$ = $[M_2]_0$; Cu(II) ppm level = 40 ppm) using and a tertiary ($k_{a0}^{chem} = k_{a22}^{chem}$; full lines) ATRP initiator full green lines: complete penultimate model (propagation and ATRP (de)activation; model 1); dashed-dotted blue lines: only PMU effects on ATRP (de)activation (model 2); dotted brown lines: only PMU effects on propagation (model 3); dashed red lines: complete terminal model (model 4); parameters: see Table D.1.*

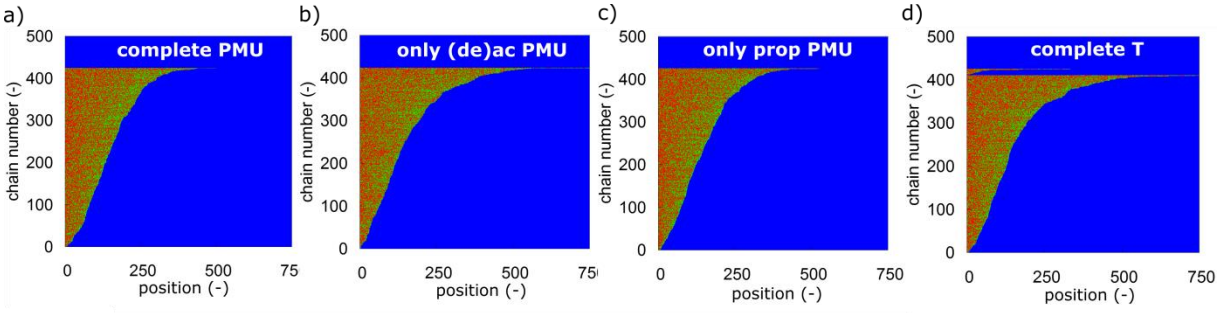

Figure D.9. *Explicit copolymer composition of ca. 400 chains out of a representative polymer sample of 150000 chains at an overall monomer conversion of 0.8 for ICAR ATRP of n-butyl acrylate (M_1; red) and methyl methacrylate (M_2; green) at 363 K ($[M]_0$:$[R_0X]_0$:$[I_2]_0$ = 200:1:0.03; $[M_1]_0$ = $[M_2]_0$; initial Cu(II) ppm level = 40 ppm) using a tertiary ATRP initiator with (a) complete penultimate model (propagation and ATRP (de)activation); (b) only PMU effects on ATRP (de)activation; (c) only PMU effects on propagation; (d) complete terminal model; parameters: see Table D.1.*

D.7 Relevance of temperature

The evolution of the gradient qualities, as related to Figure 6.10 (main text), are shown in Figure D.10. As can be seen, applying a full penultimate model at three temperatures, *i.e.* 343, 353, and 363 K, (in Figure D.10(a)), only results in minor changes in the gradient quality. However, the effect of using erroneous reactivity ratios at 293 K (brown line Figure D.10(b)), compared with the correct ones (green line Figure D.10(b)) does lead to large deviations of the obtained gradient quality, thus emphasizing the need for the determination of temperature dependent reactivity ratios.

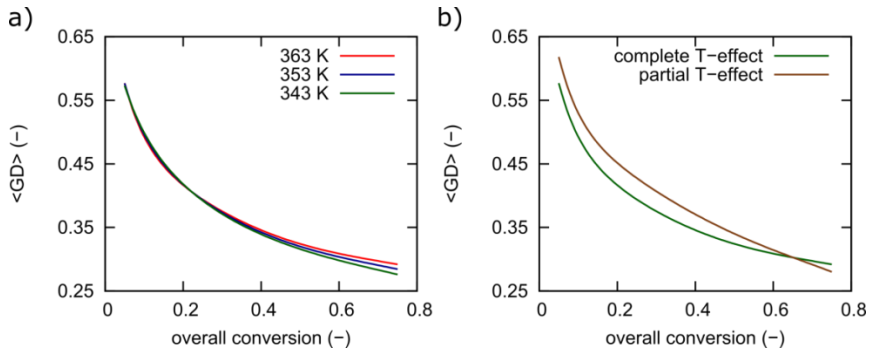

Figure D.10. *Influence of temperature effects on the gradient quality (<GD>) as a function of overall monomer conversion for batch ICAR ATRP of n-butyl acrylate (M_1) and methyl methacrylate (M_2) ($[M]_0$:$[R_0X]_0$:$[I_2]_0$ = 200:1:0.03; $[M_1]_0 = [M_2]_0$; Cu(II) ppm level = 40 ppm) using a tertiary initiator; (a) full PMU model at 363 K (red line), 353 K (blue line), 343 K (green line), (b) full PMU model at 363K using correct reactivity ratios at 363 K (green line), full PMU model at 363 K but using the typical literature values for the reactivity ratios at 293 K (brown line); parameters: see Table D.1.*

D.8 Identification of most suited multi-component fed-batch strategy

In Table D.5 the final ICAR ATRP properties are given for several analogous fed-batch strategies, *i.e.* starting with M_1 vs. M_2 and a secondary vs. tertiary R_0X type. As can be seen, starting with M_2, thus along with the naturally occurring gradient, only leads to a good ICAR ATRP if a secondary R_0X is used and this with a relatively high and thus not favorable final

dispersity. Using a tertiary R_0X results in a very inefficient R_0X initiation stage and only reaches a very low overall monomer conversion. Starting with M_1 leads to a successful ICAR ATRP using both R_0X types with very similar final properties. As a tertiary R_0X has been identified as the optimal one in the batch reference case, it was opted to also use under fed-batch conditions a tertiary R_0X starting with M_1, as this leads to the best microstructural control.

Table D.5. *Final ICAR ATRP properties for several starting configurations ICAR ATRP of n-butyl acrylate (M_1) and methyl methacrylate (M_2) at 363K using a fed-batch program as described in the main text; parameters: see Table D.1.*

		properties at end of ICAR ATRP				
starting monomer	**R_0X type**	**time (h)**	**X_m (-)**	**x_n (-)**	**$Đ$ (-)**	**EGF (-)**
M_1	**sec**	58	0.8	156	1.22	0.97
	tert	61	0.8	156	1.21	0.97
M_2	**sec**	55	0.8	157	1.42	0.98
	tert	40	0.002	417	1.65	0.99

D.9 Cumulative copolymerization compositions

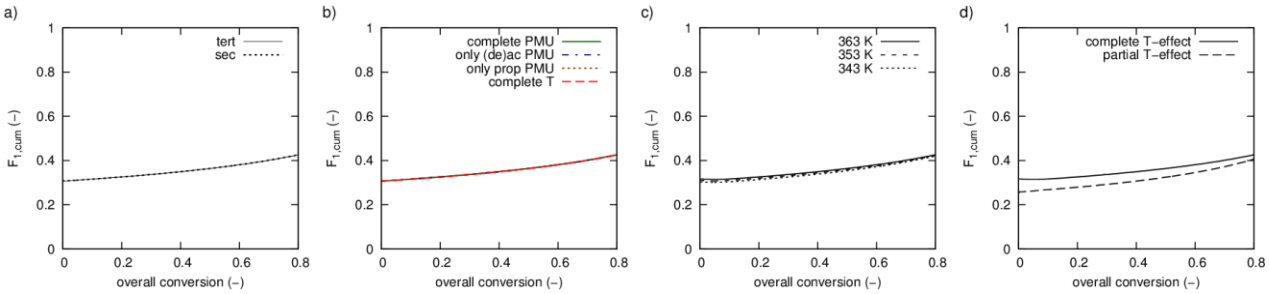

Figure D.11. *Cumulative copolymer composition ($F_{1,cum}$) as a function of overall monomer conversion for ICAR ATRP of n-butyl acrylate (M_1) and methyl methacrylate (M_2) at 363K ($[M]_0$:$[R_0X]_0$:$[I_2]_0$ = 200:1:0.03; $[M_1]_0 = [M_2]_0$; Cu(II) ppm level = 40 ppm): (a) using a secondary ($k_{a0}^{chem} = k_{a11}^{chem}$; dotted lines) and a tertiary ($k_{a0}^{chem} = k_{a22}^{chem}$; full lines) ATRP initiator (Figure 6.4 in Main text) and (b) considering several PMU effects (Figure 6.7 in Main text): full green lines: complete penultimate model (propagation and ATRP (de)activation; model 1); dashed-dotted blue lines: only PMU effects on ATRP (de)activation (model 2); dotted brown lines: only PMU effects on propagation (model 3); dashed red lines: complete terminal model (model 4); (c) full PMU model at 363 K (full lines), 353 K (dashed lines), 343 K (dotted lines); (d) full PMU model at 363K using correct reactivity ratios at 363 K (full lines), complete PMU model at 363 K but using the typical literature values for the reactivity ratios at 293 K (dashed lines); parameters: see Table D.1.*

References

1. Wang, W.; Nikitin, A. N.; Hutchinson, R. A. Consideration of Macromonomer Reactions in n-Butyl Acrylate Free Radical Polymerization. *Macromol. Rapid Commun.* **2009,** 30, (23), 2022-2027.

2. Konkolewicz, D.; Sosnowski, S.; D'hooge, D. R.; Szymanski, R.; Reyniers, M.-F.; Marin, G. B.; Matyjaszewski, K. Origin of the Difference between Branching in Acrylates Polymerization under Controlled and Free Radical Conditions: A Computational Study of Competitive Processes. *Macromolecules* **2011,** 44, (21), 8361-8373.

3. Toloza Porras, C.; D'hooge, D. R.; Reyniers, M. F.; Marin, G. B. Computer-Aided Optimization of Conditions for Fast and Controlled ICAR ATRP of n-Butyl Acrylate. *Macromol. Theory Simul.* **2013,** 22, (2), 136-149.

4. AkzoNobel https://www.akzonobel.com/polymer/our_products/polymerization_initiators/.

5. Yu, X.; Levine, S. E.; Broadbelt, L. J. Kinetic Study of the Copolymerization of Methyl Methacrylate and Methyl Acrylate Using Quantum Chemistry. *Macromolecules* **2008,** 41, (21), 8242-8251.

6. Beuermann, S.; Buback, M.; Davis, T. P.; Gilbert, R. G.; Hutchinson, R. A.; Olaj, O. F.; Russell, G. T.; Schweer, J.; van Herk, A. M. Critically evaluated rate coefficients for free-radical polymerization, 2.. Propagation rate coefficients for methyl methacrylate. *Macromol. Chem. Phys.* **1997,** 198, (5), 1545-1560.

7. Buback, M.; Kurz, C. H.; Schmaltz, C. Pressure dependence of propagation rate coefficients in free-radical homopolymerizations of methyl acrylate and dodecyl acrylate. *Macromol. Chem. Phys.* **1998,** 199, (8), 1721-1727.

8. Payne, K. A.; D'hooge, D. R.; van Steenberge, P. H. M.; Reyniers, M. F.; Cunningham, M. F.; Hutchinson, R. A.; Marin, G. B. ARGET ATRP of Butyl Methacrylate: Utilizing Kinetic Modeling To Understand Experimental Trends. *Macromolecules* **2013,** 46, (10), 3828-3840.

9. Toloza Porras, C.; D'hooge, D. R.; Van Steenberge, P. H. M.; Reyniers, M.-F.; Marin, G. B. A Theoretical Exploration of the Potential of ICAR ATRP for One- and Two-Pot Synthesis of Well-Defined Diblock Copolymers. *Macromol. React. Eng.* **2013,** 7, (7), 311-326.

10. Nanda, A. K.; Matyjaszewski, K. Effect of Penultimate Unit on the Activation Process in ATRP. *Macromolecules* **2003,** 36, (22), 8222-8224.

11. D'hooge, D. R.; Van Steenberge, P. H. M.; Reyniers, M.-F.; Marin, G. B. The strength of multi-scale modeling to unveil the complexity of radical polymerization. *Progress in Polymer Science* **2016,** 58, 59-89.

12. Mastan, E.; Li, X.; Zhu, S. Modeling and theoretical development in controlled radical polymerization. *Progress in Polymer Science* **2015,** 45, 71-101.

13. Screttas, C. G. Equivalent or alternative forms of the Evans-Polanyi-type relations. *The Journal of Organic Chemistry* **1980,** 45, (9), 1620-1623.

14. Lin, C. Y.; Coote, M. L.; Petit, A.; Richard, P.; Poli, R.; Matyjaszewski, K. Ab Initio Study of the Penultimate Effect for the ATRP Activation Step Using Propylene, Methyl Acrylate, and Methyl Methacrylate Monomers. *Macromolecules* **2007,** 40, (16), 5985-5994.

15. Hammond, G. S. A Correlation of Reaction Rates. *J. Am. Chem. Soc.* **1955,** 77, (2), 334-338.

16. Seeliger, F.; Matyjaszewski, K. Temperature Effect on Activation Rate Constants in ATRP: New Mechanistic Insights into the Activation Process. *Macromolecules* **2009,** 42, (16), 6050-6055.

17. Johnston-Hall, G.; Monteiro, M. J. Bimolecular radical termination: New perspectives and insights. *J. Polym. Sci. Pol. Chem.* **2008,** 46, (10), 3155-3173.

18. Ballard, N.; Hamzehlou, S.; Ruipérez, F.; Asua, J. M. On the Termination Mechanism in the Radical Polymerization of Acrylates. *Macromol. Rapid Commun.* **2016**, n/a-n/a.

19. Buback, M.; Günzler, F.; Russell, G. T.; Vana, P. Determination of the Mode of Termination in Radical Polymerization via Mass Spectrometry. *Macromolecules* **2009,** 42, (3), 652-662.

20. Fierens, S. K.; D'hooge, D. R.; Van Steenberge, P. H. M.; Reyniers, M.-F.; Marin, G. B. MAMA-SG1 initiated nitroxide mediated polymerization of styrene: From Arrhenius parameters to model-based design. *Chem. Eng. J.* **2015,** 278, 407-420.

21. Nesvadba, P., Radical Polymerization in Industry. In *Encyclopedia of Radicals in Chemistry, Biology and Materials*, John Wiley & Sons, Ltd: 2012.

22. Zhou, Y.-N.; Luo, Z.-H. State-of-the-Art and Progress in Method of Moments for the Model-Based Reversible-Deactivation Radical Polymerization. *Macromol. React. Eng.* **2016,** 10, (6), 516-534.

23. D'hooge, D. R.; Konkolewicz, D.; Reyniers, M.-F.; Marin, G. B.; Matyjaszewski, K. Kinetic Modeling of ICAR ATRP. *Macromol. Theory Simul.* **2012,** 21, (1), 52-69.

Appendix E. A qualitative evaluation of the impact of SG1 disproportionation and the addition of styrene in nitroxide mediated polymerization of methyl methacrylate

E.1 Overview of experimental conditions

Table E.1. *Overview of experimental conditions*

#	Temperature (set-point) (K)	TCL (-)	Initial m% sty (-)
1	333	200	0
2	343	200	0
3	353	200	0
4	363	200	2.5
5	363	200	5
6	363	200	10
7	363	500	5
8	363	500	10
9	363	750	5
10	363	750	7.5
11	363	750	10

E.2 Kinetic model

The reaction scheme (including penultimate monomer unit effects if necessary; see main text) used to simulate the nitroxide mediated polymerization of MMA with or without a small amount of styrene is given in Table E.2.

Table E.2. *Reactions and Arrhenius parameters for the simulation of NMP methyl methacrylate (M_1) and styrene (M_2) using BlocBuilder as NMP initiator (R_0X).*

Reaction			k_{chem} (363 K) ((L mol^{-1})) s^{-1}	A ((L mol^{-1})) s^{-1}	E_a (kJ mol^{-1})	ref
chain initiation	CI1	$R_0 + M_1 \xrightarrow{k_{p01}^{chem}} R_0M_1$	$10 \times k_{p11,1}^{chem}$ (1.6×10^4)	2.67×10^7	22.4	[1, 2]
	CI2	$R_0 + M_2 \xrightarrow{k_{p02}^{chem}} R_0M_2$	6.6×10^3	1.55×10^6	16.5	[3]
	CI3	$R_0M_1 + M_1 \xrightarrow{k_{pR0M1,1}^{chem}} R_{11}$	$k_{p11,1}^{chem}$ (1.64×10^4)	-	-	-
	CI4	$R_0M_1 + M_2 \xrightarrow{k_{pR0M1,2}^{chem}} R_{12}$	$k_{p11,1}^{chem}/r_1$ (3.2×10^3)	-	-	-
	CI5	$R_0M_2 + M_1 \xrightarrow{k_{pR0M2,1}^{chem}} R_{21}$	$k_{p22,2}^{chem} \times s_2/r_2'$ (6.4×10^2)	-	-	-
	CI6	$R_0M_2 + M_2 \xrightarrow{k_{pR0M2,2}^{chem}} R_{22}$	$k_{p22,2}^{chem} \times s_2$ (3.2×10^2)	-	-	-
Propagation	P1	$R_{i,11} + M_1 \xrightarrow{k_{p11,1}^{chem}} R_{i+1,11}$	1.6×10^3	2.67×10^6	22.4	[1]
	P2	$R_{i,11} + M_2 \xrightarrow{k_{p11,2}^{chem}} R_{i+1,12}$	$k_{p11,1}^{chem}/r_1$ (3.2×10^3)	-	-	-
	P3	$R_{i,21} + M_1 \xrightarrow{k_{p21,1}^{chem}} R_{i+1,11}$	$k_{p11,1}^{chem} \times s_1$ (9.6×10^2)	-	-	-
	P4	$R_{i,21} + M_2 \xrightarrow{k_{p21,2}^{chem}} R_{i+1,12}$	$k_{p11,1}^{chem} \times s_1/r_1'$ (1.9×10^3)	-	-	-
	P5	$R_{i,12} + M_1 \xrightarrow{k_{p12,1}^{chem}} R_{i+1,21}$	$k_{p22,2}^{chem} \times s_2/r_2'$ (6.4×10^2)	-	-	-
	P6	$R_{i,12} + M_2 \xrightarrow{k_{p12,2}^{chem}} R_{i+1,22}$	$k_{p22,2}^{chem} \times s_2$($3.2 \times 10^2$)	-	-	-
	P7	$R_{i,22} + M_1 \xrightarrow{k_{p22,1}^{chem}} R_{i+1,21}$	$k_{p22,2}^{chem}/r_2$ (1.8×10^3)	-	-	-
	P8	$R_{i,22} + M_2 \xrightarrow{k_{p22,2}^{chem}} R_{i+1,22}$	9.00×10^2	4.24×10^7	32.5	[4]

Table E.2. Continued

Activation	A1	$R_0X \xrightarrow{k_{a0}^{chem}} R_0 + X$	8.28×10^{-3}	1.16×10^{13}	105.3	[5]
	A2	$R_0M_1X \xrightarrow{k_{a01}^{chem}} R_0M_1 + X$	k_{a11}^{chem} (1.16)	-	-	-
	A3	$R_0M_2X \xrightarrow{k_{a02}^{chem}} R_0M_2 + X$	$k_{a22}^{chem} \times s_{a,2}$ (1.08×10^{-3})	-	-	-
	A4	$R_{i,11}X \xrightarrow{k_{a11}^{chem}} R_{i,11} + X$	1.16	2.40×10^{14}	99.5	[6]
	A5	$R_{i,22}X \xrightarrow{k_{a22}^{chem}} R_{i,22} + X$	1.65×10^{-4}	4.04×10^{17}	148.7	[5]
	A6	$R_{i,21}X \xrightarrow{k_{a21}^{chem}} R_{i,21} + X$	$k_{a11}^{chem} \times s_{a,1}$ (6.9×10^{-2})	-	-	-
	A7	$R_{i,12}X \xrightarrow{k_{a12}^{chem}} R_{i,12} + X$	$k_{a22}^{chem} \times s_{a,2}$ (1.08×10^{-3})	-	-	-
Deactivation	DA1	$R_0 + X \xrightarrow{k_{da0}^{chem}} R_0X$	2.80×10^{6}	2.80×10^{6}	0.0	[5]
	DA2	$R_0M_1 + X \xrightarrow{k_{da01}^{chem}} R_0M_1X$	k_{da11}^{chem} (1.10×10^{5})	-	-	-
	DA3	$R_0M_2 + X \xrightarrow{k_{da02}^{chem}} R_0M_2X$	$k_{da22}^{chem} \times s_{da,2}$ (1.10×10^{6})	-	-	-
	DA4	$R_{i,11} + X \xrightarrow{k_{da11}^{chem}} R_{i,11}X$	1.10×10^{5}	1.40×10^{5}	0.0	this work[a]
	DA5	$R_{i,22} + X \xrightarrow{k_{da22}^{chem}} R_{i,22}X$	1.10×10^{6}	1.10×10^{6}	0.0	[5]
	DA6	$R_{i,21} + X \xrightarrow{k_{da21}^{chem}} R_{i,21}X$	$k_{da11}^{chem} \times s_{da,1}$ (1.10×10^{5})	-	-	-
	DA7	$R_{i,12} + X \xrightarrow{k_{da12}^{chem}} R_{i,12}X$	$k_{da22}^{chem} \times s_{da,2}$ (1.10×10^{6})	-	-	-
Nitroxide side Reactions	TR1	$R_{i,11} + X \xrightarrow{k_{trM11X}^{chem}} P_i$	3.0×10^{3}	1.40×10^{7}	22.5	this work
	TR2	$R_{i,21} + X \xrightarrow{k_{trM21X}^{chem}} P_i$	3.0×10^{3}	1.40×10^{7}	22.5	this work

[a] k_{da11}^{chem} has been increased with a factor of 10 compared with its literature value.[6]

Table E.2. Continued

Termination	T1	$R_0 + R_0 \xrightarrow{k_{tc,00}^{chem}/k_{td,00}^{chem}} R_0R_0/2P_0$	RAFT-CLD-T apparent kinetic parameters to account for diffusional limitations on termination; no intrinsic parameters
	T2	$R_0 + R_{i,1} \xrightarrow{k_{tc,0i1}^{chem}/k_{td,0i1}^{chem}} P_i/P_i + P_0$	
	T3	$R_0 + R_{i,2} \xrightarrow{k_{tc,0i2}^{chem}/k_{td,0i2}^{chem}} P_i/P_i + P_0$	
	T4	$R_{i,11} + R_{j,11} \xrightarrow{k_{tc,ij,1111}^{chem}/k_{td,ij,1111}^{chem}} P_{i+j}/P_i + P_j$	
	T5	$R_{i,11} + R_{j,12} \xrightarrow{k_{tc,ij,1112}^{chem}/k_{td,ij,1112}^{chem}} P_{i+j}/P_i + P_j$	
	T6	$R_{i,11} + R_{j,21} \xrightarrow{k_{tc,ij,1121}^{chem}/k_{td,ij,1121}^{chem}} P_{i+j}/P_i + P_j$	
	T7	$R_{i,11} + R_{j,22} \xrightarrow{k_{tc,ij,1122}^{chem}/k_{td,ij,1122}^{chem}} P_{i+j}/P_i + P_j$	
	T8	$R_{i,22} + R_{j,12} \xrightarrow{k_{tc,ij,2212}^{chem}/k_{td,ij,2212}^{chem}} P_{i+j}/P_i + P_j$	
	T9	$R_{i,22} + R_{j,21} \xrightarrow{k_{tc,ij,2221}^{chem}/k_{td,ij,2221}^{chem}} P_{i+j}/P_i + P_j$	
	T10	$R_{i,22} + R_{j,22} \xrightarrow{k_{tc,ij,2222}^{chem}/k_{td,ij,2222}^{chem}} P_{i+j}/P_i + P_j$	
	T11	$R_{i,12} + R_{j,21} \xrightarrow{k_{tc,ij,1221}^{chem}/k_{td,ij,1221}^{chem}} P_{i+j}/P_i + P_j$	
	T12	$R_{i,12} + R_{j,12} \xrightarrow{k_{tc,ij,1212}^{chem}/k_{td,ij,1212}^{chem}} P_{i+j}/P_i + P_j$	
	T13	$R_{i,21} + R_{j,21} \xrightarrow{k_{tc,ij,1221}^{chem}/k_{td,ij,1221}^{chem}} P_{i+j}/P_i + P_j$	

In Table E.3 the reactivity ratios (definitions: see Equation (E.1) and (E.2)) used in this work are given.

$$r_1 = \frac{k_{p11,1}^{chem}}{k_{p11,2}^{chem}};\ r_2 = \frac{k_{p22,2}^{chem}}{k_{p22,1}^{chem}};\ r_1' = \frac{k_{p21,1}^{chem}}{k_{p21,2}^{chem}};\ r_2' = \frac{k_{p12,2}^{chem}}{k_{p12,1}^{chem}};\ s_1 = \frac{k_{p21,1}^{chem}}{k_{p11,1}^{chem}};\ s_2 = \frac{k_{p12,2}^{chem}}{k_{p22,2}^{chem}} \qquad \text{(E.1)}$$

$$s_{a,1} = \frac{k_{a21}^{chem}}{k_{a11}^{chem}}; s_{a,2} = \frac{k_{a12}^{chem}}{k_{a22}^{chem}};\ s_{da,1} = \frac{k_{da21}^{chem}}{k_{da11}^{chem}}; s_{da,2} = \frac{k_{da12}^{chem}}{k_{da22}^{chem}} \qquad \text{(E.2)}$$

The monomer reactivity ratios ($r^{(')}$) used are averaged values in the 293 – 333 K range (Table E.3). The radical reactivity ratios (*s*)have been determined at 330 K (Table E.3).[7] Hence, temperature dependency of these reactivity ratios are neglected. This is assumption is understandable, taking into account that no literature values are available and a large set of the copolymerization data is obtained under isothermal conditions for the most relevant monomer conversion range.

Table E.3. *Reactivity ratios for propagation and (de)activation in NMP of methyl methacrylate (M_1) and styrene (M_2) initiated by BlocBuilder.*

	propagation[8]						(de)activation[7]			
	r_1	r_2	r_1'	r_2'	s_1	s_2	$s_{a,1}$	$s_{a,2}$	$s_{da,1}$	$s_{da,2}$
r/s	0.49	0.49	0.49	0.49	0.60	0.36	0.06	6.7[a]	1.00	1.00

[a] determined in this work

It is however important to assess how accounting for temperature dependent reactivity ratios would influence the copolymer properties. Therefore, a sensitivity analysis has been performed on all reactivity ratios considered. It has been indicated in literature that the activation energy of reactivity ratios typically varies between 0 and 10 kJ mol^{-1}. A value of 10 kJ mol^{-1} is therefore conservatively chosen (-10 kJ mol^{-1} for s_{a2} as this is the one reactivity ratio larger than unity). The result of this sensitivity analysis is shown in Figure E.1 for a TCL of 200 at an initial styrene content of 10 m% (highest comonomer content) and 2.5 m% (most severe non-isothermal case). It can be concluded that a limited effect, mainly on dispersity at low X_M, is present. The effect is most pronounced for $r_2^{(')}$. Overall it is thus afforded – at least to a first approximation- to neglect the possible temperature dependence of the reactivity ratios.

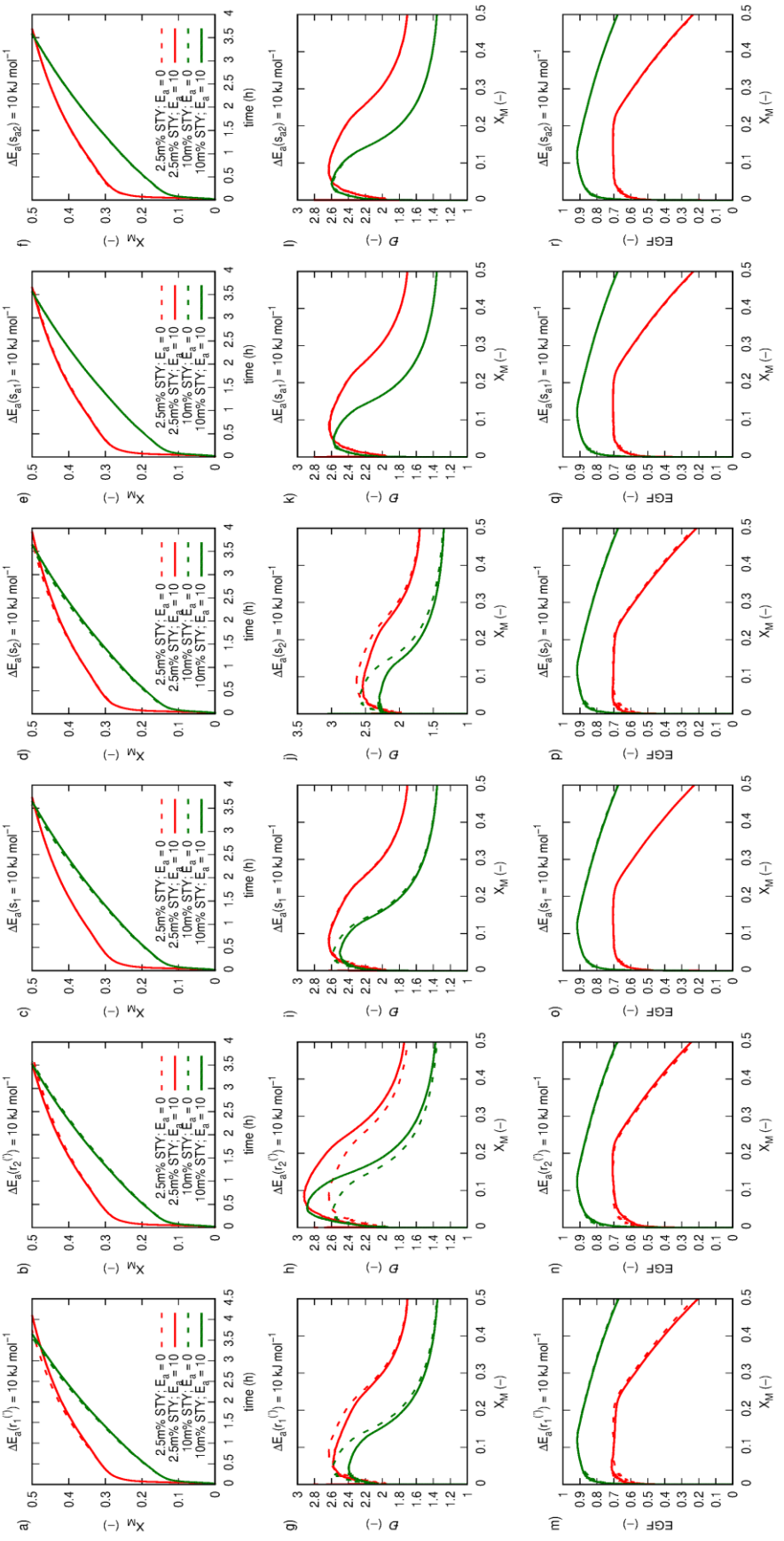

Figure E.1. *Effect of assuming activated reactivity ratios ($r_1^{(')}$ (a-g-m), $r_2^{(')}$ (b-h-n), s_1 (c-i-o), s_2 (d-j-p), s_{a1} (e-k-q), s_{a2} (f-l-r)) on NMP of MMA and styrene initiated by BlocBuilder for a T_{set} of 363 K and a TCL of 200 for various initial mass fractions of styrene (here no corrections for calibration range SEC trace): 10 m% (green lines) and 2.5 m% (red lines); (a-f) overall conversion as a function of time, (g-l) dispersity, (m-r) end-group functionality as a function of overall conversion (X_M); full lines correspond to simulation outcome if an activation energy of (+/-) 10 kJ mol^{-1} is assumed, dotted lines to non-activated reactivity ratios.*

Figure E.1. *Effect of assuming activated reactivity ratios ($r_1^{(')}$ (a-g-m), $r_2^{(')}$ (b-h-n), s_1 (c-i-o), s_2 (d-j-p), s_{a1} (e-k-q), s_{a2} (f-l-r)) on NMP of MMA and styrene initiated by BlocBuilder for a T_{set} of 363 K and a TCL of 200 for various initial mass fractions of styrene (here no corrections for calibration range SEC trace): 10 m% (green lines) and 2.5 m% (red lines); (a-f) overall conversion as a function of time, (g-l) dispersity, (m-r) end-group functionality as a function of overall conversion (X_M); full lines correspond to simulation outcome if an activation energy of (+/-) 10 kJ mol^{-1} is assumed, dotted lines to non-activated reactivity ratios.*

E.3 Calculation of apparent termination rate coefficients

For termination reactions, due to the viscosity increase of the reaction medium, apparent rate coefficients have to be considered. As the reaction medium is mainly (*p*)MMA (maximally 10 m% styrene), it is assumed that the apparent rate coefficient for MMA, as recently determined by Derboven *et al.*[9] at 353 K, in which *x* is the polymer mass fraction and *y* represents log(x_n), can be used to a first approximation.

$$\log\left(\langle k_{t,app}\rangle\right) = a + bx + c\ln(y) + dx_M{}^2 + e(\ln(y))^2 + f x_M \ln(y) + g\ x_M{}^3 + h(\ln(y))^3 + \mathrm{x_n} x(\ln(y))^2 + j\ x^2 \ln y \quad \text{(E.3)}$$

Table E.4. *Parameters used in Equation (E.3) for the calculation of $\langle k_{t,app}\rangle$.*[9]

a	b	c	d	e	f	g	h	i	j
8.399	-2.182	-1.239	3.916	1.565	2.879	-1.679	-1.214	0.730	-7.964

The value of $\langle k_{t,app}\rangle$ is then corrected for the nature of the terminal units participating in the termination and the termination mode. For methacrylates, a temperature dependent relationship between the ratio of disproportionation and recombination is reported (see Equation (E.4)).[10] For styrene, the main termination mode is recombination ($f_{rec,M2} = 1$).[2]

$$\frac{1 - f_{rec,M1}}{f_{rec,M1}} = 0.556 \exp\left(-\frac{-1.854\ kJ\ mol^{-1}}{R\ T}\right) \quad \text{(E.4)}$$

In case of termination between identical terminal units, the apparent rate coefficient is determined according to Equation (E.5)-(E.6). In case of macroradicals of different terminal nature, the apparent rate coefficient is determined according to Equation (E.7).

$$k_{tc,ij,11}^{app} = f_{rec,M1}\langle k_{t,app}\rangle;\ k_{td,ij,11}^{app} = (1 - f_{rec,M1})\langle k_{t,app}\rangle \quad \text{(E.5)}$$

$$k_{tc,ij,22}^{app} = f_{rec,M2}\langle k_{t,app}\rangle;\ k_{td,ij,22}^{app} = (1 - f_{rec,M2})\langle k_{t,app}\rangle \quad \text{(E.6)}$$

$$k_{tc,ij,12}^{app} = \frac{f_{rec,M1} + f_{rec,M2}}{2}\langle k_{t,app}\rangle;\ k_{td,ij,12}^{app} = \frac{(1 - f_{rec,M1}) + (1 - f_{rec,M2})}{2}\langle k_{t,app}\rangle \quad \text{(E.7)}$$

E.4 Experimental error on SEC traces

The error on the SEC trace can be assumed to be mainly attributed to the accuracy of the calibration. The typical experimental error on the SEC traces was determined using a collection of multiple calibration curves for polystyrene recorded at LCT during the past year. The calibration curve is based on:

$$\log(MM) = a \times t_{ret} + b$$

with MM being the molar mass, t_{ret} the retention time and *a* and *b* the calibration parameters. Following calibration parameters for 9 polystyrene calibrations, using narrow polystyrene standard samples (Medium EasiVials kit, Agilent Technologies) ranging from 4.45 10^2 to 3.49 10^5 g mol^{-1}, were obtained:

For retention times within the range typically encountered for samples taking in RDRP processes (molar mass range: *ca.* 1.0 × 10^3 g mol^{-1} - 1.0 × 10^6 g mol^{-1}) the log(MM) for all 9 calibration curves were determined and the average and standard deviations were calculated. The 0.95

confidence intervals on log(MM) were subsequently determined for the different retention times and converted to non-log scale. The average error on a linear scale, *i.e. ca*. 10%, was then used as indicative error-bar on the CLD plots provided in the main text.

Table E.5. *Overview of 9 polystyrene calibration curves for determination of the typical error on SEC measurements.*

cal. nr.	a	b
1	-0.404	10.16
2	-0.399	10.13
3	-0.401	10.14
4	-0.404	10.20
5	-0.406	10.23
6	-0.401	10.20
7	-0.407	10.23
8	-0.407	10.22
9	-0.396	10.08

E.5 Influence of macromonomer propagation

Due to the conventional termination by disproportionation, and more importantly the disproportionation reaction to nitroxide (reaction TR1-2 in Table D.1) a large amount of polymer chains containing a terminal unsaturated double bond are formed. The unsaturated dead polymer chains can function as macromonomers and thus undergo further macropropagation reactions. To investigate the influence of such reactions on the polymer properties simulations were performed including macropropagation. It was assumed that macropropagation occurs with an identical rate

coefficient as the corresponding propagation steps with methyl methacrylate monomer, which is an overestimation.[11] As can be seen in Figure E.2 a macropropagation can be neglected.

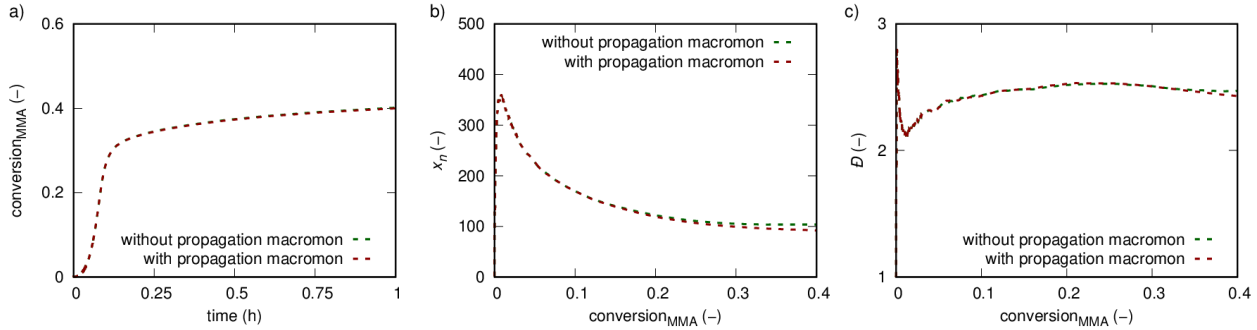

Figure E.2. *Effect of macropropagation for the NMP of MMA (TCL = 200) initiated by BlocBuilder at a Tset = 343 K : (a) MMA conversion as a function of time, (b) number average chain length, (c) dispersity as a function of MMA conversion; green lines correspond to the simulations without macropropagation and red lines to simulations with macropropagation included.*

E.6 NMP of MMA initiated by BlocBuilder

Figure E.3 shows the end-group functionality, R_0X and fraction of fraction of dead polymer products formed via the disproportionation to nitroxide, classical disproportionation, and recombination reaction as a function of (MMA) conversion (in accordance with Figure 7.2-7.3 in the main text). Note that including the non-isothermicity has a significant effect on all these characteristics and can thus not be ignored.

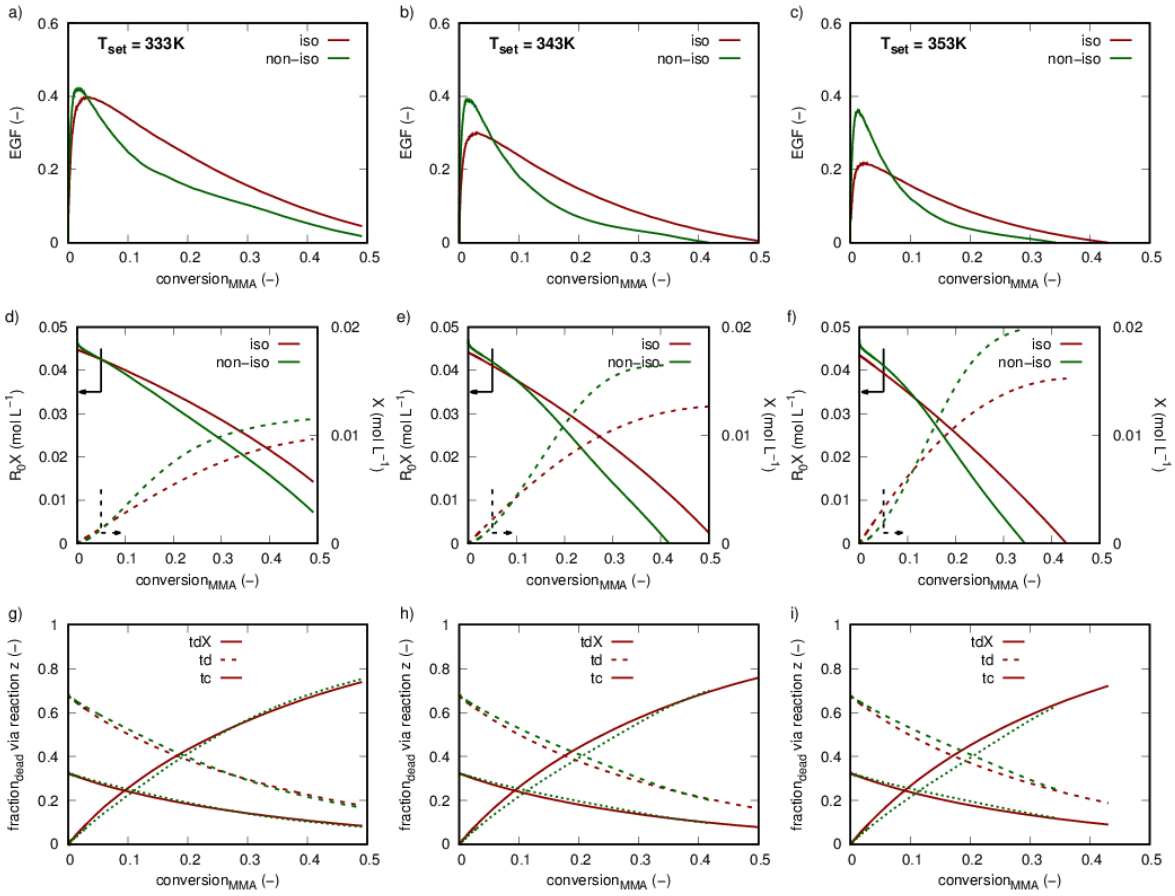

Figure E.3. *Corresponding results to Figure 7.2 (main text) displaying (a-c) end-group functionality (EGF), (d-f) R_0X concentration, and (g-i) fraction of dead polymer product formed by the disproportionation to nitroxide reaction as a function of conversion; parameters: Table S.1 (Supporting Information).*

Figure E.4. allows to clarify the control over the polymerization process by the calculation of three characteristics as explained in the main text. Figure S.4 displays the comparison with the approximate isothermal model and the literature value as highlighted in the main text.

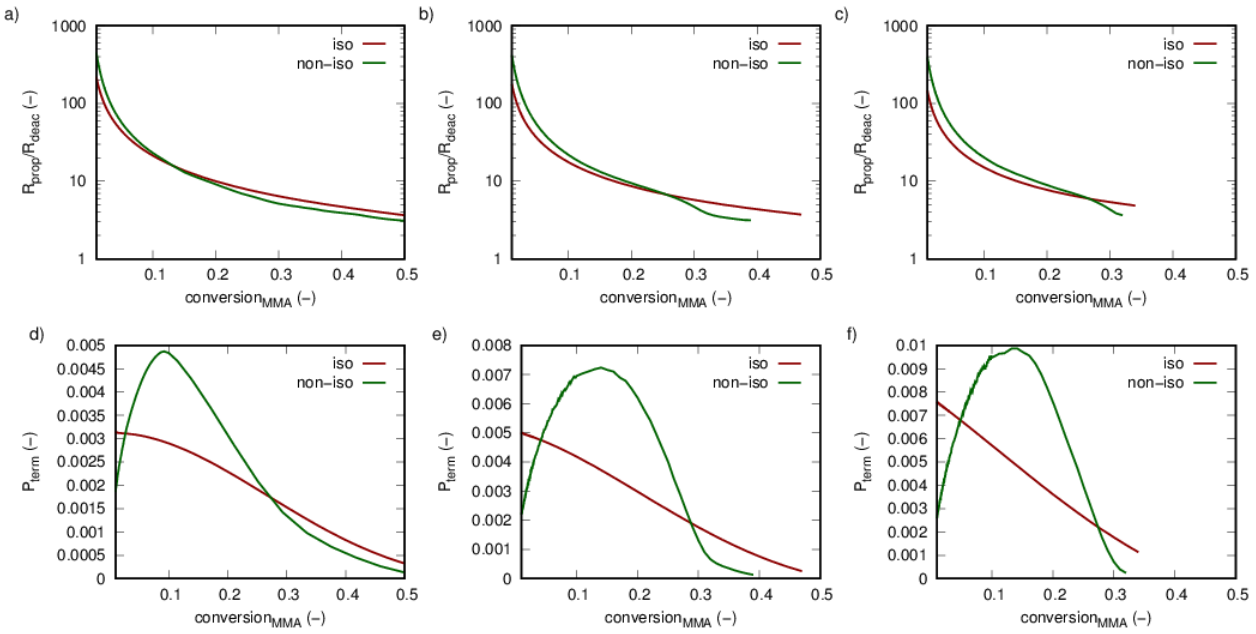

Figure E.4. *Corresponding results to Figure 7.2 (main text) displaying(a-c) propagation to deactivation ratio (R_{proop}/R_{deac}), and (d-f) termination probability (P_{term}) as a function of conversion; parameters: Table S.1(Supporting Information).*

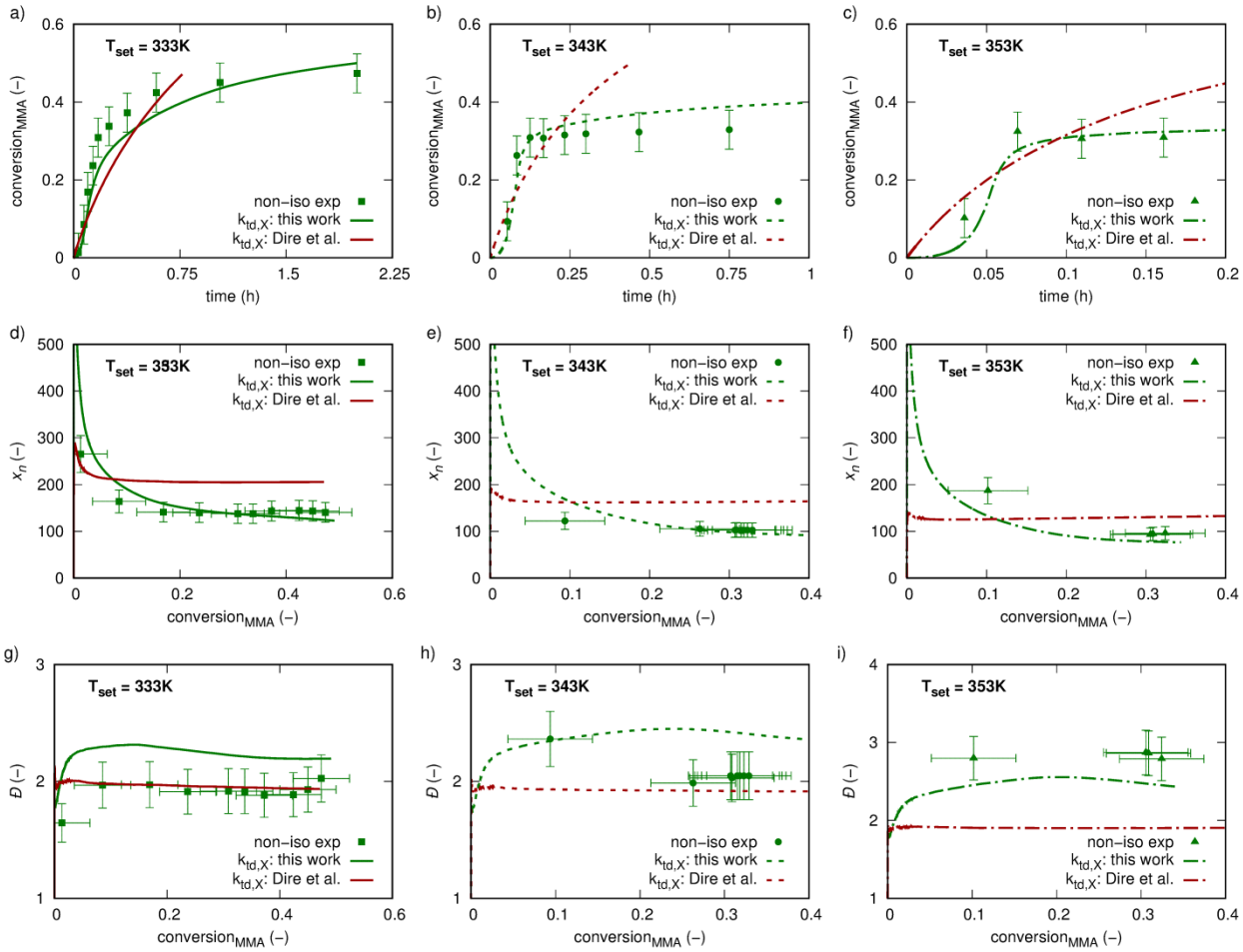

Figure E.5. *Effect of disproportionation to nitroxide reaction and isothermicity on the description of experimental data (points) for NMP of MMA (TCL = 200) initiated by BlocBuilder; (a-c) MMA conversion as a function of time, (d-f) number average chain length, (g-i) dispersity as a function of MMA conversion, green lines correspond to simulations with the* k_{tdX} *value obtained in this work, red lines correspond to isothermal simulations with* $k_{tdX} = 1.7 \times 10^3$ *L mol*$^{-1}$ *s*$^{-1}$.

E.7 NMP of MMA and a small amount of styrene initiated by BlocBuilder

NMP of MMA with a small amount of styrene improves the controlled character of the copolymerization compared with NMP of MMA. However, also in this case the isothermicity should be checked. Figure E.6 shows the recorded temperatures for the lowest ((a); 200) and highest ((b); 750) TCL considered in this work. As can be seen, in case of TCL 200, still a

temperature overshoot is present, especially in case of low initial styrene amounts, however to a lesser extent than in the homopolymerization of MMA (see Figure 7.2 (main text). The higher TCLs did not suffer from a significant overshoot, as shown for TCL 750 in Figure E.6 (b).

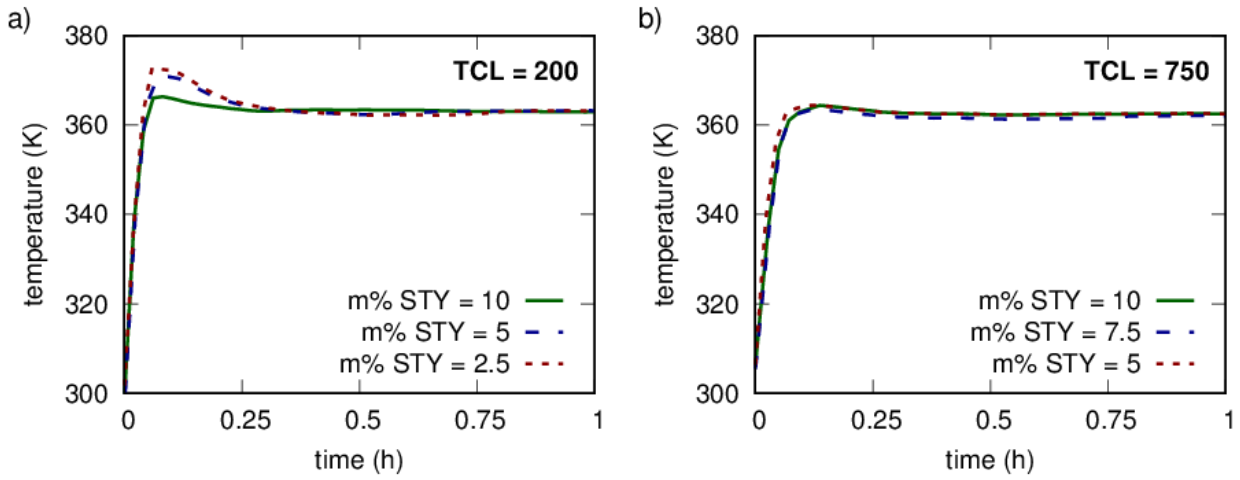

Figure E.6. *Experimentally recorded temperatures for NMP of MMA and styrene initiated by BlocBuilder for a T_{set} of 363 K; (a) a TCL of 200 and (b) a TCL of 750; for distinct initial mass fractions of styrene: 10 (green full lines/squares), 7.5 (brown dashed-dotted lines/diamonds), 5 (blue dashed lines/circles), and 2.5 (red dotted lines/triangles).*

The influence of the non-isothermicity for the most severe copolymerization, *i.e.* a TCL of 200, is shown in Figure E.7 for various initial styrene amounts. It can be seen that the effect is most pronounced for the lowest styrene amount, in compliance with the magnitude of the temperature overshoot in recorded (Figure E.6). The effect is much less pronounced than for the homopolymerization but can however still not be ignored.

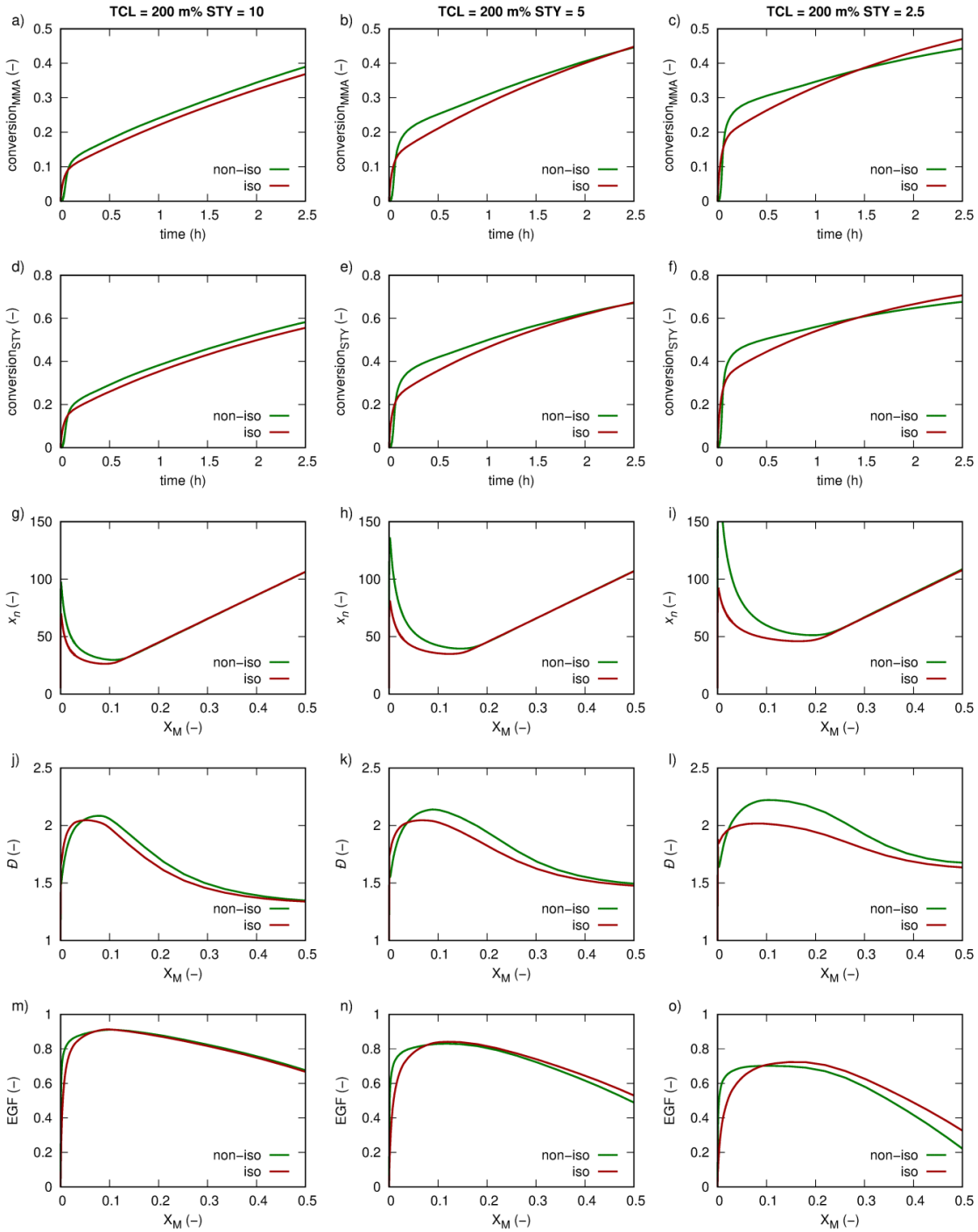

Figure E.7. *Effect of non-isothermicity NMP of MMA and styrene initiated by BlocBuilder for a T_{set} of 363 K and a TCL of 200 for various initial mass fractions of styrene: 10 m% (left), 5 m% (middle), and 2.5 m% (right); (a-c) MMA conversion, (d-f) styrene conversion as a function of time, (g-i) number average chain length, (j-l) dispersity, (m-o) end-group functionality as a function of overall conversion (X_M); red lines correspond to simulation outcome if an isothermal temperature is incorrectly assumed.*

Note that Figure E.7 (m-o) and Figure E.8 display the simulated end-group functionalities for various TCLs and initial styrene amounts. For low styrene amounts, it can be seen that towards higher conversions, a strong decrease in EGF is present for all TCLs considered. The molar fraction of MMA in the monomer feed as a function of time is displayed in Figure E.9. It can be seen that an enrichment of MMA in the feed occurs, which results in a rate enhancement towards higher times and thus a deviation from typical RDRP conversion profiles is observed via the quasi-linear X_M profiles (see Figure 7.6 in the main text).

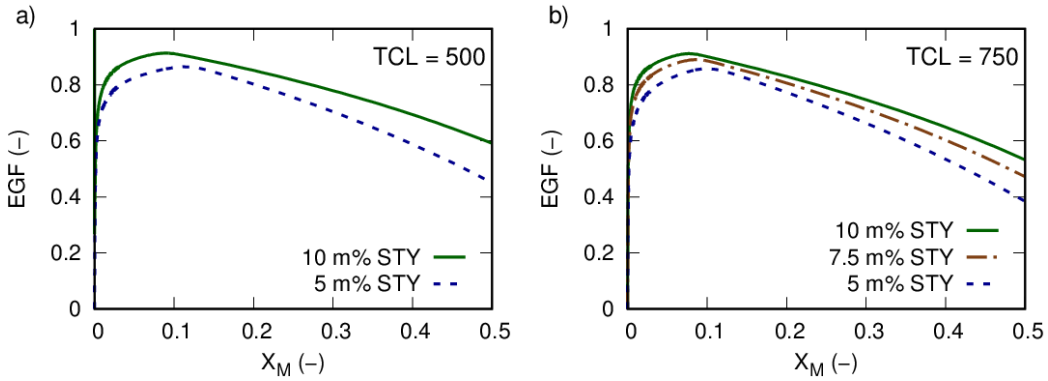

Figure E.8. *Corresponding results to Figure 7.5 (main text) displaying end-group functionality (EGF) as a function of overall conversion (X_M) for: (a) TCL = 500, and (b) TCL = 750.*

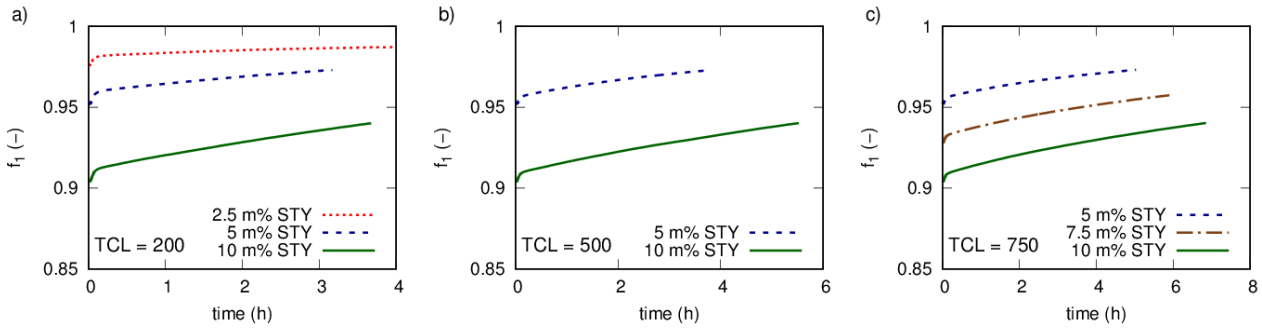

Figure E.9. *Corresponding results to Figure 7.6 (main text) displaying the molar fraction of MMA in the monomer feed (f_1) as a function of time.*

Finally, Figure E.10 shows again an interpretation based on the three general characteristics. The ratio of propagation to deactivation rate (a-c; first characteristic) displays again a strong variation,

however to a lesser extent than the homopolymerization. A lower initial styrene amount results generally in a higher R_{prop}/R_{deac}, especially at lower monomer conversions. The termination probability (d-f; second characteristic) clearly shows the onset of the persistent radical effect, as the termination probability drastically drops. Relatively low P_{term} are present with a higher initial amount of styrene. The probability for the disproportionation of the nitroxide reaction (see Figure 7.8 in Main text; third characteristic), the most important side reaction resulting in an important loss of end-group functionality, is low in the beginning as no build-up of the nitroxide has occurred. Towards higher conversions, $P_{td,X}$ increases and becomes the main termination event, in accordance with the decreasing EGF at higher conversions and the total number fraction of dead polymer product formed via this reaction which reaches 0.8 at an X_M of 0.5 (Figure E.11). This is reflected in the fraction of dead polymer product formed via the disproportionation to nitroxide reaction shown in Figure E.11. A higher initial styrene amount results in a lowering of $P_{td,X}$. This is confirmed by the mapping of the fraction of dead polymer product formed via disproportionation of the nitroxide in Figure E.12, which shows a decreasing trend as a function of the initial mass fraction of styrene.

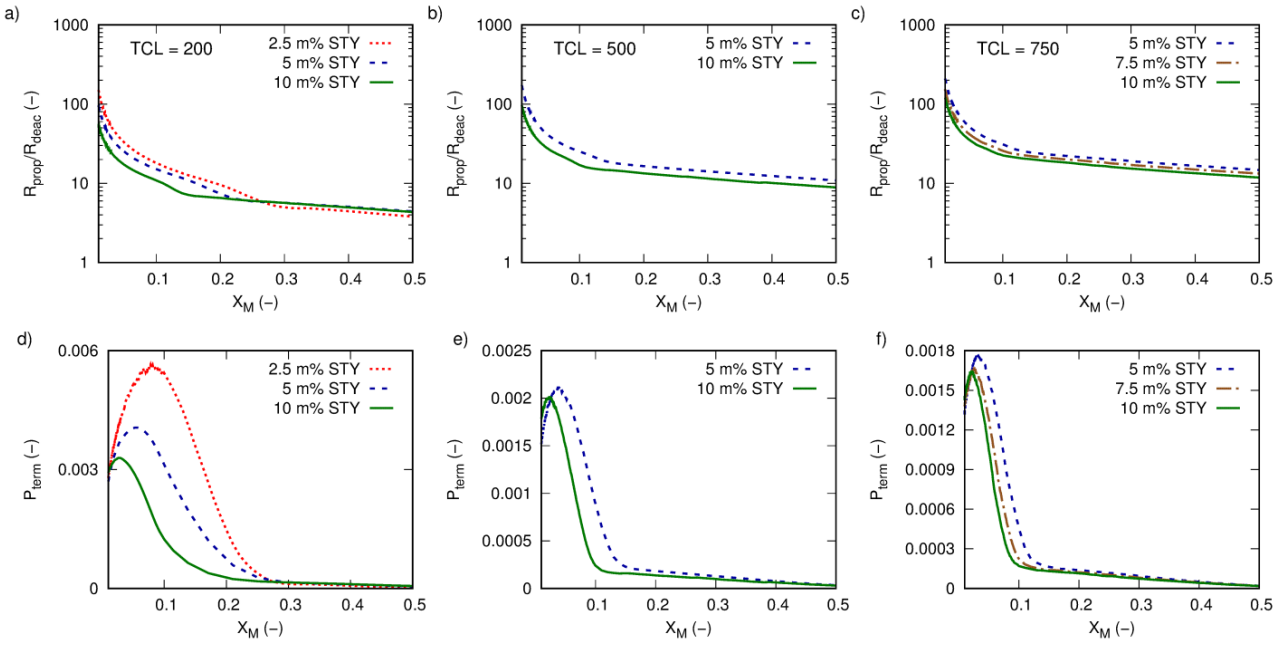

Figure E.10. *Corresponding results to Figure 7.5 (main text) displaying(a-c) propagation to deactivation rate ratio (R_{proop}/R_{deac}), and (d-f) termination probability (P_{term}) as a function of monomer conversion; parameters:* ***Table E.2*** *(Supporting Information).*

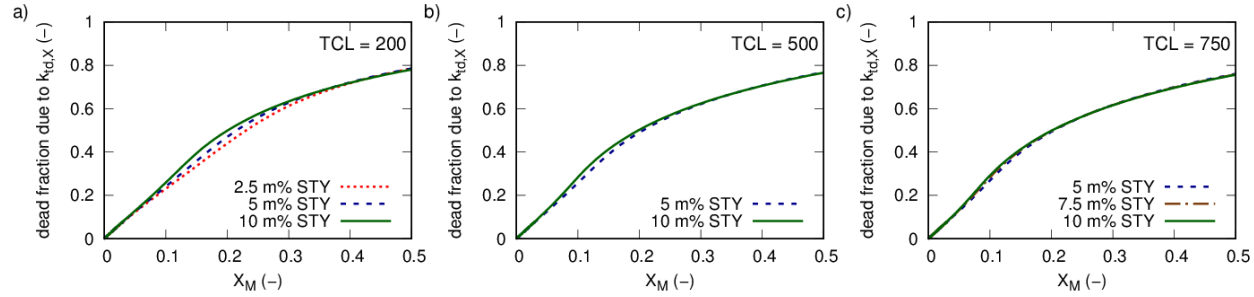

Figure E.11. *Corresponding results to Figure 7.5 (Main text) displaying the fraction of dead polymer product formed by the disproportionation to nitroxide reaction as a function of the overall conversion (X_M).*

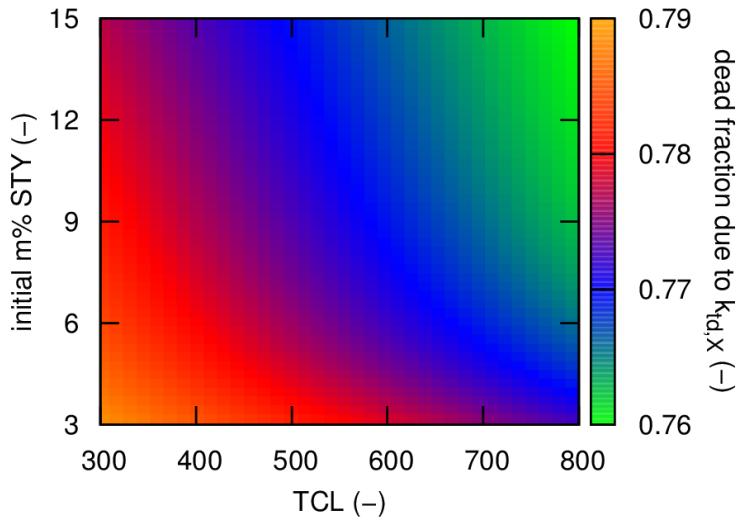

Figure E.12. *Mapping of the impact of TCL and initial mass fraction of styrene on fraction of dead polymer product formed via disproportionation of the nitroxide (X) at X_M = 0.5 for NMP of MMA and styrene initiated by BlocBuilder at 363 K.*

Figure E.13 displays per radical type R_{prop}/R_{deac} for an initial styrene fraction of 10 m%. Large differences between terminal capped MMA and styrene species are present confirming the working principle of the copolymerization approach. Related to Figure 7.9 in the main text, this also indicates that the origin of the zero-growth propagation cycles are mainly the terminal styrene capped macroradicals. This further confirmed in Figure E.14 which displays the distribution of the activation-growth-deactivation cycles, as related to Figure 7.11 in the main text, with a deactivation rate coefficient for terminal styrene capped macroradicals put formally 10 times lower than the one in the main text. The fraction of zero growth activation-deactivation cycles decreases to 0.18 further confirming that the origin of these cycles.

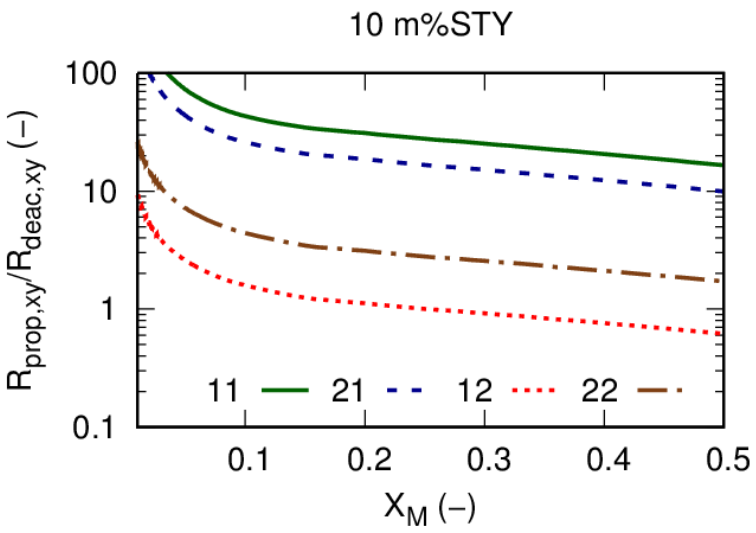

Figure E.13. *Corresponding results to Figure 7.6 (main text) displaying the propagation to deactivation rate ratio (R_{proop}/R_{deac}) per radical type for an 10 m% initial mass fraction of styrene and TCL of 200; 1: MMA; 2: styrene.*

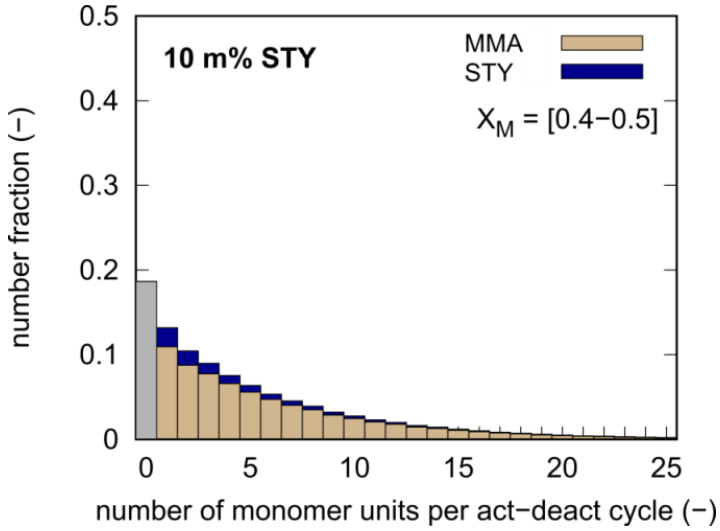

Figure E.14. *Number fraction of activation-deactivation cycles as a function of the number of propagation steps with the relative contribution of MMA and styrene indicated for X_M interval from 0.4-0.5 for the NMP of MMA and styrene (TCL = 200) initiated by BlocBuilder for a T_{set} of 363 K with an initial styrene mass fraction of 0.10 and with the deactivation rate coefficient k_{da22} formally one order of magnitude lower.*

Finally, the number fraction of chains with a given number of styrene units is shown in Figure E.15, as related to Figure 7.10 in the main text. It can be seen that a broad distribution results with an average number of 3.7, 7.1, and 13.5 number of styrene units at X_M = 0.5 for 2.5, 5, and 10 m% of initial styrene content. The coefficient of variation amounts to 1.21, 1.51, and 1.82, respectively. Thus, a relatively broader distribution results for higher styrene contents.

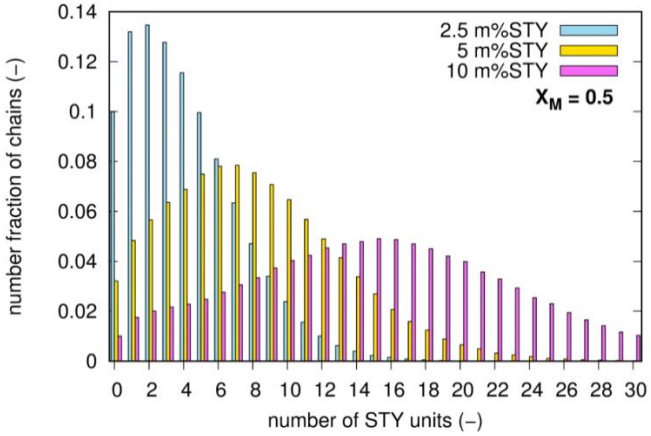

Figure E.15. *Number fraction of chains with a given number of styrene units for NMP of MMA and styrene (TCL = 200) initiated by BlocBuilder at X_M = 0.5 for a T_{set} of 363 K using an initial mass fraction of styrene of 2.5 m%(blue), 5 m% (yellow) and 10 m% (fuchsia) of styrene.*

Figure S.16 shows that the concentration of the dormant species with MMA terminal units is low.

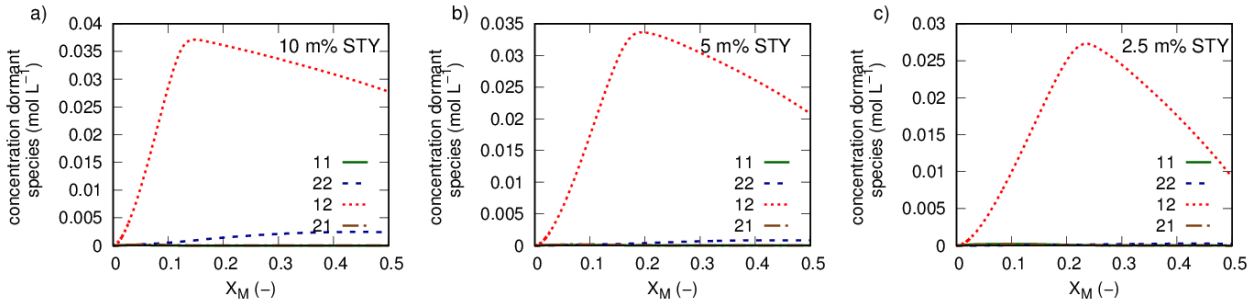

Figure E.16. *Corresponding results to Figure 7.5 (main text) displaying the concentration of dormant macrospecies type for a TCL of 200 and a (a) 10 m%, (b) 5 m%, (c) 2.5 m% initial mass fraction of styrene.*

Finally, Figure S.17 shows the relevance of the PMU on NMP activation. For completeness both reactivity ratios are included. It can be seen that a large influence on the conversion profile is present when neglecting PMU effects on activation for terminal styrene macrospecies.

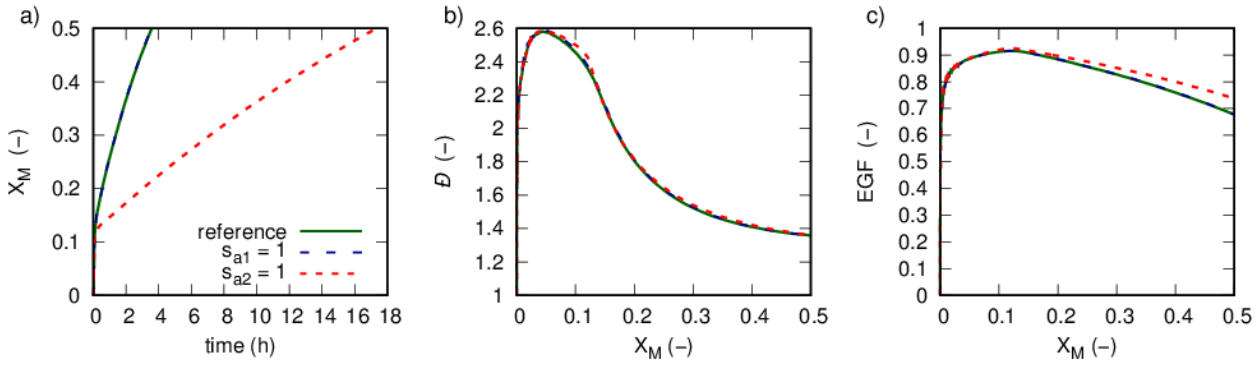

Figure E.17. *Influence of PMU effects on NMP of MMA and styrene initiated by BlocBuilder for a* T_{set} *of 363 K and a TCL of 200 for an initial mass fractions of styrene of 10 m% with* s_{a1} *= 0.06 and* s_{a2} *= 6.7 (green full lines),* s_{a1} *= 1 and* s_{a2} *= 6.7 (blue dashed lines),* s_{a1} *= 0.06 and* s_{a2} *= 1 (red dotted lines).*

References

1. Beuermann, S.; Buback, M.; Davis, T. P.; Gilbert, R. G.; Hutchinson, R. A.; Olaj, O. F.; Russell, G. T.; Schweer, J.; van Herk, A. M. Critically evaluated rate coefficients for free-radical polymerization, 2.. Propagation rate coefficients for methyl methacrylate. *Macromol. Chem. Phys.* **1997,** 198, (5), 1545-1560.

2. Matyjaszewski, K.; Davis, T. P., *Handbook of Radical Polymerization*. Wiley: 2002.

3. Chauvin, F.; Dufils, P. E.; Gigmes, D.; Guillaneuf, Y.; Marque, S. R. A.; Tordo, P.; Bertin, D. Nitroxide-mediated polymerization: The pivotal role of the k(d) value of the initiating alkoxyamine and the importance of the experimental conditions. *Macromolecules* **2006,** 39, (16), 5238-5250.

4. Buback, M.; Gilbert, R. G.; Hutchinson, R. A.; Klumperman, B.; Kuchta, F.-D.; Manders, B. G.; O'Driscoll, K. F.; Russell, G. T.; Schweer, J. Critically evaluated rate coefficients for free-radical

polymerization, 1. Propagation rate coefficient for styrene. *Macromol. Chem. Phys.* **1995,** 196, (10), 3267-3280.

5. Fierens, S. K.; D'hooge, D. R.; Van Steenberge, P. H. M.; Reyniers, M.-F.; Marin, G. B. MAMA-SG1 initiated nitroxide mediated polymerization of styrene: From Arrhenius parameters to model-based design. *Chem. Eng. J.* **2015,** 278, 407-420.

6. Guillaneuf, Y.; Gigmes, D.; Marque, S. R. A.; Tordo, P.; Bertin, D. Nitroxide-Mediated Polymerization of Methyl Methacrylate Using an SG1-Based Alkoxyamine: How the Penultimate Effect Could Lead to Uncontrolled and Unliving Polymerization. *Macromol. Chem. Phys.* **2006,** 207, (14), 1278-1288.

7. Nicolas, J.; Mueller, L.; Dire, C.; Matyjaszewski, K.; Charleux, B. Comprehensive Modeling Study of Nitroxide-Mediated Controlled/Living Radical Copolymerization of Methyl Methacrylate with a Small Amount of Styrene. *Macromolecules* **2009,** 42, (13), 4470-4478.

8. Coote, M. L.; Johnston, L. P. M.; Davis, T. P. Copolymerization Propagation Kinetics of Styrene and Methyl Methacrylate-Revisited. 2. Kinetic Analysis. *Macromolecules* **1997,** 30, (26), 8191-8204.

9. Derboven, P.; D'hooge, D. R.; Reyniers, M.-F.; Marin, G. B.; Barner-Kowollik, C. The Long and the Short of Radical Polymerization. *Macromolecules* **2015,** 48, (3), 492-501.

10. Buback, M.; Günzler, F.; Russell, G. T.; Vana, P. Determination of the Mode of Termination in Radical Polymerization via Mass Spectrometry. *Macromolecules* **2009,** 42, (3), 652-662.

11. Junkers, T.; Barner-Kowollik, C. Optimum Reaction Conditions for the Synthesis of Macromonomers Via the High-Temperature Polymerization of Acrylates. *Macromol. Theory Simul.* **2009,** 18, (7-8), 421-433.

Appendix F. Glossary

Activation-growth-deactivation cycle distribution: Distribution of the number fraction of activation-growth-deactivation cycles as a function of their number of propagation steps.

Apparent rate coefficient: Rate coefficient related to the observed kinetics, *i.e.* the rate coefficient determined by the intrinsic chemical rate coefficient and transport phenomena.

Arrhenius equation: Empirical equation that describes the dependence of the rate coefficient k of a reaction on the absolute temperature T: $k = A \exp -E_a/RT$ in which R is the universal gas constant, A the pre-exponential factor and E_a the activation energy.

Atom-transfer radical polymerization: Controlled reversible-deactivation radical polymerization in which the deactivation of the radicals involves reversible atom transfer or reversible group transfer, catalyzed usually, though not exclusively, by transition-metal complexes.

Bivariate modeling: Modeling technique involving the distribution of two variables.

Chain initiation: Chemical reaction in which initiating species add to monomer a monomer molecule to form a macrospecies.

Chain length: Number of repeating units (coming from the monomer(s)) in a polymer molecule.

Chain polymerization: Polymerization in which the growth of a polymer chain proceeds by a chain reaction mechanism.

Chain reaction: A reaction in which one or more reactive reaction intermediates (frequently radicals) are continuously regenerated, usually through a repetitive cycle of elementary steps (the 'propagation step').

Chain transfer: Chemical reaction occurring during a chain polymerization in which a reactive center is transferred from a growing macromolecule to a small molecule, to another polymer molecule or to the same polymer molecule.

Compositional drift: Deviation in the instantaneous copolymer composition originating from the changes in monomer feed composition.

Controlled radical polymerization: See *Reversible deactivation radical polymerization.*

Copolymerization: Denoting the polymerization of multiple monomer types. "Binary copolymerization" denotes the polymerization of two comonomer types. "Ternary copolymerization" denotes the polymerization of three comonomer types. Often the term "Copolymerization" is used to denote the polymerization of two monomer types.

Dead polymer molecule: Polymer molecule without end-group functionality.

Deterministic method: Method for solving of a deterministic system/model, typically a set of ordinary differential equations. A deterministic system is a system in which no randomness is involved in the temporal evolution of the system.

Diffusion: Movement of the center-of-mass of a molecule in a reaction mixture.

Dormant polymer molecule: Temporarily deactivated macroradical.

End-group functionality: Functional group allowing further chemical modification.

Explicit modeling: Modeling technique in which the complete history of reaction events and microstructure is explicitly tracked.

Functionality location distribution: Distribution of the (absolute or relative) location of functionalities along the backbone of the polymer chains.

Genetic algorithm: Algorithm inspired by the process of natural selection as occurring in nature.

Gradient copolymer: Mostly pertaining to linear polymer chains, denoting a gradual change in the monomer composition along the polymer chain.

Gradient deviation: Deviation (with respect to the theoretical ideal linear gradient profile) of the cumulative monomer composition of a single chain.

Instantaneous copolymer composition: Fraction of monomer 1 instantaneously incorporated in the copolymer, $F_{1,inst}$, as a function of the fraction of monomer 1 in the monomer feed, f_1.

Kinetic Monte Carlo: Monte Carlo method to simulate the time evolution of processes occurring in nature.

Living polymerization: Chain polymerization from which chain termination and irreversible chain transfer are absent.

Macroradical activation: Conversion of a dormant macrospecies into a macroradical.

Macroradical deactivation: Conversion of a macroradical into a dormant macrospecies.

Mayo-Lewis equation: Widely used closed-form analytical expression to describe the instantaneous copolymer composition $F_{1,inst}(f_1)$. It is based on the quasi-steady state approximation of the individual macroradical terminal unit types and depends only the (propagation) reactivity ratios.

Microstructure: Entirety of structural characteristics of a polymer on the molecular level. They determine the morphological, rheological, thermal and physical properties of polymer materials.

Monomer sequence: Fixed-order series of monomers of arbitrary number and identity.

Monomer sequence type distribution: Number fraction of a sequence with given length as a function of every possible monomer sequence.

Multi-objective optimization: Research area of multiple criteria decision making, that is concerned with mathematical optimization problems involving more than one (conflicting) objective function to be optimized simultaneously.

Nitroxide mediated polymerization: Controlled reversible-deactivation radical polymerization in which the deactivation involves reversible coupling with stable (persistent) free radicals, *i.e.* nitroxide radicals.

Overall conversion: Conversion calculated with respect to the total amount of monomer. "Total" refers to the sum of the initial monomer present in the reactor and the monomer that will be fed during the polymerization.

Pareto front: Set of optimal solutions, for which no objective can be improved without sacrificing at least one other objective, *i.e.* obeying Pareto optimality.

Pareto optimality: A concept of optimality in multi-objective optimization in which no other solution can be found which is better without making at least one objective worse.

Penultimate monomer unit: Monomer unit next to the terminal monomer unit.

Persistent radical effect: Build-up of a persistent species as a result of termination reactions leading to the reduction of the radical concentration.

Persistent species: Persistent radicals or complexes which have no mutual reactions, *i.e.* they do not react among themselves.

Polydispersity index: Ratio of the mass to number average molar mass; measure for the broadness of the molar mass distribution of the polymer.

Propagation of a macroradical: Chemical reaction between a macroradical and a monomer molecule that results in the growth of a polymer chain and the formation of a longer macroradical.

Radical polymerization*:* Chain polymerization in which the reactive centers are radicals.

Rate coefficient: Proportionality coefficient between the rate of a reaction and the product of the concentrations of the reactants.

Rate equation: Equation expressing the reaction rate as a function of concentrations or pressures of the reactants and the rate coefficient. Also called rate law.

Reversible addition-fragmentation chain transfer (RAFT) polymerization: Degenerate-transfer radical polymerization in which chain activation and chain deactivation involve a degenerative chain-transfer process which occurs by a two-step addition-fragmentation mechanism.

Reversible deactivation radical polymerization (RDRP): Radical polymerization technique in which control over the chain length distribution and livingness of the polymer is established by reversible deactivation of the macroradicals with a RDRP agent.

Segment: Consecutive sequence of comonomers of the same type in a polymer chain.

Segment length distribution: Number fraction of segments as a function of their segment lengths.

Sequence controlled polymers: Copolymer chain in which the monomer sequence distribution follows a similar arrangement in all chains, however with some deviations as opposed to sequence defined polymers.

Stochastic method: method for a model of a random process, using a random number generator to sample physical events.

Stockmayer equation: Bivariate distribution describing the joint distribution of the mass fraction of polymer chains with respect to (i) their instantaneous copolymer composition and (ii) their chain length. Valid for a basic chain polymerization.

Terminal monomer unit: Monomer unit onto which the reactive center resides.

Termination of macroradicals: Reaction consuming two radical centers leading to the formation of (a) dead polymer molecule(s).

Univariate modeling: Referring to a distribution of only one random variable. Distributions involving more than one random variable are called multivariate distributions. Distributions of two random variables are called bivariate distributions.